JOURNAL OF APPLIED PHYSICS

JOURNAL OF APPLIED PHYSICS

Vol. 19, No. 12 DECEMBER, 1948

In This Issue

	Page
Transformations in Organic Pigments F. A. Hamm and Earl Van Norman	1097
Drag Coefficients of Steel Spheres Entering Water Vertically Albert May and Jean C. Woodhull	1109
Homing and Navigational Courses of Automatic Target-Seeking Devices Luke Chia-Liu Yuan	1122
Use of an Electron Diffraction Camera as an Ultraoscilloscope, and Suggested Application to Contact Erosion J. J. Lander	1128
Erratum: The Attenuation of Spherical Shock Waves in Air Richard G. Stoner and Walker Bleakney	1129
Dielectric Measurement Methods for Solids at Microwave Frequencies W. H. Surber, Jr. and G. E. Crouch, Jr.	1130
Erratum: Twinning in Tetragonal Alloys of Copper and Manganese Francis T. Worrell	1139
Properties of a Long Antenna Erik Hallén	1140
Dissipation of Heat by Free Convection from Vertical and Horizontal Cylinders W. Elenbaas	1148
On the Theory of Biconical Antennas C. T. Tai	1155
Measurement by Radioactive Tracers of Diffusion in Liquids Andrew Gemant	1160
Physical Limitations of Omni-Directional Antennas L. J. Chu	1163
Technique for Quantitative Determination of Texture of Sheet Metals John T. Norton	1176
Letters to the Editor:	
Drag of an Airfoil in Accelerated, Supersonic Flight C. S. Gardner, H. F. Ludloff, and F. Reiche	1179
Remarks on "The Efficiency of Thermoelectric Generators" Robert M. Papet	1180
Calculation of the Temperature Development in a Contact Heated in the Contact Surface, and Application to the Problem of the Temperature in a Sliding Contact W. J. Oosterkamp	1180
On the Possibility of Hg Type Arcs with Hot Refractory Cathodes Jerome Rothstein	1181
Application of Electron Multiplier Tubes in the Measurement of X-Ray Beam Intensities and in the Determination of Crystal Structure G. Papp and K. Sasvári	1182
Homing Pigeon in Electromagnetic Fields C. L. Clark, R. A. Peck, Jr., W. F. Hollander	1183
Program of the E. F. Burton Memorial Meeting of the Electron Microscope Society of America	1186
Annual Indexes	
Author Index to Volume 19	1193
Subject Index to Volume 19	1198
In Every Issue	
Calendar of Meetings	1154
New Booklets	1184
Here and There	1184
Index to Advertisers	xxxiv

BOARD OF EDITORS

Elmer Hutchisson, *Editor*

Associate Editors

R. Bowling Barnes
Otto Beeck
W. F. Busse
W. James Lyons
Philip Morrison
Paul E. Sabine
Frederick Seitz
J. R. Townsend
John Von Neumann

Publication of the American Institute of Physics

ADMINISTRATIVE STAFF

Henry A. Barton, *Director*

Cleveland Norcross, *Assistant Director*

Ruth F. Bryans, *Publication Manager*

Theodore Vorburger, *Business Manager*

John T. Tate, *Adviser on Publications*

GOVERNING BOARD

George R. Harrison, *Chairman*

Wallace Waterfall, *Secretary*

George B. Pegram, *Treasurer*

Luis W. Alvarez
Robert B. Brode
E. U. Condon
A. J. Dempster
W. F. Fair, Jr.
Harvey Fletcher
R. C. Gibbs
W. V. Houston
Paul E. Klopsteg
F. W. Loomis
Philip M. Morse
A. H. Pfund
John T. Tate
M. W. White
A. G. Worthing

The Journal of Applied Physics, published monthly at Prince and Lemon Sts., Lancaster, Pa., is devoted to physics in its role as the science basic to other natural sciences and to the arts and industries. Previous to 1937 this publication was known as Physics. The Journal of Applied Physics publishes editorials, news of physicists, and reviews, as well as technical papers of applied physics.

Manuscripts should be submitted to Elmer Hutchisson, Editor, Case Institute of Technology, Cleveland 6, Ohio.

Subscriptions and orders for back numbers should be addressed to Prince and Lemon Streets, Lancaster, Pa. or to the American Institute of Physics, 57 East 55 Street, New York 22, N. Y.

Subscription Price

	U.S. and Canada	Elsewhere
To members and associate members of the American Institute of Physics	$7.00	$ 8.00
To all others	9.00	10.00

Back Number Prices

Complete set: Vol. 1, July, 1931–Vol. 18, 1947—$132.00
Yearly back number rate: $10.00
Single copies: $1.00 each.

Changes of address should be sent to the Business Manager, American Institute of Physics; **corrected proofs** should be sent to the Publication Manager, American Institute of Physics.

Advertising rates supplied on request. Orders, advertising copy, and cuts should be sent to the American Institute of Physics.

Entered as second class matter January 22, 1937, at the Post Office at Lancaster, Pennsylvania, under the Act of March 3, 1879.
Accepted for mailing at the special rate of postage provided for in the Act of February 28, 1925, authorized May 2, 1932.

Copyright 1948, by the American Institute of Physics.

Journal
of
Applied Physics

Volume 19, Number 12 December, 1948

Transformations in Organic Pigments

F. A. Hamm and Earl Van Norman
General Aniline and Film Corporation, Central Research Laboratory, Easton, Pennsylvania
(Received March 18, 1948)

Organic pigments are often recrystallized in various ways to effect purification and to control the particle size of the new crop of crystals. Copper phthalocyanine and indanthrene blue RS have been observed to yield crystals of varying shades, ranging from a light greenish blue to a dark reddish blue (purple). These shades have in the past been attributed only to differences in particle size because the elementary analyses strongly indicated that the samples were chemically identical. This investigation shows that both these pigments are polymorphic, and each can exist in at least two different physical forms. The shade differences, therefore, may be due to the differences in the light absorption exhibited by the structurally different polymorphic forms.

The polymorphic transformations can, for both pigments, be readily observed to take place in the electron microscope. The new form of both pigments, completely stable to the illuminating beam after the transformation, can be seen to grow from the vapor state at the expense of the original metastable solid material. The "red" shade of indanthrene blue RS and the "hard" powder of copper phthalocyanine have been labeled "metastable" because they transform in the electron microscope. The "red" shade of indanthrene blue RS can also be made to transform during its molecular distillation; the "blue" shade did not transform under any circumstances. The "hard" and "soft" powders of copper phthalocyanine can both be made to transform during their molecular distillations (not in the electron microscope) to give the same new form which is identical with the form that grew in the electron microscope at the expense of the original "hard" powder.

Electron diffraction patterns prove that the newly formed phases are structurally different from the original samples. Both these commercially important pigments are therefore at least dimorphic.

INTRODUCTION

A GREAT deal of effort is being expended toward the preparation of organic pigments which have strong hiding powers, easy dispersibility, long stability, and certain specific shades. It is not the purpose of this discussion to relate particle size to the wave-lengths of the illuminating light in order to account for shade differences. That is a tremendous subject in itself. However, we have used the electron microscope to gather data on the size, shape, and aggregation of dyestuff particles in an effort to relate this data with the quality of the pigment.

During the course of these extended investigations we observed rather spurious behavior on the part of some pigments. It developed that copper phthalocyanine and indanthrene blue RS can exist in forms which are metastable in the electron microscope during examination. Since then we have directed our efforts toward a more thorough investigation of this phenomenon. It is the purpose of this paper to report some of these findings.

There is virtually no information on the polymorphism[1] of dyestuffs in the available literature. However, a brief record of an interivew with

[1] The ability of a chemical compound to exist in two or more forms, each having different crystalline structures.

a Dr. von Susich in Germany has been recorded in British Intelligence Objectives Sub-Committee, Final Report No. 987, Item No. 22, pages 165–167. He had observed a polymorphic behavior in both copper phthalocyanine and indanthrene blue RS; however, his laboratory reports were destroyed, and his data has presumably never been published in the technical literature. It is a well established fact that polymorphic transformations, both monotropic (irreversible) and enantiotropic (reversible), may "suspend" for long periods of time so that the phase which is really metastable at room temperature may exist almost indefinitely. Sulfur, phosphorus, tin, and mercuric iodide are typical examples. In fact, severe undercooling below the transition temperature often *decreases* the rate of transformation. The image in the electron microscope is caused by the absorption and especially the scattering of the electrons passing through the sample. Kinetic energy is, therefore, in part taken up by the solid matter as heat energy. Thus, just as the hot stage light microscope is used to study polymorphism, the electron microscope is rather inadvertently used similarly.

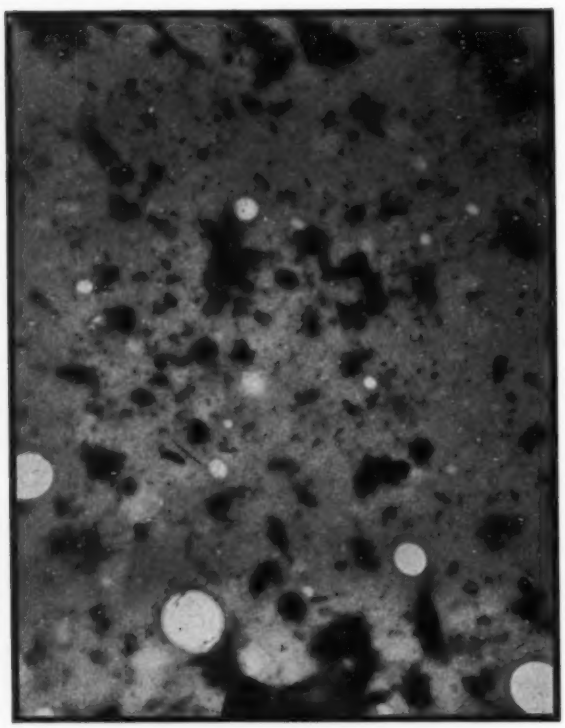

FIG. 1. Milled in Formvar dispersion of the "red" shade of indanthrene blue RS. Metastable form. 14,700×.

The samples under discussion are experimental laboratory samples.

INDANTHRENE BLUE RS

The standard plant sample of this compound always exhibits the same blue shade. However, depending upon further treatment, usually carried out for the purpose of preparing a more readily dispersed powder, pigments having different shades may be produced. This paper deals with two powders, one having a "reddish" cast and the other having the standard "bluish" cast. Both are chemically identical.

History of Samples[2]

Red Shade

A small amount of the standard material is mixed with a trace of surface active agent and dissolved in strong sulfuric acid. This solution is drowned in water with good stirring. The solid dyestuff is filtered, washed acid free, and dried at 70°C. The organic chemists feel that an acid sulfate salt is temporarily formed which is later hydrolyzed to give the free pigment.

Blue Shade

This is a standard plant sample which had been prepared by spraying a strong acid solution thereof into water, filtering off the solid pigment and drying at 70°C. It is believed that no sulfate salt is formed in this case, but that the free pigment is liberated directly.

Specimen Preparations

The "red" shade consists of extremely small particles which are severely aggregated and dispersed with great difficulty. Sonic (9 kc)[3] and ultrasonic (400 kc)[4] treatment in distilled water had little or no effect in breaking up the aggregates into individual particles (crystals). By

[2] Because of the confidential nature of these experimental samples, their complete history cannot be disclosed.

[3] Nickel magneto-constriction type of sonorator made by the Raytheon Manufacturing Company, Boston, Massachusetts.

[4] Quartz piezo-electric type of ultrasonorator Model A-500 made by Piezo Products Company, Framingham, Massachusetts.

vigorously milling the pigment in an ethylene dichloride solution of Formvar[5] on a microscope slide as usually done in this type of sample preparation, some aggregates can be dispersed into smaller aggregates or single particles. These particles are quite thin and are rather poor electron scatterers, so that it has not been possible to resolve them completely. However, it seems reasonable to assume that most of the particles are on the order of 50A or less. This sample is illustrated in Fig. 1. The surface forces binding these crystals together must be very strong.

The "blue" shade can be dispersed readily by milling in Formvar or by an ultrasonic (400 kc) treatment in distilled water. It is interesting to note that a variety of organic pigments can be ultrasonically dispersed so that electron micrographs of these samples can be used to study the size, shape, and extent of aggregation of these particles. The technique of sample preparation is as follows: About 5 milligrams of dry powder or wet paste is mixed in 5 cc of distilled water in a small test tube. The test tube is placed above the vibrating quartz crystal at the peak of the "geyser" erupting in the oil bath surrounding the quartz crystal.[6] A five minute treatment at maximum power (tuned frequency) seems to be adequate. The resultant dispersion may be stable for weeks, depending on the sample. In any case, a few drops of the mixture is immediately pipetted onto a specimen screen, previously coated with the usual thin film of Formvar. After soaking up the excess water with filter paper placed beneath the supporting specimen screen, the specimen is ready for examination.

Discussion

The crystals of the "blue" shade are relatively large and represent a wide size range. Perhaps the aggregates are more easily dispersed because the crystals are larger. However, because this is not always the case, the intercrystalline surface forces may be weaker than in the "red" shade. Figure 2 is an electron micrograph illustrating the "blue" shade after ultrasonic treatment.

FIG. 2. Ultrasonic dispersion of the "blue" shade of indanthrene blue RS. Stable form. 14,700×.

When these samples are examined in the electron microscope, the following observations can be made:

(1) The "blue" shade is very stable and only very occasionally can a transformation be observed. Thus, a small amount of the metastable form may have formed during the preparation of this sample.

(2) If the particles of the "red" shade are resting on top of a Formvar substrate, almost all of the material transforms to new crystals as soon as it is irradiated by the electron beam. This transformation is a recrystallization of the pigment from the vapor state at the expense of the original solid. This phenomenon is presumably irreversible; the new form is completely stable even at "crossover" using a self-biased gun.[7] If, however, the pigment is embedded within the Formvar, the transformation is much less complete.

[5] Shawinigan Products Corporation, Empire State Building, New York City.

[6] If a magneto-constriction type of sonorator is used, the aqueous mixture is placed in the metal cup just above the laminated nickel rod.

[7] "Crossover" is the expression used to describe the image of the thermionic emission point on the electron gun filament when focused on the specimen. Under these conditions the illumination is at a maximum. In the self-biased gun, a potential difference of some 125 volts is maintained between the filament and the grid (cathode cup) to give a higher (*ca.* 20 times) intensity electron beam than possible with the standard zero bias (no grid voltage) gun.

FIG. 3. Stable form of indanthrene blue RS "red" shade after the transformation in the electron microscope. 14,700×.

The transformation might conceivably be thermodynamic (polymorphism) or radiation-chemical[8] in nature. In any case, the Formvar may be considered to "protect" the particles embedded within it from some of the electrons, as a result of its own electron scattering power. As indicated later, the phenomenon is very probably of the usual polymorphic type. In other words, the transformation is the result of thermal effects. If the transformation temperature is somewhere below approximately 150°C, those pigment particles embedded within the Formvar may never reach the transformation temperature. Furthermore, the vapor pressure of the embedded particles because of their lower temperature may be sufficiently low so that the "vapor-to-new solid" transformation does not proceed. It follows, therefore, that those particles of the "red" shade resting on top of the Formvar are in a better position to transform because they can absorb more thermal energy given up by the scattered and absorbed electrons, which impart some kinetic energy in the form of heat.

Figure 3 illustrates crystals of the new form of indanthrene blue RS after the transformation of the "red" shade. This pigment is at least dimorphic; the particular crystalline form depends upon the preparation of the sample. It should be noted that these compounds are very thermally stable, and they do not readily decompose in a chemical sense. They are ordinarily very stable to the electron beam so that whenever a recrystallization is observed in the electron microscope, a polymorphic transformation is suggested.

The identification of the various forms was accomplished by means of their electron diffraction patterns, discussed in a later section.

COPPER PHTHALOCYANINE

This blue pigment is also important commercially and has been the subject of many investigations dealing with particle size, stability, shade differences, etc. This paper deals with a "soft" powder having a "greenish-blue" shade and a "hard" powder exhibiting a "red" shade. Both pigments are chemically identical. (A "soft" powder is one that requires little grinding to make it readily dispersible; a "hard" powder is one that requires a great deal of grinding.) From a practical point of view it is desirable to use a soft powder. However, there are times when the accompanying stability and color shade are objectionable.

Several years ago the authors recrystallized copper phthalocyanine from concentrated sulfuric acid on a microscope slide. A light microscopical study showed that as the strong acid solution took on water from the atmosphere the first crop of crystals grew as thin square plates. Soon thereafter these plates dissolved and long acicular crystals grew at their expense. This second crop of crystals was permanent. One can find in the literature[9] speculations made of various sulfuric acid salts of the basic pigment. These salts later hydrolyze in weak acid to form the free copper phthalocyanine. It may be that

[8] Radiation-chemical is the analog of photo-chemical in which high energy emanations (electrons, neutrons, alpha-particles, etc.) have an effect similar to that produced by lower energy light wave excitations.

[9] Vincent C. Vesce, *Protective and Decorative Coatings* (John Wiley & Sons, Inc., New York, Chapter 3, Vol. II).

the first crop of crystals was merely a salt complex. On the other hand, considering the results of this electron microscopical investigation it is possible that a polymorphic transformation may have occurred. In any case, the dry pigment powders under discussion are very probably polymorphs, just as in the case of the indanthrene blue RS.

History of Samples

"Soft" Powder

Plant material was mixed with a small amount of a surface active material, dried at 70°C, and hammer milled. This sample has a very strong hiding power.

"Hard" Powder

Plant material was dissolved in concentrated sulfuric acid. A relatively small amount of an aqueous dextrin solution was added after which the mixture was treated with water under pressure. The solid pigment was filtered and washed acid free. A small amount of this presscake was mixed with a trace of a surface active agent, slurried in water, filtered, and dried at 70°C. This sample is weak and has relatively poor hiding power.

Discussion

The "soft" powder can be dispersed fairly well either by milling in Formvar or by ultrasonics (400 kc) to give specimens which lend themselves to electron microscopy. Specimens prepared by pipetting an ultrasonic suspension onto Formvar are preferred because sharper micrographs are possible. It appears that large aggregates can be broken down into smaller ones, but it is difficult to find a field containing a large number of single particles.

It apparently is not possible to resolve any surface active agent which might be present as a very thin film surrounding each particle. These electron microscopical studies have not yet shed any light on the exact role placed by these surface active agents. Although these agents may be present in trace amounts, care was taken to make certain that no artifacts were introduced

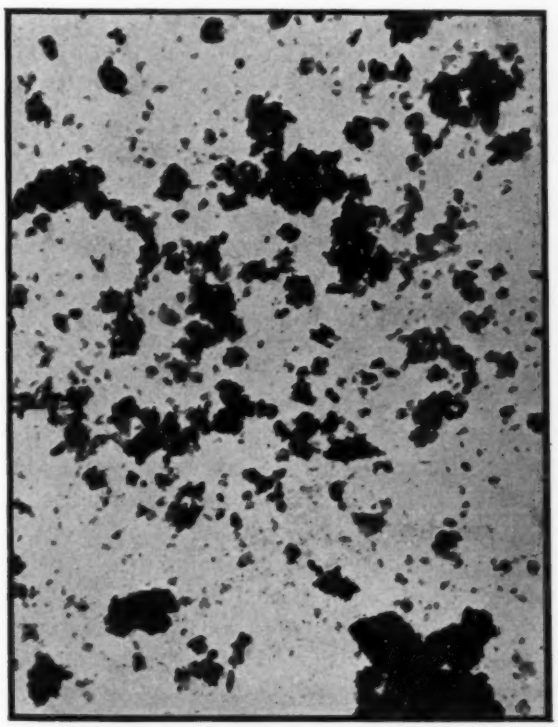

FIG. 4. Ultrasonic dispersion of the "soft" stable powder of copper phthalocyanine. 14,700×.

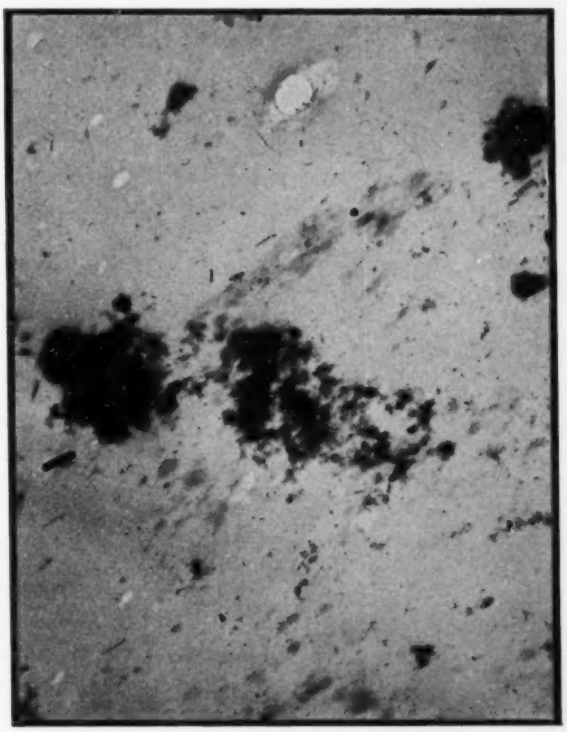

FIG. 5. Milled in Formvar dispersion of the "hard" metastable powder of copper phthalocyanine. 14,700×.

by their presence. They do not crystallize in the real sense of the word and do not give rise to diffraction patterns, so their presence in any of these samples in trace amounts is of no significance.

Figure 4 illustrates ultrasonic dispersions of the "soft" powder. Figure 5 illustrates milled in Formvar dispersions of the "hard" powder. We were unable to get electron micrographs of the "hard" powder showing good resolution of "single" particles. For one thing, the particles illustrated are probably not single particles but small aggregates thereof. Secondly, the size of these particles (aggregates) is somewhere near the limit of resolution of the electron microscope. Their contrast in Formvar is very poor so that good quality micrographs were difficult to obtain. Fortunately, our interest was not centered on ultimate particle size or size distribution, so we did not extend our efforts in this direction. We quite naturally experienced difficulty in photographing sharp diffraction patterns from these specimens.

FIG. 6. Stable form of the copper phthalocyanine "hard" powder after the transformation in the electron microscope. 14,700×.

Examination of these pigments in the electron microscope gave rise to the following salient observations:

(1) When dispersed ultrasonically and therefore resting on top of the Formvar, almost all of the "hard" powder transforms in the microscope after irradiation by the electron beam. Again the new crop of crystals grows from the vapor state at the expense of the original material. This new form is completely stable even at crossover using a self-biased gun. When embedded in Formvar, this transformation occurs only to a limited extent. Presumably the Formvar "protects" the pigment as explained in an earlier section.

(2) The "soft" powder very *rarely* exhibits this transformation, even when resting on top of the Formvar. Presumably a trace of the metastable phase formed during the preparation of this sample. In the early stages of this investigation it seemed that we were inadvertently contaminating our samples. However, our results were reproducible after carefully repeating the experiments, so that this trace of metastable form mixed with the otherwise completely stable form is a "legitimate" impurity.

(3) Based on their electron diffraction patterns, the original metastable "hard" pigment and the predominate, original stable form of the "soft" pigment are identical crystalline compounds. The new forms from both powders have the same crystal structure which is different from the original form. This pigment is, therefore, at least dimorphic. (See GENERAL DISCUSSION.)

It is interesting to note that the sample which is the most unstable ("hard" powder) is the one which was recrystallized from sulfuric acid after its initial manufacture in the plant. The same is true for the indanthrene blue RS samples. The exact role played by the sulfuric acid is not known, but this behavior on recrystallization from solvents is common in polymorphic systems. In fact, any investigations of this nature must include a consideration of the histories of the samples.

Figure 6 illustrates crystals of the new stable form after the transformation of the "hard" powder. The size range of these crystals is tremendous. These specimens are ideal for electron diffraction studies because the crystals are almost perfectly dispersed and because they are resting on top of the substrate. The growth of these new crystals during the transformation is instantaneous, and the growth itself cannot be resolved with the eye. Occasionally crystals of the original metastable forms of both pigments are reluctant to transform and require several seconds of intense illumination in order to initiate

TABLE I. The intense blue color of the following pigments permits an easy detection of first portions of the condensate.

Sample	Still pot temperature (°C)
Indanthrene blue RS "red"	148
Indanthrene blue RS "blue"	174
Copper phthalocyanine "hard"	127
Copper phthalocyanine "soft"	182

the transformation. In these cases the observer can readily see the instantaneous disappearance of the old form and the simultaneous appearance of the new crystals.

GENERAL DISCUSSION

Mention should be made of a recent paper by Burton *et al.*[10] describing a so-called "ionic-drift" in sodium chloride, potassium iodide, potassium bromide, and similar ionic compounds when examined in the electron microscope. This phenomenon was apparently slow and dynamic, wholly unlike ours. According to present day theories, slow electron migrations of this type are not plausible in covalent organic compounds such as the pigments discussed in this paper.

Because of the high energy electrons (50,000 electron volts) used in the electron microscope, it is necessary to consider the possibility of these transformations being the result of a radiation-chemical[8] effect. According to Burton,[11] some 30 or 35 electron volts of energy are required for the ionization of some organic gases. These ionized gases may decompose to give new products which may be identified in a mass spectrograph, for example. There is little or no information readily accessible on the energy of "ionization" for solids. However, the frequency of molecular collisions is greater so that there would probably be a greater dissipation of "potential ionization energy" caused by the inelastic collisional deactivation factor. Furthermore, our pigment molecules are complex, large, and strongly resonating so that their resistance to ionization, caused by high energy electrons is relatively strong. It is not the purpose of this paper to discuss the theoretical aspects of this radiation-chemical effect, but the investigators in the field of electron microscopy will perhaps have to consider this effect more carefully in the future. Aromatic hydrocarbons[11] and some of the fatty acids have been decomposed (ionization, ionic discharge, and decomposition) to give new products, some of which have been identified.

TABLE II. Indanthrene blue RS ($C_{28}H_{14}N_2O_4$).

Element	Theory	"Red" shade Analysis	"Red" shade Check	"Blue" shade Analysis	"Blue" shade Check
Carbon	76.01	74.74	74.74	74.22	74.21
Hydrogen	3.17	3.76	3.50	3.20	3.15
Nitrogen	6.35	6.36	6.24	6.22	6.30
Ash*		0.78	0.68	1.03	0.94
Copper Phthalocyanine ($C_{32}H_{16}N_8Cu$)					
		"Hard" powder		"Soft" powder	
Carbon	66.78	63.07	63.12	63.50	63.46
Hydrogen	2.78	3.02	3.10	2.82	2.87
Nitrogen	19.47	16.77	16.96	17.62	17.87

* Theoretically this compound should contain no inorganic material. However, it is practically impossible to completely purify compounds of this type by recrystallization from solvents. Copper phthalocyanine produces cupric oxide when ignited in the combustion furnace. Some of it is lost however in this type of analysis so that the copper content cannot be determined. The ash content in this sample was not reported because it is meaningless.

Fortunately we were able to corroborate our opinion that the transformations we observed in indanthrene blue RS and copper phthalocyanine were polymorphic (thermodynamic) rather than radiation-chemical in nature. Because of the greater free energy of the metastable form, its solubility, chemical reactivity, vapor pressure, etc., are greater than those for the stable form. As a simple expedient we measured the pressure and temperature, using a calibrated vacuum gage and a thermocouple in a glass high vacuum line, at which we could observe the *first signs* of condensation of sublimed pigment in the evaporation chamber. The pressures were in all cases approximately 0.1 micron. All other experimental conditions were kept as constant as possible Table I includes the temperatures at which the rate of sublimation became appreciable on slowly raising the temperature of the still pot.

As would be predicted from theory, the metastable forms do have the higher vapor pressures in this temperature range.

These samples were also sublimed directly onto specimen screens for examination in the electron microscope. Electron diffraction pat-

[10] E. F. Burton, R. S. Sennett, and S. G. Ellis, Nature **160**, 565 (1947).
[11] M. Burton, J. of Phys. & Coll. Chem. **51**, 611 (1947).

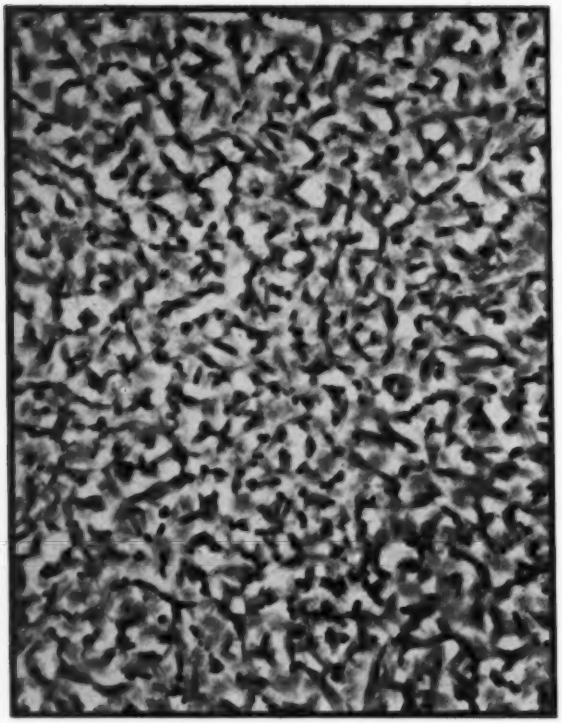

FIG. 7. Copper phthalocyanine (stable form) prepared by a molecular distillation of the "hard" powder. 14,700×.

terns (see later section) of these condensates give rise to the following information:

(1) Both original forms of indanthrene blue RS sublime without decomposition in high vacuum at elevated temperatures to give the same crystalline form. The "red" shade transformed; the "blue" shade did not.

(2) Both the "hard" and "soft" powders of copper phthalocyanine sublime similarly to given the same crystalline compound which is identical with the new form that grows in the electron microscope at the expense of the original "hard" powder. The "soft" powder, therefore, transforms during its sublimation; it does not, however, transform in the electron microscope.

These transformations took place in the vapor state because solid pseudomorphs did not form. Again there was no evidence of reversibility. These sublimation studies (no chemical decomposition) corroborate our opinion that these two pigments are polymorphic.

Both pairs of pigments without any further treatment were analyzed for carbon, hydrogen, and nitrogen as a means for checking their chemical identity. These analyses are given in Table II.

The analyses for both pigments do not accurately check the theoretical values because of the slight amounts of impurities present. Experience has shown that analyses for the elements of these high molecular weights and very insoluble compounds seldom check theory with high precision. However, the experimental analyses for both pigments agree extremely well within themselves, so that there can be no doubt about the chemical identity of both samples of each pigment.

Instrument Adjustments

Brief mention should be made of the operating conditions of the electron microscope for the micrographs shown in Figs. 1 through 7. A self-biased electron gun (500,000-ohm bias resistor) operated at about 250 microamperes was used. A 2 mil (2.5×10^{-2} radians) platinum limiting aperture was inserted in the objective pole piece. This aperture was used to enhance the gross contrast rather than to enhance the detailed contrast. A resolving power on the order of 100A was adequate for this problem. The crystals are in general quite thin so that the gross contrast was poor in the absence of an objective aperture.

Most of the images were underfocused so that they would appear more crisp (contrasty); the white halo (Fresnel diffraction fringe) is readily discernible. The pigment crystals after the polymorphic transformation were usually not in the same plane, but presented a rather severe "depth of field." Thus, some crystals may be underfocused while others are slightly overfocused. The latter are characterized by the white border just within the crystal outline and the dark band around the crystal border.

The high gain projector pole piece spacer was used. All micrographs were taken at tap 1 on the projector control; this provides an instrument magnification of about 6400×.

ELECTRON DIFFRACTION STUDIES

It was necessary to identify the various forms of these two pigments because the primary purpose of the investigation was to prove that the same chemical compounds could exist in more than one crystalline form. The electron microscope (Model EMU) modified to function as a diffraction camera adequately served this purpose.

Techniques

The arrangement of the electron microscope (Model EMB) for photographing high dispersion electron diffraction patterns by means of primary magnification was first published by Simard, Burton, and Barnes.[12] The theory and technique are well described in their paper so little more need be said about the technique. In brief, all the diffraction patterns illustrated here were photographed in the Model EMU microscope, using a 1-mil condenser aperture, having removed the objective and projector lens pole pieces. The sample was placed in the regular specimen chamber in the usual way. The projector control knob was set on tap 5 in all cases. This provided a magnification of about 2.5×, based on the conventional diffraction method using the standard diffraction adaptor. This magnification was adequate because the long interplanar spacings, typical of these organic compounds, were conveniently positioned on the photographic plate permitting convenient measurements.

At first the Leeds and Northrup Recording Microphotometer (Range 5) was used to measure the ring diameters and intensity ratios. However, the general background fog (despite the use of a central beam stop[13]) minimizes the effectiveness of the microphotometer tracing. Furthermore about 30 minutes were required for the analysis of each pattern. It was decided, therefore, to measure visually the diffraction patterns using an x-ray viewing device with a vernier scale. Only about one-third as much time is required and the ring diameter measurements can be made with an accuracy of about ±0.1 mm (except where the diffraction lines are very broad). This visual method also facilitates the measurement of faint lines which would be impossible by the microphotometer method. The intensity ratios are estimated, having assigned the value 1.0 to the strongest line. Experience would indicate that most of these organic pigment preparations, with the exception of the sublimed samples, do not lend themselves to "clean" diffraction patterns, comparable for example with inorganic oxides (smokes). When the pigment particles are embedded in the sub-

TABLE III.*

A		B		C		D	
$\frac{I}{I_0}$	d(A)	$\frac{I}{I_0}$	d	$\frac{I}{I_0}$	d	$\frac{I}{I_0}$	d
		1.0	7.80	0.9	7.90	1.0	7.80
						0.2	5.20
1.0	4.13					0.2	4.26
0.9	3.75					0.8	3.96
				0.1	3.82		
		0.8	3.62	0.8	3.64	0.7	3.62
0.4	3.48	0.8	3.43	1.0	3.52	0.9	3.42
				0.8	3.33		
0.4	3.22	0.8	3.23	0.1	3.23	0.7	3.22
0.2	3.00	0.5	3.14			0.1	3.13
				0.1	2.91	0.1	2.92
				0.1	2.76	0.1	2.70
0.8	2.48					0.2	2.56
0.5	2.22	0.1	2.26	0.1	2.26	0.1	2.26
0.5	2.06	0.1	2.16	0.2	2.16	0.3	2.07
0.3	1.86	0.1	1.82				
		0.2	1.72	0.2	1.73	0.2	1.72

* *A* Indanthrene blue RS "red" shade Original form.
B Indanthrene blue RS "blue" shade Original form.
C Indanthrene blue RS "red" shade New form (after transformation *in* the microscope).
D Indanthrene blue RS "red" shade New form (after molecular distillation).

[12] G. L. Simard, Charles J. Burton, and R. Bowling Barnes, J. App. Phys. **16**, 832 (1945).

TABLE IV.*

A		B		C		D	
$\frac{I}{I_0}$	d(A)	$\frac{I}{I_0}$	d	$\frac{I}{I_0}$	d	$\frac{I}{I_0}$	d
				1.0	5.96	0.9	6.15
						0.4	5.80
0.5	5.12	0.5	5.20				
		0.6	4.50				
				0.2	3.98	0.3	3.98
				0.7	3.60	0.9	3.63
0.5	3.45**	0.8	3.42	0.9	3.42	1.0	3.42
0.5	3.31	0.8	3.27				
0.8	3.13			0.8	3.20	0.5	3.42
0.8	3.01	1.0	3.09	0.8	3.00	0.4	3.02
		1.0	2.90				
				0.1	2.76	0.3	2.78
				0.2	2.59	0.1	2.60
				0.1	2.40		
				0.2	2.21		
				0.1	2.03	0.1	2.03
				0.3	1.92		
				0.1	1.88	0.2	1.86
				0.6	1.80		
				0.5	1.76	0.4	1.77
						0.3	1.72
0.1	1.65	0.2	1.63	0.5	1.68	0.3	1.66
				0.2	1.62		

* *A* Copper phthalocyanine "hard" powder Original form.
B Copper phthalocyanine "soft" powder Original form.
C Copper phthalocyanine "hard" powder New form (after transformation in the microscope).
D Copper phthalocyanine "hard" powder New form (after molecular distillation).
** These pairs of lines are "doublets." The shorter spacings on Sample *B* are unexplained.

[13] This accessory was designed by us and made in our own machine shop.

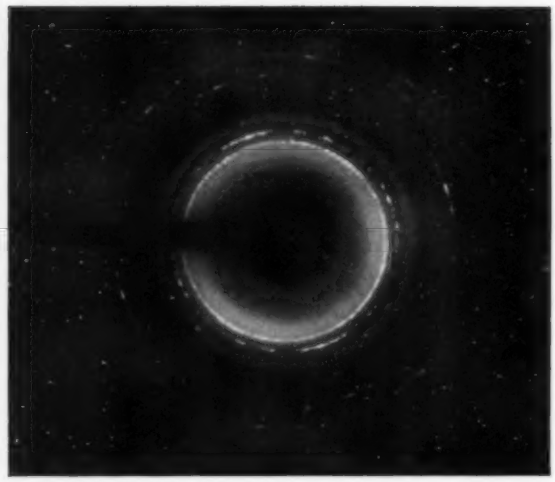

FIG. 8. Electron diffraction pattern of the original metastable form of the "red" shade of indanthrene blue RS. (See Fig. 1.)

strate, the background fog may be quite objectionable. For this reason, the intensity ratios are sometimes difficult to assign, and there may be discrepancies between the assigned value and the literature value (ASTM). However, the comparisons are normally sufficiently accurate for use in identification. No interpretation of intensity ratios should be attempted on the positive electron diffraction patterns illustrated in this paper because they were "dodged" (centers strongly exposed) during the photographic printing process.

Whenever feasible, organic compounds should be sublimed in high vacuum (molecular distillation) to prepare specimens for electron diffraction. Well formed and evenly dispersed crystals with relatively little over-lapping usually deposit in thin films. Figure 7 illustrates a specimen of copper phthalocyanine molecularly distilled onto a Formvar substrate. This sample was used to prepare the electron diffraction pattern shown in Fig. 15. Supporting substrates are often unnecessary because the crystals grow over the specimen screen openings, receiving sufficient support from the screen wires. The diffraction patterns of the original metastable forms of the indanthrene blue RS "red" shade and the copper phthalocyanine "hard" powder are comparatively poor, because out of necessity, particles embedded in Formvar had to be used.

TABLE V. Copper phthalocyanine.

(1) Lines of greatest or next to greatest relative intensity correspond to spacings in the region of 6.15A.	Lines of greatest relative intensity correspond to a spacing of about 5.12A. There are no spacings longer than 5.20A.
(2) Has a strong line at a spacing of about 3.63A.	No strong lines in this region.
(3) No distinct "doublets" are exhibited but some lines having spacings analogous to those in the doublets of the original form are present. The relative intensities are different however.	The two doublets are very characteristic. (These could not be resolved on diffraction patterns taken in the conventional way.)
(4) Several lines between the 3.00A and the 1.63A region	No lines in this region.

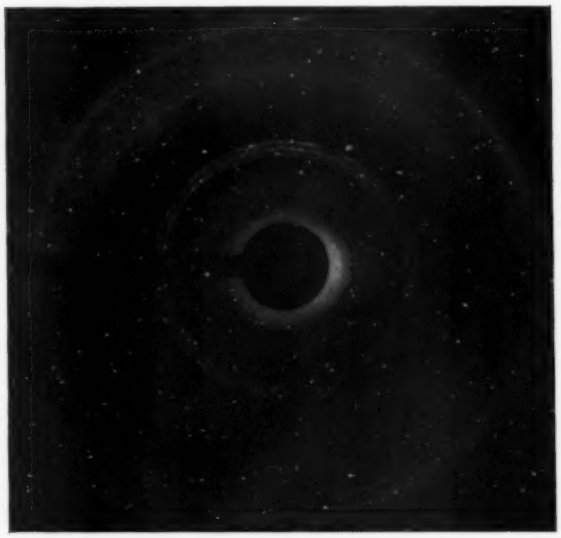

FIG. 9. Electron diffraction pattern of the original stable form of the "blue" shade of indanthrene blue RS (ultrasonic dispersion). (See Fig. 2.)

Results

The interplanar spacings listed in Tables III and IV were all taken from our own calibration curves. These calibration curves were prepared by plotting measured ring diameters against the accepted ASTM values for interplanar spacings on log-log paper. Both zinc oxide and magnesium oxide have been used. A calibration curve was usually prepared before and after a series of diffraction patterns were taken. When zinc oxide

data was used to plot the curve, the interplanar spacings for magnesium oxide were read from the curve and checked against the the ASTM values. Although some spacings agreed very closely, the average accuracy on these inorganics of five different spacings was between 1 and 2 percent.

A survey of Table III shows the following salient features:

(1) The data for the original form (*A*) were placed so that the interplanar spacings closely approach those of the new form (*B*, *C*, *D*). The absence of certain lines and the differences in intensity ratios for those lines that do agree *poorly* immediately suggest that the two forms have different crystalline structures.

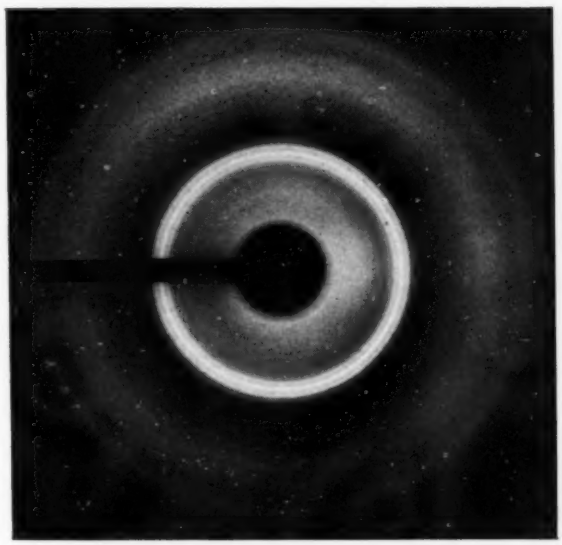

FIG. 10. Electron diffraction pattern of the new stable form of the "red" shade of indanthrene blue RS. (See Fig. 3.)

(2) The data for *D* are most complete; as was explained earlier, this is characteristic of sublimed specimens.

(3) The data for the three different specimens (*B*, *C*, *D*) of the *same* form show some discrepancies. For reasons mentioned earlier, the precision with which these measurements can be made (especially on the very small particles) is not as great as that which is commonly experienced with the inorganics. However, the comparisons are sufficiently close to justify the identification. The differences between the diffraction patterns of the two forms are not subtle, so the comparisons are left to the reader.

Table IV is a similar presentation of the data for the polymorphic forms of copper phthalocyanine.

Again there are some slight discrepancies in the electron diffraction data, but the agreement is sufficiently good so that the crystalline structures can be identified as "new" or "original." The most profound differences in the diffraction patterns of the two forms are summarized in Table V.

Care must be exercised in evaluating electron diffraction patterns for this type of specimen. The particle size and the degree to which these particles are dispersed is of utmost importance. Hillier and Baker[14] have already critically discussed these electron diffraction techniques, so that little more need be said. We had difficulty in reproducing our results with high (1 percent) accuracy for a large number of lines, especially on those samples that were embedded in Formvar (metastable forms). Despite this we felt certain that the diffraction data was significant and could be used to "fingerprint" the forms. The data presented in Tables III and IV represent only a few of a large number of patterns taken on similar specimens. The data were almost invariably in good agreement for at least a large percentage of the lines.

Figures 8 through 11 illustrate the electron diffraction patterns of the various forms of the

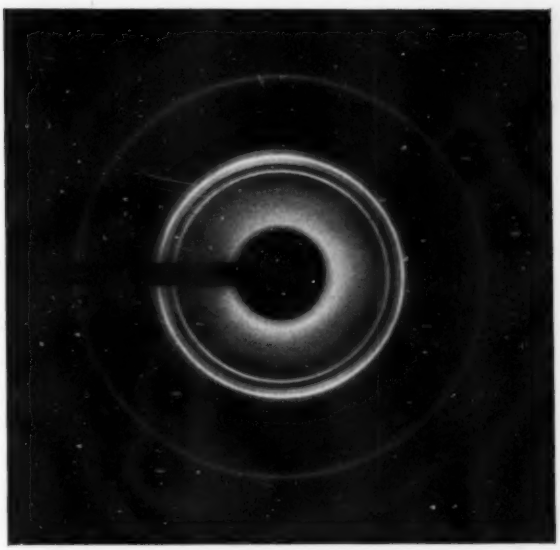

FIG. 11. Electron diffraction pattern of the new stable form of the "red" shade of indanthrene blue RS after a molecular distillation.

[14] James Hillier and R. F. Baker, J. App. Phys. **17**, 12–22 (1946).

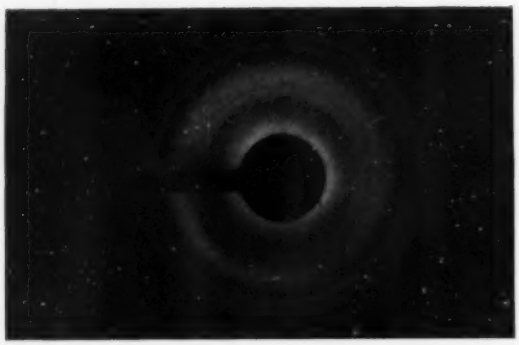

FIG. 12. Electron diffraction pattern of the original metastable form of the "hard" powder of copper phthalocyanine. (See Fig. 5.)

FIG. 13. Electron diffraction pattern of the original stable form of the "soft" powder of copper phthalocyanine. (See Fig. 4.)

indanthrene blue RS pigment listed as *A*, *B*, *C*, and *D* in Table III.

Figures 12 through 15 illustrate the electron diffraction patterns (*A*, *B*, *C*, and *D*) of the various forms of copper phthalocyanine described in Table IV.

Robertson[15] has carried out extensive x-ray diffraction studies on several phthalocyanines and has completely described the crystal structures of nickel, copper, and platinum phthalocyanine, as well as of the parent metal-free phthalocyanine. All four compounds have the same space grouping, molecules per unit cell, molecular symmetry, and the unit cell dimensions are all of the same order of magnitude. The molecules are essentially square and spread out in the crystallographic *ac* plane (monoclinic system). However, in the platinum phthalocyanine the plane containing the flat molecules

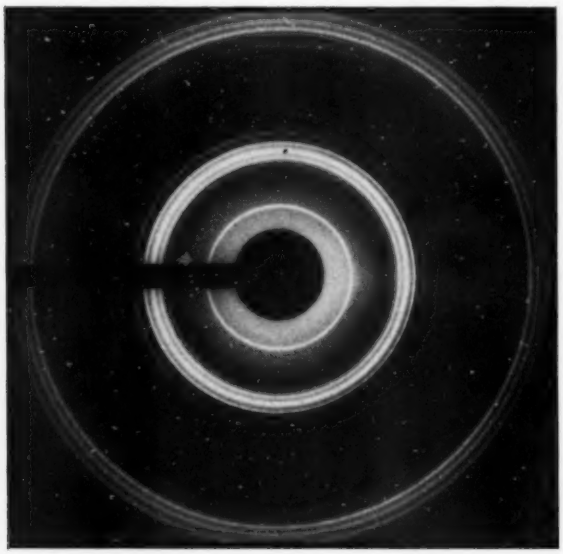

FIG. 14. Electron diffraction pattern of the new stable form of the "hard" powder of copper phthalocyanine. (See Fig. 6.)

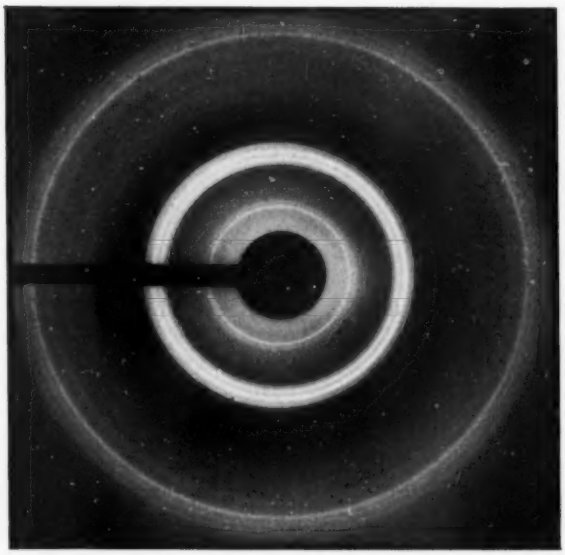

FIG. 15. Electron diffraction pattern of the new stable form of the "hard" powder of copper phthalocyanine after a molecular distillation. (See Fig. 7.)

[15] J. M. Robertson, J. Chem. Soc., 615 (1935); 1195 (1936); J. M. Robertson and I. Woodward, *ibid*, 219 (1937); 36 (1940).

makes an angle of 26.5° with the 010 plane, whereas in the nickel and copper complexes this angle is 44.2°. Robertson suggests that this represents a polymorphic modification. All of his samples[15] had been prepared by sublimation; consequently he was always working with the same crystalline structure. For this reason he did not observe a polymorphic structure in copper phthalocyanine.

CONCLUSIONS

The particle size and aggregation of these and similar pigments as related to their color shades, dispersibility, and chemical reactivity are unquestionably important and cannot be denied. It has, however, been the purpose of this paper to demonstrate the existence of polymorphic forms of these pigments and to point out the possibility of using this polymorphic behavior to account for the differences in their chemical and physical properties. Polymorphic transformations, especially in colored compounds, are almost invariably accompanied by changes in color.[16] This is to be expected because the true "body" (absorption) color of a solid is determined by its crystal structure as well as by its chemical chromophoric groups. The history of the sample, with special emphasis on its preparation, should always be considered in an investigation of this nature because it has a profound bearing on the nature of the material.

Different physical preparations of the same chemical pigments were in other studies found to give rise to much better electron diffraction patterns than those investigated in this work. Unfortunately some of the preparations described in this paper did not lend themselves to diffraction. However, they had to be used to complete the study. The resultant diffraction data is not in all cases reproducible with a desirable accuracy. Nevertheless, sufficient data were obtained to make the identification of the various forms convincing.

Since the termination of this portion of the problem, a variety of similar pigment samples have been examined. These pigments exhibited spurious properties, such as abnormal shades, solubilities, and stability. It developed that these samples were polymorphic so that added significance may be attached to this approach.

The authors are indebted to Mr. J. J. Comer whose contributions to this investigation are greatly appreciated.

[16] Phosphorus, mercuric iodide, and some of the 2,4-dinitrophenylhydrazone derivatives of organic carbonyl compounds are well-known examples.

Drag Coefficients of Steel Spheres Entering Water Vertically

ALBERT MAY AND JEAN C. WOODHULL
Naval Ordnance Laboratory, White Oak, Maryland

(Received March 29, 1948)

Drag coefficients have been determined from high speed motion pictures for ¼-inch to 1¼-inch steel spheres shot into water vertically with speeds from 25 to 208 ft./sec. These drag coefficients correspond to the entrance cavity phase and to the v-squared-law drag forces only, the immediate effects on the spheres of other forces being eliminated in the calculations. It is found that C_D is a function of both the Reynolds and Froude Numbers. Within the range investigated, the dependence may be expressed by $C_D = 0.0174 \ln(RF^4)$.

1. INTRODUCTION

THE drag coefficient of spheres completely immersed in air or water has been extensively investigated in air and water tunnels and its value has been given[1] for a wide range of values of Reynolds Number. The problem of determining the drag coefficient for spheres after vertical entry into water, while an air cavity is still attached to the sphere, is a much more complex problem. This complexity arises from the facts that the speed of the sphere is variable and that a larger variety of forces acts on the sphere.

The changing velocity of the sphere influences

[1] L. Prandtl and O. G. Tietjens, *Applied Hydro- and Aeromechanics* (McGraw-Hill Book Company, New York, 1934), p. 100.

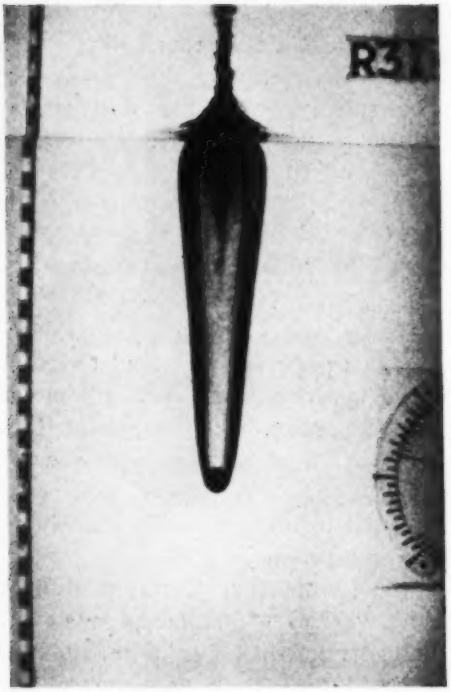

FIG. 1. High speed photograph of 1½-inch steel sphere shot into water.

the drag coefficient through its variation with Reynolds Number, already referred to. Additional forces acting on the sphere, include gravity and the difference between the buoyant force and that due to the pressure in the cavity. All of these complications result in a strong dependence of the drag coefficient on the parameters of the shot and in a large variation in its value during the sphere's flight.

Since the drag coefficient is dimensionless, the shot parameters can best be expressed in terms of such dimensionless quantities as Reynolds Number, Froude Number, or others which may be significant.

In order to simplify the approach to the problem, drag coefficients have been determined which correspond only to inertial forces, that is, to forces which accelerate the water either directly or through viscosity, and not to those forces which are peculiar to the water-entry problem. The principal merit of this approach is that the drag coefficient so defined is reasonably constant throughout the early part of a sphere's trajectory, and depends on only a small number of parameters, principally on the Reynolds and Froude Numbers.

2. EXPERIMENTAL DETAILS

In the present study, ¼-inch to 1½-inch steel spheres of specific gravity 7.77 were shot into water vertically at initial velocities from 25 to 208 ft./sec. The water was contained in glass-sided tanks so constructed that the air in the region above the water could be maintained at any pressure from several atmospheres down to $\frac{1}{32}$ atmosphere, or lower.[2] High speed motion pictures of the tank were taken during the passage of the sphere, with an Eastman high speed 16 mm camera placed outside the tank at the height of the water surface. The operating speed of the camera was generally about 1700 frames per second. A stadia rod and clock were included in the field of view as shown in the sample frame in Fig. 1.

The clock was driven by a synchronous motor with gear reduction and was equipped with a vernier permitting readings to 0.05 millisecond. Position-time data were obtained for the sphere from numerous frames of each shot.

For most of the shots used in the present study, continuous lighting was provided by a bank of Photoflood bulbs placed behind the tank. A few of the shots employed flash lighting synchronized with the camera[3] and furnished by an Arditron bulb.

3. THEORY

A body moving through a fluid experiences a resistance proportional to the square of its speed, v (except at extremely low speeds). In the absence of other forces the differential equation of motion is

$$d^2s/dt^2 = dv/dt = -\alpha v^2, \tag{1}$$

where α is the retardation coefficient; hence

$$1/v - 1/v_0 = \alpha t, \tag{2}$$

where v_0 is the speed at time $t=0$, when the body strikes the water.

[2] The phenomena which accompany the entry of spheres into water at reduced atmospheric pressure have been discussed by D. Gilbarg and R. A. Anderson, J. App. Phys. 19, 127 (1948).

[3] R. A. Anderson and W. T. Whelan, J. Soc. Motion Picture Engineers 50, 199 (1948).

The drag coefficient C_D is defined by the relation:

$$\text{Drag} = \tfrac{1}{2} C_D A \rho v^2,$$

where ρ is the density of the fluid and A is the maximum cross section of the sphere. (It should be noted that, since the motion is decelerated, a sphere of different density would presumably have a different value of C_D as here defined. This difference is real and corresponds to a different drag force resulting from a changed flow pattern. Alternatively, if the concept of apparent or virtual mass were introduced, the drag coefficient would be redefined so as to approach more nearly the value it would have for no acceleration or for spheres of other densities. Any advantages derivable from this concept appear overbalanced by the facts that the apparent mass would be difficult to determine for cavity flow and would undoubtedly vary with time.)

From Eq. (2), a plot of $1/v$ against t should give a straight graph whose slope is α, if the drag forces are proportional to v^2. The velocities are, of course, obtained by finding finite increments in distance and time and forming $\Delta s/\Delta t$. It is easily shown that the slope of the $1/v$ *versus* t graph is always equal to the instantaneous value of α, even if α is variable. This makes it possible to observe on the graphs actual or apparent variations of α throughout the flight.

As was intimated previously, the drag, regarded generally, depends on the aggregate of all of the forces acting on the sphere, but the drag coefficient, when defined by a v-squared law, may best be considered in the absence of all forces which have a different dependence on v. It will be assumed that all such forces are absent or negligible, or that the data have been adjusted so that the effects of such forces have been eliminated, as will be described below.

The equation of motion, containing the major forces acting, may be written

$$-dv/dt = \alpha v^2 - g + g\rho s A_1/m - (p - p_a)A_1/m, \quad (3)$$

instead of Eq. (1). Here g is the acceleration of gravity, $g\rho s A_1$ is the hydrostatic force due to depth alone, and $(p-p_a)A_1$ is the force due to excess pressure (i.e., relative to atmospheric pressure, p_a) in the cavity, acting on the projected wetted area A_1. It might be remarked that the dynamic pressure $\frac{1}{2}\rho_a v^2$, caused by air of density ρ_a rushing into the cavity, contributes a force proportional to v^2, also. This force is very small compared to the water drag and will be ignored.

Equation (3) may be integrated, after dividing by v^2, to give

$$1/v - 1/v_0 = \int_0^t \alpha dt - g\int_0^t \frac{1-\rho s A_1/m}{v^2} dt - \frac{A_1}{m}\int_0^t \frac{p-p_a}{v^2} dt. \quad (4)$$

The experimental data indicate, as will be shown, that C_D is approximately a linear function of $\ln(R^a F^b)$ over the range of parameters investigated, where R and F are the Reynolds and Froude Numbers, and a and b are constants. Then, if

$$\gamma \equiv \Delta C_D / \Delta \ln(R^a F^b),$$

we may write

$$C_D = C_{D_0} + \gamma(\ln R^a F^b - \ln R_0^a F_0^b),$$

where the subscript zero indicates values corresponding to the velocity at water entry. Since $R = vl/\nu$ and $F = v^2/lg$, where l is the sphere diameter and ν is the kinematic viscosity, then

$$C_D = C_{D_0} + \gamma(a+2b)\ln v/v_0.$$

For spheres, $\alpha = 3C_D/8\sigma r = \beta C_D$, (if $\beta \equiv 3/8\sigma r$), where σ and r are the specific gravity and radius of the sphere, respectively, so that

$$\alpha = \beta C_D = \alpha_0 + \beta\gamma(a+2b)\ln v/v_0.$$

Equation (4) can then be written

$$1/v - 1/v_0 = \alpha_0 t + \beta\gamma(a+2b)\int_0^t (\ln v/v_0)dt - g\int_0^t \frac{1-\rho s A_1/m}{v^2} dt - \frac{A_1}{m}\int_0^t \frac{p-p_a}{v^2} dt. \quad (5)$$

The first integral on the right of Eq. (5) expresses the fact that, if C_D increases with R and F, C_D will decrease as the velocity decreases during the sphere's flight. If the three integrals of Eq. (5) were zero, the graph of $1/v$ plotted against t should have the uniform slope α_0. This condition can be simulated by evaluating each of the integrals and subtracting their sum from the value of $1/v$, for each value of t to be plotted.

Several of the quantities in Eq. (5) require special mention. The dependence of C_D on R and F, and, of course, the slope γ, are not known in advance and must first be determined roughly. The subsequent method is one of successive approximations. The area A_1 is, from Eq. (3), presumably the projection of the wetted area of the sphere although experiment indicates that a somewhat smaller value should be used. This will be discussed in detail later. The cavity pressure may be determinable from the change of volume of the cavity after it is sealed off. Actually, it has been found impossible to determine this pressure with sufficient accuracy to permit an adequate evaluation of the last integral of Eq. (5). Because of this, the only shots included in the present study were those for which this correction would be negligible, that is, those in which the cavity did not close until late in the trajectory. This required the use of air pressures of $\frac{1}{8}$ atmosphere or less.

4. APPROXIMATE METHODS

The integrals can be evaluated numerically, using graphical procedures, but the method is long and tedious. The first two integrals of Eq. (5) can be evaluated approximately by a method which is considerably simpler. In general, the approximations are quite satisfactory, although in certain extreme cases, for example, for very small velocities, the error made may be appreciable.

The approximation method consists in obtaining analytically reducible integrals by introducing approximate relations obtained from the "ideal" Eq. (1). From Eq. (1) we obtain by integration,

$$\alpha s = \ln(\alpha v_0 t + 1). \tag{6}$$

Defining the quantity

$$w \equiv \alpha v_0 t + 1,$$

we can write Eq. (6) as

$$\alpha s = \ln w,$$

and Eq. (2) as $v_0/v = w$. Also, it is easily shown that

$$\rho A_1/m = 2\alpha k/C_D = 2\beta k,$$

where k is the fraction of the cross-sectional area of the sphere that is "wetted".

Equation (5) can then be written, dropping the last integral,

$$1/v - 1/v_0 = \alpha_0 t - \left[\frac{\beta\gamma(a+2b)}{\alpha v_0}\int_1^w \ln w\,dw + \frac{g}{\alpha v_0^3}\int_1^w w^2\,dw - \frac{2\beta k g}{\alpha^2 v_0^3}\int_1^w w^2 \ln w\,dw\right]. \tag{7}$$

It will be seen that if the quantity in brackets is calculated for each value of t of interest and is added to the values of $1/v$ to be plotted against t, the plot of these adjusted values of $1/v$ will have a slope α_0 corresponding to the velocity at water entry.

If we integrate, the quantity in brackets becomes

$$\frac{\beta\gamma(a+2b)}{\alpha v_0}(1 + w\ln w - w) + \frac{g}{3\alpha v_0^3}(w^3-1) + \frac{2\beta k g}{\alpha^2 v_0^3}\left[\tfrac{1}{9}(w^3-1) - \frac{w^3}{3}\ln w\right].$$

As has been mentioned, these approximate adjustments are generally quite satisfactory, but they must be used with discretion. For example, for a sphere entering the water at its terminal velocity in water, the approximations would be extremely poor. Usually the first adjustment term (arising from variations in the Reynolds and Froude Numbers) is preferably determined from the approximate formula, since this is not nearly so sensitive to errors in v_0 as is the graphically determined adjustment.

5. OBTAINING DATA FROM FILMS

The photographic images recorded on the 16 mm motion-picture films are never as sharp as might be desired. For various projectile velocities and photographic exposure times, the limitation may be imposed either by the blurring due to motion or to graininess of the film.

Readings are generally made on equally spaced frames, e.g., each frame might be read, or frames 1, 7, 13, 19, $\cdots$, starting just after the sphere's entrance into the water. Usually the camera is speeding up at the time of water entry and it is assumed that the acceleration is smooth. Instead of using the time interval, Δt, obtained directly

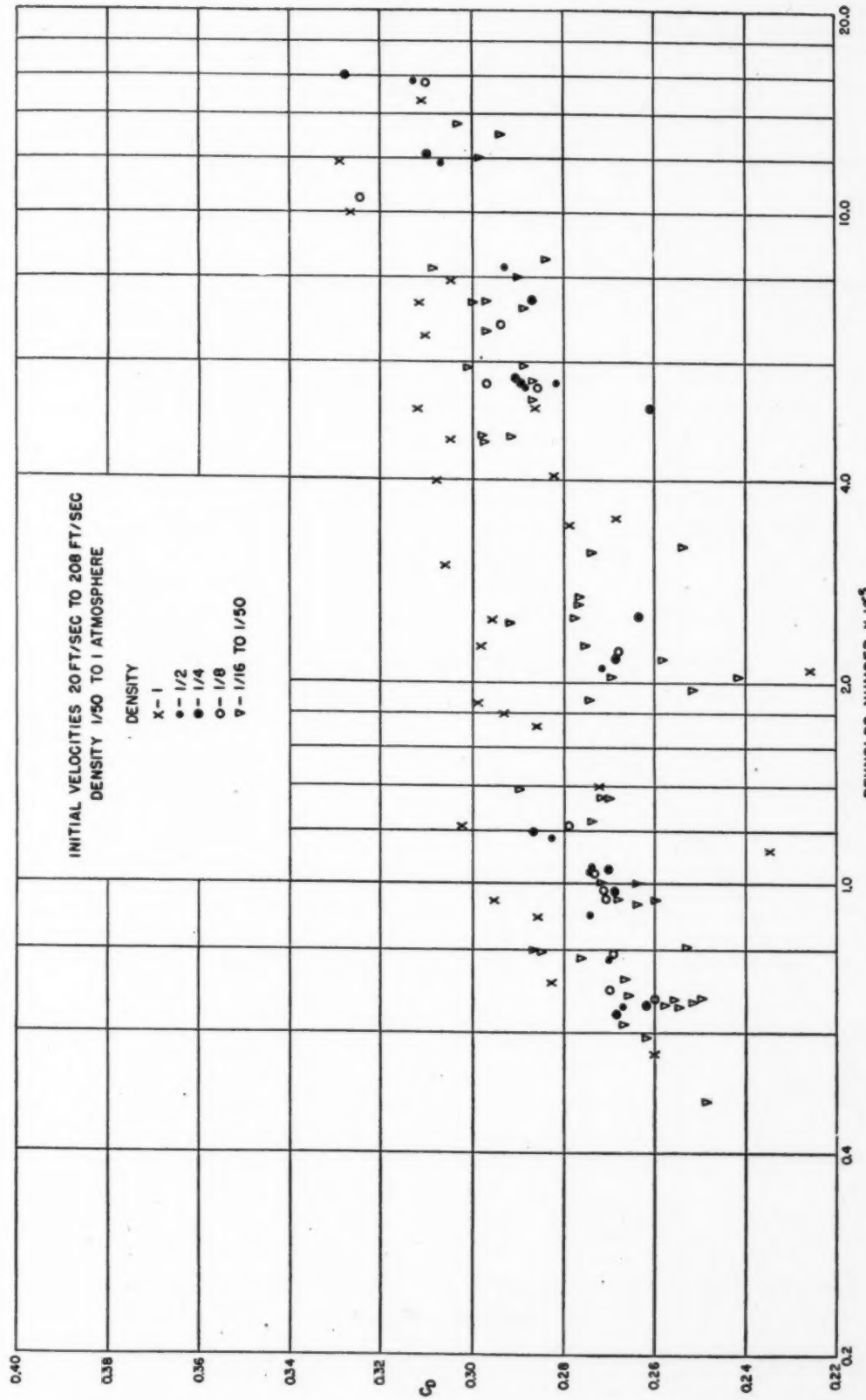

FIG. 2. Drag coefficients (calculated from total drag) for ¼- to 1¼-inch steel spheres entering water vertically.

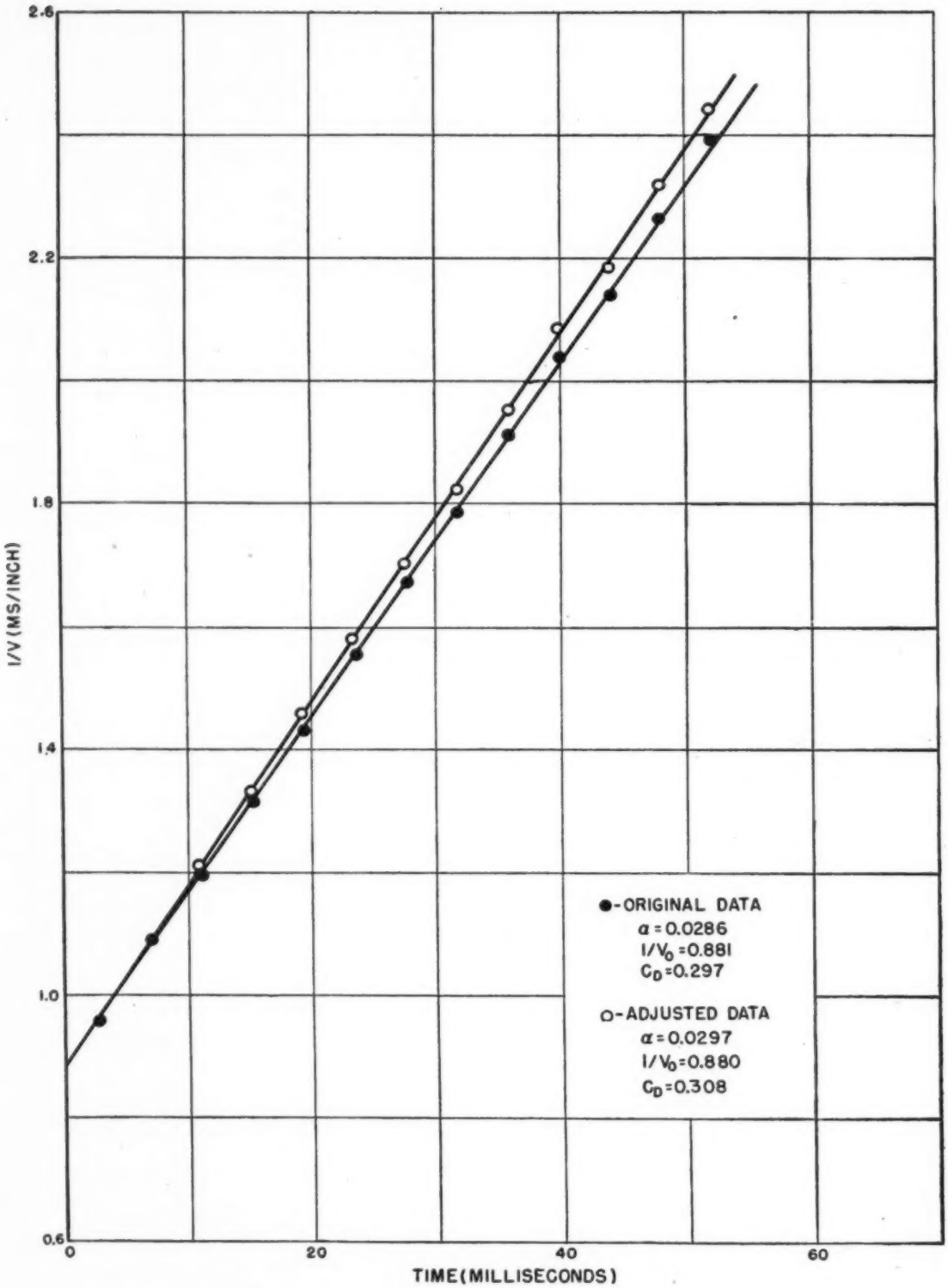

FIG. 3. Reciprocal velocity for sample shot of one-inch steel sphere before and after removing effects of gravity, of hydrostatic pressure, and of decreasing speed.

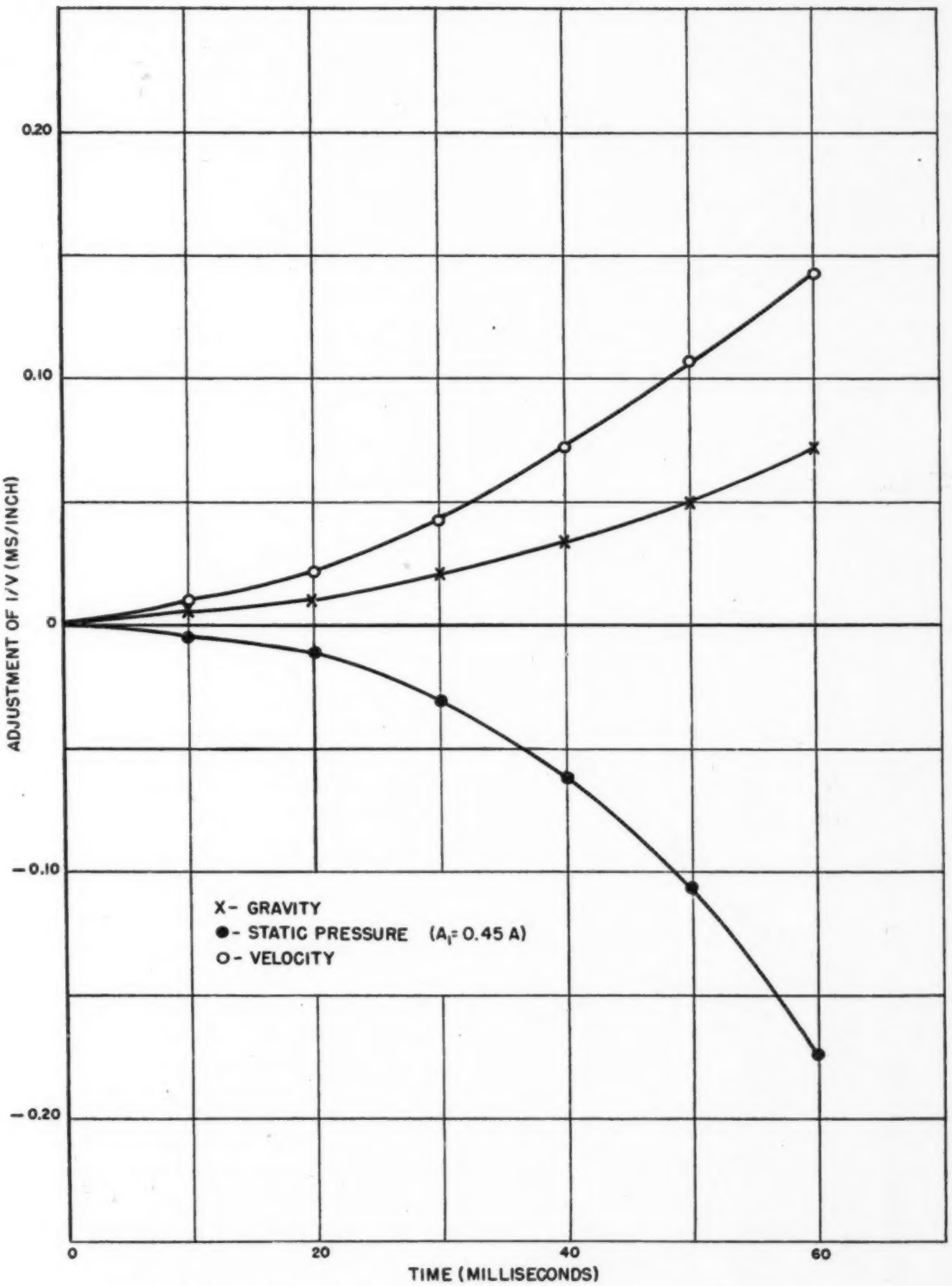

FIG. 4. Individual adjustment values used in the adjusted graph of Fig. 3.

TABLE I. Drag coefficients for steel spheres with attached entry cavities.

Source	Sphere diameter (inches)	Reynolds number $\times 10^{-5}$	C_D
Harvey-McMillen[a]	$\frac{1}{16}$ to $\frac{1}{4}$	5.0 to 50.0	0.267 to 0.315
Temperley[b]	$\frac{1}{4}$ to 1	0.2 to 3.5	0.19 to 0.34
Bauer[c]	0.43	14.0 to 60.0	0.30

[a] J. H. McMillen and E. N. Harvey, Phys. Rev. **71**, 475(A) (1947)
[b] From unpublished work of H. N. V. Temperley.
[c] W. Bauer, Ann. d. Phy. **80**, 232 (1926).

from the clock readings of two frames, the values of Δt are plotted against t and the values of Δt to be used in calculating the velocity $\Delta s/\Delta t$ are obtained from a smooth curve.

If Δt is made very small, it is difficult to obtain Δt, and especially Δs, with accuracy. The plot of $1/v$ against t will then consist of points with considerable scatter. If, on the other hand, Δt is made too large, an error will be introduced because of the curvature of the *s versus t* characteristic. A rough estimate for steel spheres indicates that a one percent error in determining α, will be caused if Δs is about twelve sphere diameters.

Instead of using large values of Δt to improve the accuracy of velocity readings, mathematical smoothing techniques can, of course, be employed.

TABLE II. Data for shots of steel spheres.

Sphere diameter (inches)	Velocity (ft./sec.)	Pressure (atm.)	Reynolds number $\times 10^{-5}$	Froude number $\times 10^{-3}$	C_D from total drag	C_D adjusted
$\frac{1}{4}$	26	1/32	0.48	1.01	0.249	0.248
	36	1/34	0.66	1.93	0.252	0.253
	36	1/32	0.66	1.93	0.255	0.255
	37	1/32	0.68	2.04	0.250	0.251
	44	1/32	0.80	2.89	0.253	0.262
	52	1/32	0.95	4.04	0.260	0.275
	54	1/32	0.93	4.35	0.264	0.276
	58	1/32	1.00	5.02	0.264	0.276
	72	1/32	1.24	7.74	0.268	0.284
$\frac{1}{2}$	38	1/25	1.34	1.08	0.271	0.271
	38	1/25	1.34	1.08	0.272	0.272
	55	1/28	2.26	1.87	0.278	0.279
	88	1/27	2.65	5.78	0.277	0.288
	89	1/26	2.68	5.91	0.277	0.289
	158	1/26	4.67	18.63	0.292	0.315
	193	1/32	7.41	27.80	0.297	0.327
	194	1/26	7.36	28.09	0.300	0.332
	208	1/25	7.98	32.29	0.290	0.319
1	25	1/16	1.95	0.23	0.252	0.264
	26	1/16	2.04	0.26	0.242	0.258
	44	1/16	3.10	0.74	0.274	0.274
	71	1/8	5.50	1.88	0.286	0.298
	72	1/16	5.58	1.94	0.298	0.306
	73	1/27	5.65	1.99	0.298	0.306
	74	1/29	5.22	2.04	0.287	0.289
	75	1/16	5.83	2.16	0.301	0.304
	96	1/29	6.68	3.44	0.297	0.308
	120	1/29	8.26	5.37	0.299	0.316
	186	1/26	13.12	12.91	0.294	0.312
$1\frac{1}{2}$	31	1/16	3.24	0.24	0.254	0.254
	41	1/8	5.57	0.42	0.275	0.283
	54	1/16	5.64	0.72	0.287	0.293
	56	1/16	5.87	0.78	0.289	0.296
	59	1/8	8.01	0.87	0.285	0.292
	69	1/16	7.24	1.18	0.289	0.298
	78	1/8	10.57	1.51	0.291	0.305
	82	1/16	8.51	1.67	0.284	0.294
	116	1/8	15.67	3.35	0.311	0.323
	128	1/16	13.21	4.08	0.299	0.313
	131	1/16	13.52	4.33	0.304	0.317

6. RESULTS

When other than inertial forces are present, the graph of $1/v$ *versus* t will not be a straight line and the drag coefficient may vary considerably during the sphere's motion. Approximate values of C_D determined for the earlier part of the trajectory, are shown in Fig. 2 plotted against the logarithm of Reynolds Number. The points plotted correspond to determinations made over wide ranges of the shot parameters. It will be seen that there is a great dependence of C_D on the density of the air above the water; higher values of C_D corresponding generally to higher densities. The drag coefficients shown in this figure correspond, of course, to the total drag and not to the drag due only to inertial forces.

Table I lists values found by other investigators, of C_D for steel spheres in water, while an entrance cavity is attached. All of these determinations were made with normal pressure air above the water. A comparison with the corresponding values in Fig. 2 shows that the latter values are generally higher than those previously reported.

The process of eliminating the effect of all forces which are not proportional to v^2, is exemplified in Figs. 3 and 4. Figure 3 gives plots of the original and adjusted values of $1/v$ for one shot. The individual adjustment values are shown in Fig. 4. The adjustments for gravity and for the change of velocity during flight are always positive and concave upward, while that for buoyant force is always negative and concave downward. The sum of the adjustments is seldom as large as some of the individual values. The retardation coefficients, α, were obtained by fitting a least-square line to the plotted points.

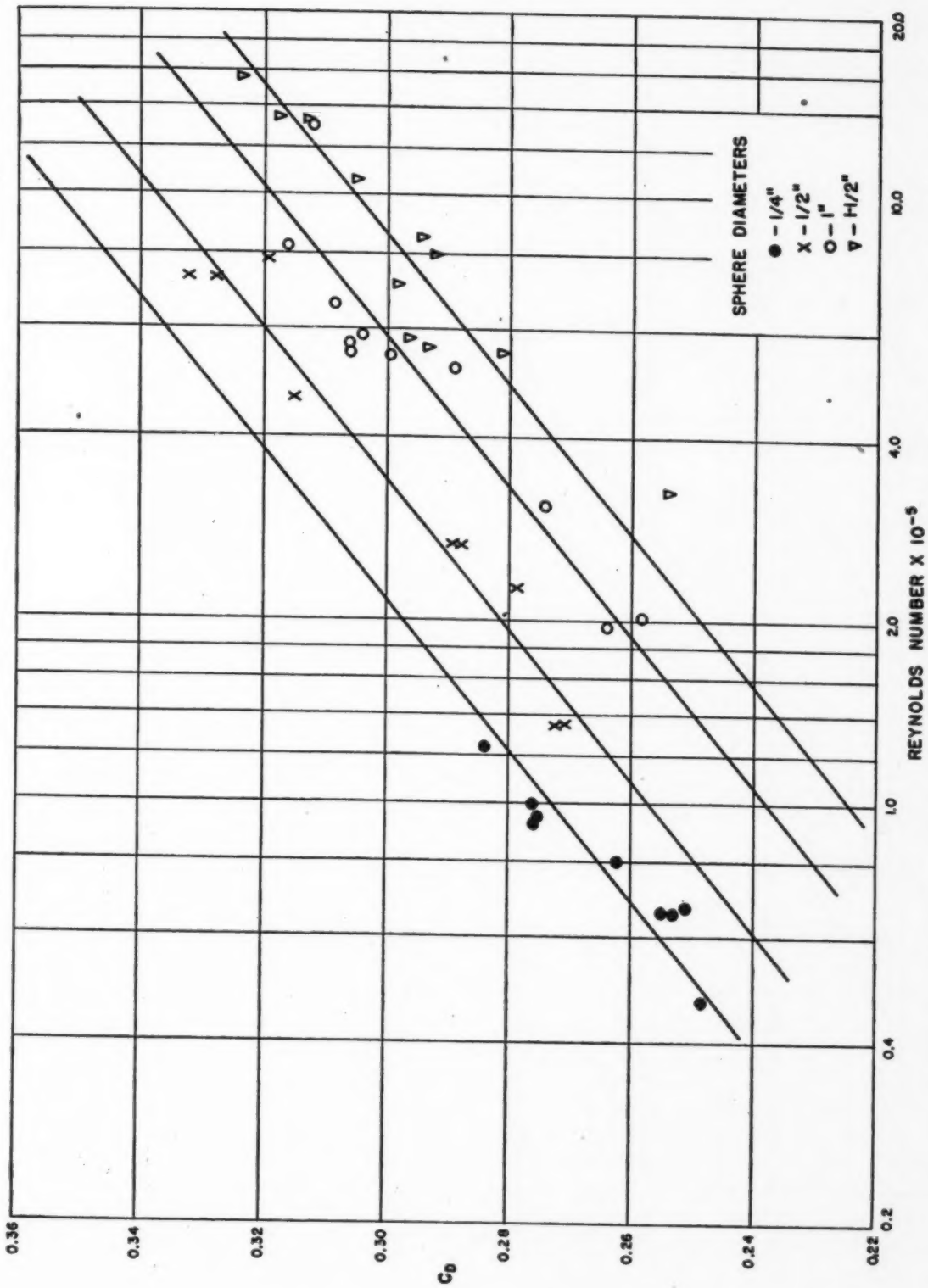

FIG. 5. Inertial drag coefficients of steel spheres after vertical entry, plotted against Reynolds Number.

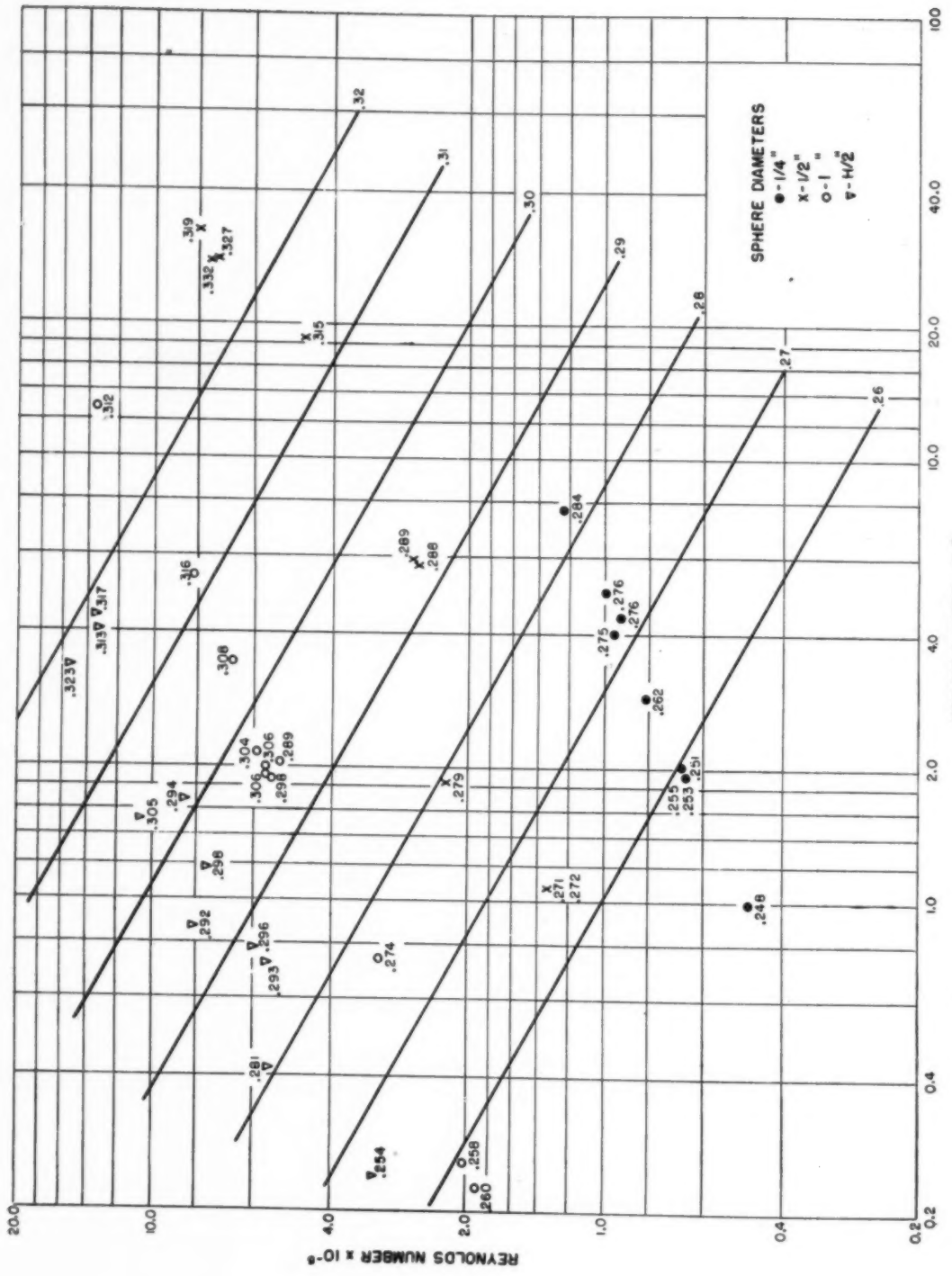

FIG. 6. Contour map of inertial drag coefficients of steel spheres after vertical entry.

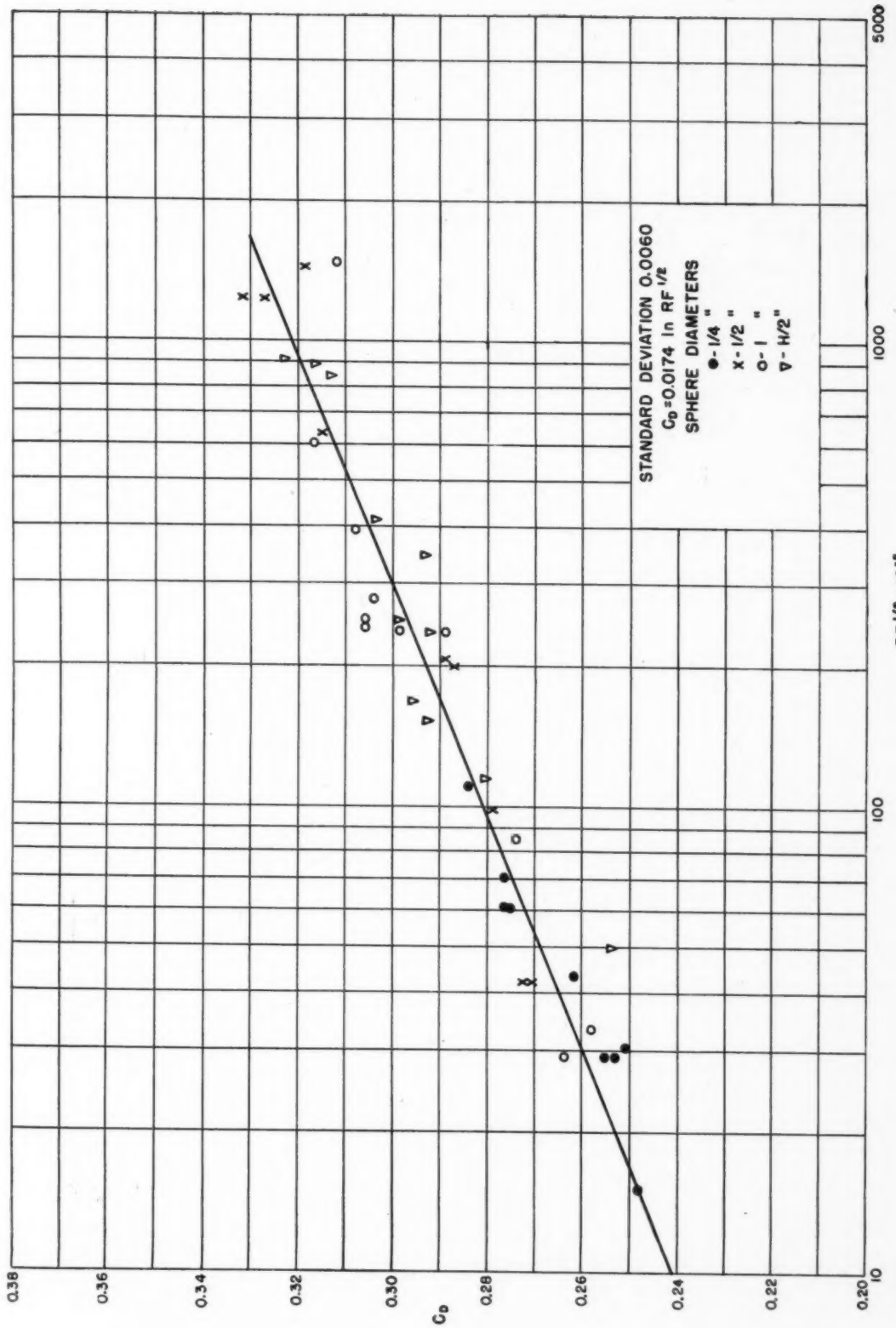

FIG. 7. Variation of inertial drag coefficient with $\ln(RF^{\frac{1}{2}})$.

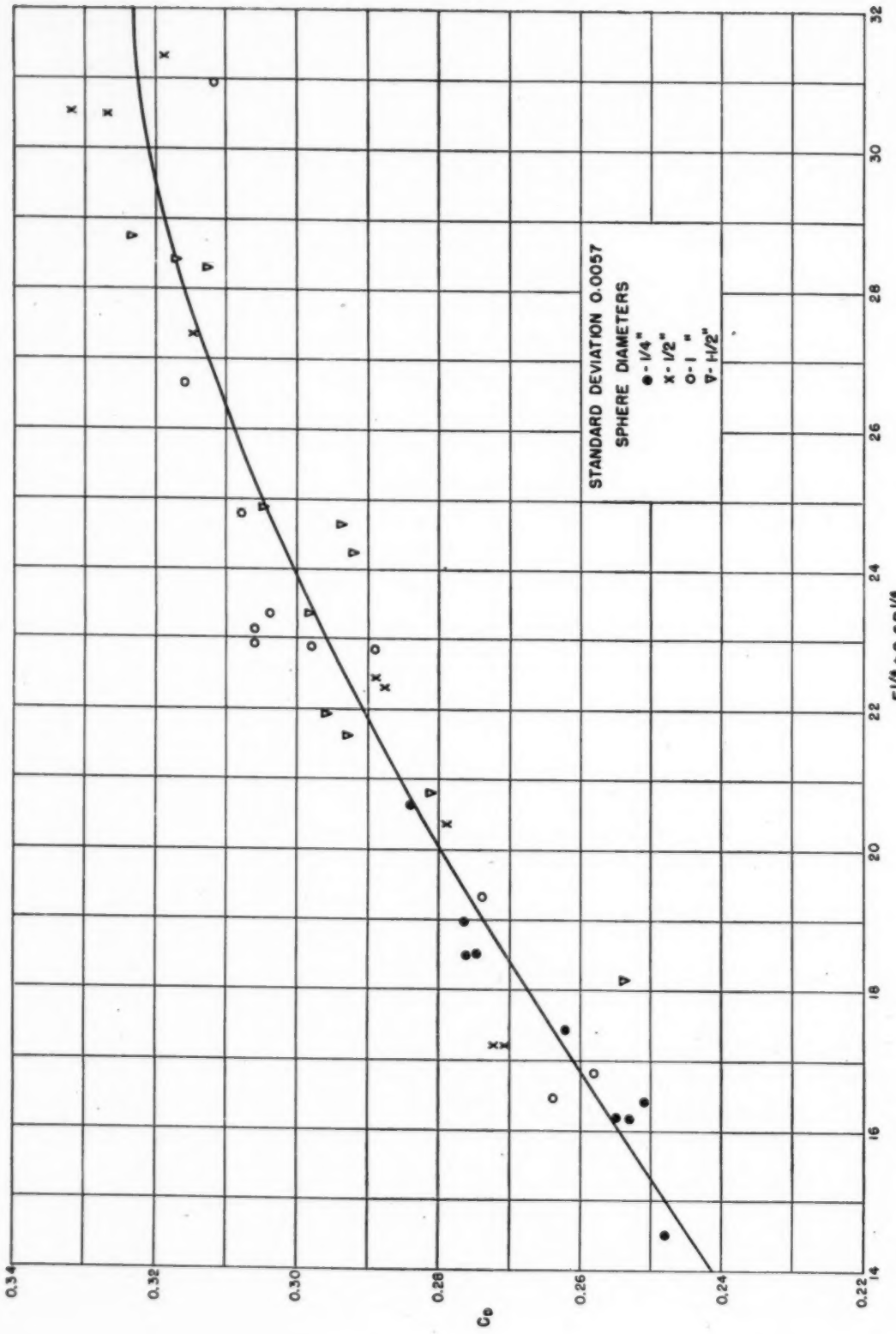

FIG. 8. Variation of inertial drag coefficient with $(F^{\frac{1}{4}}+0.6R^{\frac{1}{4}})$.

In making the adjustment for buoyant force, the wetted area, A_1, of the sphere must be known. This area may be determined roughly from the examination of photographs or from measurements of the cavity growth. Such measurements indicate that the cross section of the wetted area is about 0.8 the maximum cross-sectional area of the sphere. This value gives an adjustment of $1/v$ for buoyant force due to depth, which is apparently considerably too large, since, for trajectories which are sensitive to its value, the graph is made to curve strongly downward. A value of 0.45 of the maximum area seems most consistent with the assumption that the final graph should be a straight line, and this value has been used throughout the present study.

Table II gives various data on the 40 shots that are included in this study. It will be seen that adjusted values of C_D range from 0.248 to 0.332.

Early work in this study indicated variations of drag coefficient with the diameter and velocity of the sphere. This suggested a variation with Reynolds Number such as that well known for spheres in air. A plot of the drag coefficient against the logarithm of Reynolds Number is shown in Fig. 5. In addition to the obvious variation of C_D with Reynolds Number shown in the figure, the displacements between graphs for different diameter spheres indicate also a dependence on the Froude Number. From the points shown in Fig. 5, it appeared most reasonable to assume straight lines of the same slope for all graphs. The graphs of Fig. 5 were obtained by applying a least-square method to the complete set of points, based on the same slope for all lines, but different intercepts.

In order to determine the dependence of C_D on the Reynolds and Froude Numbers, C_D contours were drawn on axes which depended separately on the two Numbers. Such a contour map is given in Fig. 6, where the axes are the logarithms of R and F. Because of the resulting simplification, the axes were chosen so that the contours could reasonably be drawn as a family of parallel straight lines. From Fig. 6, C_D appears to be expressible as a function of the logarithm of $RF^{\frac{1}{2}}$. A plot of C_D against this function is shown in Fig. 7. This graph is straight and its equation is

$$C_D = -0.0003 + 0.0174 \ln(RF^{\frac{1}{2}}).$$

Since the value of the intercept is much smaller than experimental errors, we can write

$$C_D = 0.0174 \ln(RF^{\frac{1}{2}}).$$

This is a least-square line, drawn under the assumption that the errors in the abscissal values are negligible compared to the errors in C_D. The corresponding standard deviation is 0.0060.

As has been stated, the function $\ln(RF^{\frac{1}{2}})$ was selected as suitable for the expression of the variation of C_D, but it is quite possible that functions might be found for which the deviation would be somewhat smaller. There are no theories for the cavity which might assist in the determination of such a function. Another choice is shown in Fig. 8 where C_D is plotted against $R^{\frac{1}{2}}+0.6F^{\frac{1}{2}}$, with a standard deviation of 0.0057.

This dependence of the drag coefficient on Reynolds Number and Froude Number has, of course, been investigated here only for the case of the sphere. While a similar relation may be expected for bodies of other nose shapes, no assumptions are justified without further investigation.

7. ACKNOWLEDGMENTS

The authors wish to express their indebtedness to several members of the Hydrodynamics Subdivision; to Dr. J. Howard McMillen for stimulating discussions and helpful suggestions; to Mr. R. A. Anderson and Mr. D. J. Milano who performed the experimental work on which this report is based; and to Mrs. E. T. Dow and Mrs. B. M. Wallace who carried out a considerable part of the analysis.

Homing and Navigational Courses of Automatic Target-Seeking Devices*

LUKE CHIA-LIU YUAN
Physics Department, Princeton University, Princeton, New Jersey
(Received April 16, 1948)

A graphical and mathematical analysis of homing and navigational courses of automatic target-seeking devices is presented.

Homing courses for a seeker-to-target speed ratio of over two are likely to be impractical for target interception.

A method for obtaining a constant bearing course (navigational course) is developed. Some special cases of navigational courses have been studied graphically. It is shown that an optimum navigational ratio exists between that which leads to too slow an approach to the desired course and that which leads to instability.

Graphical analysis of navigational courses for straight as well as circular target motion is also given.

INTRODUCTION

BECAUSE of the growing interest and importance in the problem of automatic target seeking, it is deemed necessary to investigate the characteristic properties of the various possible courses traversed by a target seeker when approaching a target. The object of the present paper is to present a graphical as well as a mathematical analysis of some aspects of the problem in order that an optimum seeker course can be realized under certain conditions for achieving a satisfactory target interception in the least possible time.

We shall first consider homing courses for various target motions and attempt to analyze them by means of the correlation between the radius of curvature of the various courses and such factors as the distance between searcher and target, their relative speed ratio, the angle of approach, etc. We shall then give a brief account of the simple theory of navigational courses and a graphical analysis of them under various conditions assuming an aircraft-to-surface-vessel type of seeking.

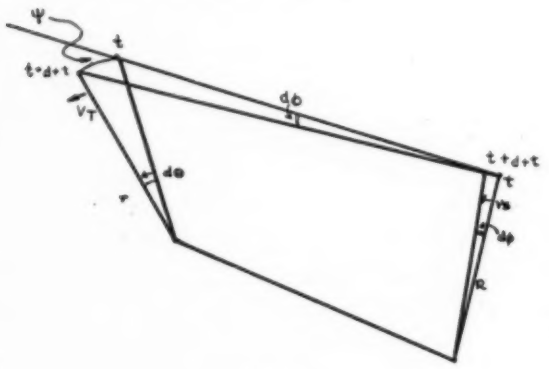

FIG. 1.

I. HOMING COURSES

A. Generalities

When a moving object directs its velocity at all times toward another object, moving or stationary, the former is said to be "homing" on the latter. This former object is called a "target seeker" or simply "seeker" while the latter is called a "target." The course thus traversed by the "seeker" is generally known as a "homing course."

When a seeker homes on a moving target whose motion is restricted within a plane, the course of the seeker is a curved path whose radius of curvature varies at various points of the path depending on the distance between and the relative speed of the two objects in question. Furthermore, the radius of the curvature also depends upon the angle between the velocity of the seeker and that of the target at the instant of consideration.

Consider as shown in Fig. 1 the elements of two paths traversed by a seeker and a target respectively between time t and $t+dt$. Suppose the seeker homes with a velocity v_S on the target moving at a velocity v_T. Let R and r be the

* This paper is based on work done for the Bureau of Ships, Navy Department, under NXsa-25337, while at the RCA Laboratories Division, Radio Corporation of America, Princeton, New Jersey.

radii of curvature of the two paths respectively at time t and let D_t be the distance between the two objects at the same instant.

Assuming that for each infinitesimal displacement on the target path in the time interval dt there is a corresponding displacement on the seeker path and that the seeker homes at all times on the target, we have

$$R=(v_S/v_T)(rd\theta/d\phi). \tag{1}$$

But

$$D_t d\phi = rd\theta \sin\psi, \tag{2}$$

where ψ is the angle between the two velocities v_S and v_T. Substituting (2) into (1) we get the radius of curvature of a homing course:

$$R=(v_S/v_T)(D_t/\sin\psi). \tag{3}$$

We see that for a constant speed ratio v_S/v_T, R is directly proportional to D_t, the distance between the two objects, and is inversely proportional to the sine of the angle between the two velocities.

In order to analyze the homing courses more clearly, we shall first consider a few special cases of target motion and then generalize them for any arbitrary motion.

B. Target Moving on a Straight Course with Constant Velocity**

The simplest case of target motion would be one in which a target moves on a straight course along the y-axis with a constant velocity v_T. Assume that the velocity v_S of the seeker is constant. We have from Eq. (3) and Fig. 2, where T is the target described by x_T, y_T, at time t, and S is the seeker described by x_S and y_S at the same instant:

$$\begin{aligned} R&=(v_S/v_T)(D_t/\sin\psi)\\ &=(v_S/v_T)(D_t^2/x_S)\\ &=Kx_S[1+(y_T-y_S/x_S)^2], \end{aligned} \tag{4}$$

where K is the speed ratio v_S/v_T. Again from Fig. 2, it is seen that

$$\frac{y_T-y_S}{x_S}=-\frac{dy_S}{dx_S}. \tag{5}$$

** The fact that a homing course in which the seeker speed is greater than twice the target speed leads to an infinitely small radius of curvature was first pointed out to the author by Dr. Jan A. Rajchman of RCA Laboratories.

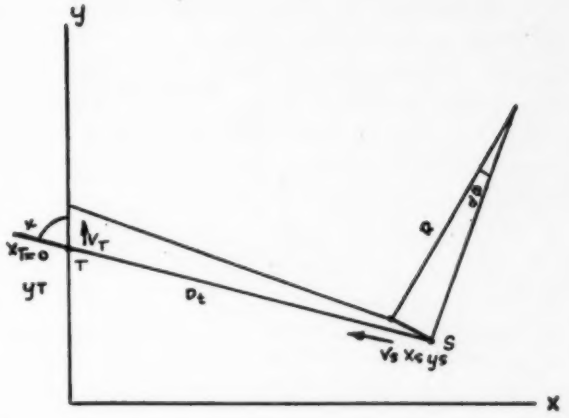

FIG. 2.

Hence (4) becomes

$$R=Kx_S[1+(dy_S/dx_S)^2], \tag{6}$$

but the radius of curvature of any path element is given by

$$R=\frac{[1+(dy_S/dx_S)^2]^{\frac{3}{2}}}{d^2y_S/dx_S}. \tag{7}$$

Equating (6) and (7) we obtain the differential equation of the homing course

$$\frac{d^2y_S}{dx_S^2}=\frac{1}{Kx_S}\left(1+\left(\frac{dy_S}{dx_S}\right)^2\right)^{\frac{1}{2}}. \tag{8}$$

Integrating (8) and assuming that the initial conditions are $x_S=x_0$ and v_S is at right angles to v_T for $t=0$, and combining with (6), we have

$$R=\frac{Kx_S}{4}\left[\left(\frac{x_S}{x_0}\right)^{1/K}+\left(\frac{x_S}{x_0}\right)^{-1/K}\right]^2. \tag{9}$$

As the seeker approaches the target and x_S tends to zero, (9) becomes

$$R\cong(Kx_0/4)^{2/K}x_S^{1-(2/K)}.$$

So that, depending on the value of K:

$$\begin{cases} R\to(x_0/2) & \text{if } K=2 \\ R\to\infty & \text{if } K<2 \\ R\to 0 & \text{if } K>2 \end{cases} \text{as } x_S\to 0. \tag{10A, 10B, 10C}$$

Thus from (10C) we see that if the speed ratio v_S/v_T is greater than two, i.e., the speed of the seeker is more than twice as great as that of the target, the radius of curvature of the homing

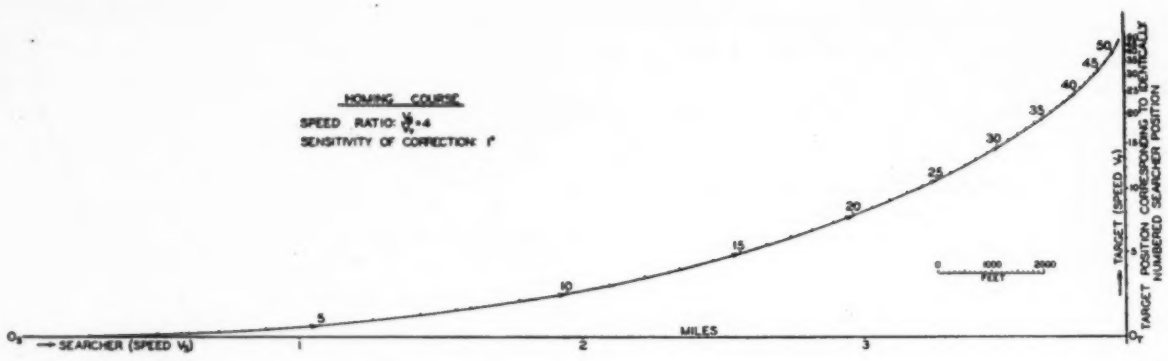

FIG. 3.

course decreases and approaches zero as the seeker approaches the target.

Since the force which must be exerted on an object moving on a curved path varies inversely as the radius of curvature, there is always a practical limit to the sharpness of a turn. Thus even for a target of a finite size, the seeker may not be able to make a sharp enough turn to follow the theoretical homing course if the speed ratio v_S/v_T is greater than two.

The path of a homing course can be easily obtained from (8) by integration and it is given by

$$y_S=\frac{x_S}{2}\left[\frac{1}{1+(1/K)}\left(\frac{x}{x_0}\right)^{1/K}-\frac{1}{1-(1/K)}\left(\frac{x}{x_0}\right)^{-1/K}\right]+\frac{(1/K)}{1-(1/K^2)}x_0. \quad (11)$$

A graphical representation of such a homing course for a seeker-to-target speed ratio of four to one is given in Fig. 3.

The target moves along the y axis on the right-hand side as indicated. The sensitivity of correction of the seeker is assumed to be 1°, i.e., the seeker makes a correction on its course only after the target is off the former's course by at least one degree. The numbers marked on the homing course indicate the positions where corrections of the course are made while the numbers on the target course show the corresponding positions of the target. The larger arrows show the directions of motion of the seeker at successive time intervals whereas the smaller arrows indicate the directions of a sighting device mounted on the seeker.

C. Target Moving on a Plane Curved Course

For a seeker homing on a target which moves along a plane curved course with a speed v_T, it can be easily shown that the radius of curvature of the seeker course can be either greater or smaller, depending on the relative motions of the target and the seeker, than that of a corresponding seeker course homing on a target which moves along a straight line with the same speed v_T.

D. Conclusions about Homing Courses

From the above analysis we may conclude that by assuming a point target, a seeker equipped with a homing device is of little practical value if its speed is more than twice as great as that of the target. However, this is not necessarily true if the target is of finite size. Even if the seeker speed could be regulated so that it would decrease as the radius of curvature of the course to prevent course from impractical curvature, still another practical drawback would remain.

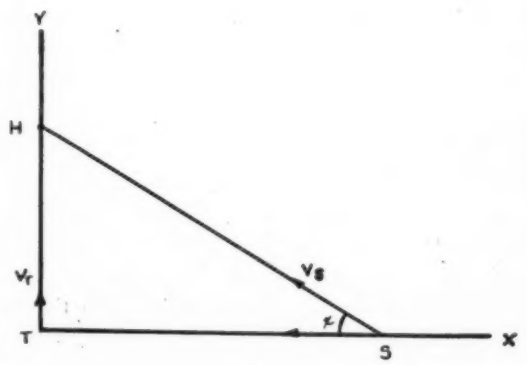

FIG. 4.

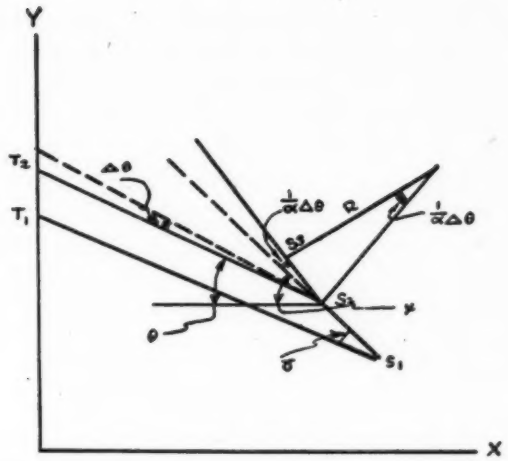

FIG. 5.

The direction of motion of the seeker is always parallel to that of the target at the point of interception so that only a comparatively small tail section is exposed to the seeker.

II. NAVIGATIONAL COURSES

A. True Navigational or Collision Courses

As we have seen from the analysis in Section I, a homing course for target interception at high seeker-to-target speed ratio

$$v_S/v_T > 2$$

is rather impractical. We shall now endeavor to analyze a more satisfactory type of seeking course which we shall call navigational course.

Suppose a target T is moving in a fixed direction with a known constant velocity v_T. It is possible to set up a straight course for the seeker to intercept the target in the least possible time. This is illustrated in Fig. 4 where the target T moves along the y axis with a constant velocity v_T, and the seeker moves with a constant velocity v_S. If the seeker S starts out at an angle ψ with respect to the x axis, such that the projected value of its velocity v_S on the direction of the target velocity is equal to the target velocity itself, it is evident that collision must result. Hence, H is the point of interception and the course $\langle SH \rangle$ is called a collision or true navigational course.

Consider further that a sighting device is provided on the seeker so that it can be rotated about an axis, normal to the xy plane, with respect to the direction of the seeker velocity. When the sighting device is kept pointing at all times toward the target, then the angle ψ between it and v_S will remain constant throughout a true navigational course.

In order to set on a true navigational course for target interception, the seeker must possess the information on the target speed and its direction of motion. In the case of pursuing an arbitrarily moving target, for instance, it is impossible to obtain such information, and besides, the target would generally not follow a definite course. Hence, a more practical way for approximating such a course without having to know the target speed and its direction of motion will be described.

B. A Method of Approximating True Navigational Courses

Now let us consider the case where the target speed v_T is unknown. Suppose at time t, the sighting device on the seeker S_1 is directed to

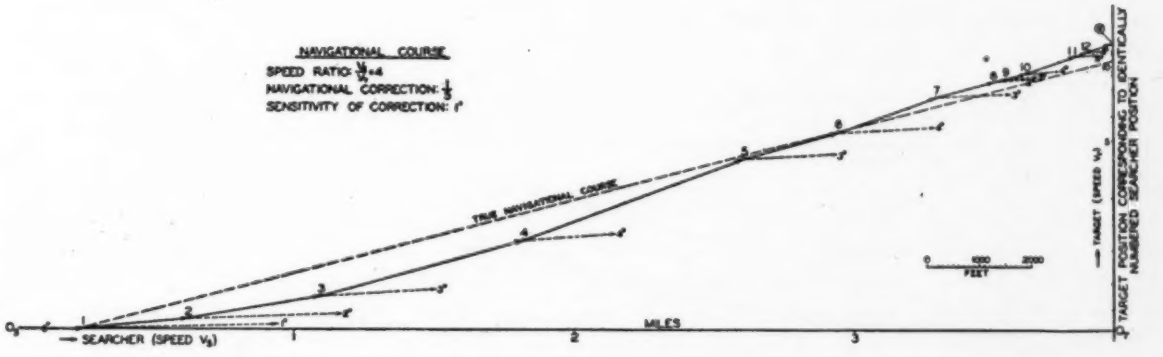

FIG. 6.

the target T_1 which makes an angle $\gamma=\psi-\theta$ with respect to the direction of the seeker velocity v_S where ψ is the angle of v_S with respect to the x axis, and θ, that of the sighting device referred to the same axis (see Fig. 5).

Suppose also that at an instant Δt later, a discrepancy $\Delta\theta$ between the direction of the sighting device and that of the new position of the target T_2 is observed. If the seeker is kept on the same course in the direction of S_1S_2, obviously it will not be able to intercept the target. However, if the seeker and the sighting device are both turned clockwise simultaneously, but through different angles, say

$$(1/\alpha)\Delta\theta \quad \text{and} \quad \Delta\theta$$

respectively, where α is a constant factor which is smaller than one, then the sighting device would again be aimed at the target T_2 and the seeker would travel in the new direction S_2S_3. By successive repetition of this process for every discrepancy $\Delta\theta$ the seeker course will gradually approach a true navigational course where the angle θ will remain unchanged. At this position the component of v_S in the direction of v_T is equal to the latter. Hence if v_T remains constant, the seeker will intercept the target on a straight course. The proportionality constant α is called the navigational correction, and the course traversed by the seeker employing such a navigational correction is called a practical navigational course, or simply a "navigational course."

Referring to Fig. 5 again, we see that the radius of curvature of the navigational course is given by:

$$R=\alpha v_S/d\theta/dt,$$

where $d\theta/dt$ is the time rate of discrepancy occurrence, and is equivalent to the time rate of corrections made at each point of the course. Hence if no discrepancy is observed throughout the course, i.e.,

$$d\theta/dt=0, \quad \text{then} \quad R=\infty,$$

and the navigational course becomes a true navigational course.

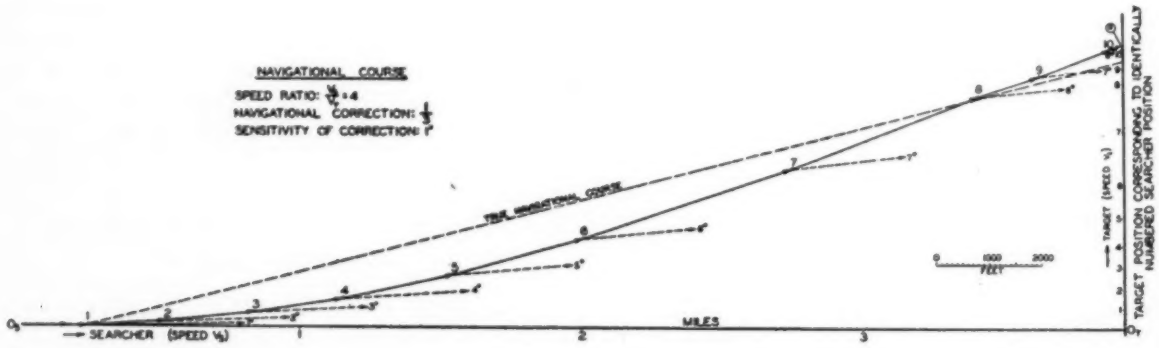

FIG. 7.

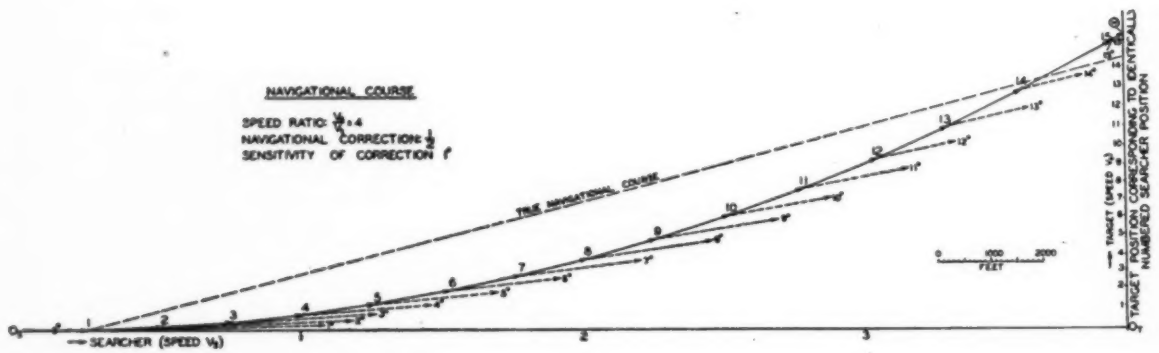

FIG. 8.

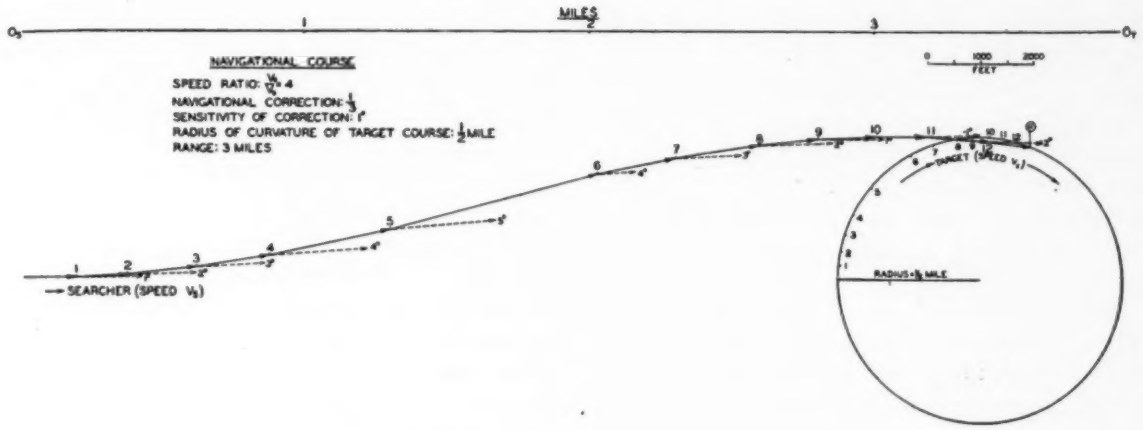

FIG. 9.

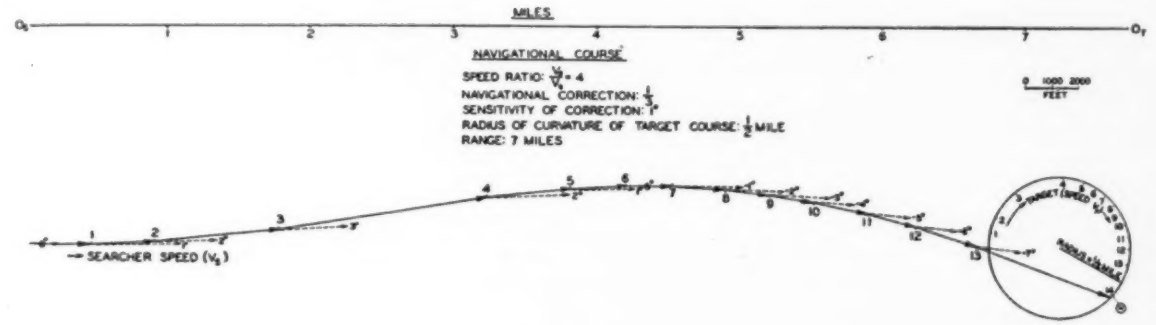

FIG. 10.

A method of achieving this in an automatic target seeking device is by coupling mechanically a sighting device (or a directional antenna system if a radar system is used) to the turning control mechanism of the seeker. It is coupled in such a way that when the sighting device is turned through the angle ϕ, the seeker is turned automatically through an angle $(1/\alpha)\phi$ in the same direction. This is most readily accomplished by reference of both directions to a gyro held fixed in direction.

C. Graphical Analysis of Navigational Courses for Straight and Circular Target Motions

For purposes of illustration, navigational courses with various navigational corrections ranging from $\alpha=\frac{1}{2}$ to $\alpha=\frac{1}{5}$ have been plotted for various cases of straight as well as circular target courses. It is assumed in all the plots that the automatic seeker has a sensitivity of correction of one degree.

Figure 6 shows a navigational course of a seeker of speed v_S intercepting a target travelling on a straight course along the y axis with a velocity v_T. The seeker-to-target speed ratio,

$$v_S/v_T$$

is assumed to be four, and the navigational correction is $\alpha=\frac{1}{3}$. The solid line represents the navigational course with the big arrows indicating the direction of the course at successive intervals. The dotted lines with small arrows indicate the directions of the sighting device at corresponding intervals of the course while the broken line represents the true navigational course. The numbers on the course denote the positions at which corrections of the course are made, while the numbers on the y axis mark the corresponding positions of the the target. H enclosed in a circle indicates the position at which the interception is made.

Similar navigational courses with different

values of α, the navigational correction, are shown in Figs. 7 and 8. Typical cases where the target moves on a circular course are shown in Figs. 9 and 10. Satisfactory interception has also been obtained in cases where there is a short time lag in correction, and where the target is heading 20° off target at the start of the course.

III. CONCLUSION

We may conclude that for automatic target seeking, a navigational course with an appropriate navigational correction has theoretical advantages over a homing course.

From the results shown, it is seen that a navigational correction of $\alpha=\frac{1}{3}$ for a seeker-to-target speed ratio of four gives a close approximation to a true navigational course without "hunting." However, the value of α within the range of $\frac{1}{3}$ to $\frac{1}{5}$ does not seem to be critical.

The author wishes to acknowledge his indebtedness to Dr. Jan A. Rajchman and to Mr. R. C. Sanders, Jr. for many valuable discussions and suggestions. He also wishes to express his thanks to Dr. Irving Wolff without whose encouragement this work would not have been possible.

Use of an Electron Diffraction Camera as an Ultraoscilloscope, and Suggested Application to Contact Erosion

J. J. LANDER
Bell Telephone Laboratories, Inc., Murray Hill, New Jersey
(Received July 8, 1948)

A high speed oscilloscope, obtained by adaptation of an electron diffraction camera, is described and a preliminary account is given of the use of this oscilloscope in a study of the "short arc" which occurs on opening mechanical contacts under certain conditions.

AN oscilloscope with time resolution of 0.001 μsec. and voltage sensitivity of ten-trace widths per volt has been obtained by superficial adaptation of the electron diffraction camera built by Dr. L. H. Germer of these Laboratories. Previous oscilloscopic work in which a high voltage beam is photographed in vacuum has been described by Rogowski and coworkers,[1] von Ardenne,[2] Hollman,[3] and Lee.[4]

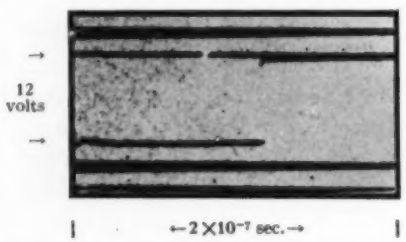

FIG. 1. Response of the oscilloscope to a unit step pulse of twelve volts. Magnification 6×.

The voltage sensitivity of about ten-trace widths per volt was obtained with deflecting plates 3 cm long, a deflecting plate to photographic plate distance of 80 cm, a trace diameter of about 0.001 cm, and an electron source at 50,000 volts negative to ground. Inductance and capacity measured at the terminals of the deflecting plates were 0.03 μH and 4 $\mu\mu F$ respectively. Since the rise time of an applied step pulse is approximately twice the square root of the product of inductance and capacity if the circuit is nearly critically damped, the calculated time resolution is about 0.0006 μsec. Figure 1 shows the response of the instrument to a step pulse of twelve volts.

The present work was undertaken in order to study transients occurring in mechanical contacts. These transients occur randomly on such a time scale. They can be observed either by tripping the sweep with the transient, meanwhile delaying the transient, or by extending the time scale beyond the period over which the occurrence of the transient is random. The sec-

[1] W. Rogowski, E. Flegler, and K. Buss, Arch. f. Elekt. **24**, 563, 1930.
[2] M. von Ardenne, Hoch: tech. u. Elek: akus. **54**, 181, 1939.
[3] H. Hollmann, Proc. I.R.E. **28**, 213, 1940.
[4] G. Lee, Proc. I.R.E. **34**, 121, 1946.

ond alternative was used successfully. With the equipment under study the transients were found to be distributed over a time interval of about 100 microseconds relative to activation of the contacts by a mercury switch. Thus, with proper sweep circuit and sweep trip, it was possible to photograph the transients by sweeping 200 lines at the rate of one line per microsecond. The lines were separated by adding a suitable voltage to the vertical plates. A triangle wave generator (obtained from an adapted Freuhauf type circuit) with about 400-volts output produced lines about one-inch long.

Figure 2 is a photograph of a transient initiated by the separation of gold electrodes in a 10 ohm circuit containing 1.0 μH inductance and a six-volt battery. The voltage across the contacts rises to about 10 volts, remains constant for about 0.04 microsecond, surges a few volts and drops to the open circuit value. This behavior is typical of a discharge characterized as the "short arc,"[5] but whereas in previous work, carried out under quite different conditions, the minimum current necessary to support such an arc between gold electrodes has been reported to be about 0.4 ampere, it is estimated that the arc of Fig. 2 was quenched at about 0.1 ampere.

The circuit conditions of Fig. 2 represent so-called "bridge erosion" conditions in which contacts are separated in a circuit with battery voltage less than the arcing potential of the contacts and with inductance reduced to a minimum. It is known that a molten bridge forms and explodes between metal contacts in the process of separation, and it is expected that under some

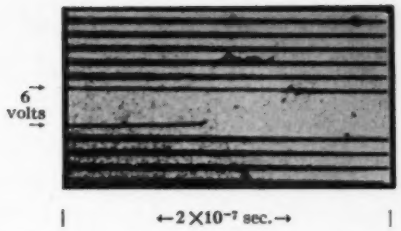

FIG. 2. "Short arc" occurring between gold contacts breaking 6 volts. The contact circuit contained 10 ohms and 1.0 μH inductance. The oscilloscope circuit contained 800 ohms. Magnification 6×.

conditions a large part of contact erosion is associated with this molten bridge.[6] Figure 2 is representative of a number of photographs obtained under similar conditions with both gold and platinum contacts. It is concluded that the "short arc" will accompany contact separation if the maximum voltage of the transient can reach a value of about 10 volts and a current larger than the minimum current necessary to support the arc can flow.

The approximate energy dissipated in the arc is simply calculated, and under the conditions of Fig. 2 it is about 0.5 Li_0^2, i_0 being the current flowing before the contacts begin to separate. Studies[7] of a "short arc" occurring between making contacts (in which stored capacitative energy is discharged) indicates that considerable energy is dissipated on the positive electrode. Under typical "bridge erosion" conditions the positive contact is also eroded and the amount of erosion can be accounted for if it is assumed that most of the inductive energy dissipated in a "short arc" is spent by boiling metal out of the contact.

[5] An account of previous work on the "short arc" is to be found in R. Holm's *Electric Contacts* (Almquist and Wiksells, 1946).

[6] J. J. Lander and L. H. Germer, J. App. Phys. **19**, 910 (1948).

[7] Germer and Haworth, Phys. Rev. **73**, 1121 (1948).

Erratum: The Attenuation of Spherical Shock Waves in Air

[J. App. Phys. **19**, 670 (1948)]

RICHARD G. STONER AND WALKER BLEAKNEY
Palmer Physical Laboratory, Princeton University, Princeton, New Jersey

AN error has been pointed out in Eq. (1) of this paper. The equation should read:

$$(P-P_0)/P_0=[2\gamma/(\gamma+1)][(V^2/a^2)-1].$$

Dielectric Measurement Methods for Solids at Microwave Frequencies*

W. H. Surber, Jr.** and G. E. Crouch, Jr.***
Princeton University, Princeton, New Jersey
(Received May 6, 1948)

An experimental method of measuring the dielectric constants of solids is described for the case of medium and high loss materials. The dielectric sample is enclosed within a section of wave guide terminated by a reflecting plane, and measurements are made of the standing wave ratio and position of the voltage minimum for both a short-circuit and an open-circuit termination. The equations for the dielectric properties of the substance may then be expressed in a relatively simple form in terms of elementary functions for media having $\tan\delta \geq 0.03$.

In order to obtain reasonable accuracy for the determination of the loss factor of low loss materials using only standard wave-guide components, it was found to be necessary to adjust the operating conditions to obtain maximum power absorption by the dielectric sample. A frequency variation method of obtaining this maximum loss sensitivity is described, the apparatus being the same as that used for the medium and high loss materials.

A set of experimental values is given for the dielectric constants of a group of common plastics at 24,000 megacycles. A brief analysis of the effect of certain of the equipment losses is included.

I. INTRODUCTION

THE dielectric properties of a non-conducting substance at microwave frequencies may be determined from the propagation characteristics of an electromagnetic wave through the medium. There are many different ways of attacking the experimental problem of measuring this propagation constant, or equivalent parameters, for a uniform sample of the material. A number of such methods are considered in Vol. 11 of the M.I.T. Radiation Laboratory Series, which includes a fairly extensive bibliography of recent work in this field.[1]

One method, which is applicable over a wide range of frequencies and of dielectric constants, is to use the standard transmission line techniques to measure the impedance at the face of a sample of the dielectric medium which is completely enclosed in a section of coaxial transmission line or hollow wave guide, and which is terminated by a perfectly reflecting plane. A general solution of the transmission line problem for such a section of dielectric-filled line has been given by S. Roberts and A. von Hipple.[2] A modification of this method of computation was developed by T. W. Dakin and C. N. Works for the case of low loss dielectrics.[3]

For medium and high loss materials the equations for the dielectric constants, may be considerably simplified if two sets of experimental measurements are made upon each sample, one with a short-circuit termination and one with an effective open-circuit termination. The sample length need not be measured in this case. For low loss media, however, it becomes difficult to correct these equations for the effects of the apparatus loses.

The dielectric constant, ϵ', of these low loss materials may readily be obtained with considerable accuracy in several ways.[1,3] The accurate determination of the dielectric loss factor, ϵ'', is more difficult, and, for a fixed sample length and a fixed frequency, requires the use of special equipment which is capable of measuring very high standing wave ratios and which minimizes or eliminates the junction loss between the dielectric-filled section of line and the slotted measuring section. By applying some form of "resonance" method, however, it becomes possible to measure small loss tangents with reasonable accuracy using only standard wave-guide components. One such method, de-

* This paper is based on work done for research programs sponsored by the Office of Naval Research under Contract N6ori–105, Task Order IV, and by the Navy Department Bureau of Ships and U. S. Army Signal Corps jointly under Contract No. W-36-039-sc-32011, File No. 10478-PH-46-91 (SCEL).

** Electrical Engineering Department, Princeton University.

*** Plastics Engineering Laboratory, Princeton University.

[1] *Technique of Microwave Measurements* (M.I.T. Radiation Laboratory Series, Vol. 11, McGraw-Hill Book Company, Inc., New York, 1947).

[2] S. Roberts and A. von Hippel, J. App. Phys. **17**, 610 (1946).

[3] T. W. Dakin and C. N. Works, J. App. Phys. **18**, 789 (1947).

scribed in this paper, is to vary the oscillator frequency until the dielectric sample is an integral multiple of a quarter wave-length long electrically. For one group of these "resonant" conditions of operation, the SWR is minimized and the wave-guide junction may be located so that its loss is negligible. This procedure is exactly analogous to the standard resonance methods for the measurement of power loss or Q, which usually consist in varying some circuit parameter, such as a tuning condenser or the position of a resonant cavity plunger, in order to obtain maximum power transfer to a dielectric load in the circuit.

II. THEORY

The general theory of the propagation of electromagnetic waves along a system of enclosed conducting surfaces is well known, and is developed in several recent texts.[4, 5] The propagation constant along the axis of a hollow wave guide of uniform cross section, having high conductivity walls and containing a non-ideal dielectric medium, may be written as:

$$\gamma_d = j(2\pi/\lambda)[\epsilon' - (\lambda/\lambda_c)^2 - j\epsilon'']^{\frac{1}{2}} \quad (1)$$

$$= \alpha_d + j(2\pi/\lambda_d), \quad (1,a)$$

where λ is the wave-length in free space, λ_c is the cut-off wave-length for the air-filled guide, λ_d is the wave-length in the dielectric-filled guide, α_d is the attenuation constant caused by dielectric power loss, and the complex dielectric constant of the medium is defined as

$$\epsilon = \epsilon_0(\epsilon' - j\epsilon''),$$

where ϵ_0 is the dielectric constant of free space in m.k.s. units.

For an ideal plane dielectric discontinuity perpendicular to the axis of a uniform wave guide, no higher modes will be excited and the standard transmission line equations for reflection and transmission at an impedance discontinuity will apply to the wave-guide circuit.[4, 5] The per unit characteristic impedance of the dielectric-filled section of wave guide is given by the equation:

$$Z_d = \left[\frac{1-(\lambda/\lambda_c)^2}{\epsilon' - (\lambda/\lambda_c)^2 - j\epsilon''}\right]^{\frac{1}{2}} = |Z_d| \exp(j\phi_d). \quad (2)$$

Thus, from an experimental measurement of the real and imaginary components of either the propagation constant or the characteristic impedance of the dielectric-filled section of guide, both the relative dielectric constant, ϵ', and the loss tangent of the medium $\tan\delta = \epsilon''/\epsilon'$, may be calculated.

III. MEASUREMENT METHODS

A. Medium and High Loss Solids

From standard transmission line theory, the characteristic impedance of a section of line of

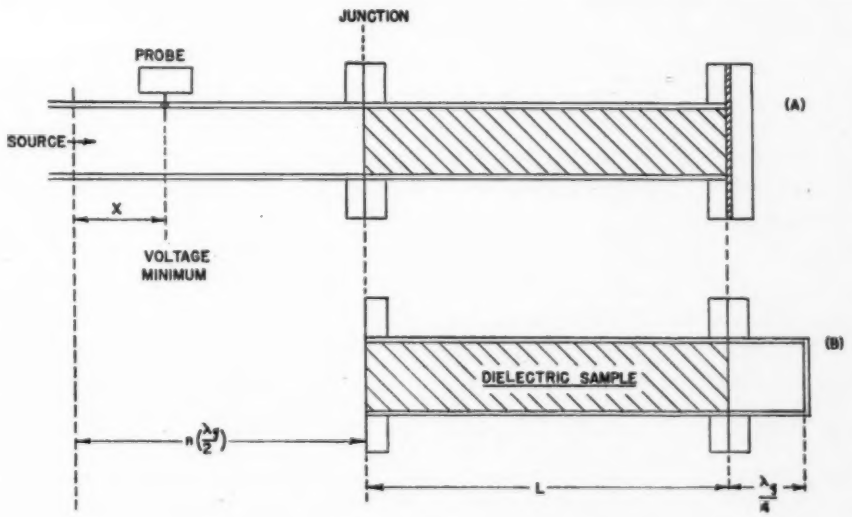

FIG. 1. Dielectric cell.

[4] J. C. Slater, *Microwave Transmission* (McGraw-Hill Book Company, Inc., New York, 1942).
[5] S. Ramo and J. R. Whinnery, *Fields and Waves in Modern Radio* (John Wiley and Sons, Inc., New York, 1944).

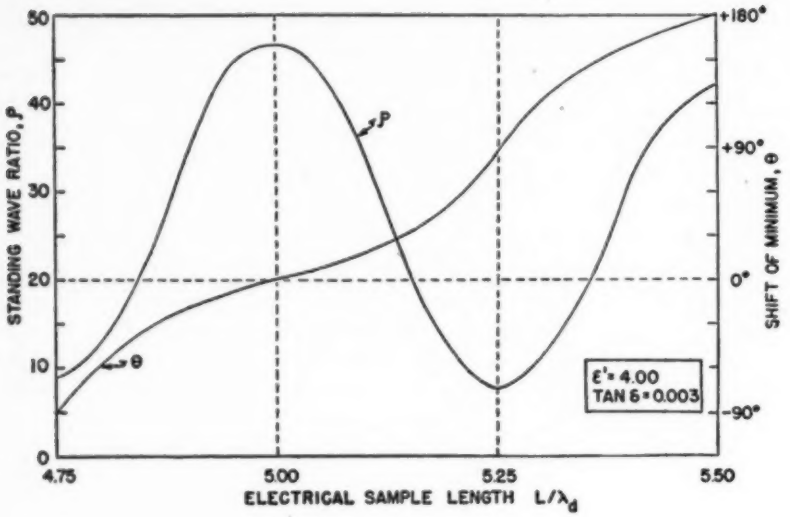

FIG. 2. Variation of VSWR and shift of the minimum with electrical sample length for a short-circuit termination.

arbitrary length is equal to the geometric mean of its observed impedances for an ideal short-circuit termination and for an ideal open-circuit termination,

$$Z_d^2 = Z_{sc} \cdot Z_{oc}. \tag{3}$$

The impedance at the face of a solid dielectric sample inserted in a section of wave guide and terminated by a reflecting plane, as shown in Fig. 1, may be measured with a slotted line connected in front of the dielectric cell. The input impedance at the dielectric cell, Z_i, is given in terms of the observed voltage standing wave ratio, ρ, and the location of the voltage minimum point by the equation

$$Z_i = \frac{1/\rho + j \tan\theta}{1 + j(1/\rho)\tan\theta}, \tag{4}$$

where $\theta = 2\pi(x/\lambda_g)$ is the angular shift of the minimum when the dielectric cell is replaced by a short circuit.

Thus, from Eqs. (2), (3), and (4), the dielectric constants of the medium may be expressed in terms of the measured ρ_1, θ_1 for a short-circuit termination, and ρ_2, θ_2 for an open-circuit termination, by the equation

$$\frac{\epsilon' - (\lambda/\lambda_c)^2 - j\epsilon''}{1-(\lambda/\lambda_c)^2} = \left(\frac{\rho_1 + j\tan\theta_1}{1 + j\rho_1 \tan\theta_1}\right) \cdot \left(\frac{\rho_2 + j\tan\theta_2}{1 + j\rho_2 \tan\theta_2}\right). \tag{5}$$

In order to obtain a more convenient algebraic expression, define

$$A = \rho_1\rho_2 - \tan\theta_1 \tan\theta_2,$$
$$B = 1 - \rho_1\rho_2 \tan\theta_1 \tan\theta_2,$$
$$C = \rho_1 \tan\theta_1 + \rho_2 \tan\theta_2,$$
$$D = \rho_1 \tan\theta_2 + \rho_2 \tan\theta_1.$$

Then the real and imaginary components of Eq. (5) may be written as:

$$\frac{\epsilon' - (\lambda/\lambda_c)^2}{1-(\lambda/\lambda_c)^2} = \frac{AB + CD}{B^2 + C^2}, \tag{5a}$$

$$\frac{\epsilon''}{1-(\lambda/\lambda_c)^2} = \frac{AC - BD}{B^2 + C^2}. \tag{5b}$$

The dielectric constants, ϵ' and ϵ'', are computed from the previous equations, neglecting the effect of the apparatus losses. This is justified only in the case of medium and high loss materials for which the power absorption in the dielectric medium is relatively large and the SWR obtained is not too high. The corrections required because of power losses in the walls of the wave guide and in the actual reflecting terminations are discussed in Appendix A. In general, for medium and high loss dielectric media, $\tan\delta \geqslant 0.03$, these terms are negligible.

Because of the manner in which the apparatus losses affect the results, this method cannot readily be extended to the case of low loss media. It provides a relatively simple and direct procedure, however, for the determination of the

dielectric constants over a loss region within which fall many types of commercial plastics.

B. Low Loss Media, Frequency Variation Method

The determination of the dielectric properties of a substance is greatly simplified if the sample is exactly an integral multiple of a quarter or half wave-length long electrically. The mathematical advantages, which follow if this is the case, are obvious since the equations for the dielectric constants reduce to a very simple form. The experimental advantages are even more important since this enables the circuit to be operated under conditions for which the wave-guide junction losses are minimized. Also, by using the proper termination, the impedance at the face of the dielectric sample will be such that the power absorbed will be in the neighborhood of a maximum. This increases the dielectric loss relative to the wave-guide losses, and thus increases the over-all sensitivity for loss measurements while decreasing the magnitude of the SWR which must be measured.

For liquids, the length of the dielectric column may be varied by using a movable reflecting plunger to terminate the sample.[6,7] In the case of solids, this procedure is considerably more difficult, since the sample must be removed from the guide and its length shaved in a series of steps until the desired multiple of $\frac{1}{4}\lambda_d$ or $\frac{1}{2}\lambda_d$ is obtained.[8]

An alternate method of adjusting the electrical length of the sample is to vary the oscillator frequency until the phase of the voltage reflection coefficient at the face of the dielectric is either 0° or 180°.[9] For low loss dielectrics, terminated by a highly conducting plane, the electrical length of the sample will then be either an odd multiple of $\frac{1}{4}\lambda_d$ or a multiple of $\frac{1}{2}\lambda_d$, respectively. By using a relatively long dielectric sample, the frequency variation required is kept small. For example, in the 1.25-cm region, a dielectric cell length of 2″ was used, which represents from about 5 to 12 wave-lengths for $2<\epsilon'<12$.

The variations of the SWR, ρ, and of the shift of the minimum point, θ, with the electrical length of a low loss sample for a short-circuit termination are indicated in Figs. 2 and 3.† From these curves it can be seen that the minimum SWR, and therefore the maximum power absorption by the dielectric load, occurs for lengths in the neighborhood of odd multiples of $\frac{1}{4}\lambda_d$. The rate of change of θ with sample length is also a maximum in this region, so that the frequency required to obtain one of this set of "resonant" lengths can be determined fairly accurately.

The dielectric constants, ϵ' and ϵ'', may then be calculated from the measured sample length,

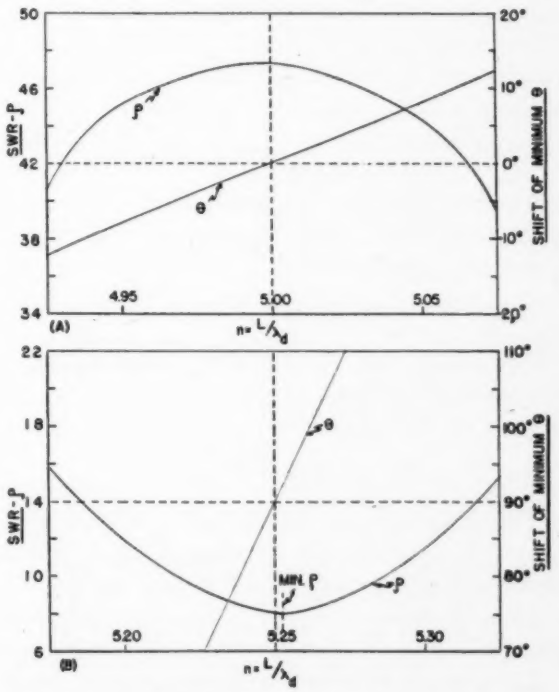

FIG. 3. Variation of VSWR and shift of the minimum with electrical sample length as in Fig. 2 for: (A) Sample length in the neighborhood of a multiple of $\frac{1}{2}\lambda_d$; (B) sample length in the neighborhood of an odd multiple of $\frac{1}{4}\lambda_d$.

[6] G. E. Crouch, Jr., J. Chem. Phys. **16**, 364 (1948).
[7] W. H. Surber, Jr., J. App. Phys. **19**, 514 (1948).
[8] E. Feenburg, Sperry Reports No. 5220-114, 5220-124, 5220-125 (April-September, 1943).
[9] W. H. Surber, Jr., *Methods of Measurement of Dielectric Constant and Loss Factor for Solids at Microwave Frequencies* (Report 3, O.N.R. Contract N6ori-105, Task Order IV, September, 1947).

† In the specific example shown, the minimum SWR occurs for an electrical length very close to an exact resonant length, $5\frac{1}{4}\lambda_d$, and the value of the minimum SWR is very close to the value at the resonant length. This is the case only for an electrically long low loss sample. For a short sample, $\frac{1}{4}\lambda_d$ or $\frac{3}{4}\lambda_d$ long, the minimum SWR might be quite appreciably smaller than the value at the exact resonant length.

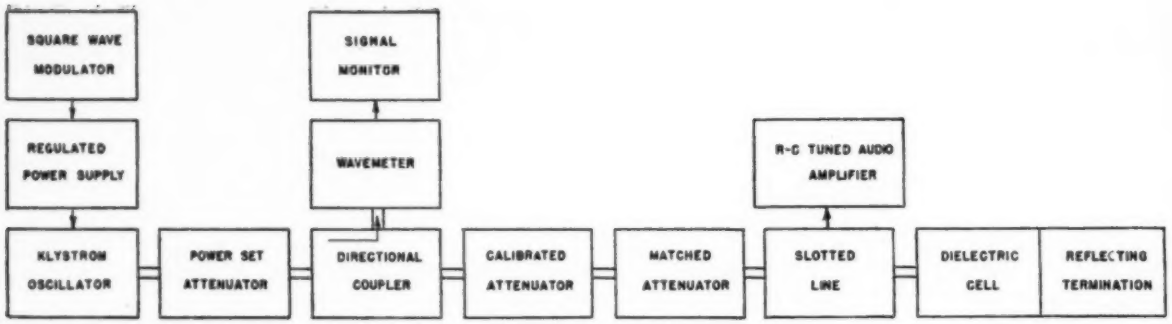

FIG. 4. Block diagram of electrical system.

L, the frequency for which it corresponds to an odd multiple of $\frac{1}{4}\lambda_d$ and the observed SWR, ρ, at that frequency. Since $L=n\lambda_d$, where n may have the values 1/4, 3/4, 5/4, $\cdots$, a multiple valued solution is possible for λ_d. To determine the correct value of λ_d, either ϵ' must be known approximately or a second measurement must be made with a different length sample. Then, as can be shown from Eqs. (1) and (1a), the exact value of ϵ' is given by the equation

$$\epsilon'=(\lambda/\lambda_c)^2+(\lambda/\lambda_d)^2\cdot[1-((\alpha_d\lambda_d)/(2\pi))^2], \quad (6)$$

where α_d is the attenuation in nepers per cm resulting from the dielectric power loss. For low loss media, this becomes

$$\epsilon'\cong(\lambda/\lambda_c)^2+(\lambda/\lambda_d)^2. \quad (6a)$$

The loss factor, ϵ'', is directly proportional to the dielectric attenuation per wave-length, and is given by the equation

$$\epsilon''=(1/\pi)(\lambda/\lambda_d)^2\cdot(\alpha_d\lambda_d). \quad (7)$$

The dielectric attenuation may be computed from the experimentally measured SWR for the resonant length, which is a function both of the total attenuation and of the per unit characteristic impedance, Z_d, of the dielectric-filled guide. Z_d may be expressed in terms of the wave-lengths, λ_d and λ_g in the dielectric- and air-filled sections of guide, respectively, by the equation:[7]

$$Z_d=|Z_d|\exp(j\phi_d), \quad (8)$$

where

$$|Z_d|=(\lambda_d/\lambda_g)\cos(\tan^{-1}\alpha_d\lambda_d/2\pi)\cong\lambda_d/\lambda_g, \quad (8a)$$

$$\phi_d=\tan^{-1}(\alpha_d\lambda_d/2\pi)\cong 0°. \quad (8b)$$

For low loss media, Z_d is approximately a pure resistance, the magnitude of which is relatively unaffected by the loss factor. The equation for the SWR, ρ, produced by a short-circuited, dielectric-filled section an odd multiple of $\frac{1}{4}\lambda_d$ in length, may then be expressed in the form:

$$1/\rho=(\lambda_g/\lambda_d)\tanh[n(\alpha_c'+\alpha_d)\lambda_d]+R_{sc}(\lambda_g/\lambda_d)^2, \quad (9)$$

where α_c' is the attenuation resulting from power loss in the walls of the section of wave guide containing the dielectric sample and R_{sc} is the per-unit resistance of the terminating plane referred to the air-filled guide. The dielectric attenuation, $\alpha_d\lambda_d$ in nepers per wave-length, computed from Eq. (9) may then be used to calculate ϵ''. The observed SWR should be corrected for losses in the air-filled wave-guide system between the dielectric cell and the slotted line probe before being inserted in this equation (see Section IV, 5).

If the electrical sample length is adjusted to be a multiple of $\frac{1}{2}\lambda_d$, then Eq. (9) should be replaced by the equation:

$$1/\rho=(\lambda_d/\lambda_g)\tanh[n(\alpha_c'+\alpha_d)\lambda_d]+R_{sc}. \quad (10)$$

In this case, the SWR obtained will be a maximum instead of near a minimum. For medium loss media, however, for which the maximum ρ is not too large to measure conveniently, this condition of operation may be desirable, since the SWR is a relatively slowly varying function in the vicinity of these $\frac{1}{2}\lambda_d$ lengths.

This type of resonance method is not applicable to high loss media for which $\tan\delta>0.1$. The phase angle, ϕ_d, of Z_d may become appreciable for these substances, so that the approximate form of Eq. (8) cannot be used. Also, the angular change in the position of the minimum

point, measured by θ, decreases as the total attenuation along the sample increases, so that it becomes difficult to determine the resonant length accurately.

IV. EXPERIMENTAL EQUIPMENT AND MEASUREMENTS

A block diagram of the electrical system is shown in Fig. 4. Two such units, both using rectangular wave guide excited in the $TE_{1,0}$ mode, were constructed, one for the 10,000-megacycle region and one for the 24,000-megacycle region. The operation of the system is apparent from the block diagram, and the experimental procedure follows the standard techniques developed for measurements in general in the microwave region.[1] The calibrated attenuator was used for SWR measurements in order to keep the operating point of the crystal and audio system constant.

The dielectric cell for the 1.25-cm unit was a standard section of $\frac{1}{2}$-in.$\times\frac{1}{4}$-in. O.D.$\times$.040-in. wall solid coin silver rectangular guide 2.06 in. long. A silver plated section of 1-in.$\times\frac{1}{2}$-in. O.D.$\times$.050-in. wall, rectangular guide 4.7 in. long and surrounded by a constant temperature bath was used for the 3.20-cm unit.

The values of the dielectric constant and loss tangent for a group of common plastics and insulators in the 24,000-megacycles region are given in Table I. These values were determined by the procedures outlined in this paper and are included to indicate the range of loss tangents which may be covered by the two methods. The correlation between the two methods may be seen by comparing data for the same materials. Measurements were made at room temperature and approximately 0 percent relative humidity except as noted.

V. SOURCES OF ERROR AND CORRECTIONS

(1) Oscillator Stabilization

The klystron oscillator used as a source should be isolated from the remainder of the system by a matched attenuating pad and should be operated from a well regulated voltage source and at thermal equilibrium in order to avoid frequency drift and changes in the power output. A high Q transmission type resonator cavity was used to continuously monitor the power output, in order to prevent any frequency change which would shift the positions of the voltage minima.

(2) SWR Measurement Errors

A certain amount of error is inherent in the precision to which very high SWR may be measured by the double minimum method, because of mechanical limitations in the design of the slotted line carriage and probe. In addition, errors in the SWR may be caused by the following effects:

(a) Frequency modulation of the source if the modulating pulses are not flat-topped or have

TABLE I. Solid dielectric measurements in the 24,000-megacycle region.

Material	Method*	λ in cm	ϵ'	tan δ
Teflon	I	1.280	2.006	0.0006
Polyethylene	I	1.233	2.17	0.0007
Polystyrene B (Lustron P2020B)	I	1.228	2.47	0.0009
Polydichlorostyrene, No. 1527-3**	I	1.245	2.55	0.0013
Polydichlorostyrene, No. 1527-10**	I	1.250	2.57	0.0023
Polydichlorostyrene, No. 1527-22**	I	1.258	2.60	0.0020
Polydichlorostyrene, No. 1527-23**	I	1.255	2.59	0.0018
Mycalex 400	I	1.264	6.49	0.0042
Mycalex 410	I	1.250	8.22	0.0042
Mica filled aniline modified phenolic (BM 262)	I	1.260	4.01	0.0129
Luctie	I	1.243	2.55	0.0071
Vinylite, VG 1800 crystal	I	1.251	2.58	0.0076
Silicone glass cloth laminate	I	1.239	3.28	0.0090
Silicone glass molding compound (Dow experimental)	I	1.238	3.47	0.0114
Plywood, (dry)	I	1.247	1.62	0.0163
	II	1.224	1.63	0.02
Plywood (52% R.H.)	I	1.234	1.74	0.063
	II	1.226	1.72	0.070
Masonite (dry)	I	1.243	2.29	0.025
Masonite (52% R.H.)	I	1.246	2.44	0.072
	II	1.250	2.40	0.075
Cellulose propionate (Forticel)	I	1.242	2.71	0.060
	II	1.253	2.69	0.068
Cellulose nitrate	I	1.253	2.79	0.082
	II	1.247	2.81	0.086
Cellulose acetate (Tenite I)	II	1.250	3.05	0.075
Cellulose acetate butyrate (Tenite II)	II	1.247	2.82	0.110
Phenolic paper laminate	I	1.277	2.94	0.045
	II	1.250	2.92	0.056
Phenolic, wood flour filled (Durez 791)	II	1.250	3.13	0.059
Phenolic, cast (Catalin, 1000 base)	I	1.237	2.35	0.037
	II	1.250	2.47	0.044
Phenolic, cast (Catalin, 500 base)	II	1.250	2.93	0.250
Melamine, α-cellulose filled (Melmac 1079) (dry)	II	1.250	4.00	0.096
Melamine, α-cellulose filled (Melmac 1079) (52% R.H.)	II	1.250	4.27	0.133

* Method *I* is the frequency variation method of obtaining a resonant length Method II is the short-circuit, open-circuit measurement method.
** Manufacturer's experimental batch numbers.

appreciable rise and decay times.[10] For a well designed modulator this effect is usually very small, and was found to be negligible for our equipment.

(b) Probe reflections resulting from excessive probe insertion. An analysis of this effect is given in reference 1.

(c) Noise level in the detector system, which may be appreciable relative to the voltage minima for high SWR. This effect may be reduced by shielding and by proper design of the receiver. Corrections for the residual noise level were included when determining the width of the double minimum.

(3) Sample Fit in Wave Guide

The dielectric sample should be fitted to the section of wave guide containing it as closely as possible. For the $TE_{1,0}$ mode in rectangular guide, the error resulting from clearance is negligible for the sides of the guide at which the electric field is zero. A correction may be applied to compensate for any clearance along the sides of the sample at which a normal electric field gradient exists.[1,11] No correction was applied for the tightly fitting samples used.

(4) Higher Mode Generation at the Dielectric

If the dielectric sample does not present a uniform plane discontinuity perpendicular to the axis of the guide, then higher modes of propagation will be set up which will introduce errors into the measured dielectric constants. If any of the higher modes are transmitted through the dielectric sample, which may be the case if ϵ' is large, then there will be a power conversion to the higher modes, and the apparent loss factor of the sample will be increased. Even if the higher modes are still beyond cut-off for the dielectric, any surface irregularity would still act effectively as a shunt admittance in parallel with the dielectric load and cause erroneous results.

The higher mode generation is a function both of the degree of departure from a plane discontinuity normal to the axis and of the amplitude of the voltage standing wave at the interface. Thus the condition for the maximum generation of higher modes occurs when the electrical sample length is adjusted so that there is a voltage maximum at the face of the sample, and the power absorption by the load is a maximum. If the irregular face of the sample were placed next to the short-circuiting plane, then the higher mode generation would be much less for the same degree of irregularity.

This effect, however, is not serious in practice since it is relatively easy to mill the sample so that there is negligible higher mode generation. Experimental tests were made on a series of samples of a medium loss material having one end tapered at angles of from 0° to 10° along the E plane and also along the H plane. For tapers less than 3°–4°, the effects on the calculated dielectric constant and loss factor were relatively small. For larger tapers, however, with the radiation incident on the tapered end of the sample, the loss tangent was considerably increased, being more than doubled for a 10° taper. With the tapered end placed next to the short-circuiting plane, the effect of the irregularity was greatly reduced. A similar investigation for imperfectly fitting coaxial samples was reported by the M.I.T. Laboratory for Insulation Research.[12]

(5) Correction of SWR for Wall Loss

The standing wave ratio measured at the probe is affected by the losses in the air-filled guide between the sample and the probe. The equivalent SWR at the face of the dielectric, ρ_e, may be found from the observed ρ, and the total attenuation between the dielectric cell and the probe, α, from the equation

$$\rho_e=\rho\left\{\frac{1-(1/\rho)\tanh\alpha}{1-\rho\tanh\alpha}\right\},$$

or

$$\frac{1}{\rho_e}\cong\frac{1}{\rho}-\alpha,$$

where

$$\alpha=\alpha_j+\alpha_{cg}+\alpha_{sg}$$

[10] M. G. Haugen and W. B. Westfall, Report XII, N.D.R.C. Contract OEMsr-191, Laboratory for Insulation Research, M.I.T.

[11] Dowker and Redheffer, Radiation Laboratory Report 483-10 (February 1945).

[12] W. B. Westphal, Report IX, Laboratory for Insulation Research M.I.T. (August, 1945).

The attenuation along the slotted section of the guide, α_{sg}, is somewhat larger than the wall loss attenuation, α_{cg}, along the unslotted guide. The junction power loss is represented by α_j in nepers, and is discussed in Appendix B. For a voltage maximum at the junction, α_j is negligibly small.

(6) Conductor Losses in Dielectric Cell

The loss in the reflecting termination for the dielectric sample must be measured experimentally and included in the equations as previously indicated.

The wall loss attenuation, α_c, must also be measured experimentally for the air-filled guide. The observed loss is found to be larger than that calculated from the specific conductivity of the metal. This effect is thought to be caused by the surface formation, i.e., small scratches or irregularities on the tube.[13] When a dielectric medium is inserted, the theoretical conductor attenuation, α_c', is a function of the dielectric constant, ϵ', and the ratio $(\alpha_c'\lambda_d/\alpha_c\lambda_g)$ may be plotted in terms of ϵ', as indicated in Appendix B. Then, using the experimental value of $\alpha_c\lambda_g$, the appropriate value of $\alpha_c'\lambda_d$ may be found from this curve for any given ϵ'. There is some doubt, however, as to whether the excess attenuation caused by the type of surface will vary in the same manner with ϵ' as in the case of an ideal surface.

(7) Conditioning of Dielectric Sample

The dielectric constants of some materials are greatly affected by their moisture content and thus depend on the humidity of the atmosphere to which they have been exposed. The test specimens were conditioned as recommended by the A.S.T.M.[14] Unless otherwise specified, samples were kept at 0 percent relative humidity within a calcium chloride desiccator. A relative humidity of 52 percent, obtained with a saturated solution of $Na_2Cr_2O_7$, was also used for certain samples as indicated.

(8) Estimated Accuracy of Measurement

For low loss media, using the resonance method, the dielectric constant, ϵ', may be determined quite accurately, within 1 percent or less, since it depends primarily on measurements of length and of frequency. For medium loss materials, this accuracy is somewhat less, within 1–3 percent by the resonance method and 2–5 percent by the short-circuit, open-circuit method.

The loss factor, ϵ'' depends on the determination of the circuit losses and on the measurement of the SWR. For the low loss materials, the estimated accuracy of the $\tan\delta$ determination with the standard equipment used is about 3–5 percent, or to within 0.0003, whichever is larger. This accuracy could be considerably improved by using a resonance method with a specially constructed slotted line instrument. For medium loss materials, the measurement of $\tan\delta$ should be within 5 percent by the resonance method and within 5–10 percent, depending on the loss region, for the short-circuit, open-circuit method.

[13] E. Maxwell, J. App. Phys. **18**, 629 (1947).
[14] A.S.T.M. Standards on Plastics, Committee D-20 (May, 1945).

APPENDIX A

Effect of Non-Ideal Terminations on Open-Circuit, Short-Circuit Measurements

For the circuits shown in Figs. (1a) and (1b), if the terminating impedances, R_{sc} and R_{oc}, are not zero and infinite, respectively, the equation for the impedance at the face of the dielectric sample may be written in the two forms:

$$Z_{sc}=Z_d(\tanh\gamma_d L+(R_{sc}/Z_d))/(1+(R_{sc}/Z_d)\tanh\gamma_d L), \quad (11a)$$

$$Z_{oc}=Z_d(\coth\gamma_d L+(Z_d/R_{oc}))/(1+(Z_d/R_{oc})\coth\gamma_d L). \quad (11b)$$

Combining these equations, expanding the result, and neglecting small quantities of the second order, the approximate equation

$$Z_{sc}\cdot Z_{oc}=Z_d^2(1+K-\cdots) \quad (12)$$

is obtained, where the first-order complex correction factor, K, is

$$K=(2/\sinh 2\gamma_d L)(R_{sc}/Z_d-Z_d/R_{oc}). \quad (13)$$

Provided the short- and open-circuit terminations are well made, K is negligibly small except in the immediate vicinity of a minimum of the "sinh $2\gamma_d L$" function. Since $\gamma_d=\alpha_d+j\beta_d$ is complex, the values of the minima of $\sinh 2\gamma_d L$, which occur for $L=n\lambda_d/4$, are determined by the total sample attenuation, $\alpha_d L$. The value of

$\alpha_d L$ will be large enough for medium and high loss dielectrics, so that K is always negligible. However, the minimum may be sufficiently small for low loss dielectrics, so that K becomes appreciable in the vicinity of certain critical electrical sample lengths. Either these critical points must be avoided, or the calculations must be modified to include the correction factor.

APPENDIX B

Equipment Losses

(1) *Wall Loss Attenuation*

The calculated and measured values of the attenuation per wave-length resulting from conductor loss in the walls of $\frac{1}{2}$-in.$\times\frac{1}{4}$-in. O.D. $\times$0.040-in. wall rectangular wave guide for the $TE_{1,0}$ mode are given in Table II for drawn

TABLE II. $\lambda = 1.25$ cm.

Wave guide	Calculated: $\alpha_c\lambda_g$ nepers	Measured: $\alpha_c\lambda_g$ nepers
Copper	0.00059	0.00091
Coin silver	0.00065	0.00094

deoxidized copper tubing and for coin silver wave guide.

The theoretical variation of $\alpha_c'\lambda_d$ relative to $\alpha_c\lambda_g$ as a function of ϵ' for a dielectric medium filling the wave guide may be obtained from the equation

$$\left(\frac{\alpha_c'\lambda_d}{\alpha_c\lambda_g}\right) = \left[\frac{\epsilon'+2(b/a)(\lambda/\lambda_c)^2}{1+2(b/a)(\lambda/\lambda_c)^2}\right]\cdot\left[\frac{1-(\lambda/\lambda_c)^2}{\epsilon'-(\lambda/\lambda_c)^2}\right], \quad (14)$$

where a, b are the dimensions of the wave guide, $a>b$, and $\lambda_c=2a$ is the cut-off wave-length for the $TE_{1,0}$ mode for $\epsilon'=1.0$.

(2) *Power Loss in Terminating Element*

The power loss in a metallic short-circuiting plane perpendicular to the axis and integral with the walls of a wave guide may be easily computed.[15] For any TE mode in a wave guide of arbitrary cross section, the per unit resistance of such a termination, R_{sc}, which may be determined either from the calculated power loss or from the characteristic impedance of the metal, is given by the equation

$$R_{sc} = (\epsilon_0/\mu_0)^{\frac{1}{2}}\cdot(\mu\omega/2\sigma)^{\frac{1}{2}}\cdot[1-(\lambda/\lambda_c)^2]^{\frac{1}{2}}. \quad (15)$$

For a silver shorting plane at 24,000 megacycles in $\frac{1}{2}$-in.$\times\frac{1}{4}$-in. O.D.$\times$0.040-in. wall wave guide, $R_{sc}=0.00085$. Assuming the same increase in effective resistivity as for the coin silver wave guide, this would become $R_{sc}\cong 0.00012$, which represents the lower limit for any actual shorting plane in this type of guide. The per unit resistence, R_{sc}, is equal to one-fourth the power attenuation in nepers at the short circuit.

The conductance of a quarter wave-length section of empty guide terminated by a short-circuit may be determined from the equation

$$G_{oc}=1/R_{oc}\cong R_{sc}+\tfrac{1}{4}\alpha_c\lambda_g.$$

The experimentally measured approximate values of R_{sc} for certain types of reflecting terminations for $\lambda=1.25$ cm were as follows:

(a) Silver plate soft-soldered to end of guide: $R_{sc}\cong 0.000$.
(b) Silver foil soft-soldered to brass plate and clamped to a flange on the guide: $R_{sc}\cong 0.000$.
(c) Choke-type plunger, copper plated, new: $R_{sc}=0.001$.
(d) Choke-type plunger, brass, old: $R_s=0.0077$.

(3) *Junction Attenuation*

In coupling two sections of wave guide, the flange-flange type of butt joint was chosen rather than the choke-flange or choke-choke joint, since it is extremely broad-banded, introduces negligible phase shift, and causes no appreciable higher mode generation. The type of flange studied experimentally in the 1.25-cm wave-length region is of an extremely simple construction, being merely a 1-in. diameter brass disk with the center portion cut out for a coin silver rectangular wave guide.

It was experimentally determined that the power loss at a flange-flange butt joint is proportional to the square of the component of current in the wave-guide walls perpendicular to the edge of the joint. This is, of course, exactly what would be expected theoretically, since it is this component of current which acts as a source for the radiation of energy down the

[15] W. H. Surber, Jr., *Microwave Dielectric Measurement Methods for Liquids and Solids*, A Dissertation presented to the Faculty of Princeton University in candidacy for the degree of Doctor of Philosophy (May, 1948).

slot between the flanges. The junction loss, α_j in nepers, may then be expressed in terms of the SWR, ρ, which exists behind the junction by the equation:[15]

$$\alpha_j = 2(\alpha_j)_1 \cdot \left[\frac{\rho^2+1}{(\rho+1)^2} + \left(\frac{\rho-1}{\rho+1} \right) \cos 2\theta' \right], \quad (16)$$

where

$(\alpha_j)_1$ = junction loss in nepers for $\rho = 1.0$,
$\theta' = 2\pi(x/\lambda_g)$ = angular distance of a voltage minimum from the junction, and
x = distance from the junction to a voltage minimum point in the line.

For $\rho \ll 1$, this reduces to the form

$$\alpha_j = 4(\alpha_j)_1 \cos^2\theta'.$$

The maximum value of the junction loss, which occurs at a voltage minimum, $\theta' = 0°$, is

$$|\alpha_j|_{\max} = 4(\alpha_j)_1(\rho/\rho+1)^2,$$

and the minimum value of the junction loss, which occurs at a voltage maximum, $\theta' = 90°$, is

$$|\alpha_j|_{\min} = 4(\alpha_j)_1(1/\rho+1)^2.$$

Curves showing the theoretical variation of the junction loss as a function of θ' are given in Fig. 5, together with experimental points determined for a high SWR behind the junction. The experimental data were taken for groups of 1, 2, 4, and 6 standard butt joints separated by one wave-length in the guide, i.e., effectively in parallel.

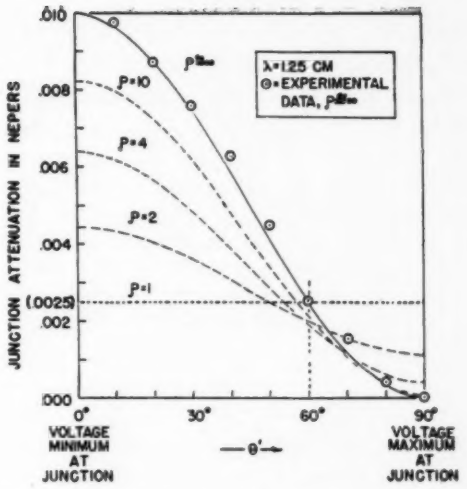

FIG. 5. Variation of wave guide junction loss *vs.* position of voltage minimum relative to junction.

For an ordinary junction of this type, connected with normal pressure, the maximum loss observed varied from 0.0080 neper to 0.0103 for an SWR of from 50 to 200 behind the junction. The mean maximum loss was about 0.010 neper for an infinite ρ, which corresponds to an $(\alpha_j)_1 = 0.0025$ neper.

By using carefully smoothed silver plated flanges tightly clamped, the maximum loss could be reduced to less than 0.001 neper.

Erratum: Twinning in Tetragonal Alloys of Copper and Manganese

[J. App. Phys. 19, 929 (1948)]

FRANCIS T. WORRELL
Institute for the Study of Metals, University of Chicago, Chicago, Illinois

AN error in our manuscript was found too late for correction in the printed *Journal*. In the first column on page 931, end of the second line, the word should be "ethyl" instead of "methyl."

Properties of a Long Antenna

ERIK HALLÉN†
Cruft Laboratory, Harvard University, Cambridge, Massachusetts
(Received May 13, 1948)

Although exact integral expressions for the outgoing current waves on a long antenna have long existed, they have never been brought in such a form that a numerical or graphical description of the wave has been possible. The author shows how to transform them into good series expansions valid for all distances from the feeding point. Graphs show the result. The traveling current waves can also be extracted from the author's expression for the current on a finite transmitting antenna published in Nova Acta Upsal, 1938. Both ways give identical series.

IN a paper some time ago, Schelkunoff[1] pointed out that it would be of interest to study certain properties of antennas with the help of an infinite antenna which is easy to treat mathematically. His own attempt cannot, however, be considered as successful and he complains over the difficulty in handling the exact integral expressions. Those difficulties can be overcome.

The idea of treating an infinite cylindrical antenna occurred to me also when I wrote my article[2] on antennas in Nova Acta Upsal 1938, and I still have from that time an unpublished paper with the short deduction of the exact integral formula which follows. It convinced me of the usefulness of an integral equation but probably did I, as Schelkunoff, resent the form of the expression. The latter is, with one small exception, the same as has long since been published by Schelkunoff[3] and by Stratton and Chu.[4] The "small exception" (which is due to a tube instead of solid cylinder) has, however, put me in a better position than Schelkunoff when it comes to useful results.

An infinite antenna does not exist. But the behavior of outgoing traveling current waves on an antenna of finite length must be the same as if it were infinite. If we have correctly determined the current on a finite antenna, which is the more difficult problem, we must necessarily be able to extract expressions for the traveling waves. In other words, the solution for the infinite antenna must be included in the solution for the finite one. This gives a good check on the more difficult problem.

For a center-fed transmitting antenna of the length $2l$ I found from my integral equation the following expression[2] for the antenna current

$$I(x)=\frac{4\pi}{\mu_0 c}V \times\frac{1}{\Omega}\frac{j\sin p(l-|x|)+\varphi_1(x)\Omega^{-1}+\varphi_2(x)\Omega^{-2}}{\cos pl+a_1\Omega^{-1}+a_2\Omega^{-2}} \quad (1)$$

where $2V$ is the feeding voltage and $\Omega=2\log 2l/\rho$ if ρ is the radius of the cross section. For tables over $\varphi_1(0)$, $\varphi_2(0)$, a_1 and a_2 see another paper by the author.[5] Recurrence formulas for higher terms in the two series in numerator and denominator were also given. In two other papers[6,7] I have pointed out the two possibilities of varying the outward form of (1), one consisting in expanding in powers of $(\Omega-\Delta)^{-1}$ instead of Ω^{-1}, the other in multiplying numerator and denominator term by term by a series $1+\mu_1\Omega^{-1}+\mu_2\Omega^{-2}$. In whatever way we solve the integral equation correctly by iteration, we always come to a form within this group. Schelkunoff's[3] im-

† Now at the Royal Institute of Technology, Stockholm, Sweden.

[1] S. A. Schelkunoff, "Concerning Hallén's Integral Equation for Cylindrical Antennas," Proc. I.R.E. **33**, 873, 876 (1945).

[2] E. Hallén, "Theoretical Investigations into the Transmitting and Receiving Qualities of Antennae," Nova Acta Upsal (4) **11**, 10, 14, 15, 21 (1938).

[3] S. A. Schelkunoff, "Theory of antennas of arbitrary size and shape," Proc. I.R.E. **29**, 501, 509, 510, 520 (1941).

[4] J. A. Stratton and L. J. Chu, "Steady-state solutions of electromagnetic field problems," J. App. Phys. **12**, 233 (1941).

[5] E. Hallén, "On antenna impedances," Trans. Roy. Inst. Tech. (Stockholm, 1947) No. 13.

[6] E. Hallén, "Über die elektrischen Schwingungen in drahtförmigen Leitern," Arsskrift, Uppsala **1**, 8, 22–23, 47–53 (1930).

[7] E. Hallén, "Further investigations into the receiving qualities of antennae: the absorption of transient unperiodic radiation," Arsskrift, Uppsala **4**, 6–8, 15 (1939).

pedance formulas—for $x=0$—belong to the group. Even in Miss Gray's[8] and King's and Middleton's[9] papers appear variations of (1) which belong to the group though they have added minor arbitrary approximations which destroy the analytical character of (1). They have, however, been unaware of my previous discussion and forgotten the second of the two possibilities mentioned which makes their results arbitrary. In these authors' papers appear curves which are ascribed to my formula but which do not at all agree with it.[10]

The way to extract the traveling waves is to use the two mentioned variations to create a denominator of the type $1+ke^{-j2pl}$ where k is an aperiodic series in Ω^{-1}. The result[11] which first was made public in a lecture,* is a series of current waves I_n which, if starting in direction of positive x after n reflections have the form

$$I_n(x)=\pm\frac{4\pi}{\mu_0 c}Vk_0(l)k_l(2l)\times k_{2l}{}^{n-2}(2l)\psi_{2l}(2p(l\pm x))e^{-jp(2nl\pm x)}$$

where for the outgoing, the once and the twice reflected waves we have to substitute the middle factor by respectively ψ_0, $k_0(l)\psi_l$, $k_0(l)k_l(2l)\psi_{2l}$. All the ψ:s and k:s are the same functions of two parameters, one of which is shown as an index. Thus $k_0(0)=1$. Expecially the outgoing wave, which will occupy us here is

$$I(x)=\frac{4\pi}{\mu_0 c}V\psi(2p|x|)e^{-jp|x|} \tag{2}$$

where the complex amplitude function ψ for positive x is

$$\psi(2px)=\Omega_x{}^{-1}+\Omega_x{}^{-3}\left[2\,\mathbf{l}^{11}2px-\mathbf{l}^{2}2px-\frac{\pi^2}{6}\right] \tag{3}$$

and

$$\Omega_x=2\log\frac{1}{\gamma_1 p\rho}+\mathbf{l}_0 2px+\mathbf{l}2px-j\pi$$

$$=\log\frac{\lambda x}{\pi\rho^2}-\gamma+\mathbf{l}2px-j\frac{\pi}{2} \tag{4}$$

$$\mathbf{l}_0 z=\log\gamma_1 z+j\frac{\pi}{2} \tag{5}$$

$$\gamma=\log\gamma_1=0.577215.$$

$\mathbf{l}z$ and $\mathbf{l}^{11}z$ are aperiodic amplitude functions associated with sine and cosine integrals and iterated sine and cosine integrals, to be given below. They have been tabulated.[12,13] For $z=0$ we have $\mathbf{l}_0 z+\mathbf{l}z=0$ and $2\,\mathbf{l}^{11}z-\mathbf{l}^2 z-\pi^2/6=\pi^2/3$. For great z both $\mathbf{l}$ and $\mathbf{l}^{11}$ vanish as $1/z$. The amplitude function ψ is shown in Fig. 1 for $\lambda/\rho=1000$. Figure 2 shows the phase angle between the current wave and the potential wave and the phase velocity of the current wave. The potential wave has constant amplitude[2,7] and travels with ve-

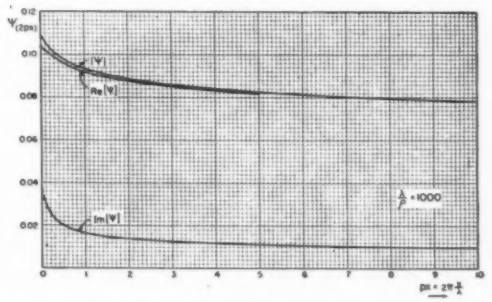

FIG. 1. Amplitude function for outgoing current wave on antenna.

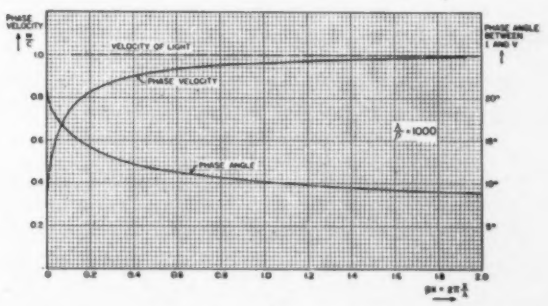

FIG. 2. Phase angle between current and potential. Phase velocity for outgoing wave on antenna.

[8] M. Gray, "A modification of Hallén's solution of the antenna problem," J. App. Phys. **15**, 61 (1944).

[9] R. King and D. Middleton, "The cylindrical antenna, current and impedance," Quart. Appl. Math. **3**, 302 (1946).

[10] E. Hallén, "Admittance diagrams for antennas and the relation between antenna theories," Cruft Laboratory Technical Report **46** (1948).

[11] E. Hallén, "Travelling waves and unsymmetrically-fed antennas," Cruft Laboratory Technical Report **49** (1948).

* Physics and Applied Science Colloquium, Harvard, April 12, 1948.

[12] E. Hallén, "Iterated sine and cosine integrals," Trans. Roy. Inst. Tech. (Stockholm, 1947) No. 12.

[13] E. Hallén, "Further investigations into iterated sine and cosine integrals and their amplitude functions" (to be published).

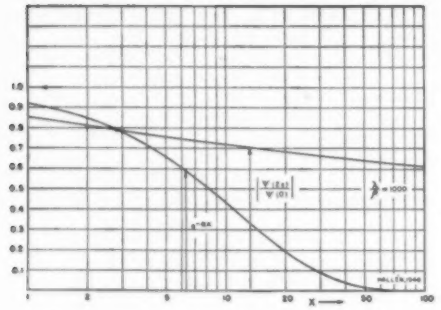

FIG. 3. Comparison between antenna wave amplitude and exponential. Intersection points $X=0$ and $X=2.8$ radians (arbitrary).

locity of light. Figure 3 shows the great difference between ψ and an exponential.

This is the way I first found a useful expression for ψ. It has not been numerically or graphically described before.

We now turn to the exact integral expression. For a perfect conductor with rotational symmetry there are two equivalent simple methods of getting an exact integral equation with the help of the retarded potentials. Both have been used by the author.[2,6,14] One expresses for a solid conductor that the electric field, created by the currents and charges on the surface of the conductor, along its axis is equal to zero, the other that the tangential component of the field in the surface is zero. The former method needs only one coordinate and gives[2,6] for a solid conductor

$$\frac{\partial}{\partial x}\int\frac{\dfrac{dI}{d\xi}e^{-jpr}}{r}d\xi+p^2\int\frac{I(\xi)e^{-jpr}}{r}d\xi=0 \qquad (6)$$

where $r=((x-\xi)^2+\rho^2(\xi))^{\frac{1}{2}}$. The other gives for a circular infinite tube of constant radius ρ

$$\int_{-\infty}^{\infty}I(\xi)d\xi\frac{1}{2\pi}\int_0^{2\pi}\frac{e^{-jpr}}{r}d\varphi=\frac{4\pi}{\mu_0 c}Ve^{-jp|x|} \qquad (7)$$

where $r=((x-\xi)^2+4\rho^2\sin^2\frac{1}{2}\varphi)^{\frac{1}{2}}$ and $2V$ as before the voltage across an infinitely small gap. The Eq. (7) can also be found in a paper by Schelkunoff.[1] Singularly enough he stated[1,15] that only (7) but not (6) should be mathematically exact, which is a mistake. He has mistaken my location of the current which is on the surface of the conductor if this is a perfect one. Here we use, however, the tube equation (7). Dissolving the kernel of (7) in a Fourier integral we get

$$\frac{1}{2\pi}\int_0^{2\pi}\frac{e^{-jpr}}{r}d\varphi$$

$$=\frac{1}{2\pi}\int_{-\infty}^{\infty}e^{j\alpha(x-\xi)}2I_0(\rho(\alpha^2-p^2)^{\frac{1}{2}})K_0(\rho(\alpha^2-p^2)^{\frac{1}{2}})d\alpha$$

where, in Watson's notation, I_0 and K_0 are Bessel functions. Between $\alpha=-p$ and $\alpha=p$ the values $I_0(jz)=J_0(z)$, $K_0(jz)=-j(\pi/2)H_0^{(2)}(z)$ should be taken. Further is

$$e^{-jp|x|}=\frac{j}{2\pi}\int_\Gamma\frac{2p}{\alpha^2-p^2}e^{j\alpha x}d\alpha$$

where Γ is a contour in the complex plane shown in Fig. 4. Consequently (7) takes the form

$$\frac{1}{2\pi}\int_{-\infty}^{\infty}I(\xi)d\xi\int_\Gamma e^{j\alpha(x-\xi)}2I_0K_0(\rho(\alpha^2-p^2)^{\frac{1}{2}})d\alpha$$

$$=\frac{4\pi}{\mu_0 c}V\frac{j}{2\pi}\int_\Gamma\frac{2p}{\alpha^2-p^2}e^{j\alpha x}d\alpha$$

where I_0 and K_0 have real positive values outside $-p/p$. For great α the product I_0K_0 approaches $1/2\rho(\alpha^2-p^2)^{\frac{1}{2}}$. We conclude

$$\int_{-\infty}^{\infty}I(\xi)e^{-j\alpha\xi}d\xi=\frac{4\pi}{\mu_0 c}Vj\frac{p}{(\alpha^2-p^2)I_0K_0(\rho(\alpha^2-p^2)^{\frac{1}{2}})},$$

$$I(x)=\frac{4\pi}{\mu_0 c}V\frac{j}{2\pi}\int_\Gamma\frac{e^{j\alpha x}pd\alpha}{(\alpha^2-p^2)I_0K_0(\rho(\alpha^2-p^2)^{\frac{1}{2}})}.$$

The sign in the exponential can apparently be changed and if we put $\alpha=p\beta$ we get the following exact expression for the outgoing current wave

$$I(x)=\frac{4\pi}{\mu_0 c}V\frac{j}{2\pi}\int_{\Gamma_1}\frac{e^{-ip\beta x}d\beta}{(\beta^2-1)I_0K_0(p\rho(\beta^2-1)^{\frac{1}{2}})} \qquad (8)$$

where Γ_1 avoids ±1 in the same way as Γ avoids $\pm p$.

[14] E. Hallén, "Lösung zweier Potentialprobleme der Elektrostatik," Arkiv f. Mat., Astr. och Fysik **21A**, 32 (1929).

[15] S. A. Schelkunoff, "Principal and complementary waves in antennas," Proc. I.R.E. **34**, 1 (1946).

As

$$\frac{1}{(\beta^2-1)I_0K_0(p\rho(\beta^2-1)^{\frac{1}{2}})} = \frac{p\rho}{(\beta^2-1)^{\frac{1}{2}}}\left(\frac{K_1}{K_0}-\frac{I_1}{I_0}\right)_{p\rho(\beta^2-1)^{\frac{1}{2}}}$$

we can divide (8) into two terms, one containing Hankels functions, the other Bessel functions. Those two terms in reality represent one solution for the outer problem (solid cylinder) and one solution for the inner guided waves. As we only consider the case when $\rho/\lambda \ll 1$ the latter term is negligible. The term containing Hankel functions is the solution of Schelkunoff[3] equation (163) and of Stratton and Chu[4] Eq. (14). An integration over a distributed emf can immediately be carried out and does not constitute anything essential. Stratton and Chu have, however, even the ohmic resistance.

We add to (8) the complex conjugate of $I(x)$, in which the integration path avoids ± 1 on the other side, and reverse the direction of integration. Thus, we find the real part of $I(x)$

$$\mathrm{Re}[I(x)] = \frac{4\pi}{\mu_0 c} V \frac{j}{4\pi} \times \int_{\Gamma_2} \frac{e^{-i\beta px}d\beta}{(\beta^2-1)I_0K_0(p\rho(\beta^2-1)^{\frac{1}{2}})} \quad (9)$$

where Γ_2 is the contour Fig. 5. As here β is finite and $p\rho \ll 1$ we can substitute

$$I_0K_0 = \tfrac{1}{2}\Omega_{0r} - \tfrac{1}{2}\log\frac{\beta^2-1}{4}$$

where

$$\Omega_{0r} = 2\log\frac{1}{\gamma_1 p\rho} = 2\log\frac{\lambda}{\gamma_1 2\pi\rho}$$

which is the real part of (4) for $x=0$. Thus,

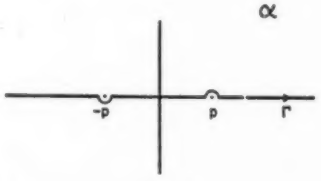

FIG. 4.

expanding the denominator in power series of Ω_{0r}^{-1} we find

$$\mathrm{Re}[I(x)] = \frac{4\pi}{\mu_0 c} V \sum_{n=0}^{\infty} \Omega_{0r}^{-n-1} \frac{j}{2\pi}\int_{\Gamma_2} e^{-i\beta px}\frac{\log^n\frac{\beta^2-1}{4}}{\beta^2-1}d\beta$$

where we have neglected terms of the order of magnitude $(\rho/\lambda)^2$ in the exact expression (9). The series converges for sufficient great Ω_{0r}. We write

$$\frac{j}{2\pi}\int_{\Gamma_2} e^{-i\beta px}\frac{\log^n\frac{\beta^2-1}{4}}{\beta^2-1}d\beta = A_n + B_n$$

where

$$A_n = e^{-ipx}\frac{j}{4\pi}\int_{\Gamma_2}\frac{\log^n\frac{\beta^2-1}{4}}{\beta-1}d\beta - e^{ipx}\frac{j}{4\pi}\int_{\Gamma_2}\frac{\log^n\frac{\beta^2-1}{4}}{\beta+1}d\beta,$$

$$B_n = -e^{-ipx}\frac{j}{4\pi}\int_{\Gamma_2}\frac{1-e^{-j(\beta-1)px}}{\beta-1}\log^n\frac{\beta^2-1}{4}d\beta + e^{ipx}\frac{j}{4\pi}\int_{\Gamma_2}\frac{1-e^{-j(\beta+1)px}}{\beta+1}\log^n\frac{\beta^2-1}{4}d\beta.$$

We must start the integrations in the same point of the loop. We find without difficulty

$$A_0 = \cos px$$
$$A_1 = 0$$
$$A_2 = -\tfrac{2}{3}\pi^2\cos px.$$

For B_n we observe that it vanishes for $x=0$ and that dB_n/dx can be expressed with the help of

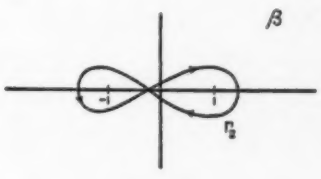

FIG. 5.

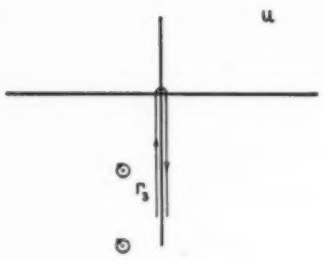

FIG. 6.

B_{n-1}. Thus, by recurrence we get

$$B_0=0$$

$$B_1=-\tfrac{1}{2}[e^{-ipz}\mathrm{L}^*2px+e^{ipz}\mathrm{L}2px]$$

$$B_2=e^{-ipz}[\mathrm{L}^{01}*2px-\mathrm{L}^{11}2px]+e^{ipz}[\mathrm{L}^{01}2px-\mathrm{L}^{11}*2px]$$

where for $z>0$

$$\mathrm{L}z=\int_0^z\frac{1-e^{-i\xi}}{\xi}d\xi=\mathrm{l}_0z+e^{-iz}\mathrm{l}z$$

$$\mathrm{L}^{01}z=\int_0^z\frac{\mathrm{L}\xi}{\xi}d\xi=\tfrac{1}{2}\mathrm{l}_0{}^2z+\frac{\pi^2}{12}-e^{-iz}\mathrm{l}^{01}z$$

$$\mathrm{L}^{11}z=\int_0^z\frac{e^{i\xi}\mathrm{L}\xi}{\xi}d\xi=\mathrm{L}^{01}*z-\mathrm{L}^*z\,\mathrm{l}_0z+\tfrac{1}{2}\mathrm{l}_0{}^2z+\frac{\pi^2}{4}-\mathrm{l}^{11}z$$

$$\mathrm{l}z=\int_0^\infty\frac{e^{-juz}}{1+u}du$$

$$\mathrm{l}^{01}z=\int_0^\infty\frac{\log(1+u)}{1+u}e^{-juz}du$$

$$\mathrm{l}^{11}z=\int_0^\infty\frac{\log(1+u)}{u}e^{-juz}du.$$

Introducing the amplitude functions l, l^{01}, l^{11} we find for the terms in our series expressions the form $e^{-ipz}f(x)+e^{ipz}g(x)$. If we change the sign of j in the latter we can write

$$\mathrm{Re}[I(x)]=\frac{4\pi}{\mu_0 c}V\,\mathrm{Re}[\psi(2p|x|)e^{-ip|x|}],$$

where for positive x

$$\psi(2px)=\Omega_{0r}{}^{-1}-\Omega_{0r}{}^{-2}[\mathrm{l}_02px+\mathrm{l}2px-j\pi]+\Omega_{0r}{}^{-3}\left[(\mathrm{l}_02px+\mathrm{l}2px-j\pi)^2+2\,\mathrm{l}^{11}2px-\mathrm{l}^2 2px-\frac{\pi^2}{6}\right].$$

If we expand this series in terms of $\Omega_x{}^{-1}$ instead of $\Omega_{0r}{}^{-1}$ we regain (3). We have thus in reality found not only the real part but even the imaginary part of (2). The latter, however, without proof. Apparently the real part of (2), found by iteration of an integral equation is for sufficient big Ω an analytical solution.

In order to be able to discuss the best value of the expansion parameter and to make sure that the imaginary part of $I(x)$ is correct we must however study even (8), which we write

$$I(x)=\frac{4\pi}{\mu_0 c}V\psi_0(2p|x|)e^{-ip|x|},$$

where

$$\psi_0(2p|x|)=\frac{j}{2\pi}\int_{\Gamma_1}\frac{e^{-i(\beta-1)p|x|}d\beta}{(\beta^2-1)I_0K_0(p\rho(\beta^2-1)^{\frac{1}{2}})}\qquad(10)$$

is the exact value of ψ, the index used to distinguish it from the series (3). Putting for positive x $(\beta-1)px=u$ we get, because $p=2\pi/\lambda$

$$\psi_0(2px)=\frac{j}{2\pi}\int_{\Gamma_3}\frac{e^{-iu}du}{u\left(1+\dfrac{u}{2px}\right)2I_0K_0\left(2\left(\dfrac{\pi\rho^2}{\lambda x}\right)^{\frac{1}{2}}\left(u\left(1+\dfrac{u}{2px}\right)\right)^{\frac{1}{2}}\right)}$$

where Γ_3 consists of an infinite number of circles around the zeros of I_0 and a double line along the negative imaginary axis encircling the origin in negative direction (Fig. 6). For great values of λ/ρ and x we may still substitute I_0K_0 by a logarithm. Thus

$$2I_0K_0=\log\frac{\lambda x}{\gamma_1{}^2\pi\rho^2u\left(1+\dfrac{u}{2px}\right)}=\log\frac{\lambda x}{\gamma_1\pi\rho^2}-\frac{\pi}{2}-\log\left[\gamma_1 ue^{-i\pi/2}\left(1+\frac{u}{2px}\right)\right].$$

We then get

$$\frac{1}{2I_0K_0}=\sum_{n=0}^{(\infty)}\Omega'^{-n-1}{}_x\log^n\left[\gamma_1 u e^{-j\pi/2}\left(1+\frac{u}{2px}\right)\right],$$

where $\Omega_x'=\Omega_x-1|2px$. It is easily seen that we cannot dispose over x in any other way if the terms are to be kept small for very great x. The factor $e^{-j(\pi/2)}$ within the logarithm ensures symmetry with respect to the imaginary axis and keeps the imaginary part of the logarithm as small as possible. The factor γ_1 is not motivated until we have carried out the integration.

The poles give only a negligible contribution. The series expansion is valid only up to a certain great value of $|u|$ but on account of the exponential we may extend the integration up to $u=-j\infty$. The result is that instead of (10) we get

$$\psi(2px)=\sum_{n=0}^{(\infty)}\Omega_x'^{-n-1}C_n, \qquad (11)$$

where we find C_n by carrying out the complex integration along Γ_3 term by term and use the relations

$$\int_0^1\frac{du}{u}\left[1-\exp\left(-j\frac{u}{\gamma_1}\right)\right]-\int_1^\infty\frac{du}{u}\exp\left(-j\frac{u}{\gamma_1}\right)=j\frac{\pi}{2}$$

$$\int_0^1 du\frac{\log u}{u}\left[1-\exp\left(-j\frac{u}{\gamma_1}\right)\right]-\int_1^\infty du\frac{\log u}{u}\exp\left(-j\frac{u}{\gamma_1}\right)=\frac{\pi^2}{24}$$

$$1^{01}z+1_0z1z+\int_0^\infty\frac{\log u}{1+u}e^{-jzu}du=0$$

the latter of which is a functional equation between our amplitude functions. I have only found a rather tedious proof for it. Thus, I find

$$C_0=1$$

$$C_1=-1|2px$$

$$C_2=2\,1^{11}|2px-\frac{\pi^2}{6}$$

and consequently,

$$\psi(2px)=\Omega_x'^{-1}-\Omega_x'^{-2}1|2px+\Omega_x'^{-3}\left(2\,1^{11}|2px-\frac{\pi^2}{6}\right). \qquad (12)$$

The expression (11) represents ψ_0 with an accuracy which neglects terms of the order of magnitude $\rho^2/\lambda|x|$. For smaller values of $|x|$ (but not $x=0$) we may use the same integration path but another expansion parameter, for which we may chose Ω_0. We need not repeat the calculation. Now $1z$ vanishes as $1/z$ for great z-values and 1_0z+1z vanishes for $z=0$. The common expansion parameter Ω_z, Eq. (4), which we have formerly found in a natural way from the old iteration solution of the linearized integral equation, is thus here justified both for great and small values of x. Expanding (12) in power series of Ω_z^{-1} instead of $\Omega'^{-1}{}_x$ we immediately get (3). The integration path Γ_3 has thus directly led to an expression in terms of the associated amplitude functions 1 and 1^{11}.

I have even determined the fourth term in (3) which is

$$\Omega_x^{-4}\left(-6\,1^{111}|2px+6|2px|1^{11}|2px-2\,1^3|2px-2\sum_1^\infty\frac{1}{n^3}\right)$$

where

$$\sum_1^\infty\frac{1}{n^3}=1.2020569$$

and 1^{111} is an amplitude function associated with iterated sine integrals of the third order

$$1^{111}z=\int_0^\infty\frac{e^{-jzu}}{1+u}du\int_0^u\frac{\log(1+\xi)}{\xi}d\xi.$$

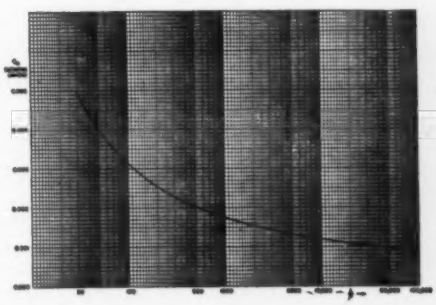

FIG. 7. Wave conductance of cylindrical antenna.

The complex integral along the infinite path Γ_3 is, however, very laborious and several new functional equations appear, whereas the whole term comes out quite easily when we use the loop Γ_2 for determining the real part of $I(x)$. For iterated sine integrals and their amplitude functions see two other papers by the author.[12,13]

There remains the value $x=0$ and its immediate neighborhood. In that case equation (10) gives for $\psi_0 e^{-jp|x|}$ a finite term plus

$$\frac{j}{2\pi}2p\rho\int_{\Gamma_1}\frac{e^{-j\beta p|x|}d\beta}{(\beta^2-1)^{\frac{1}{2}}}=p\rho H_0^{(2)}(p|x|)$$

which has a logarithmically infinite imaginary part for $x=0$. The exact value of the real part of $\psi_0(2p|x|)e^{-jp|x|}$ remains finite and can be computed from (9). For $x=0$ I find from (9) *the wave conductance* of an antenna, i.e., the input conductance of an infinite antenna

$$G_0=\frac{\mathrm{Re}[I(0)]}{2V}=\frac{1}{60}\left\{\frac{1}{\pi}\operatorname{arctg}\frac{\pi}{\Omega_{0r}}+\int_0^1\frac{du}{u}\frac{\log(1-u)[2\Omega_{0r}-2\log u-\log(1-u)]}{[\pi^2+(\Omega_{0r}-\log u(1-u))^2][\pi^2+(\Omega_{0r}-\log u)^2]}\right.$$
$$\left.+4\pi^2\left(\frac{\rho}{\lambda}\right)^2\int_0^1\frac{\pi^2+[\Omega_{0r}+\log 4-\log(1-u^2)]^2+2\Omega_{0r}+2\log 4-2\log(1-u^2)}{[\pi^2+(\Omega_{0r}+\log 4-\log(1-u^2))^2]^2}du\right\} \quad (13)$$

where the last term is only about 1 percent even down to $\lambda/\rho=20$, when our series expansion in terms of Ω^{-1} is no more valid. The first term alone is a rather good approximate value.

The expression is correct with the exception of terms of the order of magnitude $(\rho/\lambda)^4$. The integrands remain finite and I find from 13 the value shown in Fig. 7 for the region through which Schelkunoff[3] has drawn only an extrapolated curve given in a very small scale. He gives his function in his Fig. 21 as input impedance. This is wrong. It ought to be inverted value of the input conductance. The input impedance is smaller.

For the imaginary part of the current (2,3) give a finite value even for $x=0$. The determining of the currents created by a finite voltage jump across an infinitely small gap is the fundamental problem in antenna theory as well as in all other circuit theory. From that starting point every other problem can be solved. The solution belonging to a distributed enforced emf or external electromagnetic field is created by exchanging $2V$ against $E(\xi)d\xi$ and x against $x-\xi$ and integration with respect to ξ, if $E(\xi)$ is the electrical field component in the direction of the antenna. It is in that case no inconvenience that the exact expression (8) has a logarithmical singularity at $x=0$. But if the final result, as is most likely, must be expanded in terms of some parameter to be made useful, it is of course equally correct and much simpler to start from a finite series expansion (3).

It is when we consider a transmitting antenna fed in some way in a "point" that differences arise. Then the "exact" solution (10) is useless because it gives an infinite input susceptance. The infinitely small gap is then an absurdity. The series, however, gives with a finite number of terms, which at first rapidly decrease, a finite value of the wave susceptance. This is a kind of extrapolated value. For a sufficiently thin antenna this value is well determined. For fatter antennas there is a latitude of undeterminedness. It is necessary to use a correction term, a "positive or negative parallel base capacitance." As the vector potential in a finite gap has a component in the direction of the antenna, there is no mathematically exact definition of the input impedance of the antenna proper, the impedance must then be referred to a point in the feeding line. With an emf distributed over a certain interval Δ of an antenna without a gap, one can, of course, define an admittance of the antenna proper which will then depend upon Δ. For sufficiently thin antennas this impedance will seemingly tend to an extrapolated limit when Δ decreases.

It is possible to show that the imaginary part of (3) for $x=0$ forms a series, whose terms finally diverge. Thus even in this respect the series (3) behaves as the exact expression (10). But in general the terms of the series (3) decrease very rapidly. The vicinity of $x=0$ is the only exception.

In Schelkunoff's[16] discussion of the feeding gap from practical point of view, which otherwise is quite good, he has tried to use the necessary undeterminedness in the input susceptance to make my theory suspicious. As I have shown in another place[10] the terms in his impedance expressions are not analytically different from the terms of corresponding order in my expression. His accusations are for this reason meaningless. But, in addition, I, unlike Schelkunoff, determined the current in any point and the value in an exceptional point does not afflict the solution as such.

Using the same Fourier expansion as before we get for a finite, cylindrical, center-fed antenna instead of (7) the exact equation

$$\frac{1}{2\pi}\int_\Gamma 2I_0K_0(\rho(\alpha^2-p^2)^{\frac{1}{2}})e^{j\alpha z}d\alpha\int_{-l}^{l}I(\xi)e^{-j\alpha\xi}d\xi = -j\frac{4\pi}{\mu_0 c}(V\sin p|x|+A\cos px).$$

If we here substitute

$$2\log\frac{2}{\gamma_1\rho(\alpha^2-p^2)^{\frac{1}{2}}}=\Omega+\log\frac{1}{\gamma_1^2l^2(\alpha^2-\epsilon^2)}+\log\frac{\alpha^2-\epsilon^2}{\alpha^2-p^2}$$

for $2I_0K_0$ and carry out the integration with respect to α we get after passing to limit $\epsilon\to 0$

$$\Omega I(x)+I(x)\log\frac{l^2-x^2}{l^2}+\int_{-l}^{l}\frac{I(\xi)e^{-jp|x-\xi|}-I(x)}{|x-\xi|}d\xi = -j\frac{4\pi}{\mu_0 c}(V\sin p|x|+A\cos px). \quad (14)$$

This is my linearized integral equation[2] in this special case. As ρ is small the substitution means that we have replaced the most high frequent of the Fourier components by other. Thereby we violate the shape only in regions with extreme curvature. We have got an equation where the radius has disappeared except in the parameter Ω. As the current must be continuous we still keep an accuracy of the order of magnitude $(\rho/l)^2$. There is no special elegance in postponing this normal and necessary technical "approximation" to a later stage. When Schelkunoff incessantly repeats "approximate integral equation" he ought to add "approximate" to practically every equation in electrotechnics. His own efforts in antenna theory are much more approximate.

Most of my successors have hesitated to use the logical form $\log(l^2-x^2/l^2)$ in the second term of (14) and substituted it by some finite but still approximate factor. This is not only less consistent and more complicated, it is even less accurate. I have invented the integral equation, (14), under much more general conditions, and the method of solving it with the intention to simplify and yet keep the same accuracy as is usual concerning all kinds of electrical equations related to wires. My iteration method and perhaps even the integral equation itself have apparently been misunderstood as some sort of arbitrary approximation. This comparison with an exact formula for outgoing waves may help to bring about a correct conception.

Long ago Pocklington,[17] Rayleigh,[18] and Oseen[19] succeeded in extracting some rather approximate results concerning free oscillations in wires from integro-differential equations derived from retarded potentials. A consistently built, analytically solvable integral equation, of which (14) is a special case, is quite another thing. For a point on the axis outside the antenna of revolution, the right side of the exact integral Eq. (6) has to be changed into $4\pi jpE/\mu_0 c$. The Eqs. (3.16) and (5.10) in the recent papers of Albert and Synge[20] and Synge[21] are identical with this old equation in my papers (reference 2, p. 10, and reference 6, p. 8, 10). (In their Eq. (5.10) V/η should be changed into $-2E$). Since Albert and Synge[20] (footnote 2) refer to my equations as "less exact" than their equation (3.16), they have apparently not been aware of the identity.

[16] S. A. Schelkunoff, "Antenna theory and experiment," J. App. Phys. **15**, 56, 60 (1944).

[17] H. C. Pocklington, Proc. Camb. Phil. Soc. **9**, 324 (1897).

[18] Lord Rayleigh, Physik. Zeits. **13**, 842 (1912).

[19] C. W. Oseen, Arkiv f. Mat., Astr. och Fys. **9**, No. 30 (1914).

[20] G. E. Albert and J L. Synge, "The general problem of antenna radiation and the fundamental integral equation, with application to an antenna of revolution—part I." Quart. App. Math. **6**, 117 (1948).

[21] J. L. Synge, "—Part II," Quart. App. Math. **6**, 133 (1948).

The Dissipation of Heat by Free Convection from Vertical and Horizontal Cylinders

W. ELENBAAS
Physical Laboratory of the Lighting Department of N. V. Philips' Gloeilampen fabrieken, Eindhoven, Holland
(Received May 21, 1948)

This paper gives a simpler deduction of formulas given previously [W. Elenbaas, Physica 9, 285, 665, (1942)] for the dissipation of heat of horizontal and vertical cylinders with natural cooling.

SYMBOLS

Index w means that the magnitude must be taken at the wall temperature.
Index $\sim$ means that the magnitude must be taken at the ambient temperature.
Index m means that the mean of the quantity in the interval $T_w - T_\sim$ must be taken, for instance:

$$\lambda_m = \frac{1}{T_w - T_\sim} \int_{T_\sim}^{T_w} \lambda(T) dT.$$

$\mathrm{Nu} = \alpha l/\lambda$ = Nusselt's number.
$\mathrm{Gr} = l^3 g \rho^2 \beta \theta_w / \eta^2$ = Grashof's number.
$\mathrm{Pr} = C_p \eta / \lambda$ = Prandtl's number
α = coefficient of heat transfer = average heat dissipation per unit of surface, per unit of time and per unit of temperature difference.
β = cubic expansion coefficient of the surrounding medium. For gases $\beta = 1/T_\sim$.
b = outside diameter of the Langmuir layer around a cylinder.
C_p = specific heat of the surrounding medium at a constant pressure.
d = cylinder diameter.
$e = 2.7183\cdots$.
η = viscosity of the surrounding medium.
g = acceleration of gravity.
h = height of the vertical cylinder.
λ = heat conductivity of the surrounding medium.
l = determining linear dimension of similar bodies.
ρ = density of the medium.
r = distance between a given point in the medium and the cylinder axis.
R = cylinder radius.
θ = difference in temperature from remote points in the medium ($\theta = T - T_\sim$).
T = temperature in °K.
Φ = heat transfer by conduction and convection per sec. per cm of cylinder length.

I. INTRODUCTION

THE dissipation of heat of wires with natural cooling has been studied frequently in connection with its importance in the manufacture of incandescent lamps. This is because lamp filaments originally heated in a vacuum, were later, in order to reduce evaporation, made to burn in a gaseous atmosphere. However, this has the disadvantage that part of the energy supplied is lost by conduction and convection. With a view to improving the construction of the incandescent lamp it was, therefore, of importance to know the magnitude of the heat dissipation as a function of the determining factors (wire diameter and wire temperature, the position of the filament, the nature and the pressure of the gas). It was in this connection that Langmuir[1] made his well-known experiments, which revealed the remarkable fact that with very small wire diameters, the loss of heat per cm of length is practically independent of the diameter. This led to the practice of coiling the filament, resulting in a considerable reduction of length and consequently of the loss of heat by convection.

Langmuir was able to explain the heat dissipation of thin wires as a function of the diameter by assuming the following:

1. Around the wire there is a layer wherein the gas is stagnant and the entire temperature difference from the surroundings is located. Thus the transport of heat in the layer takes place exclusively by conduction.
2. On the outside of this layer the temperature gradient is independent of the wire diameter (δ in Fig. 2 independent of d).

We can interpret these assumptions in some measure as follows:

(1) On the surface, the velocity of flow is zero, and since the viscosity increases with the temperature, the flow is also impeded close to the wire, while, in addition, the conduction of heat in the proximity of the wire is large owing to the increase in the coefficient of heat conduction with the increasing temperature. Therefore it is in the immediate vicinity of the wire that the transport of heat mainly takes place by conduction.

[1] I. Langmuir, Phys. Rev. **34**, 401 (1912).

Further, a laminar flow round the wire will have but little influence on the *radial* heat flow.

(2) The cylindrical outer surface of the layer is considered to be the boundary between the laminar flow inside the layer and the turbulent flow outside the layer. This boundary will therefore occur where a particular dT/dr is obtained, independently of the wire diameter. Owing to the turbulent flow outside the layer the temperature of the surroundings will prevail there. So the value of dT/dr on the outer surface of the layer may depend on several factors influencing the flow (the nature and the pressure of the gas, the acceleration resulting from gravity, the ambient temperature), but not on the wire diameter, since the curvature of the surface plays no part.

The cooling of bodies is determined by the state of flow of the surrounding medium. With natural cooling this state of flow is the result of the temperature difference in the medium, and causes the warmer and consequently lighter parts of the medium to rise. From the differential equations determining this flow and the balance of energy, Nusselt[2] deduced that for similar bodies in a certain gas the value $\alpha l/\lambda$ is a function of $l^3 g\rho^2\beta\theta_w/\eta^2$, the shape of this function depending on that of the body, the size of which is denoted by l. The meaning of the different symbols is given in the table of symbols. $\alpha l/\lambda(=\mathrm{Nu})$ is termed Nusselt's number and $l^3 g\rho^2\beta\theta_w/\eta^2(=\mathrm{Gr})$ Grashof's number, so that the following holds for a certain shape of body:

$$\mathrm{Nu}=f_1(\mathrm{Gr}). \qquad (1)$$

If one wishes to compare the heat dissipation in different gases, it appears that apart from Gr the Nu number also depends on Prandtl's number $\mathrm{Pr}=c_p\eta/\lambda$, so that

$$\mathrm{Nu}=f_2(\mathrm{Gr},\mathrm{Pr}). \qquad (2)$$

Since Pr is only dependent on the number of atoms per molecule, we may use Eq. (1), when comparing the cooling in gases having an equal number of atoms per molecule. If this is not the case, then since the velocities are usually low with natural cooling, and therefore the forces of inertia are negligible, Eq. (2) may be written in the following shape:

$$\mathrm{Nu}=f_3(\mathrm{Gr.Pr}). \qquad (3)$$

[2] W. Nusselt, Gesundheitsing. **38**, 477 (1915).

In Eq. (3) the values λ, η, β, c_p have been supposed to be independent of the temperature, whereas in reality they vary with the temperature. This dependence can, as a first approximation, be expressed by writing (3) as follows:[2,3]

$$\mathrm{Nu}=f_4(\mathrm{Gr.Pr},\ \theta_w/T\sim). \qquad (4)$$

As stated above, the shape of the function f_4 depends on the shape of the body (the shape of Eq. (4) for several bodies is given by the author.[4] Equation (4) is very useful in expressing experimental results since the latter would otherwise have to be represented as functions of l, ρ, η, T_w etc. In Fig. 1 we have drawn the measuring-results of horizontal cylinders obtained by various authors as summarised by Hermann.[3] It appears that the dependence on $\theta_w/T\sim$ only occurs with small Grashof numbers. The scattering of the measurements about the lines drawn is fairly considerable. Log Nu is uncertain to approximately ± 0.04 (uncertainty in Nu about 10 percent). Hermann[3] calculated the function f_4 for horizontal cylinders for large Grashof numbers. These calculations are fully analogous to those which Schmidt, Pohlhausen, and Beckmann[5] made for vertical flat plates. Hermann found $\mathrm{Nu}_{d,w}=0.37\ \mathrm{Gr}^{\frac{1}{4}}_{d,w}$ for the horizontal cylinder in

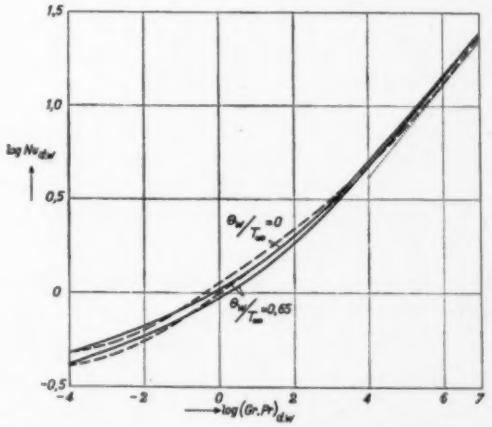

FIG. 1. – – – – Heat transfer in air of horizontal cylinders as measured by various authors and summarized by Hermann (see reference 3), ····· calculated according to formula (5), ——— calculated according to formula (24).

[3] R. Hermann, Forschungsheft 379, Beilage Forsch. auf dem Geb. des Ing. W. 1936.

[4] W. Elenbaas, DeIngenieur **60**, 0.21 (1948); Philips Res. Rep. 3, Oct. and Dec. 1948.

[5] E. Schmidt and W. Beckmann, Tech. Mech. und Thermodyn. **1**, 341 and 391 (1930).

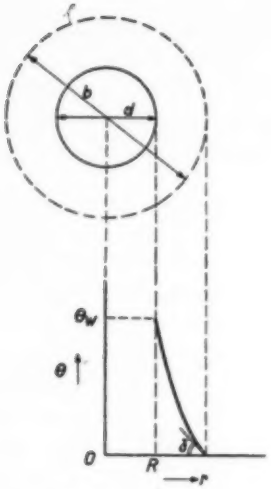

FIG. 2. Temperature course in the Langmuir layer. Langmuir assumes the angle δ to be independent of the diameter d.

air, so that, since for air Pr = 0.73, we can write:

$$\mathrm{Nu}_{d,w} = 0.40(\mathrm{Gr.Pr})^{\frac{1}{4}}_{d,w}. \tag{5}$$

The index d means that in the dimensionless number the diameter must be inserted for the linear dimension l, and the index w that the material constants must be inserted for the temperature operative at the cylinder wall. In Fig. 1 the relation (5) has likewise been drawn (dotted line).

In deducing (5) three simplifying suppositions have been made:

1. The cylinder is infinitely long, so that the only determining dimension is the diameter.
2. The flow in the border layer is laminar.
3. The thickness of the layer in which the temperature falls from the wall temperature to the ambient temperature (the thickness of the Langmuir layer) is small as compared with half the circumference of the cylinder.

Because of the last two conditions Eq. (5) only holds for $10^4 < \mathrm{Gr.Pr} < 3\,10^8$. The lower limit is the outcome of the third supposition, while above the upper limit the second supposition is no longer fulfilled.

We shall now derive formulas for the cooling of vertical and horizontal cylinders valid for a larger range of Gr.Pr. To this end we use:

1. Langmuir's suppositions (see Fig. 2).

2. The knowledge that Nu must be a function of Gr.Pr and of $\theta_w/T\sim$.

3. The assumption that the formula for the vertical plate as deducted by Schmidt, Pohlhausen, and Beckmann[5], *viz.*

$$\mathrm{Nu}_{h,w} = 0.6(\mathrm{Gr.Pr})^{\frac{1}{4}}_{h,w}, \tag{6}$$

is correct, with respect also to the dependence on $\theta_w/T\sim$. By inserting all the material constants at the wall temperature, we find no explicit dependence on $\theta_w/T\sim$ in (6).

II. THE VERTICAL CYLINDER

Vertical cylinders are mutually similar for a constant proportion d/h, so that we must extend Eq. (4) as follows:

$$\mathrm{Nu}_d = f_5(\mathrm{Gr}_d.\mathrm{Pr},\ d/h,\ \theta_w/T\sim), \tag{7a}$$

or, since $d^3/h^3 = (\mathrm{Gr.Pr})_d/(\mathrm{Gr.Pr})_h$, we can also write:

$$\mathrm{Nu}_d = f_6(\mathrm{Gr}_d.\mathrm{Pr},\ \mathrm{Gr}_h.\mathrm{Pr},\ \theta_w/T\sim). \tag{7b}$$

By the insertion of $\theta_w/T\sim$ it is not necessary to indicate at what temperature the values λ, η etc. must be inserted. We can do this at choice. However, the function f_6 will be dependent on our choice. We can represent the heat transfer Φ per second and per cm of cylinder length for the stagnant medium in the Langmuir layer, as follows:

$$\Phi = -2\pi r\lambda(T)dT/dr. \tag{8}$$

The upward flow of the medium in the Langmuir layer is accounted for by assuming dT/dr to be dependent not only on r, but also on z (the height at which the zone is above the bottom of the cylinder).

Equation (8) determines the temperature variation in the Langmuir layer, assuming the temperature for $r = R$ (R = the radius of the cylinder) to be equal to the cylinder temperature and for $r = \frac{1}{2}b$ to be the ambient temperature. Thus b is the diameter of the Langmuir layer, and depends on all the magnitudes, including z. Integrating (8), we find:

$$\ln(b/d) = \frac{2\pi}{\Phi}\int_{T\sim}^{T_w}\lambda(T)dT. \tag{9}$$

We now define the mean coefficient of heat conduction λ_m as:

$$\lambda_m = \frac{1}{\theta_w}\int_{T\sim}^{T_w}\lambda(T)dT, \tag{10}$$

so that we can write (9) as follows:

$$\Phi = 2\pi\theta_w\lambda_m/\ln(b/d). \tag{11}$$

The heat transfer Φ per cm of length would consequently be known, if b were known. On account of the definition of α we have:

$$\Phi \equiv \alpha\pi d\theta_w. \tag{12}$$

From (11) and (12) follows:

$$\frac{\alpha d}{\lambda_m} \equiv \mathrm{Nu}_{d,m} = \frac{2}{\ln(b/d)}. \tag{13}$$

We shall now use Langmuir's second supposition. From (8) and (11) it follows that:

$$(dT/dr)_{r=\frac{1}{2}b} = -\frac{\Phi}{\pi b\lambda_\sim} = -\frac{2\theta_w\lambda_m}{b\lambda_\sim \ln(b/d)}. \tag{14}$$

According to Langmuir $(dT/dr)_{r=\frac{1}{2}b}$ is independent of d, so that we find that $b\ln(b/d)$ must be independent of d. We write:

$$b\ln(b/d) = 2B. \tag{15}$$

Thus B may be a function of all the magnitudes, except d. (It is readily to be understood that B is the layer thickness for $d=\sim$.) Equation (13) yields:

$$b = d\exp(2/\mathrm{Nu}_{d,m}). \tag{16}$$

On inserting (13) and (16) in (15) we find:

$$\frac{\exp(2/\mathrm{Nu}_{d,m})}{\mathrm{Nu}_{d,m}} = \frac{B}{d}. \tag{17}$$

Now, according to (7b) Nu_d is a function of $\mathrm{Gr}_d.\mathrm{Pr}$, $\mathrm{Gr}_h.\mathrm{Pr}$ and $\theta_w/T_\sim$, so that according to (17) B/d is likewise a function of these magnitudes, and since B must be independent of d, we write:

$$\frac{B}{d} = \frac{B_0}{(\mathrm{Gr}_d.\mathrm{Pr})^{\frac{1}{4}}} \cdot f_7(\mathrm{Gr}_h.\mathrm{Pr}, \theta_w/T_\sim), \tag{18}$$

in which B_0 represents a numerical value. As d appears in the third power in Gr_d, d disappears from (18), and B is thus really independent of d. The function f_7 is still unknown.

Equations (17) and (18) give:

$$B_0\,\mathrm{Nu}_{d,m}\exp(-2/\mathrm{Nu}_{d,m}) = (\mathrm{Gr}_d.\mathrm{Pr})^{\frac{1}{4}}/f_7(\mathrm{Gr}_h.\mathrm{Pr}, \theta_w/T_\sim). \tag{19}$$

To determine the function f_7 we introduce the condition that (19) must change for $d\to\sim$ into Eq. (6), which holds for the vertical plate. Equation (19) gives for $d\to\sim$:

$$\frac{B_0\alpha}{\lambda_m} = \left(\frac{g\rho^2\beta\theta_w\,\mathrm{Pr}}{\eta^2}\right)^{\frac{1}{4}} \Big/ f_7(\mathrm{Gr}_h.\mathrm{Pr}, \theta_w/T_\sim). \tag{20}$$

So we can write (20) also as:

$$\frac{\alpha h}{\lambda_w} = \frac{\lambda_m}{\lambda_w B_0}\left(\frac{h^3 g\rho^2\beta\theta_w\,\mathrm{Pr}}{\eta^2}\right)^{\frac{1}{4}} \Big/ f_7 = \frac{\lambda_m}{\lambda_w B_0}(\mathrm{Gr}_h.\mathrm{Pr})^{\frac{1}{4}}/f_7(\mathrm{Gr}_h.\mathrm{Pr}, \theta_w/T_\sim).$$

Now, according to (6):

$$\frac{\alpha h}{\lambda_w} = 0.6(\mathrm{Gr}.\mathrm{Pr})^{\frac{1}{4}}_{h,w},$$

so that

$$\frac{\lambda_m}{\lambda_w B_0}(\mathrm{Gr}_h.\mathrm{Pr})^{\frac{1}{4}} \Big/ f_7(\mathrm{Gr}_h.\mathrm{Pr}, \theta_w/T_\sim) = 0.6(\mathrm{Gr}.\mathrm{Pr})^{\frac{1}{4}}_{h,w},$$

or

$$f_7(\mathrm{Gr}_h.\mathrm{Pr}, \theta_w/T_\sim) = \frac{\lambda_m}{\lambda_w B_0}\,\frac{(\mathrm{Gr}_h.\mathrm{Pr})^{\frac{1}{4}}}{0.6(\mathrm{Gr}.\mathrm{Pr})^{\frac{1}{4}}_{h,w}}. \tag{21}$$

On inserting (21) in (19) we get:

$$\frac{\lambda_m}{\lambda_w}\mathrm{Nu}_{d,m}\exp(-2/\mathrm{Nu}_{d,m}) = 0.6(\mathrm{Gr}.\mathrm{Pr})^{\frac{1}{4}}_{h,w}\left(\frac{\mathrm{Gr}_d}{\mathrm{Gr}_h}\right)^{\frac{1}{4}},$$

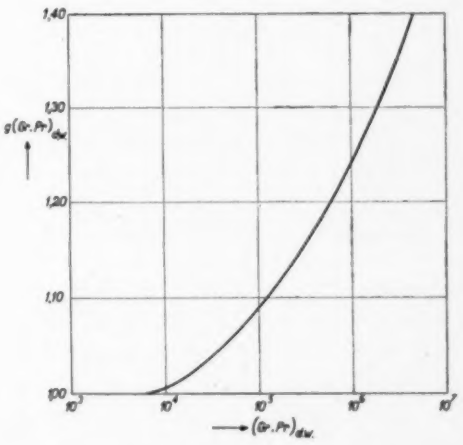

FIG. 3. $g(\mathrm{Gr}.\mathrm{Pr})_{d,w}$ as it appears in (24).

or:

$$\mathrm{Nu}_{d,w}\exp(-2/\mathrm{Nu}_{d,m})=0.6(\mathrm{Gr.Pr})^{\frac{1}{4}}_{h,w}d/h, \quad (22a)$$

or:

$$\mathrm{Nu}_{d,w}\exp(-2/\mathrm{Nu}_{d,m}) =0.6(\mathrm{Gr.Pr.}\ d/h)^{\frac{1}{4}}_{d,w}, \quad (22b)$$

or:

$$\mathrm{Nu}_{d,w}\exp(-2/\mathrm{Nu}_{d,m})=0.6\frac{(\mathrm{Gr.Pr})^{\frac{1}{4}}_{d,w}}{(\mathrm{Gr.Pr})^{1/12}_{h,w}}. \quad (22c)$$

So we see that we can express the dependence on $\theta_w/T\sim$ by inserting both $\mathrm{Nu}_{d,w}$ and $\mathrm{Nu}_{d,m}$.[6] The denominator of Eq. (22c) can be interpreted as being caused by the heating of the gas as the latter flows upwards along the side of the cylinder. As h appears to the third power in Gr_h, the right-hand term decreases by the $\frac{1}{4}$ power of the height. With the vertical plate, too, the cooling decreases in the same way by the height z of the relative zone above the bottom rim.

III. THE HORIZONTAL CYLINDER

We consider an infinitely long cylinder so that we can use Eq. (4) for this case:

$$\mathrm{Nu}_d=f_3(\mathrm{Gr}_d.\mathrm{Pr},\ \theta_w/T\sim). \quad (23)$$

What has been said about the temperature gradient in the Langmuir layer holds for the horizontal cylinder as well as for the vertical one. The only difference is that the effect of the heating of the medium, which effect is expressed by the factor $1/(\mathrm{Gr.Pr})^{1/12}_{h,w}$ in Eq. (22c), must now be a function of $(\mathrm{Gr.Pr})_{d,w}$, since the medium flows upwards along the circumference of the cylinder. So as an analogy to (22c) we write for the horizontal cylinder:

$$\mathrm{Nu}_{d,w}\exp(-2/\mathrm{Nu}_{d,m}) =C(\mathrm{Gr.Pr})^{\frac{1}{4}}_{d,w}/g(\mathrm{Gr.Pr})_{d,w}, \quad (24)$$

in which the function $g(\mathrm{Gr.Pr})_{d,w}$ stands for the heating-effect, though for the rest it is unknown.

On comparison with the measurements it will be found that $g(\mathrm{Gr.Pr})_{d,w}$ is constant for small values of $(\mathrm{Gr.Pr})_{d,w}$. We choose C so that $g(\mathrm{Gr.Pr})_{d,w}=1$ in this range. From the experiment it appears then that we must take $C=0.16$. Hence in the range of small (Gr.Pr) numbers no correction of Langmuir's theory is required. Figure 3 gives the function g of (24) as it has been determined experimentally. The fact that the left-hand term of (24) comprises both $\mathrm{Nu}_{d,w}$ and $\mathrm{Nu}_{d,m}$, is responsible for the fact that, if we draw $\mathrm{Nu}_{d,w}$ as a function of $(\mathrm{Gr.\ Pr})_{d,w}$, we get a series of diverging curves dependent on $\theta_w/T\sim$. However, in full accordance with experiment the diversion does not manifest itself for large values of $(\mathrm{Gr.Pr})_{d,w}$, since here the e-power is almost constant because of the large value of $\mathrm{Nu}_{d,m}$ $[(\exp-2/\mathrm{Nu}_{d,m})\approx 1]$.

IV. COMPARISON WITH EXPERIMENTAL RESULTS

A. The horizontal cylinder

The heat emission of the horizontal cylinder in bi-atomic gases (Pr=0.73) has been widely investigated. The diameter and the wall temperature were usually taken as variables. After Nusselt[2] had shown that for similar bodies Nu must be a function of Gr, all the measurements could be united in a single graph. As far back as 1915 Nusselt[2] already gave the most probable course of this relation for the horizontal cylinder in air. Later on Hermann[3] re-arranged the material and also considered the dependence of $\theta_w/T\sim$. In Fig. 1 the broken lines represent this course as a function of $(\mathrm{Gr.Pr})_{d,w}$.

The scattering of the measuring-points round about the broken lines of Fig. 1 is great. The full lines in Fig. 1 represent the course calculated with Eq. (24) for the same values of $\theta_w/T\sim$. The constant C and the factor $g(\mathrm{Gr.Pr})_{d,w}$ have been adapted to the measurements. We give C the value 0.16, so as to obtain the value 1.0 for the function g in the field $(\mathrm{Gr.Pr})_{d,w}<10^4$. The course of g for $\mathrm{Gr.Pr}>10^4$ is drawn in Fig. 3. The calculation of $\mathrm{Nu}_{d,w}$ as a function of $(\mathrm{Gr.Pr})_{d,w}$ with the aid of (24) is done as follows: with $\theta_w/T\sim=0$, $\mathrm{Nu}_{d,w}=\mathrm{Nu}_{d,m}$, so that we can calculate $\mathrm{Nu}_{d,w}$ for each value of the right-hand term of (24). For $\theta_w/T\sim=0.65$ is with $T\sim=293$, $\theta_w=0.65\times 293=190$, so that $T_w=483°\mathrm{K}$. For air we then get $\lambda_m/\lambda_w=1.19$. We now write (24) in the shape of

$$\mathrm{Nu}_{d,m}\exp(-2/\mathrm{Nu}_{d,m}) =(\lambda_w/\lambda_m)0.16(\mathrm{Gr.Pr})^{\frac{1}{4}}_{d,w}/g(\mathrm{Gr.Pr})_{d,w},$$

[6] W. Elenbaas, Physica 9, 285 and 665 (1942).

so that we can calculate $Nu_{d,m}$ for each value of $(Gr.Pr)_{d,w}$. We get the value of $Nu_{d,w}$ by dividing by 1.19.

As Fig. 1 shows, the deviation between the measured and the calculated value of $\log Nu_{d,w}$ is in no place larger than 0.04 so that the heat dissipation measured and that calculated by means of (24), differ by less than 10 percent in the whole range of $(Gr.Pr)_{d,w}$ from 10^{-4} to 10^{7}. Since the measurements are uncertain up to about 10 percent, the agreement between theory and experiment is satisfactory. Now, this is not surprising for $(Gr.Pr)_{d,w} > 10^{4}$, since the function f in this field has been chosen so that correspondence must be obtained. We chose the function $g(Gr.Pr)_{d,w}$ in accordance with our own measurements[6] and those by Jodlbauer.[7] This is why the curve calculated with (24) does not exactly coincide with the course indicated by Hermann.[3] However, here, too, the deviations are smaller than 10 percent. As shown by Fig. 1, the dependence on $\theta_w/T\sim$ is well described by (24). As for the function $g(Gr.Pr)_{d,w}$ we want to turn attention to the following two points:

1. The function g varies only slightly as a function of $(Gr.Pr)_{d,w}$, which is what we may expect, if g is really the consequence of the heating of the upward flowing gas. Thus the broad trend of Nu as a function of Gr.Pr is already represented relatively well without the experimental function $g(Gr.Pr)_{d,w}$.

2. The function g starts deviating from 1 at a value of $(Gr.Pr)_{d,w}$, which we expect on the ground of our considerations. We may expect that no correction of the heating-effect will appear as long as the thickness of the Langmuir layer is comparable to one-half of the circumference, i.e., at about $b/d > 2$. (In Fig. 2, $b/d = 2$ has been chosen.) If the layer thickness becomes smaller, the gas will grow perceptibly hotter on passing through the layer.

According to (13) $Nu_{d,m}$ then is $< 2/\ln 2$. With (24) we find:

$$(2/\ln 2)\exp(-\ln 2) > 0.16(Gr.Pr)^{\frac{1}{4}}_{d,w},$$

or

$$(Gr.Pr)_{d,w} < (1/0.16\ln 2)^{3} \approx 10^{3}.$$

As shown in Fig. 3, the function g really starts deviating from 1 at $(Gr.Pr)_{d,w} \approx 5.10^{3}$.

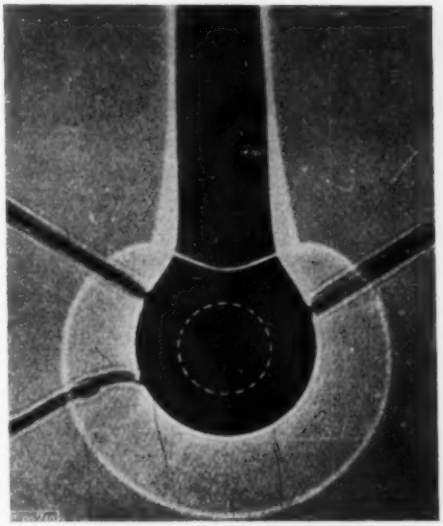

a

b

FIG. 4. "Schlierenaufnahmen" taken by E. Schmidt (see reference 7) of heat dissipating horizontal cylinders. (a) Cylinder diameter 16 mm, $T\sim = 297°K$, $\theta_w = 165°$, $(Gr.Pr)_{d,w} = 1.510^{4}$. (b) Cylinder diameter 150 mm, $T\sim = 297\frac{1}{2}°K$, $\theta_w = 180°$, $(Gr.Pr)_{d,w} = 1.2\ 10^{7}$. The dotted line represents the cross section of the cylinder. The first boundary indicates the outside of the Langmuir layer, while the distance between the cylinder and the heart-shaped line is proportional to the local heat transfer.

[7] K. Jodlbauer, Forsch. auf dem Geb. des Ing. W. **4**, 157 (1933).

The calculations by Hermann[7] were based on a small thickness of the Langmuir layer as compared with one-half of the circumference, so there $(Gr.Pr)_{d,w}$ must be larger than the limit determined in the present case. Hermann's theory thus holds for $(Gr.Pr)_{d,w} > 10^4$.

To illustrate the Langmuir layer we give in Fig. 4 two "Schlierenaufnahmen" of heat-dissipating horizontal cylinders taken by Schmidt.[8] By this method a pointed luminous source is placed at a great distance from the cylinder in line with the cylinder axis. On the opposite side of the cylinder at some distance from it is a screen on which the image represented in Fig. 4 is thrown. The dotted line, which marks the outline of the cylinder, is not visible in the actual image. Rays of light passing along the surface through the Langmuir layer are deflected by the radial temperature gradient, so that no light falls on the screen where the projection of the Langmuir layer appears. In Fig. 4 the black ring round about the dotted line consequently represents the Langmuir layer. Owing to the heating-effect the latter is rather wider at the top than at the bottom.

The light deflected by the Langmuir layer, is thrown on the screen at a place further away from the image of the cylinder. Since the temperature gradient is largest close to the surface, the rays of light skimming the surface will be deflected most. This is responsible for the heart-shaped outline in Fig. 4. The distance from this line to the dotted line is proportional to dT/dr on the surface and consequently proportional to the heat dissipation at that point. Quite in accordance with the larger thickness of the top portion of the Langmuir layer, the heat dissipation is smallest there. It is the deviation of the heart-shaped line from the circle as determined by the lower part of the heart-shaped line, that is responsible for the appearance of the function g in formula (24).

[8] E. Schmidt, Forsch. auf dem Geb. des Ing. W. **3**, 181 (1932).

B. The vertical cylinder

Much less experimental work has been done on the vertical cylinder than on the horizontal one. One of the reasons for this is probably that there is an additional variable in this case, *viz.* the height h. It is true that the length of the horizontal cylinder also plays its part, but, since the various zones are cooled by parallel currents, they do not influence one another in sections that are far enough away from the ends, and the coefficient of heat transmission thus reaches a limit with increasing length, in contradiction to the vertical cylinder, where α decreases with increasing height. Thus with the horizontal cylinder this variable may be dispensed with, provided that it is chosen sufficiently long, whereas the length is an essential element with the vertical cylinder.

Formulas (22) were tested[6] on cylinders having diameters of $1\frac{1}{2}$ to 10 cm, heights of 10 to 60 cm, and values of θ_w from 10 to 300°C. We found differences up to 15 percent between the measured values and the values calculated with (22). However, these deviations may be due to inaccuracies in the measurements.

Summarising we may say that formulas (22) and (24) describe the heat dissipation with natural cooling of the cylinder for a wide range of Gr.Pr values within the errors of measurement.

Calendar of Meetings

December

16–18 American Society for X-Ray and Electron Diffraction

26–27 Central Association of Science and Mathematics Teachers, Indianapolis, Indiana

26–28 American Physical Society (Pacific Coast Meeting), Berkeley, California

28–31 American Astronomical Society, Columbus, Ohio

29–30 American Chemical Society (Division of Industrial and Engineering Chemistry), Chicago, Illinois

31 Mathematical Association of America, Columbus, Ohio

January, 1949

10–12 Conference on High Frequency Measurements (American Institute of Electrical Engineers, Institute of Radio Engineers, National Bureau of Standards), Washington, D. C.

10–14 Materials Handling Show and American Society of Mechanical Engineers Conference on Materials Handling, Philadelphia, Pennsylvania

27–29 American Physical Society and American Association of Physics Teachers, New York, New York

February

28–March 4 American Society for Testing Materials (Spring Meeting), Chicago, Illinois

On the Theory of Biconical Antennas*

C. T. Tai
Cruft Laboratory, Harvard University, Cambridge, Massachusetts
(Received June 4, 1948)

The investigation contained in this paper gives a general treatment of the theory of biconical antennas based upon Smith's formulation of the problem. For the case of small-angle cones, an expression of the effective load admittance is obtained which is the same one that Schelkunoff derived based upon two rather ingenious methods, both of which, however, are not as rigorous as the present one. As an illustration of another application of the analysis, a treatment is given of the characteristics of biconical antennas where the space between the cones is filled with a dielectric other than air.

INTRODUCTION

BICONICAL antennas, assumed to be perfectly conducting, were first introduced by Schelkunoff[1] as a convenient model to study the characteristics of a radiating system, particularly its input impedance. As was shown by Schelkunoff, if one defines the voltage between two points on the upper and lower cones as the line integral of the electric intensity along a meridian, then the input impedance of the antenna can be expressed as the input impedance of a conical transmission line, formed by the lateral surfaces of the cones, terminated by an effective load impedance z_t or admittance y_t, which is, of course, related to the amplitudes of the complementary waves. The problem of determining the input impedance of the antenna then reduces to that of finding the value of y_t.

In Schelkunoff's original paper, a solution of y_t was obtained for small-angle cones based upon two rather ingenious methods. For convenience, we shall call the first "the method of partial matching," and the second "the e.m.f. method." The result of the first method gives an expression of y_t in terms of a series of products of Bessel and Hankel functions, while the e.m.f. method gives an expression of y_t in terms of finite terms of sine integrals, cosine integrals, trigonometrical functions, and logarithmic functions. There is, however, no mention of the mathematical relation between these two expressions, derived from two apparently different methods. Later, Rice[2] published a paper giving a mathematical proof of the identity of these two expressions. This is, to some extent, a quite surprising result, in view of the fact that Schelkunoff's method of partial matching involves a rather complicated analysis. The e.m.f. method, on the other hand, is a rather simple one, but it is known to be very delicate and its validity is still doubtful. There is, however, one important step which is common to both methods, i.e., a sinusoidal distribution of current has been used as an approximate current distribution to evaluate some of the coefficients, or functions, occurring in the analysis. This is, perhaps, the most essential step involved in Schelkunoff's treatment. In addition to the foregoing remarks, we may also mention the fact that in the method of partial matching, Schelkunoff limits himself to cones of small angles, so he neglects the boundary condition at the end surfaces at the very beginning of his analysis.

In a later paper,[3] Schelkunoff formulated the problem again by taking into account all the boundary conditions. It is a rigorous formulation. As a result, he obtained an infinite set of linear equations relating the effective load admittance, y_t, and the amplitudes of the interior and exterior complementary waves. The equations involve some general integrals of Legendre's functions of fractional order, the analytical nature of which was not discussed.

* The research reported in this document was made possible through support extended Cruft Laboratory, Harvard University, jointly by the United States Navy, Office of Naval Research, and the United States Army Signal Corps, under ONR Contract N5ori-76, T.O.I.

[1] S. A. Schelkunoff, "Theory of antennas of arbitrary size and shape," Proc. I.R.E. **29**, 493–521 (1941).

[2] S. O. Rice, "Sum of series of the form $\sum_0^\infty A_n J_{n+\alpha}(z) \times J_{n+\beta}(z)$," Phil. Mag. **35**, Ser. 7, 686 (1944).

[3] S. A. Schelkunoff, "Principal and complementary waves in antennas," Proc. I.R.E. **34**, 23–32 (1946).

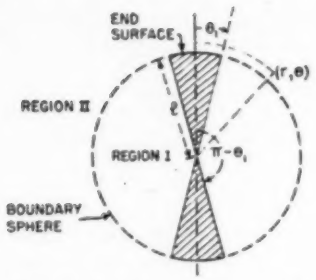

Fig. 1. The biconical antenna.

Recently, Smith[4] restated the same problem. He obtained sets of equations which are essentially the same as those obtained by Schelkunoff. There is, however, one great improvement in his formulation: instead of dealing with the integrals of Legendre's functions directly, he expresses those integrals in terms of the characteristic value of these functions, and their derivatives which can be handled much more easily. To solve this set of equations Smith considers only the principal wave, one interior complementary wave, and two exterior complementary waves.

The present work will include a discussion on Smith's formulation by including more high order complementary waves. In the limiting case of small-angle cones, we will show that it is possible to take into consideration all complementary waves. The expression of y_t thus obtained is precisely the same on which Schelkunoff derived from his first method. Since we have solved the problem based upon a more rigorous method, we are justified in saying that Schelkunoff's result is correct, but the mathematical implications of his two methods need further investigation. This will be discussed in a companion paper, to be published later, which will contain a critical study of the e.m.f. method.

To illustrate another application of the present analysis, a treatment is also give of the characteristics of biconical antennas where the space between the cones is filled with a dielectric other than air. It would be extremely difficult to apply either of Schelkunoff's methods to treat this problem.

GENERAL FORMULATION AND THE SOLUTION

Without going into the details of the derivation, we will simply write down most of the equations derived previously by Smith, with all the notations practically unchanged. The principal wave existing in region I (Fig. 1) is given by

$$\begin{cases} E_\theta = [Vz_0/(r\sin\theta)] \\ \quad \times[(1+Ky_t)\exp[-j\beta(r-l)] \\ \quad +(1-Ky_t)\exp[j\beta(r-l)]], \quad (1)^{**} \\ H_\phi = [V/(r\sin\theta)] \\ \quad \times[(1+Ky_t)\exp[-j\beta(r-l)] \\ \quad -(1-Ky_t)\exp[j\beta(r-l)]], \quad (2) \end{cases}$$

where V is an arbitrary constant, y_t is the effective load admittance to be determined, and K is the characteristic impedance of the cones if they are infinitely long. The complementary waves existing in region I are

$$\begin{cases} E_r = \dfrac{-j}{\omega\epsilon_0 r^2}\sum_n \dfrac{a_n}{2\pi}\dfrac{S_n(\beta r)}{S_n(\beta l)}L_n(\theta), & (3) \\ E_\theta = \dfrac{-jz_0}{r}\sum_n \dfrac{a_n}{2\pi}\cdot\dfrac{1}{n(n+1)}\cdot\dfrac{S_n'(\beta r)}{S_n(\beta l)}\cdot\dfrac{\partial L_n(\theta)}{\partial\theta}, & (4) \\ H_\phi = \dfrac{-1}{r}\sum_n \dfrac{a_n}{2\pi}\cdot\dfrac{1}{n(n+1)}\cdot\dfrac{S_n(\beta r)}{S_n(\beta l)}\cdot\dfrac{\partial L_n(\theta)}{\partial\theta}, & (5) \end{cases}$$

where

$$\begin{cases} z_0 = (\mu_0/\epsilon_0)^{\frac{1}{2}} \doteq 120\pi \text{ ohms}, & (6) \\ S_n(\beta r) = (\beta r)^{\frac{1}{2}}J_{n+\frac{1}{2}}(\beta r), & (7) \\ S_n'(\beta r) = [dS_n(\beta r)/d(\beta r)], & (8) \end{cases}$$

and $L_n(\theta)$ denotes a class of Legendre functions which vanishes at $\theta=\theta_1$, $\pi/2$, and $\pi-\theta_1$. n is, therefore, a root of the equation $L_n(\theta_1)=0$, or one characteristic value of the Legendre equation with the specified boundary conditions.

The complementary waves existing in region II are given by the following formulas:

$$\begin{cases} E_r = \dfrac{-j}{\omega\epsilon_0 r^2}\sum_{k=1,3,\cdots}\dfrac{b_k}{2\pi}\dfrac{R_k(\beta r)}{R_k(\beta l)}P_k(\theta), & (9) \\ E_\theta = \dfrac{-jz_0}{r}\sum_{k=1,3,\cdots}\dfrac{b_k}{2\pi} \\ \quad \cdot\dfrac{1}{k(k+1)}\dfrac{R_k'(\beta r)}{R_k(\beta l)}\dfrac{\partial P_k(\theta)}{\partial\theta}, & (10) \\ H_\phi = \dfrac{-1}{r}\sum_{k=1,3,\cdots}\dfrac{b_k}{2\pi}\dfrac{1}{k(k+1)}\dfrac{R_k(\beta r)}{R_k(\beta l)}\dfrac{\partial P_k(\theta)}{\partial\theta}, & (11) \end{cases}$$

[4] P. D. P. Smith, "The conical dipole of wide angle," J. App. Phys. 19, 11 (1948).

** The constant V was omitted in Smith's original paper. The final solution of y_t, however, is independent of V. It is kept here simply for completeness.

where

$$\begin{cases} R_k(\beta r) = (\beta r)^{\frac{1}{2}} H_{k+\frac{1}{2}}(\beta r), & (12) \\ R_k'(\beta r) = dR_k(\beta r)/d(\beta r), & (13) \end{cases}$$

$H_{k+\frac{1}{2}}(\beta r)$ being the Hankel function of the second kind, and $P_k(\theta)$ denoting the Legendre polynomials. It was shown by Smith that by matching the H_ϕ and E_θ components of the interior and exterior fields across the boundary sphere, and at the end surfaces, where E_θ is zero, the system of equations thus obtained can be solved by making use of the orthogonal properties of the Legendre functions. The formal solution of y_t then satisfies the following equation:

$$y_t = \frac{z_0}{4\pi^2 K^2} \sum_{k=1,3,\cdots} \left(\frac{b_k}{V}\right) \frac{1}{k(k+1)} P_k(\mu_1), \quad (14)$$

while (b_k/V) satisfies the following set of linear equations:

$$4\pi P_r(\mu_1) = (b_r/V) W_r + r(r+1) P_r(\mu_1) \times \sum_n \sum_{k=1,3,\cdots} \left(\frac{b_k}{V}\right) \frac{P_k(\mu_1) s_n}{(r,n)(k,n)}, \quad r = 1, 3, \cdots, \quad (15)$$

where

$$\begin{cases} s_n = j \dfrac{2n+1}{n(n+1)} (1-\mu_1^2) \dfrac{dn}{d\mu_1} \dfrac{S_n'(\beta l)}{S_n(\beta l)}, & (16) \\ (r,n) = r^2 + r - n^2 - n, & (17) \\ W_r = \dfrac{j}{(2r+1)} \dfrac{R_r'(\beta l)}{R_r(\beta l)}, \quad \mu_1 = \cos\theta_1 & (18) \end{cases}$$

Equations (14) and (15) contain the exact solution of y_t that applies to biconical antennas of any angle. The problem of finding the explicit solution of y_t then reduces to that of solving the coefficients (b_k/V) from Eq. (15). To that effect, Smith limits himself to one term of n and two terms of b_k contained in the double summation sign of Eq. (15). Physically, it implies that in addition to the principal wave, only one interior complementary wave and two exterior complementary waves have been considered. Smith's subsequent work discusses in considerable detail the numerical values of this approximate solution of y_t for cones of various sizes. In the case of small-angle cones, he shows that his approximate expression of y_t reduces to the following form:

$$(y_t)_1^2 = \frac{z_0 \beta l}{2K^2} \left[(3/2) J_{3/2} H_{3/2} + (7/12) J_{7/2} H_{7/2} \left(1 - \frac{R_3}{R_3'} \frac{S_3'}{S_3}\right)\right]. \quad (19)$$

The superscript 2 implies two exterior complementary waves, and the subscript 1 implies one interior complementary wave. Their significance will be discussed later. It is understood that all the J-, H-, R-, and S-functions defined in Eq. (19) have the argument βl. It is recalled that Schelkunoff's formula of y_t is given by

$$y_t = \frac{z_0 \beta l}{2K^2} \left[(3/2) J_{3/2} H_{3/2} + (7/12) J_{7/2} H_{7/2} + (11/30) J_{11/2} H_{11/2} + \cdots \right]. \quad (20)$$

Now if we compare Eqs. (19) and (20), it can perhaps be anticipated that if Schelkunoff's formula is correct it should be possible to obtain this formula from this more general formulation by taking into consideration all the interior and exterior complementary waves. This is indeed the case, proof of which is given as follows.

Since it is almost impossible to solve the system of equations defined by Eq. (15) for an arbitrary value of μ_1, nevertheless one can obtain a degenerated form of this set of equations by limiting the value of μ_1 to be very near unity, which corresponds to a small value of θ_1. It is known[1] that the limiting values of n for a small value of θ_1 is given by

$$n = k + [1/\log(2/\theta_1)], \quad k = 1, 3, \cdots. \quad (21)$$

Hence

$$\lim_{\mu_1 \to 1} (1-\mu_1^2)(dn/d\mu_1) = -(n-k)^2, \quad k = 1, 3, \cdots. \quad (22)$$

It can be easily shown that

$$\lim_{n \to k} (k, n) = -(2k+1)(n-k). \quad (23)$$

Thus, the function $[s_n/(r,n)(k,n)]$ occurring in

Eq. (15) takes the form

$$\lim_{\mu_1 \to 1} \frac{s_n}{(r, n)(k, n)} = \begin{cases} 0; \ k \neq r, \text{ and } k = r \neq n \\ -j \dfrac{S_r'(\beta l)}{r(r+1)(2r+1) \ S_r(\beta l)}; \\ k = r \doteq n. \end{cases} \quad (24)$$

By making use of Eq. (24) and the relation

$$\lim_{\mu_1 \to 1} P_k(\mu_1) = 1, \quad (25)$$

we obtain the degenerated form of Eq. (15) for small values of θ_1.

$$4\pi = (b_r/V)W_r - [j/(2r+1)][S_r'(\beta l)/S_r(\beta l)](b_r/V). \quad (26)$$

Substituting the values of W_r, S_r, and S_r' defined by Eqs. (7), (8), (12), (13), and (18) into (26), and making the necessary simplification of the Bessel functions, we obtain the following expression of (b_r/V):

$$b_r/V = 2\pi^2(2r+1)\beta l J_{r+\frac{1}{2}}(\beta l) H_{r+\frac{1}{2}}(\beta l). \quad (26)'$$

Substituting this value of b_r/V into Eq. (14) and making use of Eq. (25), we come out with Schelkunoff's expression. As we have mentioned earlier, Schelkunoff, in his method of partial matching, obtained this expression in a rather ingenious way. The steps involve an assumption of a sinusoidal distribution of current, a matching of the E_r component of the field across the foundary sphere, and a relation between the currents associated with the principal wave and the interior complementary waves, by assuming a vanishing of the total current at the ends of the antenna. Some of these steps lack the mathematical rigor needed in a boundary value problem. The main difference between the present analysis of small-angle cones and Schelkunoff's is, therefore, a question of rigor and not of results, since these are the same.

In the light of this analysis, it is obvious that Smith's approximate expression, $(y_t)_1^2$, is actually not a very good one, at least for small-angle cones. This can be seen by comparing the numerical value of $K^2(y_t)_1^2$ with $K^2 y_t$ for values of

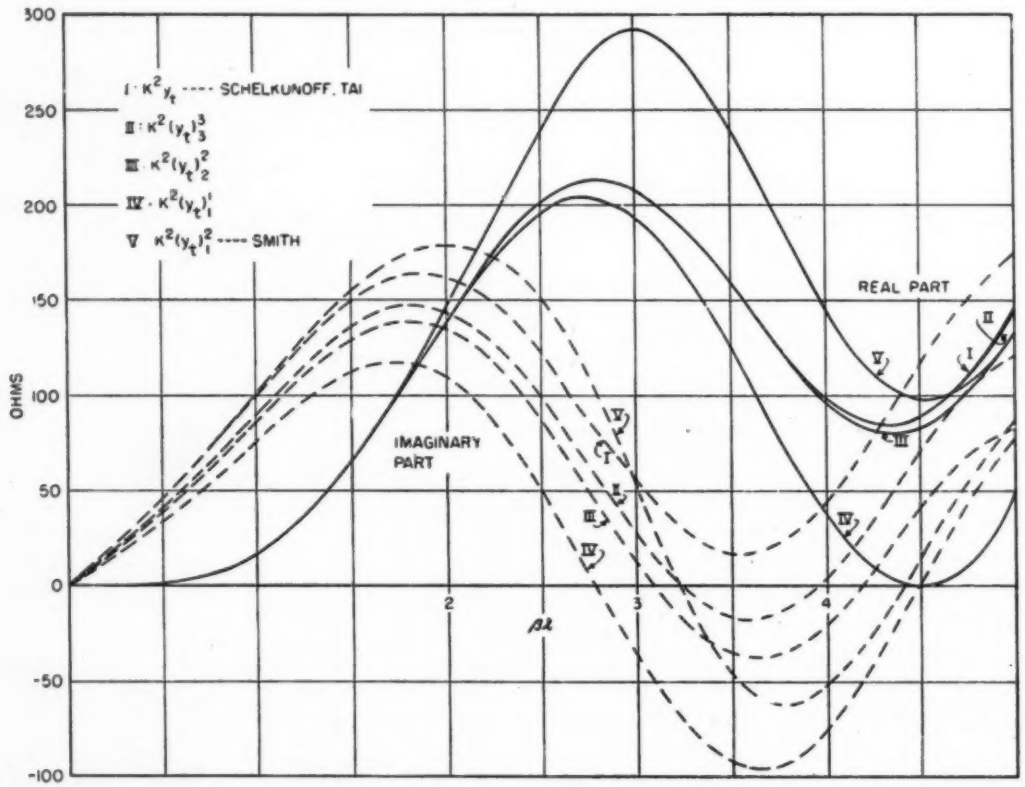

FIG. 2. A comparison of solutions of different orders for small-angle biconical antennas.

$\beta l < 5$, as shown in Fig. 2. If we take an additional value of n, but still keep two terms of b_k, then the new approximate expression of $(y_t)_2{}^2$ for small-angle cones is given by the first two terms of the series y_t. Values of $K^2(y_t)_r{}^r$ up to $r=3$ are also plotted in Fig. 2. Thus we can interpret each term of the series y_t as the effective load admittance contributed by a pair of interior and exterior complementary waves of comparable order. A similar interpretation, for a set of exterior waves alone, was used by Stratton and Chu[5] in their investigation of the input impedance of a spherical antenna. As Smith has already pointed out, the spherical antenna is only a degenerated case of a wide-angle biconical antenna. For wide-angle cones, high order solutions can be obtained by including more n's and b's. A paper will be published later on the numerical value of $(y_t)_2{}^2$ for wide-angle cones, where it involves a computation of Bessel functions of fractional order.

DIELECTRIC FILLED-BICONICAL ANTENNAS

To illustrate another application of this analysis, we shall consider the same biconical antenna shown in Fig. 1, but with region I filled by a dielectric other than air. The formulation is similar to the previous one except that some constants need to be changed. Thus, for the principal wave and the interior complementary waves defined by Eqs. (1)–(5), z_0, K, ϵ_0, and β should be replaced by z_1, K_1, ϵ_1, and β_1, where

$$z_1 = z_0/(\epsilon)^{\frac{1}{2}}, \quad K_1 = K/(\epsilon)^{\frac{1}{2}}, \quad \epsilon_1 = \epsilon\epsilon_0, \quad \beta_1 = (\epsilon)^{\frac{1}{2}}\beta, \tag{27}$$

and ϵ is the dielectric constant of the material filling region I. There will be no change in the constants occurring in Eqs. (9)–(11), unless the whole antenna is immersed in a medium other than air, such as a dissipative one. By performing the same operation as outlined previously, we can derive the following equations corresponding to Eqs. (14) and (15). They are

$$\bar{y}_t = \frac{z_1}{4\pi^2 K_1{}^2} \sum_{k=1,3,\cdots} \left(\frac{b_k}{V}\right) \times \frac{1}{k(k+1)} P_k(\mu_1), \tag{28}$$

$$4\pi P_r(\mu_1) = (\epsilon)^{\frac{1}{2}}\left(\frac{b_r}{V}\right) W + r(r+1)P_r(\mu_1) \times \sum_n \sum_{k=1,3,\cdots} \left(\frac{b_k}{V}\right) \cdot \frac{P_k(\mu_1)\delta_n}{(r,n)(k,n)}, \quad r=1, 3, \cdots, \tag{29}$$

where δ_n is similar to that defined by (16), except that the argument of the Bessel functions is changed into $\beta_1 l$. The remaining functions have the same meaning as before. For the limiting case of small-angle cones, Eq. (29) degenerates into the form

$$(b_k/V) = \frac{-j4\pi(2r+1)}{\left[(\epsilon)^{\frac{1}{2}}\dfrac{R_k'(\beta l)}{R_k(\beta l)} - \dfrac{S_k'(\beta_1 l)}{S_k(\beta_1 l)}\right]}, \tag{30}$$

The final expression of $\bar{y}_t$ is then given by

$$\bar{y}_t = \frac{-jz_1}{\pi K_1{}^2} \sum_{k=1,3,\cdots} \frac{2k+1}{k(k+1)} \cdot \frac{1}{\left[(\epsilon)^{\frac{1}{2}}\dfrac{R_k'(\beta l)}{R_k(\beta l)} - \dfrac{S_k'(\beta_1 l)}{S_k(\beta_1 l)}\right]}. \tag{31}$$

The function occurring in the bracket of the denominator of Eq. (29) cannot be further simplified. Similar functions appeared in the problem of diffraction of plane electromagnetic waves by a dielectric sphere.[6] It is obvious by comparing Schelkunoff's two methods with the present analysis that it will be extremely difficult to apply either of his two methods to treat this problem.

CONCLUSION

A theoretical investigation has been made on the impedances of biconical antennas based upon Smith's formulation. It has been shown that for small-angle cones it is possible to determine the effective load admittance of the antenna by taking all the interior and exterior complementary waves into consideration. As a result, we derived Schelkunoff's expression for y_t without

[5] J. A. Stratton and L. J. Chu, "Steady-state solutions of electromagnetic field problems. Part II, J. App. Phys. 12, 236 (1941).

[6] Unpublished notes by the author.

imposing any approximation based upon physical intuitions, except the mathematical approximation of the Legendre functions occurring in the final stage of the analysis. For those antennas whose angles are not small, it has been demonstrated that Smith's approximation is not a very good one. For a better approximation one should take at least one additional interior complementary wave into consideration. To illustrate another application of this analysis, a treatment is also given of the characteristics of biconical antennas where the space between the cones is filled with a dielectric other than air.

ACKNOWLEDGMENT

The author wishes to thank Misses Betty Finn and Julie Klimas for carrying out all the numerical calculations.

Measurement by Radioactive Tracers of Diffusion in Liquids

ANDREW GEMANT

Research Department, The Detroit Edison Company, Detroit, Michigan

(Received June 14, 1948)

A method, using a radioactive tracer technique, for the measurement of diffusion coefficients in liquids is described. Results for uranyl nitrate solutions, revealing the diffusion of Th-234, in water and dioxane are presented.

IN connection with recent investigations of the the author[1] concerning electrolytically conducting solutions in hydrocarbons, it was found that it is important to know the size of the dissolved particles. It was thought that if the diffusion coefficient of the solute were known, the size of the particles could be determined by means of Stokes' relation. In order to measure the diffusion coefficient, a radioactive tracer method was developed. The tracer principle for diffusion measurements is generally known; a study by Adamson[2] on the diffusion of radiosodium in solution, and a study by Kuczynski[3] on the diffusion in solids, are mentioned as examples. The method developed by the author[4] is believed to have novel features, and is described briefly in this paper, together with some measurements on uranyl nitrate solutions in water and dioxane.

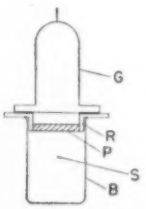

FIG. 1. Diagram of diffusion cell.

In this method the pure solvent is confined within an inert porous structure with which the solution is in direct contact (Fig. 1). Bonded fiberglass mat was found suitable for such a porous structure (3-vol. percent of glass); in some tests agar gel was used instead. The porous structure P was prepared inside a metal ring R which was placed on top of a glass beaker B, containing the solution S. A Geiger-Müller counter tube G was then placed on top of the metal ring. The porous structure was sufficiently thin (a few mm) for the counter to record the progress of diffusion within one or two hours.

In order to evaluate the rate of increase of counts in terms of the diffusion constant, the concentration of the solute at each depth below the surface, and for any time, must be known. This relation depends on the condition of the solution below the solvent. If the solution is at rest, and in addition has a depth appreciably greater than that of the solvent layer, we have,[5] for the concentration c at any depth x below the

[1] Andrew Gemant, J. Chem. Phys. **14**, 424 (1946).
[2] A. W. Adamson, J. Chem. Phys. **15**, 762 (1947).
[3] A. C. Kuczynski, J. App. Phys. **19**, 308 (1948).
[4] Andrew Gemant, Science **107**, 622 (1948).

[5] R. V. Churchill, *Modern Operational Mathematics in Engineering* (McGraw-Hill Book Company, Inc., New York, 1944), pp. 196 and 210.

surface, and any time t,

$$c=1-0.5[\mathrm{erf}(1+(x/l))/(2(kt)^{\frac{1}{2}}/l) + \mathrm{erf}(1-(x/l))/(2(kt)^{\frac{1}{2}}/l)], \quad (1)$$

where l = depth of the solvent layer, k = diffusion constant, and the bulk concentration of the solvent, approximately constant, is taken as unity. Figure 2 shows c *vs.* (x/l) for various values of kt/l^2. The condition for which Eq. (1) is valid was maintained for all tests using fiberglass structures.

If the solution is well stirred, the bulk concentration (unity) of the solution is practically constant up to the boundary. For the solvent layer one has[5]

$$c=1-\frac{4}{\pi}\sum_{n=1}^{\infty}((-1)^{n-1})/(2n-1) \times\cos((2n-1)\pi x)/(2l) \times\exp[-((2n-1)^2\pi^2kt)/(4l^2)]. \quad (2)$$

Figure 3 shows c *vs.* (x/l) for various parameters kt/l^2. The condition necessary for Eq. (2) to be valid was maintained in the agar tests.

Next, one must know the effect of absorption upon the activity reaching the counter. This effect was obtained by calibration. It can be approximated for uranium by an exponential relation; the intensity I after absorption is given by

$$I=I_0\exp(-6.15\rho x), \quad (3)$$

where I_0 = initial intensity, ρ = density in g/cm³, and x is in cm. The factor 6.15 shows that what we measured was essentially the beta-radiation of UX_2. It has a maximum energy of 2.32 Mev, and its maximum range is known to be 1.1 g/cm². The alpha-radiation from U^{238} and U^{234} is not measured in the arrangement above, and the contribution of betas from UX_1, because of their much higher absorption, is rather small. The absolute counts from a solution agreed rather closely with those calculated from the known concentration of the solution and the absorption coefficient of betas from UX_2.

Finally, the variation of the geometric factor with varying depth must be known. This effect, too, was obtained by calibration; the result is seen in Fig. 4. The abscissa gives depth in cm

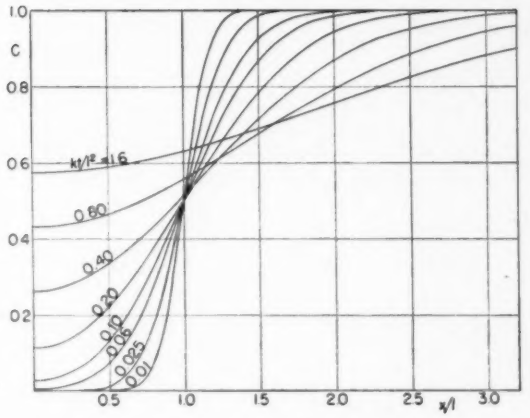

FIG. 2. Calculated trend of diffusion with time for solution at rest (Eq. (1)).

below the guard ring of the counter, and the ordinates are counts per minute in relative units.

By multiplying the three factors represented by Figs. 2 and 4 and Eq. (3), numerical integration over the entire depth gives the relative increase of counts per minute with time. Because of the limited length of the diffusion layer, it is enough to proceed with the numerical integration to a depth equal to a few times of l; farther layers contribute merely a time-independant amount to the activity which increases the background count. Curve 1 of Fig. 5 gives the result for the solution at rest and a fiberglass layer having a thickness of 0.215 cm. The abscissa is kt in cm², and the ordinates are counts per minute in fractions of the final equilibrium value. The curve has a rather constant slope up to the ordinate 0.2. In comparing this calculated

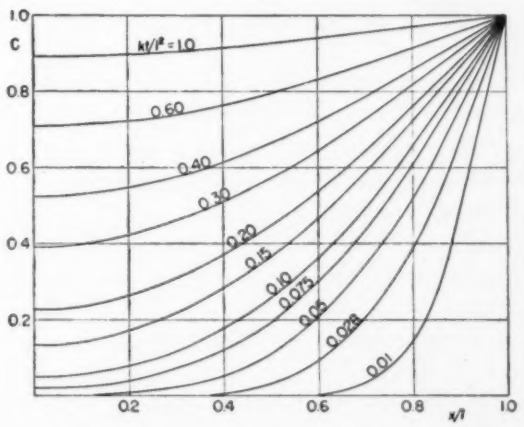

FIG. 3. Calculated trend of diffusion with time for well stirred solution (Eq. (2)).

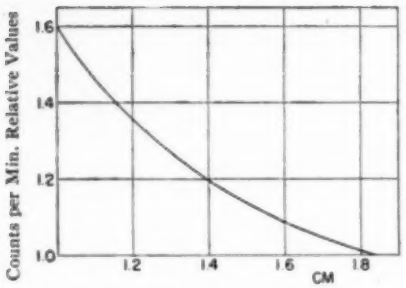

FIG. 4. Counts per min., in relative units, *vs.* distance of a thin layer from guard ring of counter (geometric factor).

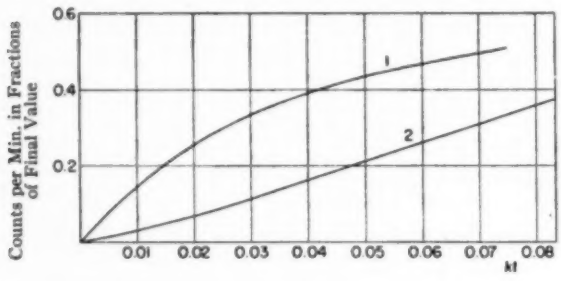

FIG. 5. Calculated counts per min. *vs.* time: curve 1, solution at rest, $l=0.215$ cm; curve 2, well stirred solution, $l=0.59$ cm.

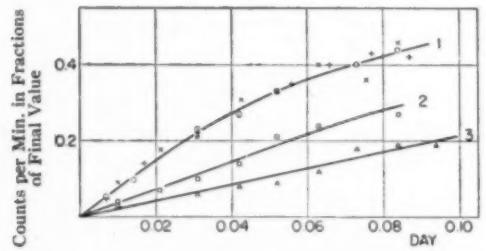

FIG. 6. Experimental data of counts per min. *vs.* time with aqueous 0.02-m uranyl nitrate solution and fiberglass layer: curve 1, viscosity 0.9 centipoise; curve 2, viscosity 1.8 centipoise; curve 3, viscosity 3.6 centipoise (different symbols indicate repeated runs).

curve with the data of an experimental run, k is obtained. Curve 2 of Fig. 5 gives the corresponding result of numerical integration from Fig. 3 for the stirred solution and an agar layer of 0.59-cm thickness. The average slope up to the ordinate 0.4, in conjunction with experimentally obtainable data, yields the diffusion constant.

As an illustration of this technique, experiments were carried out with aqueous uranyl nitrate solutions. Some doubt might be expressed regarding the identity of the cations, the diffusion of which is measured in this case. As mentioned, the beta-ray activity of UX_2 was counted. Since, however, the half-life of the latter is only 1.14 minutes, while the test takes a few hours to complete, it must be the diffusion of UX_1, the parent of UX_2, which is essentially measured. UX_1 (thorium-234) has a half-life of 24.5 days and is everywhere in the course of its diffusion practically in equilibrium with its daughter product UX_2, which acts as its tracer.

Concerning the experimental technique, it should be mentioned that the products of $UO_2(NO_3)_2$ are easily adsorbed by glass. In order to minimize this complication, fiberglass that already contained the adsorbate was used; its activity merely increased the background count. While this adsorption is not irreversible, the adsorbate was found rather stable, and its amount probably did not change much in the course of the diffusion process.

Figure 6, curve 1 shows experimental results on 0.02-molar solutions in 0.1-molar nitric acid.

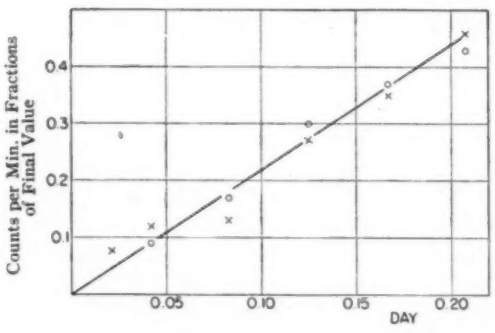

FIG. 7. Experimental data of counts per min. *vs.* time with aqueous 0.02-m uranyl nitrate solution and agar gel layer (different symbols indicate repeated runs).

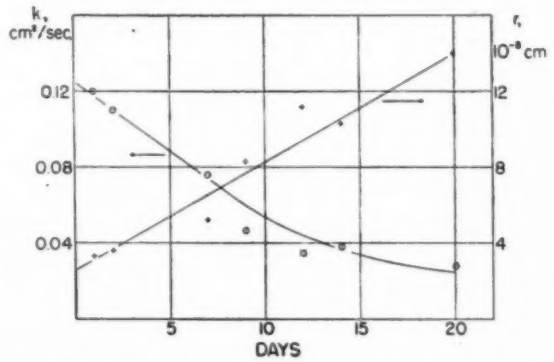

FIG. 8. Diffusion constant and molecular radius *vs.* age. 0.02-m uranyl nitrate solution in 2:1-dioxane-castor oil mixture.

The final equilibrium count per min. resulting from the solution present in the fiberglass layer was 370. The curve has a trend very similar to that of the calculated curve 1, Fig. 5; from the initial slopes 0.50 cm²/day is obtained for k. Curve 2 refers to a similar solution containing, in addition, 25-wt. percent glycerine, having a viscosity of 1.8 centipoise at 25°C; curve 3 refers to 43-wt. percent glycerine solution with a viscosity 3.6 cp. From curve 2, $k=0.24$, and from curve 3, $k=0.14$. In first approximation, the product of k and the viscosity is expected to be constant; the products obtained from Fig. 6 are 0.45, 0.43, and 0.50. Definite deviation from this relation would indicate a change of size of the solute molecules or ions.

Figure 7 shows data on 0.5-percent agar gel as the porous structure. In this case diffusion took place from an 0.02-molar uranyl nitrate solution into an 0.01-molar solution. Comparison of the slope with that of curve 2, Fig. 5, results in $k=0.50$, which is in good agreement with the previous value obtained from the considerably thinner fiberglass layer and entirely different boundary condition.

TABLE I.

Solvent	Viscosity, cp (η)	k, cm²/day	$k\eta$
Dioxane	1.16	0.50	0.58
Dioxane with 33-vol. percent castor oil	5.1	0.11	0.56

Results of measurements with $UO_2(NO_3)_2$ solutions in dioxane are given in Table I.

Figure 8 presents k in dioxane plus 33-vol. percent castor oil as a function of age. It may be seen that k decreases with age. It is possible that larger aggregates are formed with time; the increase of the molecular radius was computed by using Stokes' relation

$$r=(\bar{k}T)/(6\pi\eta k), \tag{4}$$

where $\bar{k}$ = Boltzmann constant and T = absolute temperature. The computed radii are also shown in Fig. 8. Even if the absolute validity of Eq. (4) may be questioned, comparative molecular sizes derived from it are certainly useful.

The technique as described will next be used for the study of solutions in hydrocarbon oils, as mentioned in the introduction.

Physical Limitations of Omni-Directional Antennas*

L. J. CHU
Massachusetts Institute of Technology, Research Laboratory of Electronics, Boston, Massachusetts
(Received May 27, 1948)

The physical limitations of omni-directional antennas are considered. With the use of the spherical wave functions to describe the field, the directivity gain G and the Q of an unspecified antenna are calculated under idealized conditions. To obtain the optimum performance, three criteria are used, (1) maximum gain for a given complexity of the antenna structure, (2) minimum Q, (3) maximum ratio of G/Q. It is found that an antenna of which the maximum dimension is 2a has the potentiality of a broad band width provided that the gain is equal to or less than $4a/\lambda$. To obtain a gain higher than this value, the Q of the antenna increases at an astronomical rate. The antenna which has potentially the broadest band width of all omni-directional antennas is one which has a radiation pattern corresponding to that of an infinitesimally small dipole.

I. INTRODUCTION

AN antenna system, functioning as a transmitter, provides a practical means of transmitting, to a distant point or points in space, a signal which appears in the form of r-f energy at the input terminals of the transmitter. The performance of such an antenna system is judged by the quality of transmission, which is measured by both the efficiency of transmission and the signal distortion. At a single frequency, trans-

* This work has been supported in part by the Signal Corps, the Air Materiel Command, and O.N.R.

mission efficiency is determined by the power gain of the antenna system in a desired direction or directions. The distortion depends not only on the frequency characteristics of the antenna input impedance, but also on variations of phase and of power gain with frequency. It is common practice to describe the performance of an antenna system in terms of its power gain and the band width of its input impedance.

Designers of antennas at *VLF* range have always been faced with the problems of excessive conduction losses in the antenna structure and a narrow band width. At this frequency range, the physical size of the antenna is necessarily small in terms of the operating wave-length. For a broadcasting antenna, with a specified distribution of radiated power in space, it was found that the antenna towers must be spaced at a sufficient distance apart so as not to have excessive currents on the towers. At microwave frequencies, where a high gain has been made possible with a physically small antenna, there seems to be a close relationship between the maximum gain thus far obtainable and the size of the antenna expressed in terms of the operating wave-length. At optical frequencies where a different language is used, the resolving power of a lens or a reflector is proportional to the ratio of the linear dimension to wave-length. Thus, over the entire frequency range, there seems to be a practical limit to the gain or the directivity of a radiating or focussing system.

From time to time, there arises the question of achieving a higher gain from an antenna of given size than has been obtained conventionally. Among published articles, Schelkunoff[1] has derived a mathematical expression for the current distribution along an array which yields higher directivity gain than that which has been usually obtained. It is mentioned at the end of this article that an array carrying this current distribution would have a narrow band width as well as high conduction loss. In 1943, LaPaz and Miller[2] obtained an optimum current distribution on a vertical antenna of given length which gives the maximum possible field strength on the horizon for a given power output. The result was disputed in a later paper by Bouwkamp and deBruijn[3] who developed a method of realizing an arbitrarily sharp vertical radiation pattern by a suitable choice of the current distribution. In a later report by Laemmel of the Polytechnic Institute of Brooklyn, a method was presented for finding a source distribution function which results in an arbitrarily large gain relative to an isotropic radiator and which at the same time is contained within an arbitrarily small region of space.

In all the above articles, the authors invariably have computed the source distribution required to obtain a directivity gain higher than that obtained in practice with an antenna of a given size. As a result, it can be said that there is no mathematical limit to the directivity gain of an antenna of given size. The possibility of arranging on paper the current distribution on an antenna at r-f frequencies exists because of the absence of the severe restriction which must be observed, on account of the incoherent nature of the energy, in designing a system at optical frequencies.

In 1941, Stratton demonstrated the impracticality of supergain antennas. In his unpublished notes he derived the source distribution within a sphere of finite radius for any prescribed distribution of the radiation field in terms of a complete set of orthogonal, spherical, vector wave functions.[4] Mathematically, the series representing the source distribution diverges as the directivity gain of the system increases indefinitely. Physically, high current amplitude on the antenna, if it can be realized, implies high energy storage in the system, a large power dissipation, and a low transmission efficiency.

This paper presents an attempt to determine the optimum performance of an antenna in free space and the corresponding relation between its

[1] S. A. Schelkunoff, Bell System Tech. J. **22**, 80–107 (1943).

[2] L. ŁaPaz and G. A. Miller, Proc. I.R.E. **31**, 214–232 (1943).

[3] C. J. Bouwkamp and N. G. deBruijn, Philips Research Reports **1**, 135–158 (1946). This work was extended to the current distribution over an area by H. J. Riblet (Proc. I.R.E. **36**, 620–623 (1948)). Raymond M. Wilmotte, commenting on Riblet's work in a letter to the Editor (Proc. I.R.E. **36**, 878 (1948)), discussed the exceedingly low radiation resistance associated with discrete current distributions which have an abnormally high directivity.

[4] J. A. Stratton, *Electromagnetic Theory* (McGraw-Hill Book Company, Inc., New York, 1941). Chap. 7, p. 392.

gain and the band width of the input impedance under various criteria. Let the largest linear dimension of the antenna structure be $2a$, such that the complete antenna structure including transmission lines and the oscillator can be enclosed inside a geometrical spherical surface of radius a. The field outside the sphere as a result of an arbitrary current or source distribution inside the sphere can be expressed in terms of a complete set of spherical vector waves.[4] Each of these waves represents a spherical wave propagating radially outward. However, the current or source distribution *inside* the sphere is not uniquely determined by the field distribution *outside* the sphere. It is mathematically possible to create a given field distribution outside the sphere with an infinite number of different source distributions. We shall confine our interest to the most favorable source distribution and the corresponding antenna structure. To circumvent the difficult task of determining the latter, the most favorable conditions will be assumed to exist inside the sphere. The current or source distribution inside the sphere necessary to produce the desired field distribution outside will be assumed to require the minimum amount of energy stored inside the sphere so that one has a pure resistive input impedance at a single frequency. Also, to simplify the problem, the conduction loss will be neglected.

Under these conditions it is not possible to calculate the behavior of this antenna over a finite frequency range since the exact nature of the antenna structure is not known. At one frequency we can determine the radiation characteristics of the system from the expressions for the field, including the directivity gain of the antenna in a given direction. The directivity gain is equal to the power gain in the absence of conduction loss in the antenna structure. We shall utilize the conventional concept of Q, computed from the energy and power at a single frequency, to obtain the frequency characteristics of the input impedance by extrapolation. It is understood that the physical interpretation of Q as so computed becomes rather vague whenever the value of Q is low.

After obtaining the gain and Q of the antenna corresponding to an arbitrary field distribution outside the sphere, we then proceed to determine the optimum distribution of the field outside the sphere under different criteria and the corresponding gains and Q through the process of maximization and minimization.

Antennas can be classified according to their radiation characteristics as follows: (1) omnidirectional antennas, (2) pencil-beam antennas, (3) fanned-beam antennas, and (4) shaped-beam antennas. The first type of antenna will be discussed in detail in this article. The physical limitations of pencil-beam antennas will be dealt with in an article to be publsihed later.

The problem has been worked out independently by Ramo and Taylor** of Hughes Aircraft with a slightly different procedure. Their results are essentially in agreement with what follows.

II. ANALYSIS

A. Field of a Vertically Polarized Omni-Directional Antenna

The type of antenna under consideration here gives rise to an omni-directional pattern. It is commonly used as a beacon or broadcasting antenna. The radiated power is distributed uniformly around a vertical axis, which we take as the axis of a spherical coordinate system (R, θ, ϕ). We shall discuss first the case where the electric field lies in planes passing through the axis of symmetry. The antenna is schematically shown in Fig. 1 and lies totally within a spherical surface of radius a. For an arbitrary current distribution and antenna structure, the field outside the sphere can be expressed in terms of a complete set of orthogonal, spherical waves, propagating radially outward. For the type of antenna under consideration only TM_{n0} waves are required to describe the circularly symmetrical field with the specified polarization. By ignoring

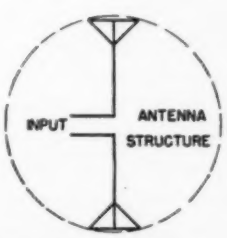

FIG. 1. Schematic diagram of a vertically polarized omni-directional antenna.

** See Ramo and Taylor, Proc. I.R.E. 36, 1135 (1948).

all the other spherical waves we have the expressions of the three non-vanishing field components:

$$H_\phi = \sum_n A_n P_n^1(\cos\theta) h_n(kR),$$

$$E_R = -j\left(\frac{\mu}{\epsilon}\right)^{\frac{1}{2}} \sum_n A_n n(n+1) \times P_n(\cos\theta) \frac{h_n(kR)}{kR},$$

$$E_\theta = j\left(\frac{\mu}{\epsilon}\right)^{\frac{1}{2}} \sum_n A_n P_n^1(\cos\theta) \times \frac{1}{kR} \frac{d}{dR}[Rh_n(kR)], \quad (1)$$

where $P_n(\cos\theta)$ is the Legendre polynomial of order n, $P_n^1(\cos\theta)$ is the first associated Legendre polynomial, $h_n(kR)$ is the spherical Hankel function of the second kind, $k=\omega(\epsilon\mu)^{\frac{1}{2}}=2\pi/\lambda$, $(\mu/\epsilon)^{\frac{1}{2}}$ is the wave impedance of a plane wave in free space and $1/(\epsilon\mu)^{\frac{1}{2}}$ is the velocity of a plane wave in free space. The time factor $e^{j\omega t}$ is omitted throughout the paper and the rationalized m.k.s. unit system is used. The coefficients A_n's are, in general, complex quantities. In synthesis problems, the A_n's are specified by the desired radiation characteristics. When the antenna structure is given, the A_n's are determined from the boundary conditions on the surfaces of the antenna structure. For the time being, the A_n's are a set of unspecified coefficients.

B. Radiation Characteristics

At a sufficiently large distance from the sphere, the transverse field components become asymptotically

$$\left.\begin{aligned} E_\theta &= (\mu/\epsilon)^{\frac{1}{2}} e^{-jkR}/kR \times \sum_n A_n(-1)^{(n+1)/2} P_n^1(\cos\theta) \\ H_\phi &= (\epsilon/\mu)^{\frac{1}{2}} E_\theta \end{aligned}\right\}. \quad (2)$$

The angular distribution of the radiation field is given by the series of the associated Legendre polynomials. This series behaves somewhat like a Fourier series in the interval from $\theta=0$ to $\theta=\pi$. Using the conventional definition for the directivity gain, we have

$$G(\theta) = \frac{4\pi|E_\theta|^2}{\int_0^\pi \int_0^{2\pi} |E_\theta|^2 \sin\theta d\theta d\phi} = \frac{|\sum_n A_n(-1)^{(n+1)/2} P_n^1(\cos\theta)|^2}{\sum_n |A_n|^2 \frac{n(n+1)}{2n+1}}. \quad (3)$$

The denominator is obtained from the orthogonality of the associated Legendre polynomials:

$$\int_0^\pi [P_n^1(\cos\theta)]^2 \sin\theta d\theta = \frac{2n(n+1)}{2n+1},$$

and

$$\int_0^\pi P_n^1(\cos\theta) P_{n'}^1(\cos\theta) \sin\theta d\theta = 0 \text{ for } n \neq n'.$$

We shall limit our attention to the gain in the equatorial plane $\theta=\pi/2$. In this plane,

$P_n^1(0)=0$ for n even, and

$$P_n^1(0) = (-1)^{(n-1)/2} \frac{n!}{2^{n-1}\left(\frac{n-1}{2}!\right)^2} \text{ for } n \text{ odd.}$$

Thus the terms of even n do not contribute to the radiation field along the equator. In order to have a high directivity gain in the equatorial plane it is necessary to have

$$A_n = 0 \text{ for } n \text{ even}$$

while all the rest of the A_n's must have the same phase angle. From here on, we shall consider all A_n's to be positive real quantities for odd n and zero for even n. Thus the directivity gain on the equatorial plane becomes

$$G\left(\frac{\pi}{2}\right) = \frac{[\sum' A_n(-1)^{(n+1)/2} P_n^1(0)]^2}{\sum' A_n^2 \frac{n(n+1)}{2n+1}}, \quad (4)$$

where $\sum'$ represents the sum over odd n only.

C. Power and Energy Outside the Sphere

With the field of the omni-directional antenna outside the sphere given by Eqs. (1), the total

complex power computed at the surface of the sphere is the integral of the complex Poynting vector over the same sphere:

$$P(a)=j2\pi\left(\frac{\mu}{\epsilon}\right)^{\frac{1}{2}}\Sigma'\left\{\frac{A_n}{k}\right\}^2\frac{n(n+1)}{2n+1}\rho h_n(\rho h_n)', \quad (5)$$

where

$$\rho=ka, \quad h_n=h_n(\rho), \quad (\rho h_n)'=\frac{d}{d\rho}\rho h_n(\rho).$$

The average power radiated is the real part of (5):

$$P_{Rn}=2\pi\left(\frac{\mu}{\epsilon}\right)^{\frac{1}{2}}\Sigma'\left\{\frac{A_n}{k}\right\}^2\frac{n(n+1)}{2n+1}. \quad (6)$$

It is possible to calculate the total electric energy and the magnetic energy stored outside the sphere. On the *c-w* basis the total stored energy is infinitely large provided any one of the A_n's is finite, since the radiation field which is inversely proportional to the radial distance extends to infinity. As in the case of an infinite transmission line with no dissipation, most of the energy appears in the form of a traveling wave which propagates toward infinity and never returns to the source. The total energy calculated on this basis has no direct bearing upon the performance of the antenna. It is difficult to separate the energy associated with the local field in the neighborhood of the antenna from the remainder. The energy is not linear in the field components and hence the law of linear superposition cannot be applied directly to it. The imaginary part of the integral of the complex Poynting vector is proportional only to the difference of the electrical and magnetic energy stored outside the sphere. In order to separate the energy associated with radiation from that associated with the local field, we shall reduce the field problem to a circuit problem where the radiation loss is replaced by an equivalent conduction loss.

D. Equivalent Circuits for Spherical Waves

Because of the orthogonal properties of the spherical wave functions employed, the total energy, electric or magnetic, stored outside the sphere is equal to the sum of the corresponding energies associated with each spherical wave,

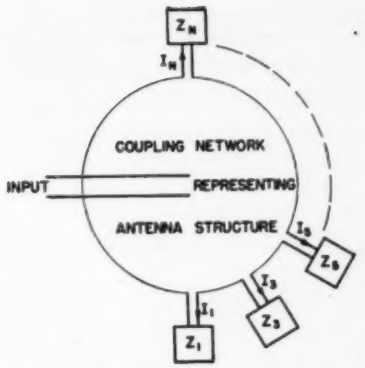

FIG. 2. Equivalent circuit of a vertically polarized omni-directional antenna.

and the complex power transmitted across a closed spherical surface is equal to the sum of the complex powers associated with each spherical wave. Insofar as the total energies and power are concerned, there is no coupling between any two of the spherical waves outside the sphere. Consequently, we can replace the space outside the sphere by a number of independent equivalent circuits, each with a pair of terminals connected to a box which represents the inside of the sphere. From this box, we can pull out a pair of terminals representing the input to the antenna as shown in Fig. 2. The total number of pairs of terminals is equal to the number of spherical waves used in describing the field outside the sphere, plus one. We have now managed to transform a space problem to the problem of its equivalent circuit.

When the field outside the sphere has been specified by Eqs. (1), the current, voltage, and impedance of the equivalent circuit for each spherical wave are uniquely determined except for an arbitrary real transformer ratio by equating the complex power associated with the spherical waves to that of the circuits. We shall define the voltage, current, and impedance of the equivalent circuit for the TM_n wave as:

$$V_n=\left(\frac{\mu}{\epsilon}\right)^{\frac{1}{2}}\frac{A_n}{k}\left(\frac{4\pi n(n+1)}{2n+1}\right)^{\frac{1}{2}}j(\rho h_n)'$$

$$I_n=\left(\frac{\mu}{\epsilon}\right)^{\frac{1}{2}}\frac{A_n}{k}\left(\frac{4\pi n(n+1)}{2n+1}\right)^{\frac{1}{2}}\rho h_n, \quad (7)$$

and

$$Z_n=j(\rho h_n)'/\rho h_n.$$

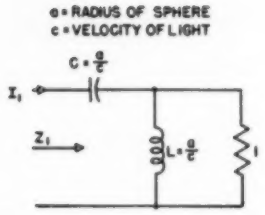

FIG. 3. Equivalent circuit of electric dipole.

The voltage is proportional to the θ component of electric field and the current is proportional to the magnetic field H_ϕ of the TM_n wave on the surface of the sphere. The normalized impedance Z_n is equal to the normalized radial wave impedance on the surface. It can be shown that not only is the complex power which is fed into the equivalent circuit equal to the complex power associated with the TM_n wave but the instantaneous powers are also equal to each other. The impedance Z_n of the equivalent circuit is a physically realizable impedance and Eqs. (7) are valid at all frequencies.

Using the recurrence formulas of the spherical Bessel functions, one can write the impedance Z_n as a continued fraction:

$$Z_n=\cfrac{n}{j\rho}+\cfrac{1}{\cfrac{2n-1}{j\rho}+\cfrac{1}{\cfrac{2n-3}{j\rho}+\cdots\cfrac{1}{\cfrac{3}{j\rho}+\cfrac{1}{\cfrac{1}{j\rho}+1}}}}. \quad (8)$$

This can be interpreted as a cascade of series capacitances and shunt inductances terminated with a unit resistance. For $n=1$, the impedance consists of the three elements shown in Fig. 3. This is the equivalent circuit representing a wave which could be generated by an infinitesimally small dipole. At low frequencies, most of the voltage applied to the terminal appears across the capacitance, and the unit resistance is practically short-circuited by the inductance. At high frequencies, the impedance Z_1 is practically a pure resistance of amplitude unity. At intermediate frequencies, the reactance of Z_1 remains capacitive. The equivalent circuit of Z_n is schematically shown in Fig. 4. The circuit, for all values of n, acts as a high-pass filter. With the dissipative element hidden at the very end of the cascade, the difficulty of feeding average power into the dissipative element at a single frequency increases with the order of the wave. The dissipation in the resistance is equal to the radiation loss in the space problem. The capacitances and inductances are proportional to the ratio of the radius of the sphere to the velocity of light. The increase of the radius of the sphere has the same effect on the behavior of the equivalent circuit as the increase of frequency.

TABLE I. The maximum gain *versus* N.

N	1	3	5.....N
Gain	1.5	3.81	4.10 $2N/\pi$

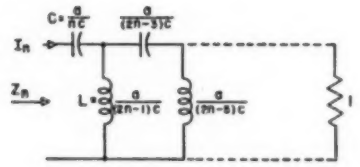

FIG. 4. Equivalent circuit of TM_n spherical wave.

Except for the equivalent circuit of the electric dipole, it would be tedious to calculate the total electric energy stored in all the capacitances of the equivalent circuit for Z_n. We shall therefore approximate the equivalent circuit for Z_n by a simple series RLC circuit which has essentially the same frequency behavior in the neighborhood of the operating frequency. We compute R_n, L_n, and C_n of the simplified equivalent circuit by equating the resistance, reactance, and the frequency derivative of the reactance of Z_n to those of the series RLC circuit. The series resistance R_n is of course equal to the real part of Z_n at the operating frequency. The results are the following:

$$R_n=|\rho h_n|^{-2},$$

$$C_n=\frac{2}{\omega^2}\left[\frac{dX_n}{d\omega}-\frac{X_n}{\omega}\right]^{-1},$$

$$L_n=\frac{1}{2}\left[\frac{dX_n}{d\omega}+\frac{X_n}{\omega}\right],$$

where

$$X_n=[\rho j_n(\rho j_n)'+\rho n_n(\rho n_n)']|\rho h_n|^{-2},$$

and j_n and n_n are the spherical Bessel functions of the first and second kind. Except for the frequency variation of the resistance R_n in the original equivalent circuit, the simplified circuit is accurate enough to describe Z_n in the immediate neighborhood of the operating frequency.

Based upon this simplified equivalent circuit, the average power dissipation in Z_n is

$$P_n=\left(\frac{\mu}{\epsilon}\right)^{\frac{1}{2}}\frac{2\pi n(n+1)}{2n+1}\left(\frac{A_n}{k}\right)^2 \qquad (10)$$

and the average electric energy stored in Z_n is

$$W_n=\left(\frac{\mu}{\epsilon}\right)^{\frac{1}{2}}\frac{\pi n(n+1)}{2(2n+1)}\times\left(\frac{A_n}{k}\right)^2|\rho h_n|^2\left[\frac{dX_n}{d\omega}-\frac{X_n}{\omega}\right], \qquad (11)$$

which is larger than the average magnetic energy stored in Z_n. We shall define Q_n for the TM_n wave as

$$Q_n=\frac{2\omega W_n}{P_n}=\frac{1}{2}|\rho h_n|^2\left[\rho\frac{dX_n}{d\rho}-X_n\right]. \qquad (12)$$

The band width of the equivalent circuit of the TM_n wave is equal to the reciprocal of Q_n, when it is matched externally with a proper amount of stored magnetic energy. When Q_n is low, the above interpretation is not precise, but it does indicate qualitatively the frequency sensitivity of the circuit.

In Fig. 5, Q_n of the TM_n waves is plotted against $2\pi a/\lambda$. We observe that Q_n is of the order of unity or less whenever the abscissa $2\pi a/\lambda$ is greater than the order n of the wave. Here the stored electric energy in the equivalent circuit of the wave is insignificant and the circuit behaves essentially as a pure resistance. When $2\pi a/\lambda$ is less than n, the circuit behaves essentially as a pure capacitance. Q_n increases at an astronomical rate as the abscissa decreases. In terms of wave propagation, the TM_n wave will propagate from the surface of the sphere without an excessive amount of energy stored in the neighborhood of the sphere only when the radius of the sphere is greater than $n\lambda/2\pi$.

E. Equivalent Circuit of the Antenna

The complete equivalent circuit of the antenna system is shown in Fig. 2. The circular box is a coupling network representing the space inside the geometrical sphere shown in Fig. 1. It couples the system feeding the input terminals to the various equivalent circuits of the TM waves connected externally to the box. The voltage V_n and current I_n are those given by Eqs. (7).

In Section B on radiation characteristics, it was pointed out that for each term to contribute positively to the gain of the antenna in the equatorial plane, it is necessary for all A_n's to have the same phase angle. The spherical Hankel function $h_n(\rho)$ is essentially a positive imaginary quantity when its argument is less than the order n. Thus, the currents of the equivalent circuits Z_n for n greater than the argument, are essentially in phase, and the instantaneous electric energies stored in all the equivalent circuits oscillate in phase.

We have calculated the power dissipation as well as the average energy stored in Z_n for the simplified circuit of the TM_n wave. The total electric energy stored and the power dissipated in all the circuits connected to the coupling network is equal to the summation of W_n and

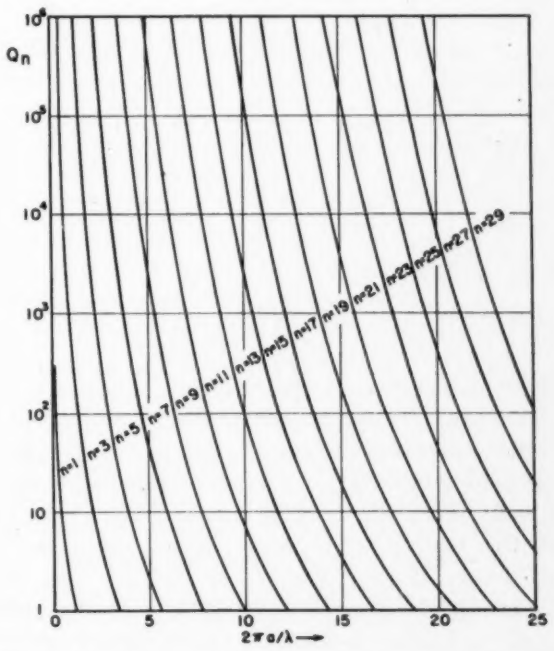

FIG. 5. Q_n of the equivalent circuit of TM_n or TE_n wave.

P_n, respectively. The total power dissipated $\sum' P_n$ is, of course, equal to the total power radiated into space, while the total electric energy stored $\sum' W_n$ is that associated with the local field outside of the sphere.

Theoretically, there is no unique antenna structure or source distribution inside the sphere which generates the field distribution given by Eqs. (1). Consequently, the coupling network representing the space inside the sphere is not unique. The process of determining the optimum antenna structure for a given field distribution outside or the optimum coupling network is by no means a simple matter. To simplify the problem and to give the best antenna structure the benefit of doubt, the following most favorable conditions for energy storage and power dissipation inside the sphere will be assumed:

1. There will be no dissipation in the antenna structure in the form of conduction loss.
2. There will be no electrical energy stored except in the form of a traveling wave.
3. The magnetic energy stored will be such that the total average electric energy stored beyond the input terminals of the antenna is equal to the average magnetic energy stored beyond the terminals at the operating frequency.

By Poynting's theorem it can be shown that the input impedance of the antenna is a pure resistance at the operating frequency under these conditions.

With this particular antenna structure, and its corresponding equivalent circuit, we can proceed to define a quantity Q at the input terminals:

$$Q=\frac{2\omega \text{ times the mean electric energy stored beyond the input terminals}}{\text{power dissipated in radiation}}.$$

If this Q is high, it can be interpreted as the reciprocal of the fractional frequency band width of the antenna. If it is low, the input impedance of the antenna varies slowly with frequency and the antenna has potentially a broad band width. The ratio Q can therefore be used in the latter case as a crude indication for a broadband.

Upon summing up the mean electric energy stored in all the simplified equivalent circuits representing the spherical waves outside the sphere, and the total power radiated, the Q of the idealized antenna is

$$Q=\frac{\sum' A_n^2 \frac{n(n+1)}{2n+1} Q_n(\rho)}{\sum' A_n^2 \frac{n(n+1)}{2n+1}}, \qquad (13)$$

where Q_n is given by Eq. (12).

We have defined and calculated two fundamental quantities G and Q for this somewhat idealized antenna. We have imposed a number of conditions on the coefficients A_n as well as on the energy and power inside the sphere. Otherwise, the set of coefficients A_n is yet unspecified. Additional conditions must be imposed on G and Q to determine the ultimate limits of antenna performance under various criteria.

F. Criterion I: Maximum Gain

Whenever the antenna structure must be confined within a small volume, and high gain is required, the logical criterion would be to demand maximum gain with an antenna structure of given complexity. The series of Legendre polynomials representing the field distribution behaves angularly in the same fashion as a Fourier series. The complexity of the source distribution required to generate the nth term increases with the order n. To specify the number of terms in Eqs. (1) to be used is therefore equivalent to specifying the complexity of the antenna structure. We shall therefore exclude all the terms for $n>N$, where N is an odd integer, and proceed to calculate the maximum gain as a function of N.

Differentiating the gain in the equatorial plane, [Eq. (4)], with respect to the coefficient A_n and setting the derivative to zero, we have

$$A_n=(-1)^{(n+1)/2}\frac{2n+1}{n(n+1)}P_n^1(0) \times \frac{\sum' A_n^2 \frac{n(n+1)}{2n+1}}{\sum' A_n(-1)^{(n+1)/2}P_n^1(0)}.$$

There are as many equations of this form as the number of terms in the series. We can therefore solve for A_n in terms of the first coefficient A_1:

$$A_n=(-1)^{n-1/2}\frac{2(2n+1)}{3n(n+1)}P_n^1(0)A_1. \quad (14)$$

The corresponding gain and Q of the antenna are

$$G\left(\frac{\pi}{2}\right)=\sum_1^N{}' a_n, \quad (15)$$

$$Q=\sum_1^N{}' a_nQ_n \Big/ \sum_1^N{}' a_n, \quad (16)$$

where

$$a_n=\frac{2n+1}{n(n+1)}[P_n^1(0)]^2. \quad (17)$$

Except for the first few terms,

$$a_n\cong 4/\pi. \quad (18)$$

The formula (15) for the maximum gain was previously obtained by W. W. Hansen.[5]

The value of the maximum gain for different values of N is given in Table I. For $N=1$, the gain is that of an electric dipole. For large values of N, the gain is proportional to N. Under the present criterion, the gain is independent of the size of the antenna. It indicates that an arbitrarily high gain can be obtained with an arbitrarily small antenna, provided the source distribution can be physically arranged.

Figure 6 shows the Q of an antenna designed to obtain the maximum gain with a given number of terms, as a function of $2\pi a/\lambda$. While the terms in the denominator of Eq. (16) have approximately equal amplitudes, the numerator is an ascending series of $(N+1)/2$ terms. For any given value of $2\pi a/\lambda$, Q_n increases with n at a rapid rate as shown in Fig. 5. The numerator is essentially determined by the last few terms of the ascending series. For $2\pi a/\lambda$ greater than N, Q is of the order of unity or less, indicating the potentiality of a broad-band system. For $2\pi a/\lambda$ less than N, the value of Q rises astronomically as $2\pi a/\lambda$ decreases. The transition occurs for

$$2\pi a/\lambda\cong N \quad (19)$$

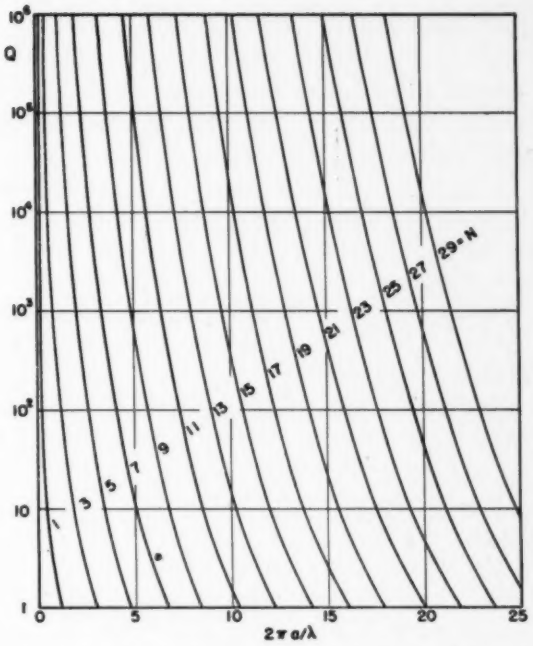

FIG. 6. Q of omni-directional antenna. Criterion: Max. gain with fixed number of terms.

corresponding to a gain

$$G\cong\frac{2}{\pi}\cdot\frac{2\pi a}{\lambda}=\frac{4a}{\lambda}. \quad (20)$$

The gain of an omni-directional antenna as given by Eq. (20) will be called the normal gain. It is equal to the gain obtained from a current distribution of uniform amplitude and phase along a line of length $2a$. In Fig. 7, curve I shows the Q of an antenna of normal gain. To increase the gain by a factor of two, we have to use twice as many terms, and pay dearly in Q as shown by Curve II. The slope of Curve II indicates the increasing difficulty of obtaining additional gain as the normal gain increases.

Under the present criterion, no special conditions have been imposed on Q. It can be shown that the Q obtained here is by no means the minimum for a given gain and antenna size. Since the gain is maximized [Eq. (15)] with respect to A_n, a small variation of A_N will not affect the gain. Instead, the Q will vary rapidly as indicated by Eq. (13) when $N>2\pi a/\lambda$.

G. Criterion II: Minimum Q

In this section, we shall proceed to find a combination of A_n's to give the minimum Q with

[5] W. W. Hansen, "Notes on Microwaves," M.I.T. Rad. Lab. Report T-2.

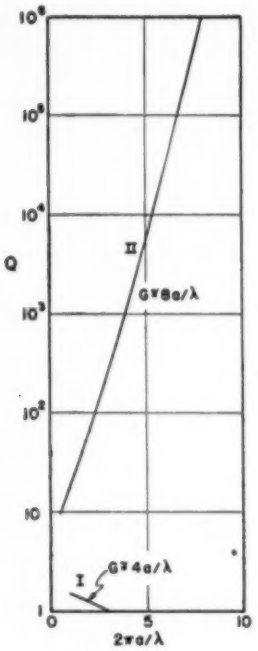

FIG. 7. Q for omni-directional antenna. Criterion: Max. G with fixed number of terms. I—normal gain. II—twice the normal gain.

no separate conditions imposed on the gain of the antenna. Differentiating Q with respect to A_n we have the following equation:

$$Q_n \sum' A_n^2 \frac{n(n+1)}{2n+1} = \sum' A_n^2 \frac{n(n+1)}{2n+1} Q_n.$$

For any given value of $2\pi a/\lambda$, all the Q_n's have different values. Hence, the above equation can be satisfied when there is only one term under the summation sign. The corresponding Q of the antenna is equal to the Q_n of the term used. Since Q_1 has the lowest amplitude, we conclude that the antenna which generates a field outside the sphere corresponding to that of an infinitesimally small dipole has potentially the broadest band width of all antennas. The gain of this antenna is 1.5.

H. Criterion III: Maximum G/Q

As a compromise between the two criteria just mentioned, we shall now maximize the ratio of the gain to Q. The process can be interpreted as the condition for the minimum Q to achieve a certain gain or as the condition for the maximum gain at a given Q. The problem is that of finding the proper combination of A_n's for maximum G/Q. From Eqs. (4) and (13), we have

$$\frac{G}{Q} = \frac{[\sum' A_n(-1)^{(n+1)/2} P_n^1(0)]^2}{\sum' A_n^2 \frac{n(n+1)}{2n+1} Q_n}. \tag{21}$$

With the same method used before, we obtain

$$A_n = (-1)^{(n-1)/2} \frac{2(2n+1)}{3n(n+1)} P_n^1(0) \frac{Q_1}{Q_n} A_1. \tag{22}$$

The corresponding values of G, Q, and the ratio G/Q are

$$G = \frac{[\sum' a_n/Q_n]^2}{\sum' a_n/Q_n^2}, \tag{23}$$

$$Q = \frac{\sum' a_n/Q_n}{\sum' a_n/Q_n^2}, \tag{24}$$

$$G/Q = \sum' a_n/Q_n, \tag{25}$$

where a_n is given in Eq. (17). The gain and G/Q are plotted against $2\pi a/\lambda$ with N as a parameter in Figs. 8 and 9, respectively. In using the above formulas, Q_n is arbitrarily considered to be unity whenever its actual value is equal to or less than unity. The Q for all the points on the curve is about unity. Since the two series involved in Eqs. (23) and (24) converge rapidly as N is increased indefinitely, the gain approaches asymptotically the approximate value of $4a/\lambda$ which is the normal gain derived under criterion I. There is a definite limit to the gain if the Q of the antenna is required to be low. It is this physical limitation, among others, which limits the gain of all the practical antennas to the approximate value $4a/\lambda$.

I. Horizontally Polarized Omni-Directional Antenna

By interchanging E and H in Eq. (1), and replacing $(\epsilon/\mu)^{\frac{1}{2}}$ by $-(\mu/\epsilon)^{\frac{1}{2}}$, we have the field outside the geometric sphere, for a horizontally polarized omni-directional antenna, expressed as a summation of circularly symmetrical TE_n

waves:

$$E_\phi = \left(\frac{\mu}{\epsilon}\right)^{\frac{1}{2}} \sum' B_n P_n^1(\cos\theta) h_n(kR),$$

$$H_r = j \sum' B_n n(n+1) P_n(\cos\theta) \frac{h_n(kR)}{kR}, \qquad (26)$$

$$H_\theta = -j \sum' B_n P_n^1(\cos\theta) \frac{1}{kR} \frac{d}{dR}[Rh_n(kR)],$$

where the B_n's are arbitrary constants. As before, each TE_n wave at the surface of the sphere can be replaced by a two-terminal equivalent circuit defined on the same basis as that of the corresponding TM_n wave. The voltage, current, and admittance at the input of the circuit are the following:

$$V_n = \left(\frac{\mu}{\epsilon}\right)^{\frac{1}{2}} \frac{B_n}{k} \left(\frac{4\pi n(n+1)}{2n+1}\right)^{\frac{1}{2}} \rho h_n, \qquad (27)$$

$$I_n = \left(\frac{\mu}{\epsilon}\right)^{\frac{1}{2}} \frac{B_n}{k} \left(\frac{4\pi n(n+1)}{2n+1}\right)^{\frac{1}{2}} j(\rho h_n)', \qquad (28)$$

$$Y_n = j(\rho h_n)'/\rho h_n.$$

The admittance is equal to the normalized wave admittance of the TE_n wave on the surface of the sphere, and is also equal to the impedance Z_n of the equivalent circuit for the TM_n wave. This circuit is a cascade of shunt inductances and series capacitances terminated with a unit conductance as shown in Fig. 10. At low frequencies, the admittance is practically that of the first inductance. The admittance remains inductive at all frequencies and approaches a pure conductance of unit amplitude as the frequency increases.

The analysis of the horizontally polarized omni-directional antenna follows exactly that of the vertically polarized one. The formulas for G, P_n, W_n, Q_n, and Q remain unchanged if we replace all the A_n's by B_n's. The quantity W_n is now to be interpreted as the mean magnetic energy stored in the simplified equivalent circuit of the TE_n wave (a parallel RLC circuit). Results obtained previously apply to the present problem without further modification.

J. Circularly Polarized Omni-Directional Antenna

The field of an elliptically polarized omni-directional antenna can be expressed as a sum

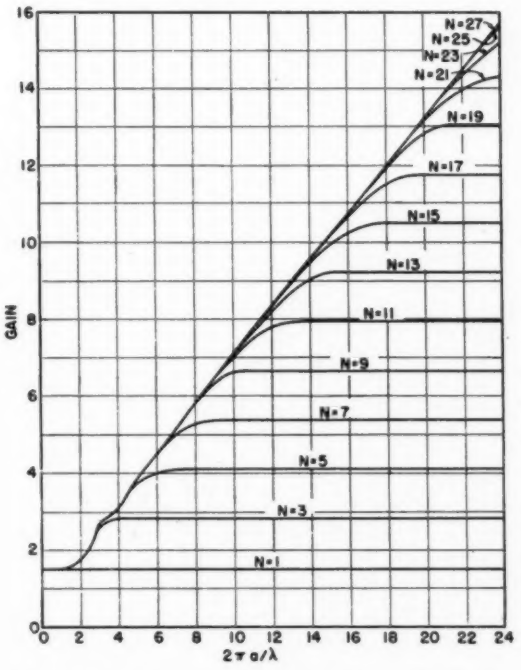

FIG. 8. Gain of omni-directional antenna. Criterion: Max. G/Q. When $Q_n < 1$, it is considered to be unity.

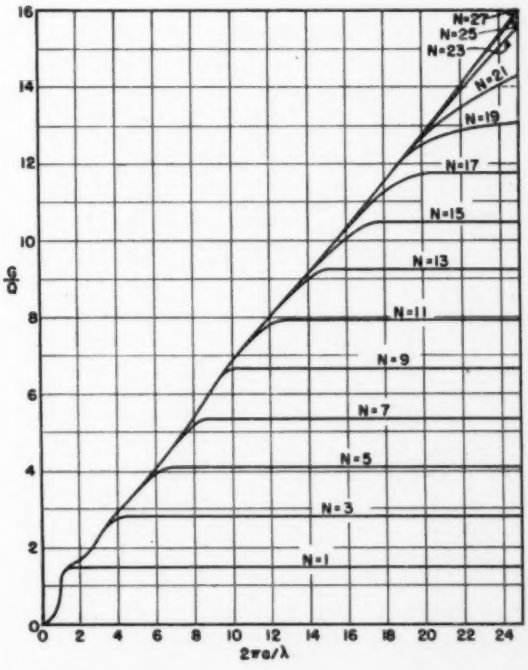

FIG. 9. G/Q of omni-directional antenna. Criterion: Max. G/Q. When $Q_n < 1$, it is considered to be unity.

of TM_n waves [Eqs. (1)] and TE_n waves [Eqs. (26)]. To obtain circular polarization everywhere, we must have

$$B_n = \pm jA_n. \tag{30}$$

Under this condition, the gain of the circularly polarized antenna is again given by Eq. (3).

The equivalent circuit of the circularly polarized omni-directional antenna consists of $2N+1$ pairs of terminals where N is the highest order of the spherical waves used. If we are only interested in the gain along the equator, the even terms of the series can be excluded. The number of pairs are reduced to $N+2$ including the input pair. It is interesting to observe that the instantaneous total energy density at any point outside the sphere is independent of time when Eq. (30) is satisfied. The difference between the mean electric energy density and the mean magnetic energy density is zero at any point outside the sphere enclosing the antenna. Furthermore, the instantaneous Poynting vector is independent of time. This implies that the power flow from the surface of the sphere enclosing a truly circularly polarized omni-directional antenna is a d.c. flow, and the instantaneous power is equal to the radiated power. These relationships are due to the dual nature of TE waves and TM waves as well as the 90° difference in time phase between the two sets of waves.

To obtain the Q of the antenna, it is convenient to combine the energies and dissipation in Z_n of the TM_n wave with that in Y_n of the TE_n wave and define a new Q_n as $2\omega W_n/P_n$ where W_n is the mean electric or magnetic energy stored in Z_n and Y_n, and P_n is the total power dissipated in both. Then

$$Q_n = \tfrac{1}{2}|\rho h_n|^2 \rho \frac{dX_n}{d\rho}, \tag{31}$$

where X_n is the imaginary part of Z_n. For $\rho = 2\pi a/\lambda > n$, this Q_n is approximately equal to

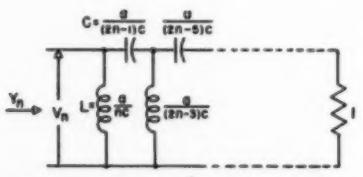

FIG. 10. Equivalent circuit of TE_n spherical wave.

one-half of the previous Q_n defined for Z_n or Y_n alone, [Eq. (12)]. If no conduction loss and no stored energy inside the sphere are assumed, the expression for Q of a circularly polarized omni-directional antenna turns out to be identical with that given by Eq. (13), except that Q_n is given by Eq. (31) instead of Eq. (12).

With expressions for G and Q identical with what were obtained previously, we expect similar numerical results for the present case under the various criteria, and the same physical limitation applies.

III. FURTHER CONSIDERATIONS

A. Practical Limitations

The above analysis does not take into consideration many practical aspects of antenna design. In the following, a qualitative discussion will be given of some of the practical limitations.

It is assumed in the analysis that the antenna under consideration is located in free space. The results, with a minor modification are applicable to the problem of a vertically polarized antenna above a perfectly conducting ground plane. In practice, this condition can seldom be fulfilled. The performance of an antenna designed on the free-space basis will be modified by the presence of physical objects in the neighborhood. Currents will be induced on the objects. They will give rise not only to an additional scattered radiation field but also to a modification of the original current distribution on the antenna structure. Both the gain and Q of the antenna will be changed from their unperturbed values. The currents set up on the objects vary as the unperturbed field intensity at the locations of the objects. For the same power radiated, the r.m.s. amplitude of the unperturbed field intensity in the neighborhood of the antenna is approximately proportional to the square root of Q. In view of the rapid increase of Q as the gain of an antenna is increased above the normal value shown in Fig. 6, the disturbance of the field distribution in space by physical objects in the neighborhood of the antenna becomes increasingly serious.

It is tacitly assumed in the analysis that physically it is possible to design an antenna to achieve an arbitrary current distribution which

satisfies the condition for minimum energy storage as discussed in Section II, E. To obtain a gain above normal, additional higher-order spherical waves must be generated outside the sphere with a proper control of amplitudes and relative phases. The corresponding current distribution will have rapid amplitude and phase variation inside the sphere. The practical difficulty of achieving this current distribution will increase with the gain.

We have avoided the question of conduction losses on the antenna structure. In practice, the antenna structure will have conductivities differing from zero or infinity. Neglecting the losses on the transmission line, it can be shown that the minimum conduction loss of the antenna under consideration varies approximately as the mean square of the electric or magnetic field on the surface of the sphere. For a high-Q antenna, the ratio of the minimum conduction loss to the power radiated is therefore approximately proportional to the Q of the antenna computed in the absence of losses. Although this conduction loss is helpful in reducing the Q at the input terminals, it reduces the efficiency and the power gain of the antenna.

The condition of minimum energy storage within the sphere is not always realizable. On account of the unavoidable frequency sensitivities of the elements of the antenna structure or the matching networks, the Q of a practical antenna computed on the no conduction-loss basis will be usually higher than the one derived in this paper.

B. Band Width and Ideal Matching Network

We have computed the Q of an antenna from the energy stored in the equivalent circuit and the power radiated, and interpreted it freely as the reciprocal of the fractional band width. To be more accurate, one must define the band width in terms of allowable impedance variation or the tolerable reflection coefficient over the band. For a given antenna, the band width can be increased by choosing a proper matching network. The theoretical aspect of this problem has been dealt with by R. M. Fano.[6] Figure 11 given here through his courtesy illustrates the relations among the fractional band width, absolute amplitude of the reflection coefficient, and the parameter $2\pi a/\lambda$ of an antenna which has only the TM_1 wave outside the sphere. As shown in Section II, F this antenna has the lowest Q of all vertically polarized omni-directional antennas and its equivalent circuit is shown in Fig. 3. The curve of Fig. 11 is computed on the assumption that the input impedance of the antenna is equal to Z_1, and an ideal matching network is used to obtain a constant amplitude of the reflection coefficient over the band. The phase of the reflection coefficient, however, varies rapidly near the ends of the band.

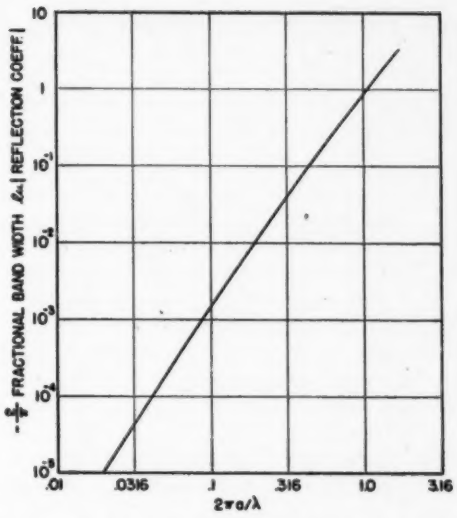

FIG. 11. Bandwidth of an ideal dipole with ideal matching network.

[6] R. M. Fano, "Theoretical Limitations on the Broadband Matching of Arbitrary Impedances," R.L.E. Technical Report No. 41, January 2, 1948.

A Technique for Quantitative Determination of Texture of Sheet Metals

JOHN T. NORTON*
Massachusetts Institute of Technology, Cambridge, Massachusetts
(Received July 6, 1948)

A method is described for making a pole figure of rolled sheet employing an x-ray unit equipped with a G-M counter for measuring intensities. Small rods are cut from the sheet with their axes parallel to the plane of the sheet and making various angles with the rolling direction. With the counter tube set at the correct diffraction angle for the desired crystallographic plane, each rod in turn is placed in the beam and rotated continuously about its axis. The recorder chart, synchronized with the rod rotation, plots a curve of intensity *vs.* angular position. Thus the record for each rod provides information for a specific diameter of the pole figure and all have a common point at the center. Since all rods are cylindrical and of the same diameter, there is no absorption correction to be applied. Contours for the pole figures may be drawn as closely together as desired. For special purposes where the complete pole figure is not required but quantitative comparisons are to be made between specimens, certain simplified techniques based on the same principle have proved useful.

INTRODUCTION

A METHOD of obtaining information for the construction of pole figures of sheet with preferred orientation, which employs an x-ray unit with a G-M counter tube has recently been described by Decker, Asp, and Harker.[1] This method employs a thin sheet specimen which can be rotated about two mutually perpendicular axes so that the intensity of the reflected beam and hence the pole density can be determined, point by point. In this paper, a factor was developed to correct the observed intensities for the changing angular position of the specimen with respect to the incident beam. The method does not permit the central portion of the pole figure to be obtained and a large number of individual points must be measured if a proper coverage is to be secured. A somewhat different technique will provide the missing information and eliminates the need for the angular correction factor.

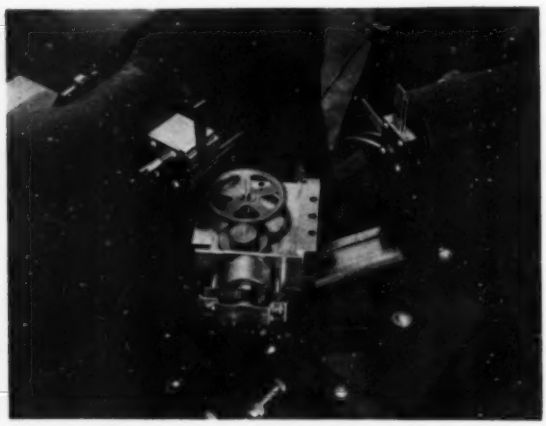

FIG. 1. Photograph of rod specimen mount in Norelco recording x-ray spectrometer.

In the technique here described, small cylindrical rods are cut from the sheet in such a way that the rod axis lies in the plane of the sheet and makes various angles with the rolling direction. Each rod is placed in turn in the x-ray beam and rotated about the rod axis so that the reflected intensity in a plane perpendicular to the rod axis is measured. The measured intensities from each rod, which will be proportional to pole density, will, when plotted, lie on a diameter of the pole figure. Since all rods are the same diameter and have rotational symmetry about the axis, the absorption correction is constant and may be disregarded. As many rods may be prepared as is necessary to obtain the desired coverage of the pole figure.

In order to decrease the rather tedious job of using the counter to obtain the intensity of each point, the rod may be rotated continuously at constant speed and the output signal from the G-M counter tube connected to a strip chart recorder in such a way that the paper motion is synchronized with the specimen rotation. The result is a continuous curve of the intensity *vs.* angle for each diameter of the pole figure. All of

* Professor of Metallurgy, Massachusetts Institute of Technology, Cambridge, Massachusetts.
[1] Decker, Asp, and Harker, J. App. Phys. **19**, 388 (1948).

these curves should give the same intensity value for the center of the pole figure which serves as a useful check on the results. From the intensity curves, it is a very simple matter to draw horizontal sections and transfer the information to the pole figure in the form of contours.

PREPARATION OF SPECIMENS

The preparation of the rod specimens offers no particular difficulty. The direction of the rod axis is inscribed on the sheet surface and a rough blank cut out with a band saw. The blank is then placed in a jeweler's lathe and carefully turned down to cylindrical form. The finished rod should be about 0.75″ long with one end turned to a taper which fits a matching tapered hole in the specimen mount. The opposite end of the rod is filed to a chisel edge to indicate the original rolling plane. The final diameter of the rod is not critical provided all of the rods of a set are of the same diameter. A diameter of 0.30″ is a convenient size to work with but rods of smaller diameter can be made with sufficient care. It is also possible to file out a rod by hand, making first a square and then an octagonal cross section and finishing to cylindrical shape with a lapping device made of a small split brass block using grinding paste.

The final surface finish is important and is obtained by polishing with fine abrasive paper to remove the cold work of turning and then etching to remove the polished layer. The light polishing and etching may be repeated two or three times until a constant intensity curve results. Cold-rolled sheet frequently has surface layer of different orientation from the interior and, for this reason, the final rod diameter should be not more than 75 percent of the original sheet thickness.

EXPERIMENTAL ARRANGEMENT

The equipment employed is the commercial Norelco recording x-ray spectrometer with a special specimen mount which fits into the socket used for the standard mount. The special mount consists of a vertical shaft accurately mounted in a bearing which can be moved by means of a slide so that the shaft axis can be made to coincide with the spectrometer axis or displaced in a horizontal direction by any desired amount. At the top of this shaft is a chuck containing a tapered

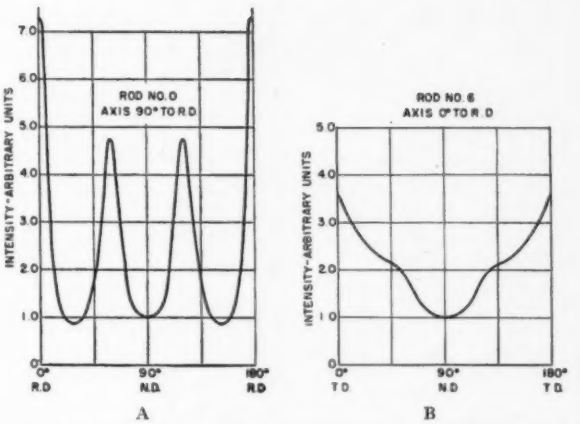

FIG. 2. Typical curves showing change in 110 intensity as rods are rotated through 180°. (A): Rod axis parallel to transverse direction. (B): Rod axis parallel to rolling direction.

hole into which the rod specimen fits, the whole capable of rotation without any eccentricity. The shaft is rotated by a gear train and synchronous motor at a speed of 20° per minute. Means are available for disengaging the gears so that the specimen may be rotated by hand if desired.

The slit defining the x-ray beam is wide enough to illuminate the whole specimen and high enough to cover a specimen length of about 0.375″. In cold-rolled sheet, the grain size is small enough to give a satisfactory statistical picture of a specimen of this size. The G-M tube slit is set at maximum width to include as much of the reflected beam as possible. Figure 1 shows the experimental arrangement.

With the rod stationary and at the angle corresponding to maximum pole density, the reflected line is scanned in the usual manner to establish the background intensity and the angle of maximum intensity for the chosen set of lattice planes. The counter tube is then set at this angle and a 360° rotation of the rod is recorded. The exact angular position of the original rolling plane can be determined from an examination of the record.

Each record should be symmetrical about a direction in the rolling plane and a direction perpendicular to it. Frequently the records are not exactly symmetrical due to some slight misalignment and it is satisfactory to average the four portions of the curve representing one complete revolution. It will be found that the angular positions of the peaks and valleys will be substantially the same but that the intensities may

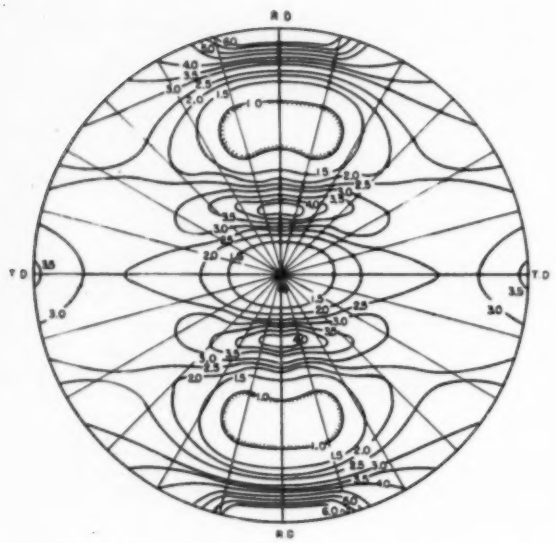

FIG. 3. Pole figure of 110 poles for low carbon steel sheet with a cold reduction of 43 percent.

vary, especially if the peaks are quite sharp. Experience has shown that if several rods are cut from the same specimen, the averaged curves are consistent even though the individual curves are somewhat unsymmetrical. Tracings of typical intensity curves are shown in Fig. 2.

TYPICAL RESULTS

In Fig. 3 is shown a pole figure of the 110 poles of a specimen of low carbon steel sheet reduced 43 percent by cold-rolling. The scale of pole densities is an arbitrary one and the density in the normal direction (center of pole figure) was taken as unity. In one quadrant are the actual points taken from the intensity curves which are used in drawing the contours.

There are two limitations to the pole figure method described above which must be recognized. The first is that the sheet under investigation must be thick enough so that a suitable rod can be prepared. The lower limit of thickness appears to be about 0.015". It is conceivable that several layers might be soldered or cemented together to form a blank from which a rod could be machined but so far attempts have not been very successful. The other limitation is that the grain size of the rod must be such that enough crystals are illuminated to give a proper statistical picture. Recrystallized metals often give very irregular response curves and, for this reason, it has not been possible to study recrystallization orientations in a satisfactory manner. For cold-worked materials, however, the results have proved very satisfactory and represent a considerable improvement over the photographic methods previously employed for studying problems of preferred orientation.

There are many cases where it is desired to compare the crystallographic anisotropy of two lots of materials, but knowledge of the complete pole figure is unnecessary. Suppose, for instance, one wishes to observe the anisotropy in the plane of the sheet. Several pieces of the sheet are placed, one on top of the other, with the rolling direction parallel and are screwed together to make a block about 0.375" thick. The block is then placed in the lathe and turned to a disk with its axis perpendicular to the rolling plane. The disk is placed on the rotating device so that the beam is just tangent to its edge when the counter tube is at zero degrees on the scale. The tube is then turned to the correct angle for reflection from the desired family of planes and the disk rotated, making a continuous record of the intensities. Such response curves of the several lots of material may then be compared directly. Other modifications of the technique will occur to the reader.

Letters to the Editor

Drag of an Airfoil in Accelerated, Supersonic Flight*

C. S. GARDNER, H. F. LUDLOFF, AND F. REICHE
College of Engineering, New York University, New York, New York
September 13, 1948

IF a thin airfoil of profile form $f(\bar{x})$ moves at the supersonic speed $U=U_0+b\cdot t$, b being a constant acceleration, into still air, the disturbance caused by the airfoil can be expressed by a perturbation potential $\bar{\varphi}$, which obeys the differential equation

$$a_0^2(\bar{\varphi}_{\bar{x}\bar{x}}+\bar{\varphi}_{\bar{y}\bar{y}})-\bar{\varphi}_{\bar{t}\bar{t}}=0, \tag{1}$$

and the boundary condition:

$$\begin{cases}\text{for:}\quad -U_0\bar{t}-\frac{1}{2}b\bar{t}^2<\bar{x}<-U_0\bar{t}-\frac{1}{2}b\bar{t}^2+l,\\ (\bar{\varphi}_{\bar{y}})_{\bar{y}=0}=(U_0+b\cdot\bar{t})\cdot f';\end{cases} \tag{2}$$

here f' stands for the slope of the airfoil surface at any station at a given time $\bar{t}$, a_0 is the sound velocity, and $\bar{x}$, $\bar{y}$ are coordinates, fixed in still air. l is the chord length.

As (1) represents a wave equation in the $\bar{x}-\bar{t}$-plane, it appears appropriate to introduce characteristic coordinates ξ, $\eta=\bar{x}\pm a_0\cdot\bar{t}$, whereupon the solution can be obtained merely by two quadratures. In this way $\bar{\varphi}$ finally becomes

$$\bar{\varphi}(\xi_0,\eta_0)_{\bar{y}=0}\sim-\int_{\eta_1}^{\eta_0}d\eta\int_{\xi_0}^{\xi_1(\eta)}d\xi \times((\bar{\varphi}_{\bar{y}})_{\bar{y}=0})/(((\xi-\xi_0)(\eta_0-\eta))^{\frac{1}{2}}). \tag{3}$$

(3) can be interpreted as a "supersonic source" distribution. The integration has to be extended over a quasi-triangular area in the $\xi-\eta$-plane, which is bounded by the two characteristics $\xi=\xi_0$ and $\eta=\eta_0$, going through $P(\xi_0\eta_0)$, and a parabolic arc, representing the accelerated motion of the leading edge. The integrals to be evaluated in (3) are rather complicated combinations of elliptic integrals, which will be discussed in a separate paper.

Here, however, an alternative approach will be followed. By introducing dimensionless coordinates which are *fixed* in the *airfoil*,

$$x=\frac{\bar{x}+U_0\cdot\bar{t}+\frac{1}{2}b\cdot\bar{t}^2}{l},\quad y=\bar{y}/l,\quad t=(\bar{t}\cdot a_0)/l,$$

and also

$$M_0=U_0/a_0,\quad B=(bl)/a_0^2,\quad \varphi=\bar{\varphi}/a_0l,$$

(1) and (2) transform into D.E.:

$$[(M_0+Bt)^2-1]\varphi_{xx}-\varphi_{yy} +2(M_0+Bt)\varphi_{xt}+B\cdot\varphi_x+\varphi_{tt}=0,$$

and B.C.:

$$(\varphi_y)_{y=0}=(M_0+B\cdot t)f'(x). \tag{4}$$

Assuming that the acceleration $B\ll1$, we expand φ, D.E. and B.C. in powers of B:

$$\varphi=\varphi^0+B\cdot\varphi'+B^2\cdot\varphi^2+\cdots.$$

Using characteristic coordinates $\xi,\eta=x\mp(M_0^2-1)^{\frac{1}{2}}\cdot y$, we obtain **with B^0:**

$$4(M_0^2-1)\varphi_{\xi\eta}{}^0=0;$$

$$\varphi_\eta{}^0-\varphi_\xi{}^0=\frac{M_0}{(M_0^2-1)^{\frac{1}{2}}}\cdot f'(x)\text{ for }\xi=\eta=x.$$

Solution on the airfoil surface $y\sim0$:

$$(\varphi^0)_{y=0}=-\frac{M_0}{(M_0^2-1)^{\frac{1}{2}}}\cdot f(x). \tag{5}$$

With B^1: Putting $\varphi^1=\varphi^{11}+t\cdot\varphi^{12}$, where φ^{11} and φ^{12} are independent of t:

$$4(M_0^2-1)\varphi_{\xi\eta}{}^{12}=\frac{2M_0^2}{(M_0^2-1)^{\frac{1}{2}}}\cdot f''(\xi),$$

with

$$\varphi_\eta{}^{12}-\varphi_\xi{}^{12}=\frac{f'(x)}{(M_0^2-1)^{\frac{1}{2}}},\text{ for }\xi=\eta=x.$$

Similarly,

$$4(M_0^2-1)\varphi_{\xi\eta}{}^{11}=-2M_0(\varphi_\xi{}^{12}+\varphi_\eta{}^{12})+\frac{M_0}{(M_0^2-1)^{\frac{1}{2}}}\cdot f'(\xi),$$

with

$$\varphi_\eta{}^{11}-\varphi_\xi{}^{11}=0\text{ for }\xi=\eta=x.$$

Solution:

$$(\varphi^1)_{y=0}=(t)/((M_0^2-1)^{3/2})\cdot f(x) -\tfrac{1}{2}(M_0)/((M_0^2-1)^{5/2})\cdot\int_0^x f(x')dx'. \tag{6}$$

With B^2: Putting $\varphi^2=\varphi^{21}+t\cdot\varphi^{22}+t^2\cdot\varphi^{23}$, we get

$$4(M_0^2-1)\varphi_{\xi\eta}{}^{23}=-2M_0(\varphi_{\xi\xi}{}^{12}+\varphi_{\eta\eta}{}^{12}+2\varphi_{\xi\eta}{}^{12}) +\frac{M_0}{(M_0^2-1)^{\frac{1}{2}}}\cdot f''(\xi),$$

with:

$$\varphi_\eta{}^{23}-\varphi_\xi{}^{23}=0\text{ for }\xi=\eta=x.$$

Similar differential equations and boundary conditions are obtained for φ^{22} and φ^{21}.

On the airfoil surface ($y\sim0$), the solution reduces to

$$(\varphi^2)_{y=0}=-(15M_0(4M_0^2+3))/(8(M_0^2-1)^{9/2}) \cdot\int_0^x dx'\int_0^{x'}dx''\cdot f(x'') +t\cdot\frac{3(4M_0^2+1)}{2(M_0^2-1)^{7/2}}\cdot\int_0^x dx'\cdot f(x') -t^2\frac{3\cdot M_0}{2\cdot(M_0^2-1)^{5/2}}\cdot f(x). \tag{7}$$

If necessary, the contributions of higher order, $B^n\cdot\varphi^n$, can be readily deduced. It can be shown by a more involved argument that the so obtained perturbation potential, $\varphi=\varphi^0+B\cdot\varphi^1+B^2\cdot\varphi^2+\cdots$, vanishes at the characteristic surface $y=\psi(x,t,B)$ of D.E. (4), as it must be.

Using the adiabatic $p-\rho$-relation and Bernoulli's law, we find, by disregarding consistently higher orders of the velocity components, the pressure relative to that in still air:

$$\Delta p/\rho=-\bar{\varphi}_{\bar{t}}=-a_0^2[(M_0+Bt)\varphi_x+\varphi_t], \tag{8a}$$

and at zero angle of attack, for symmetrical profiles, the drag per unit length

$$D'=2l\int_0^1 dx f'(x)\cdot\Delta p. \tag{8b}$$

Upon substituting the values of φ_s and φ_t from (5)–(7) into (8a,b), one obtains D' and the "instantaneous" drag coefficient:

$$c_D=(D')/(\tfrac{1}{2}\rho U^2\cdot l)=(4)/(M^2-1)^{\frac{1}{2}}\cdot\int_0^1[f'(x)]^2dx$$
$$-6\cdot B^2(M^4+(27/4)M^2+1)/(M^2(M^2-1)^{9/2})$$
$$\cdot\int_0^1[f(x)]^2dx. \quad (9)$$

The first term in (9) represents the well-known expression for the wave drag of an airfoil, except for the fact that M refers to the *instantaneous speed*, $M=(U_0+bt)/a_0$, rather than to the uniform speed, $M_0=U_0/a_0$. In other words, the contributions to c_D which are proportional to B^0 and B^1 have been combined, with the result that neither U_0 nor t appear explicitly in (9), but only by way of M. This is rather satisfactory. Thus, up to the first power of B, the result can be obtained by quasi-stationary treatment. The second term in (9), however, adds a new feature by indicating that as a result of the acceleration B, the drag is decreasing proportional B^2, the rate of decrease depending on the speed M and the profile form $f(x)$ as indicated.

Of course, (9) holds only for "small" accelerations; this is the case which is ordinarily considered. For some purposes (in explosion processes), however, it will be interesting to explore the behavior of c_D for very large accelerations B. This can be accomplished by evaluating (3).

* Investigation sponsored by O.N.R., Fluid Mechanics Branch.

Remarks on "The Efficiency of Thermoelectric Generators"

ROBERT M. PAPET
Engineer, the Société d'Etudes Mécaniques et Energétiques, Paris and Lyon, France
April 29, 1948

SYMBOLS: W_e=electrical energy produced in the thermocouple (watt), N=total efficiency, n_e=electrical efficiency, n_t=thermal efficiency, and all other symbols are as in the original article.

In the article entitled as above, published in the J. App. Phys. **18**, 1116 (December 1947), the author, Maria Telkes, states that "the maximum power output of a thermoelectric generator is obtained when its internal resistance is nearly equal to the external load resistance."

The "efficiency calculations" are based on this operating condition, for which the Watt output is half of the total electrical energy produced:

$$W_0=\tfrac{1}{2}EI.$$

As a matter of fact, *any* electrical generator works with a bad efficiency, if the external resistance is equal to the internal one, since half of the electrical energy is consumed for the production of internal Joule heat.

I think a confusion of the maximum output and the maximum efficiency ought to be avoided. The output is given by

$$W_0=(E/R_e+R)^2\cdot R_e,$$

which is maximum for $R_e=R$; but the electrical efficiency n_e is

$$n_e=\frac{R_e}{R_e+R},$$

which is maximum for $R_e\to\infty$.

The total efficiency of the thermoelectric generator is equal to the product of the partial efficiencies n_e (electrical) and n_t (thermal)

$$N=n_e\cdot n_t=(R_e)/(R_e+R)\cdot(W_e)\Big/\left(\frac{W_e\cdot T_h}{\Delta t}+Q_e\right).$$

If we suppose that all other conditions (temperatures, external form, material) are constant and that the electrical resistance of the wire is variable by changing its diameter, we may assume that the heat conducted away by the wire is proportional to the electrical conductance of the wire plus a certain constant amount of heat,

$$N=(R_e)/(R_e+R)\cdot(W_e)\Big/\left(\frac{W_eT_h}{\Delta t}+k_1+\frac{k_2}{R}\right)$$
$$=(R_e)/(R_e+R)\cdot(R)/(a+bR),$$

with $a=k_2/W_e$ and $b=T_h/\Delta t+k_1/W_e$.

This expression is maximum for

$$dN/dR=0;\quad d^2N/dR^2<0,$$

and we obtain

$$R_e=b/a(R^2).$$

This formula is of practical value only if a and b are known, but, anyhow, it shows that the efficiency calculated with $R_e=R$ should not be compared with that one of an ordinary electrical generator. The real working condition will depend on the purpose. 1. If maximum output for minimum weight is desired, regardless to efficiency, the internal resistance may be made approximately equal to the external one. 2. If maximum efficiency is preferred, the factors a and b should be determined by practical research, and the condition

$$(R_e=b/aR^2),$$

should be approached.

Calculation of the Temperature Development in a Contact Heated in the Contact Surface, and Application to the Problem of the Temperature in a Sliding Contact

W. J. OOSTERKAMP
Research Laboratory, N. V. Philips Gloeilampenfabrieken, Eindhoven, Netherlands
September 15, 1948

RECENTLY a paper by Holm[1] on this subject appeared in this journal. It may be worth while to call attention to the fact that the problem of heat dissipation treated by Holm is similar to that of the heat dissipation in the anode of an x-ray tube, in which the focal spot—where the electron beam originating from the cathode strikes the anode—is taking the place of the contact area in the contact problem. The stationary contact is identical with the

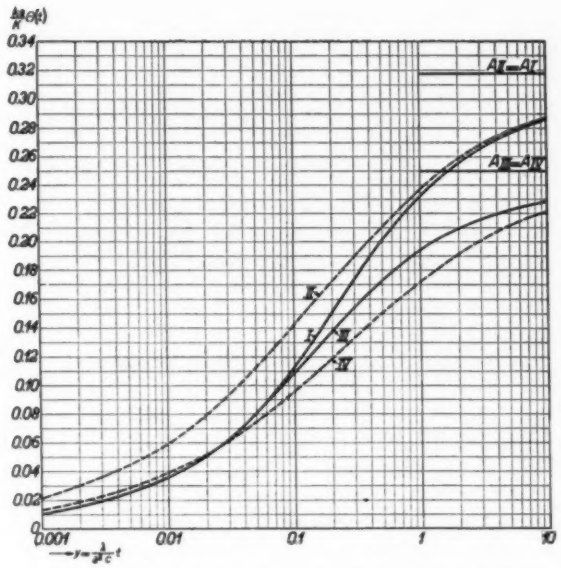

FIG. 1. The temperature rise as a function of time of contact. Curve *I*: maximum temperature according to Oosterkamp; curve *II*: maximum temperature according to Holm ($b=0.5a$); curve *III*: average temperature in contact area according to Oosterkamp; curve *IV*: average temperature in contact area according to Holm ($b=2/\pi=0.64a$). A_I, A_{II}, A_{III}, A_{IV}: asymptotes of the curves *I*, *II*, *III*, and *IV*, respectively.

loading of an x-ray tube with stationary anode, whereas the problem of the sliding contact is similar to that of an x-ray tube with rotating anode.

The temperature rise in the anode of an x-ray tube has been calculated and experimentally verified by various authors,[2] though sometimes only for very specific restricted conditions. A complete treatment has appeared in my thesis,[3] part of which has been republished in the Philips Research Reports.[4] The formulas obtained can be applied right away to the contact problem. In Holm's notation, my Eqs. (8) and (12) give for the temperature rise at the center of a circular stationary contact at the time $t=(a^2c)/(\lambda)y$:

$$\theta(t)=(2K)/(\pi^{\frac{1}{2}}a\lambda)y^{\frac{1}{2}}[1-\exp(-1/4y)+(\pi^{\frac{1}{2}})/(2y^{\frac{1}{2}})\{1-\phi((y^{-\frac{1}{2}})/(2))\}],$$

and for the temperature rise in the stationary state ($t=\infty$):

$$\theta(\infty)=(K)/(\pi a\lambda).$$

These relations are shown in Fig. 1, curve *I*. Curve *II* gives the results of Holm's calculations, when the radius b of the hemisphere is chosen such that the correct value of the maximum temperature in the stationary state, occurring at the center of the contact area, is obtained ($b=0.5a$). Curve *III* gives the results of my method of calculation applied to the average temperature to be compared with curve *IV*, according to Holm ($b=2/\pi=0.64a$).

It will be noted that Holm's calculations give values that are too high at short contact times—the difference being larger in the case of maximum temperature than in the case of average temperature. It is possible, using Holm's method, to obtain the correct temperature at short contact times by putting $b=\frac{1}{2}a\sqrt{2}=0.71a$; (area hemisphere =actual circular contact area) but then the calculated temperature in the stationary state will be too low. Thus, by treating the temperature development in a flat contact area as a hemispherical problem, only approximate data can be obtained, if the full range of possible values of the contact time has to be covered, because of the difference of divergence of the flow of heat in both cases.

Other results of calculations on x-ray tubes can be used to calculate the temperature during the cooling down period, and to treat the problem of a sliding contact. In this respect I refer to the publications[3,4] mentioned before.

[1] R. Holm, J. App. Phys. **19**, 361 (1948).
[2] A. Bouwers, Zeits. f. tech. Physik **8**, 271 (1927); A. Bouwers, Physica **10**, 125 (1930); J. E. de Graaf and W. J. Oosterkamp, J. Sci. Inst. **15**, 293 (1938); J. E. de Graaf, W. J. Oosterkamp, and L. Philips, Tech. Rev. **3**, 259 (1938); A. Muller, Proc. Roy. Soc. **117**, 30 (1927); J. W. M. DuMond, B. B. Watson, and B. Hicks, Rev. Sci. Inst. **6**, 183 (1935); A. Muller, Proc. Roy. Soc. **125**, 507 (1929).
[3] W. J. Oosterkamp, thesis (Delft, 1939).
[4] W. J. Oosterkamp and L. Philips, Res. Rep. **3**, 49 (1948); **3**, 161 (1948); **3**, 303 (1948).

On the Possibility of Hg Type Arcs with Hot Refractory Cathodes

JEROME ROTHSTEIN
Evans Signal Laboratory, Belmar, New Jersey
September 27, 1948

FURTHER consideration of a theory recently proposed to account for the behavior of Hg type arc spots[1] has led to the conclusion that such spots can occur even with refractory cathodes like W. Cold C and W arcs[2] are, of course, well known, but the type under consideration, unlike these, should occur even with pure inert gases and with the cathode hot enough to ensure that it is thoroughly outgassed.

The Hg type spot is characterized by a discontinuous glow-arc transition (DGA). It is thought that when increasingly larger glow currents are drawn there is increased sputtering of Hg from the cathode, thus local increased vapor density, concomitant rise in current density, and increased ionization of the vapor, hence still more bombardment of the cathode, more sputtering, and so on. At a critical value of the current density the glow becomes unstable against formation of an arc spot as the culmination of this process. Experiments of Plesse[3] and others indicate that a DGA is indeed facilitated by the presence of metal vapor near the cathode and that a more or less definite transition current density exists for a given set of conditions.

The thermionic arc, on the other hand, is characterized by a continuous glow-arc transition (CGS). The intense ionic bombardment occurring in the abnormal glow heats the cathode until it emits enough electrons thermionically to satisfy the external circuit.

The Hg spot regime would seem to arise whenever cathode vaporization or other cooling processes prevent the attainment of temperatures high enough to supply the electrons required by the external circuit by conventional thermionic emission. It thus seems reasonable to expect a

spot of the Hg type to develop even on clean W, say, if the external circuit is unsatisfied by the thermionic current available at the cathode temperature determined by the balance between heating by ionic bombardment and cooling by radiation, evaporation (atoms, electrons, ions), and, to some extent, thermal dissociation or ionization of the gas, conduction, and convection.

A simple way to realize such an arc experimentally is to employ a W cathode of very small area, thereby requiring large current densities at the cathode for moderate currents in the external circuit. Of great interest in this connection are the observations of Druyvesteyn[4] on the glow-arc transition for W in rare gases. He obtained a CGA for W spheres and wires of various diameters down to 250 microns. For a wire diameter of 100 microns, however, only a DGA was obtained. Furthermore, his $V-i$ curves indicate a lower arc drop for the 100-micron wire. It is proposed that in this case the Hg spot mechanism is operative. More rapid "evaporation" of the cathode, possibly the presence of r. f. transients on transition, and the appearance of spectral lines of the cathode vapor, a different spectral distribution at the spot than that ascribable to high temperature, and other Hg spot characteristics absent for thermionic arcs, should be observable here. Similar phenomena should be observed with other refractory metals capable of supporting thermionic arcs, e.g., Mo, Ta, and Pt. The high temperature arcs with Cu, Fe, Ni, Ag, or Au cathodes may be of a similar nature,[5] the high temperature serving to supply metal vapor for the Hg spot mechanism rather than electrons by thermionic emission.

[1] J. Rothstein, Phys. Rev. **73**, 1214 and **74**, 228 (1948).
[2] O. Becken and K. Sommermeyer, Zeits. f. Physik **102**, 551 (1936).
[3] H. Plesse, Ann. d. Physik **22**, 473 (1935).
[4] M. J. Druyvesteyn, Zeits. f. Physik **73**, 727 (1932).
[5] M. J. Druyvesteyn and F. M. Penning, Rev. Mod. Phys. **12**, 153, Table XI, Col. III, 154 (1940).

The Application of Electron Multiplier Tubes in the Measurement of X-Ray Beam Intensities and in the Determination of Crystal Structure

G. Papp and K. Sasvári
Institute of Atomic Physics and Institute of Chemical Physics, University of Technical and Economic Sciences, Budapest, Hungary
April 8, 1948

In the Tungstram Research Laboratory, electron multiplier tubes have been developed whose dark current is almost entirely eliminated, and each electron emitted by the cathode—after an average multiplication of the order 10^9—can be detected at the collector plate of the tube by macroscopical measurements.[1] Such multiplier tubes were used in the measurement of x-ray intensities and its particular applicability for the determination of crystal structure was shown.

For measuring x-ray intensities the number of pulses of the electron multiplier tube can be used. The total multiplication (T) of our tube is so high, that already at a comparatively small number of impulses per second it yields a macroscopically measurable plate current. At a given supply voltage the plate current is perfectly reproducible and proportional to the number of electrons emitted by the cathode. With the variation of the supply voltage the total multiplication (T) of the tube can be varied within a very wide range. Transition from the discrete to the continuous region of current takes place continuously.

The method of counting single impulses allows the measurement of smallest intensities ranging from about one pulse per hour to about 10^4 pulses per second. The lower limit of the measurable continuous current corresponds to about 1 pulse per second, and there is practically no upper limit of the continuous current region. The possibility of measuring throughout such a wide range is due to the fact that the impulse period of the electron multiplier is very short[2] ($<10^{-8}$ sec.), and that the multiplication of the tube depends only on the interstage voltages which are practically not affected by the pulses themselves. These are the features that make electron multiplier tubes preferable to G.-M. counter tubes in measuring x-ray intensities.

The efficiency of our tube having silver cathode was determined by the comparison of the number of impulses given by the tube and the intensity of the incident Mo K_α radiation measured with the aid of an ionization chamber. According to these measurements the quantum-efficiency $w=2.75\cdot10^{-3}$ electron/photon was found.

The total multiplication of the tube was determined by measuring the plate current and the number of impulses simultaneously. If n electrons are emitted by the cathode per second and the total multiplication of the tube is T, the plate current is $i=n.T.e.$, e being the charge of the electron. Thus at a supply voltage $3060V$, $T=1.46\cdot10^{-9}$ was found. The variation of T as a function of the supply voltage is shown in Fig. 1.

Comparing the current given by a perfectly absorbing ionization chamber (filled with air) and our multiplier tube in case of the same radiation (Mo K_α line in our case) of the same intensity, the electron multiplier yields a current

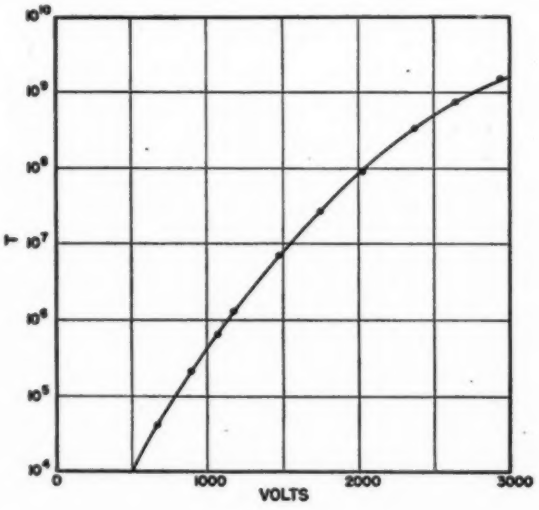

Fig. 1.

10^{-4} times greater than the ionization chamber. Thus the multiplier tube allows the use of a quite ordinary current measuring instrument whereas electric charge is to be measured with the aid of an electrometer if an ionization chamber is used.

A radiation producing 10^{-14}A ion-current in an ionization chamber—which is practically the lowest limit of such a measurement—yields one pulse per second in an electron multiplier tube, which can be measured as a continuous current, if the measuring instrument averages the discontinuous current pulses for the period of about 100 pulses. This was realized by measuring the voltage drop across a resistance R shunted by a capacity C. The period of averaging is determined by the time constant RC, and it is chosen as required by the circumstances.

The usefulness of the above method was shown in the determination of crystal structures. In the x-ray spectroscope the ionization chamber is substituted by an electron multiplier tube. Thus the output current is increased by a factor of about 10^4 which is most advantageous in adjusting the apparatus, in reading the current intensity and in the duration of the measurements.

The application of electron multiplier tubes in the examination of materials and determination of the fine structure of surfaces is going on.

Further details on the method, apparatus, and results were published in the "Publications of the University of Technical Sciences" (Budapest, 1947), Vol. 1, p. 171.

[1] Z. Bay, Zeits. f. Physik **117**, 227 (1941).
[2] G. Papp, Rev. Sci. Inst. **19**, 568 (1948).

Homing Pigeon in Electromagnetic Fields

C. L. Clark and R. A. Peck, Jr.
Sloane Physics Laboratory, Yale University, New Haven, Connecticut

and

W. F. Hollander
Larson College, New Haven, Connecticut

September 7, 1948

In an attempt to make manifest a possible sensitivity of homing pigeons to electromagnetic fields,[1] a female Racing Homer of the Trenton strain has been subjected to the diverse fields described below. This pigeon, a vigorous, normal representative of the breed, had been trained in free flight near Akron, Ohio, though never trained for long distance racing. Since its shipment to New Haven in 1947, it had never been released. The experiments were performed with the idea that any sensory apparatus can be stimulated to the point where the subject's discomfort will be objectively observable.

Magnetic Fields: (a) Uniform field of electromagnet (15-cm pole pieces, 18-cm gap). Field at first steady, then pulsed to 200-gauss maximum (rise time 1 sec., fall 1 sec.), later to 700 gauss (rise 8 sec., fall 6 sec.). Bird held loosely in gap.

(b) Fringing field of cyclotron magnet, tapering from 3000 to 500 gauss. Bird first in cardboard cage, later in hand; held stationary, and also moved about (~50 cm/sec.).

(c) Air-core solenoid. Field ~100 gauss, rapidly reversed with approximately 1-second period. Bird at rest in hand just outside end of solenoid.

(d) Lecture demonstration bar magnet. Waved to and fro, period approximately 2 seconds, 10–20 cm from bird in chicken-wire cage.

Electric Fields: Table model Wimshurst machine, operated continuously in all cases.

(a) Static and slowly varying, inhomogeneous fields. One pole of machine connected by light chain (1) to vertical metal cylinder (10 cm in diameter, 40 cm long) and thence (2) to feet of bird in cardboard cage on insulating stool 50 cm from cylinder. Other pole connected to metal wand, manipulation of which caused large changes in highly inhomogeneous field around bird. Wand waved around with frequency about 1 to about 30 per minute. Moving the wand caused appreciable variation in charge induced on bird's neck, as shown by electroscope and proof plane.

(b) Corona discharge. As above, obtaining corona discharge from bird's back, wings, tail with wand thrust into cage.

(c) Static and transient charging by conduction. Bird free in dark (observed by flashlight), perched on insulated metal stand connected to one pole of machine 50 cm away; both with and without spark discharges at machine terminals.

Radiation Fields: (a) 81-Mc/sec. Cenco demonstration oscillator in lecture hall (about 1 volt per meter at 20 cm; dipole antenna). Pulsed and steady operation with bird at rest. In dark, bird at rest and moved about by hand; with lights on, bird at rest and also allowed to fly around—both with and without oscillator in each case.

(b) 50-Mc/sec. 10-kw oscillator; sixty 250-microsecond pulses per second. Bird in cardboard cage about 1 meter from aperture radiating a few percent of power (diathermy incipient).

(c) 10-Mc/sec. 6-kw (cyclotron) oscillator, steady operation and also pulsed as follows: up in about 15 seconds, down in less than 1 second. Bird in cardboard cage just outside aperture radiating a few percent of power.

In no case did the bird show any concern or any deviation from normal behavior. It was supremely indifferent to all the experiments except when it received an accidental spark discharge from the Wimshurst machine. However, it should be emphasized that (1) only one pigeon was tested, (2) this pigeon was not in free flight during any of the experiments, and (3) the observed indifference does not prove complete insensitivity to these fields—it shows only that the bird, if perceiving the fields, was not overstimulated to the point of obvious discomfort.

[1] H. L. Yeagley, J. App. Phys. **18**, 1035 (1947); also three letters, by J. Slepian, R. H. Varian, L. Davis, J. App. Phys. **19**, 306–7 (1948). Further relevant information is in G. H. Henderson, Science **105**, 597 (June 4, 1948) and D. R. Griffin, The Auk **57**, 61 (1940). For an earlier review of the general problem see D. R. Griffin, Quart. Rev. Biol. **19**, 15 (1944).

New Booklets

Microfilm Service, 2153 Florida Avenue, Washington 8, D. C., has announced that the following publications are now available to libraries on 35-mm microfilm: *Zeitschrift fur Physicaische Chemie*, well known journal in the field of physical chemistry, for the years 1925 to date; *The Collected Works of James Clerk Maxwell*, British physicist.

Corning Glass Works, Corning, New York, has published a booklet, No. C-248, entitled *Glass Color Filters*, 22 pages. Fifty cents per copy, but free to bonafide scientists and others whose work is concerned with glass color filters.

Panoramic Radio Corporation, 92 Gold Street, New York 7, New York, has issued a six-page leaflet on its *Panoramic Sonic Analyzer*. Free on request.

Leeds and Northrup Company, 4934 Stenton Avenue, Philadelphia 44, Pennsylvania, has announced publication of two revised catalogues: ND4A(1), *L & N Electric Control, Position-Adjusting Type*, 40 pages; ND4A(2), *Duration-Adjusting Type of L & N Electric Control*, 36 pages. Free on request.

The Reliable Electric Company, 3145 Carroll Avenue, Chicago 12, Illinois, has issued a series of five catalogues covering the company's complete line of products (electrical equipment). All five are bound and indexed in a sturdy binder and are available to anyone interested upon request to E. Freimuth at the address above.

Burrell Technical Supply Company, 1942 Fifth Avenue, Pittsburgh 19, Pennsylvania, has published its Bulletin No. 213 entitled *Burrell Industro Gas Analyzer*. 8 pages, free on request.

Superior Electric Company, Bristol, Connecticut, has issued a small 8-page leaflet entitled EM *is an important part of* AM, FM, TV *broadcasting*. Request Bulletin 448.

Grove Regulator Company, 65th and Hollis Streets, Oakland 8, California, has published two new Bulletins: 800-B, 16 pages, describing the applications of Grove "Flexflo" expansible tube valves, and 610-B, describing the operation and performance of Grove "Chex-flo check valves." Free on request.

Miniature Precision Bearings, Inc., Keene, New Hampshire, recently issued a new catalogue on its miniature ball bearings. 8 pages, free on request.

National Bureau of Standards published the following physics articles in August. Copies may be obtained at listed prices from the Superintendent of Documents, Government Printing Office, Washington 25, D. C. *Divided Flow, Low-Temperature Humidity Test Apparatus*, Arnold Wexler, 8 pp., 10 cents. *Ionospheric Radio Propagation*, 209 pp., $1.00.

Laboratory Furniture Company, 37-18 Northern Boulevard, Long Island City 1, New York, recently issued a 16-page brochure on industrial research, as defined and appraised by eminent scientists, executives, and educators. Attractively illustrated with many photographs. Free on request. Title is *Research*.

The Brown Instrument Company, Wayne and Roberts Avenues, Philadelphia 44, Pennsylvania, publishes quarterly a journal entitled *Instrumentation*. The issue of the third quarter of 1948 has 32 pages and is magazine size.

Amperex Electronic Corporation, 25 Washington Street, Brooklyn 1, New York, has announced a new 296-page catalogue, covering its lines of electronic tubes for communications, industrial, amateur, and electro-medical uses. Send request on your business letterhead.

Gow-Mac Instrument Company, 22 Lawrence Street, Newark 5, New Jersey, has published a 4-page leaflet entitled *Ever-Tite Thermal Conductivity Units*. Free on request.

National Carbon Company, Inc., 60 East 42d Street, New York 17, New York, offers two new booklets: Catalogue Section B-2106 deals with standardization of carbon, graphite, and metal-graphite brushes for motors and generators; Catalogue Section M-8800B covers the company's "Karbate" brand pipe and fittings.

Bausch and Lomb Optical Company, Rochester 2, New York, has issued a 20-page booklet entitled *Bausch and Lomb Stereoscopic Wide Field Microscopes*. It is Catalogue D-15, free on request.

Fish-Schurman Corporation, 230 East 45th Street, New York 17, New York, announces a bulletin ZL-321S describing its "Zirconarc" photomicrographic lamp. Free on request. 4 pages.

Kinney Manufacturing Company, Boston 30, Massachusetts, has published Bulletin 2448 entitled *Kinney Vacuum Tight Valves*. 4 pages, free on request.

Here and There

New Appointments

Joseph P. Maxfield, for 31 years associated with the Bell Telephone Laboratories, has accepted appointment to the position of Superintending Scientist of the U. S. Navy Electronics Laboratory, San Diego, California. He is in charge of the Laboratory's scientific and technical research in radio, radar, and sonar.

H. F. McMurdie has been named Chief of the Constitution and Microstructure Section of the Mineral Products Division of the National Bureau of Standards.

Edwin F. Dillaby has been appointed by Tracerlab, Inc., Boston, Massachusetts, to be chief engineer in charge of its newly formed Tube Division.

Earl R. Spangenberg has been apointed head of the Electronics Branch of the Office of Naval Research. Dr. Spangenberg has been granted leave of absence from the Department of Electrical Engineering, Stanford University, to assume his duties for the Navy.

Robert A. Stauffer has been named assistant director of research of National Research Corporation, Cambridge, Massachusetts. James H. Moore will succeed him as director of the metals department.

Necrology

Dr. Samuel E. Sheppard, widely known for his research on the sensitivity of photographic materials, died in Rochester, New York, on September 29 at the age of 66. He had been in retirement since January 1948, after 35 years with Kodak Research Laboratories. He was born in England and obtained his Doctor of Science degree at the University College of London.

Awards

Presidential Certificates of Merit were awarded September 20 to Loren F. Jones and Hugh H. Spencer, both of Radio Corporation of America, for their contributions to the development of direction-finding equipment and guided missiles during World War II.

Franklin Medals, highest honors of the Franklin Institute of the State of Pennsylvania, will be awarded this year to Wendell M. Stanley, biochemist, and Theodore von Karman, aeronautical engineer.

Research Administration Clinic

A conference on administration of scientific research was held September 13 to 15 at State College, Pennsylvania. Attended by research executives for government, industry, education, and other fields, the clinic was sponsored by Pennsylvania State College School of Chemistry and Physics and the School of Engineering.

High Vacuum Symposium

A High Vacuum Convention was held at Gleneagles, Perthshire, Scotland, on October 12 and 13, with Sir Charles Darwin, Director of the National Physical Laboratory, presiding. A number of American scientists participated.

APS Has Fluid Dynamics Division

The Division of Fluid Dynamics, which was established by the Council of the American Physical Society in June 1947, has now been completely organized. R. J. Seeger is chairman, H. L. Dryden, vice-chairman, and H. W. Emmons, secretary-treasurer. The Division assisted in sponsoring in Los Angeles, California, in June 1948 a three-day symposium on heat transfer and fluid mechanics.

Special Committee on Technical Information Formed

In September Dr. Vannevar Bush, then chairman of the Research and Development Board, National Military Establishment, announced the formation of a Special Committee on Technical Information to promote effective exchange of research and development information among the departments of the National Military Establishment. Chairman is Dr. Detlev W. Bronk, recently appointed president of Johns Hopkins University, and the other members include Professor John E. Burchard, Dean of Humanities, Massachusetts Institute of Technology; Herman Henkle, Director of the John Crerar Library; Lt. Col. F. L. Walker, Jr., Army; Captain W. H. Leahy, Navy; Colonel Bernard A. Schriever, Air Force. Norman T. Ball is executive director of the committee.

Bulletin of Mathematical Biophysics

Following is the table of contents of the December 1948 issue of the Bulletin of Mathematical Biophysics:

A Note on Biological Periodicities—N. Rashevsky

A Note on the Probabilistic Approach to the Cancer Problem—N. Rashevsky

Steady States in Random Nets: I—Anatol Rapoport and Alfonso Shimbel

Steady States in Random Nets: II—Anatol Rapoport

Book Review—John H. Northrop, Moses Kunitz and Roger M. Herriott, *Crystalline Enzymes*—John Z. Hearon

The University of Chicago Press, Chicago, Illinois, Volume 10, Number 4.

Pittsburgh Conference

The sixth annual Pittsburgh Conference on X-Ray and Electron Diffraction was held at the Carnegie Institute of Technology and the University of Pittsburgh November 19 and 20. Featured address was delivered by Sir Lawrence Bragg, Nobel Laureate, Director of Cavendish Laboratory, Cambridge University, Cambridge, England, on "The X-Ray Structure of Proteins and Other Organic Molecules."

Site near Schenectady Chosen for New Atomic Power Reactor

The United States Atomic Energy Commission announced in September that it would acquire 4500 acres of land in Saratoga County, New York, as the location of an experimental atomic power plant for studies of the generation of electric power from nuclear energy. The plant will be part of the facilities of the Knolls Atomic Power Laboratory, operated for the Commission by the General Electric Company at Schenectady.

Symposium at Brooklyn Polytechnic

A symposium on "Ultrasonics and Macromolecules" was sponsored on October 23 by the Institute of Polymer Research of the Polytechnic Institute of Brooklyn. Chairman was Dr. J. W. Ballou of Dupont de Nemours and Company.

Nuclear Laboratory Opened at Cornell

The new $2,000,000 Laboratory of Nuclear Studies at Cornell University was formally opened in October, with the dedication ceremony on October 7. Dr. Robert R. Wilson is director of the Laboratory, which houses a 300-million-electron-volt synchrotron.

PROGRAM OF THE E. F. BURTON MEMORIAL MEETING OF THE ELECTRON MICROSCOPE SOCIETY OF AMERICA

THE E. F. Burton Memorial Meeting of the Electron Microscope Society of America was held at the University of Toronto, Toronto, Canada, September 9, 10, and 11, 1948.

Titles and abstracts of the papers presented are given below:

1. Comparison of Inorganic and Organic Replicas. C. J. CALBICK, *Bell Telephone Laboratories, Murray Hill, New Jersey.*—The terraces surface structure developed by sintering nickel-manganese oxide powders[1] is favorable for a comparison of replica techniques because of the sharply defined topography. Inorganic replicas show greater resolving power and less deterioration under the action of the electron beam in the microscope. They are also more suitable for stereoscopic micrography, which serves to delineate the geometrical form of a surface without the necessity for an interpretation of density variations in the micrographs.

[1] H. Christensen and C. J. Calbick, Bull. Am. Phys. Soc. **23**, 3, 23 (1948).

2. An Evaluation of Several Types of Replicas. J. J. COMER AND F. A. HAMM, *General Aniline and Film Corporation, Easton, Pennsylvania.*—The use of replicas is often necessary in the study of surfaces that cannot be examined directly in the electron microscope. The possibility of introducing artifacts must always be considered. This paper is concerned with a comparison of several types of replicas within themselves, as well as with a comparison of these replicas with the original sample which could be examined in the electron microscope. The sample is a modified surface of a foil cast from organic solvents. Four different types of specimens have been compared. They are as follows: (1) The original cast foil. (2) A chrome-shadowed foil. The advantages of shadowing are clearly illustrated inasmuch as the foil itself is a very poor electron scatterer. (3) A chrome-shadowed silica replica prepared via a *one*-step method. Silica is evaporated onto the foil. The silica is shadowed after removal of the foil. (4) A chrome-shadowed silica replica prepared via a *two*-step process. A negative resin replica is prepared first. This is stripped from the foil and silica is evaporated onto that side of the resin which had made contact with the foil. This positive silica replica is then chrome-shadowed. Although the thin organic foil does not produce sufficient contrast to reveal its complete structure, the reliability of the replicas may be at least partially evaluated by comparison. The chrome-shadowed foil is very easily prepared, and is the most accurate type of specimen. The two-step replica technique is cumbersome and exhibits some artifacts. The one-step replica exhibits good qualities, but offers no advantages over the more readily prepared chrome-shadowed foil. The relative merits of each type specimen from the standpoint of resolution, contrast, and reproducibility will be presented.

3. A Method of Examination of Sections of Fine Metal Powder Particles with the Electron Microscope. LAURENCE DELISLE, *Sylvania Electric Products Inc., Bayside, L. I., New York.*—This note describes a method for the mounting, polishing, and etching of fine metal powders for the examination of cross sections of the particles with the electron microscope by the replica technique. The method was applied to three types of metal powders, tungsten, carbonyl iron, and carbonyl nickel powders, and permitted the observation of structural details which could not be brought out by other methods of examination. Photomicrographs illustrate the results obtained. The method could likely be applied to many other metal powders consisting of particles less than ten microns in diameter.

4. Electron Microscope Investigation of Opal Glass. THOMAS F. BATES AND MARY V. BLACK, *Department of Earth Sciences, Pennsylvania State College, Pennsylvania.*—The electron microscope is a useful tool for the detailed study of glasses containing a dispersed phase (gases and crystals) which cannot be disclosed with the light microscope. Eleven samples of commercial opal glass and two opalescent glasses made in the laboratory have been subjected to a preliminary investigation by means of the replica technique. Calcium fluoride glasses show well defined fluorite octahedrons and cubes either in clusters or scattered uniformly over the surfaces studied. Sodium fluoride glasses commonly contain clusters of globular forms having within them small crystals which appear to be cubic. The crystals found projecting from the broken glass surfaces range from 0.04 to 0.8 micron in diameter while in some samples a group of larger crystals (1.0 to 3.0 microns) also is present. In the specimens studied there are from 10^7 to 10^8 crystals per square centimeter of surface. Bubbles are present in all the glasses investigated. They vary in number from approximately 10^8 to 10^9 per square centimeter of surface and in diameter from 0.03 to 0.08 micron in the various samples.

5. Some Uses of Uniform Sized Spherical Particles. R. C. BACKUS AND R. C. WILLIAMS, *Department of Physics, University of Michigan, Ann Arbor, Michigan.*—Polystyrene Latex, No. 580, made by the Dow Chemical Company, consists of a water suspension of spherical particles of remarkable uniformity of size. The provisional value of the particle diameter is 2540±15A, with most of the uncertainty residing in the errors of measurement rather than in true dispersion of size. Examples of the usefulness of particles of this nature will be discussed: They provide

ideal objects for calibration of electron microscopic magnification. The shape and length of their shadows allow a precise determination to be made of the shadow-casting angle in any small region of the specimen, and for generally determining the quality of the shadows and any local distortion of the substrate film. The growth of the evaporated film on the exposed side of the particle during shadowing allows the thickness of the film on the substrate to be measured, and allows an estimate to be made of the extent to which much smaller objects are distorted by the film used in shadowing.

6. The Determination of Molecular Weights of High Polymers with the Electron Microscope. BENJAMIN M. SIEGEL,* DWIGHT H. JOHNSON,** AND HERMAN F. MARK, *Polytechnic Institute of Brooklyn, Institute of Polymer Research, Brooklyn, New York.*—The electron microscope has been used to determine the molecular weights of three polystyrene fractions. The carefully fractionated polymer samples had the following osmotic molecular weights: 4.8×10^5, 1.1×10^6, and $\sim2.5\times10^6$. Extremely dilute solutions ($\sim$1 ppm.) in cyclohexane were deposited onto collodion substrates in minute droplets of approximately 2 micron radius. Shadowcasting with 3A of uranium gave the necessary contrast for observing the dispersion of the single spheroidal particles obtained by this method of deposition. Assuming that the particles were single molecules and that their density could be taken for a first approximation as the same as the density of bulk polystyrene, the molecular weights obtained were 6.4×10^5, 9.6×10^5, and 2.5×10^6. These values agree well within the limits of accuracy obtainable from measurements of osmotic pressure and particle size with the electron microscope. The electron microscope should thus provide a useful method for characterizing polymeric materials whose molecular weight is greater than one million.

* Associate of the Weizmann Institute of Science, Rehovoth, Israel.
** At present at Princeton University.

7. Ultrasonic Disintegration of Cellulose Fibers Before and After Acid Hydrolysis. F. F. MOREHEAD, *American Viscose Corporation, Marcus Hook, Pennsylvania.*—Metal shadowed electron micrographs of natural and regenerated cellulose fibers, disintegrated by ultrasonic vibrations before and after acid hydrolysis, show a distinct fibrillar structure. In both the unhydrolyzed natural and regenerated fibers, the length of the fibril resulting from ultrasonic disintegration is largely dependent on the orientation and crystallinity of the fiber, i.e., the greater the degree of orientation and crystallinity the longer the fibril. When the sample is degraded by mild acid hydrolysis to its "basic" or limiting degree of polymerization (chain length) as measured by cupra-ammonia fluidity, a much shorter length fibril results. These "limiting D.P. fibrils" are distinctly different for the unhydrolyzed fibrils, being not only much shorter, but also of smaller diameter in the regenerated fiber. Good agreement with the limiting D.P. values and the measured lengths of the natural fiber are shown. The same trend is not so pronounced in the regenerated fiber but that may be merely a reflection of the difficulties of obtaining accurate measurements here.

The possibility of their "limiting D.P. fibrils" being related to the original structure and properties of the fiber are discussed.

A Symposium on Replica Techniques

Chairman: S. G. ELLIS, *RCA Laboratories, Princeton, New Jersey*

8. Oxide and Polystyrene—Silica Techniques. R. D. HEIDENREICH, *Bell Telephone Laboratories, Murray Hill, New Jersey.*

9. Techniques in the Preparation of Shadow-Cast Collodion Replicas. ROBLEY C. WILLIAMS, *Department of Physics, University of Michigan, Ann Arbor, Michigan.*

10. Handling and Washing Fragile Replicas. MARY S. JAFFE, *Lamp Department, General Electric Company, Cleveland, Ohio.*

11. Miscellaneous Techniques and Applications. JAMES HILLIER, *RCA Laboratories, Princeton, New Jersey.*

12. A Study of Bacterial Flagellation with the Delft Electron Microscope (Invited paper). A. L. HOUWINK, *Technical Physics Department, Delft, Netherlands, Communicated by* MISS WOUTERA VAN ITERSON, *National Institute of Health, Bethesda, Maryland.*—This paper deals with some of the results of research on the structure of bacteria now being carried out at the Institute for Electron Microscopy at Delft, Netherlands. It is confined to observations on flagellation.

The flagella of *Azotobacter agilis* show near the cell body a single composite strand, which at some distance from the body breaks up into several separate flagella equal in length.

In electron micrographs of a number of bacteria belonging to the genera *Aerobacter* and *Bacterium* (*Erwinia, Eberthella*), clear evidence was obtained that indeed several flagella were attached to various parts of the surface of the same bacterial cell. These observations are of interest in connection with the recently expressed doubt regarding the occurrence of peritrichous flagellation amongst bacteria. In some bacteria the presence of very fine threads in addition to ordinary flagella was observed.

13. Electron Microscopy of Mycobacteria Tuberculosis. E. M. BRIEGER, *Papworth and Strangeways Laboratories, Cambridge* AND V. E. COSSLETT, *Cavendish Laboratory, Cambridge.*—A number of strains of Avian Tubercle Bacilli have been grown on various media and examined in the electron microscope. The cultures may be removed directly from the surface of the growth medium in a collodion film, or may be grown directly on collodion-covered metal grids. By these methods the cultures can be observed without disturbing their natural mode of growth. They are normally fixed in osmic acid vapor and formalin before examining in the electron microscope. The bacteria so prepared are usually exceedingly transparent to the electron beam, so that changes in their internal structure may be followed through the early stages of development. Gold-shadowing reveals additional details of internal structure and other features associated with bacterial growth.

14. On the Possibility of Demonstrating an Intermediate Level of Structure in Normal Bacteria. JAMES HILLIER, *RCA Laboratories, Princeton, New Jersey.*—Simultaneous bombardment of normal *Escherichia coli* grown on collodion with electrons and water vapor has revealed the existence of numerous discrete granules and fibers with dimensions in the range 400A–800A. Similar structures have been found in the debris of freshly autolyzed or phagolyzed cells of several organisms. As yet it has not been possible to demonstrate these structures in untreated cells either by chemical or electron optical methods.

15. On the Presence of Dense Particles in the Neurotubules of Nerves Infected with Poliomyelitis Virus. E. DEROBERTIS AND F. O. SCHMITT, *Department of Biology, Massachusetts Institute of Technology, Cambridge, Massachusetts.*—With the assistance of Dr. H. Farber and Miss R. Silverberg, Stanford Medical School, sciatic nerves of Rhesus monkeys were transsected and dipped in a 20 percent suspension of a strain (CAM) of human poliomyelitis virus. After varying periods of time the nerves were extirpated, fixed in formalin, fragmented, and examined with the electron microscope. In some of the neurotubules examined very dense particles were observed, ranging in size from about 200 to 400A and usually appearing as dense granules or as ovoid bodies having low density centers; in some instances the edges of the ovoids are streaked, giving the appearance of pairs of slightly curved rodlets. The particles are found in the central region or at the inner edges of the neurotubules. Indirect evidence indicates that the virus moves centrally in the nerve axon at a velocity of the order of 2 mm per hour. The same order of velocity of migration of the dense particles may be inferred from their concentration in neurotubules at varying distances from the infected ends of the nerves and from the time intervals between infection and extirpation of the nerves. The possible relation between the dense particles and the virus will be discussed.

16. Quantitative Virus Counts with the Electron Microscope. D. GORDON SHARP, *School of Medicine, Duke University, Durham, North Carolina.*—It is a common experience that the number of virus particles seen per unit area of electron micrographs is not proportional to the virus concentration of the suspension dried on the film. In the present work studies have been made to devise a method for estimating the number of virus particles in suspension by electron micrography. For this purpose a sector-shaped cell containing 1 cc of swine influenza virus suspension and having a 1 cm^2 piece of thin glass lying on the bottom was spun at 16,500 G for 20 minutes, a procedure which sedimented all the virus on the collodion coating the glass. Afterward this collodion was stripped from the glass and electron micrographs were taken of the virus deposited on it. As examination was made of seven twofold dilutions in the range 0.004 to 0.00006 mg of virus per ml, and pictures were taken at a magnification of 4800×. Virus particle counts were in excellent agreement with the dilution factors and within a few percent of the number to be expected from calculations based on particle weight, density, water content, etc. The method seems promising for quantitative work.

17. The Ultrastructure of the Retinal Rods of the Guinea Pig Eye. FRITIOF S. SJÖSTRAND, *Department of Biology, Massachusetts Institute of Technology, Cambridge, Massachusetts.*—Dispersions of outer limbs of retinal rods from guinea pig eyes were fixed in osmic acid, centrifuged, thoroughly washed in water and subjected to sonic fragmentation. This results in cleavage of the cylindrical rods into very thin disks whose diameters (about 2μ) are similar to rod diameters. The disks show a peripheral thickening and dense spots fairly uniformly distributed over the surface. Disks tend to rupture at a particular structural discontinuity in the peripheral region. From preparations of disks shadowed with chromium at 10°, estimates have been made of thicknesses of various regions in the disks. The peripheral thicker region averages 130 to 160A in thickness. Fragments of the central region had thickness of the order of 50A or less. Disks frequently cleave in packets with thickness equal to multiples of the single thickness. The average rod outer limb would correspond to a stack of about 1000 disks. These findings are consistent with the results of the polarization optical analysis (W. J. Schmidt) which reveal negative uniaxial (platelet) form birefringence in the outer limbs.

18. Morphology of Nucleoprotein of Spinal Cord as Revealed by Electron Microscopy. JOSEPH T. MELNICK, *Yale University School of Medicine, New Haven, Connecticut.*—Nucleoproteins, prepared from monkey spinal cords according to the method of Mirsky and Pollister, were characterized by their high viscosity, by their solubility in distilled water and in 1.0 *M* NaCl and insolubility in 0.14 *M* NaCl, and by their tendency to form fibers when precipitated in the cold at the latter salt concentration. Ultraviolet absorption spectra were determined in water and in 1.0 *M* NaCl, and in both instances the protein solution exhibited the characteristic absorption maxima of nucleic acid at 260–265 mμ. Fibrous structures were observed in the electron microscope. The suggestion of uni-

form spacings seen in unshadowed preparations became strikingly apparent when the preparations were obliquely shadowcast before examination. The nucleoprotein is made up of long threads of discoid segments each about 120 mμ (±35) in diameter and about 57 mμ (±7) in length. The spacing between these discoid segments is about 10 mμ (±2). The differences in the diameters of the various preparations appear to be a reflection of the condition of the fiber, depending on whether or not the fiber is "deflated." Mirsky and Pollister have suggested that nucleoproteins prepared in this fashion may be nuclear chromatin threads made up of highly polymerized units. These electron micrographs are compatable with such a concept.

19. Observations on Chromosome Structure in Resting Cells with the Electron Microscope. BENJAMIN M. SIEGEL,* FERNANDO CALVET,** AND KURT G. STERN, *Polytechnic Institute of Brooklyn, Brooklyn, New York.*—The chromatin structure present in the resting nucleus of calf thymus lymphocytes has been studied in some detail with the electron microscope. Pure suspensions of thymus lymphocytes were obtained and were ruptured for study in the electron microscope either mechanically or by vacuum drying. The cytoplasmic components were then washed away with physiological saline and the chromatin nature of the residue demonstrated with the light microscope using standard nuclear stains. Examination of this material under the electron microscope reveals a loose mesh of cross-linked fibers of indeterminant length and with widths varying from 200–700A. When the thymus lymphocytes are treated with lanthanum acetate after rupture, the chromatin network is further resolved into bundles of fine ultrafibrils of fairly uniform thickness of 80 to 100A. The lanthanum reagent also acts as an "electron stain" and micrographs of these treated fibrils show that they possess a definite fine structure with a high order of regularity. There is a banded appearance with individual "bands" or "disks" of about 30 to 40A and these are spaced at approximately the same distance apart.

* Associate of the Weizmann Institute of Science, Rehovoth, Israel.
** Research Fellow, Spanish Cultural Relation Board.

20. Fibrillar Structure in Rat Fibroblasts as Seen by Electron Microscopy. F. B. BANG AND G. O. GEY, *The Johns Hopkins Hospital, Baltimore, Maryland.*—During the course of some comparative studies of a normal rat fibroblast and its malignant cell derivative, we have obtained preparations of both of these cell types which under the electron microscope* show an unmistakable fibrillar structure in the thinly spreading endoplasmic sheet. These fibrils of an estimated thickness of 25 to 100 mμ may converge and diverge in fan-like formations of great regularity, but are more often seen gathered together in long bands of varying widths. They are apparently composed of long thin converging fibrils which in general radiate from the dense perinuclear region. That the fibrils are not produced by a wrinkling of the membrane on which the cell is stretched is indicated by their uniformity, by their sharp change in direction in certain areas of the periphery, and by their fine converging and diverging structure. Besides this, no wrinkles were seen in the membrane outside of the cellular area where clear visualization is possible. This fibrillar structure when present is clear and definite but is not present in every cell and thus may well represent a phase in either the growth or migration of the cells. Such structures have not previously been described in electron microscope studies of similar cells, and many types of cells will have to be studied before their general significance can be established. However, it has been supposed for some time that cytoplasm may have a basic fibrillar structure. This is based on the demonstration of the elasticity of protoplasm —both to externally applied tensions and to internally displaced foreign bodies and on the viscosity of the cytoplasm.

* Our technique of study of tissue cultured cells is essentially that of Porter with the exception that fixation and staining has been limited to ten minutes exposure to osmic acid vapors.

21. Replica Studies of Collagen Fibers. J. GROSS, *Department of Biology, Massachusetts Institute of Technology, Cambridge, Massachusetts.*—Specimens of human skin collagen were deposited on glass slides and plastic film replicas made of dried material and of preparations still slightly moist. After stripping, the replicas were shadowed at small angles with chromium. Imprints of dried fibrils reproduce the axial macroperiod very clearly, and in favorable specimens considerable detail of intraperiod structure is shown. Imprints of moist fibrils show much less, and sometimes no contouring, indicating that the banded structure results primarily from water loss at specific intraperiod regions. The role of the plastic solvent in this procedure will be discussed. Replicas of tissue smears show fibrils frequently arranged in parallel bundles, adjacent fibrils being in register with respect to cross-bands. This technique offers considerable promise as a means of studying tissue fragments, as from biopsy material, both in the dry and in the moist condition.

22. Sectioning Techniques for the Electron Microscope using a Conventional Microtome (Invited paper). RICHARD F. BAKER AND DANIEL C. PEASE, *Departments of Anatomy and Experimental Medicine, School of Medicine, The University of Southern California, Los Angeles, California.*—Techniques for consistently cutting 0.2-micron sections of biological material with a conventional microtome are described. Double embedding in a high melting point paraffin and hard collodion together with a small block area and a sharp knife are necessary factors. The knife tilt is critical. Several mounting methods are discussed. The necessity for careful preliminary treatment of the material is emphasized. The principal artefacts are those of the original fixation. The technique is illustrated with micrographs of various biological preparations.

23. A New Method of Sectioning Single Filaments of Synthetic Fibers for the Electron Microscope. MARSHALL D. EARLE AND JEAN A. MINKIN, *The Franklin Institute, Philadelphia, Pennsylvania.*—A method has been devised in which a piece of rayon yarn consisting of thirty or forty single filaments is prepared for sectioning with the ultramicrotome in such a way that the boundaries of individual

filaments can be identified when viewed in the electron microscope. The yarn is mounted in a special holder in which the filaments are spread out radially. They are then coated with a thin film of evaporated gold in the vacuum unit. These filaments are allowed to fall parallel to each other again. They are embedded in a very thin layer of low melting point paraffin and sectioned with the ultramicrotome. The thin film of gold makes it possible to determine whether or not the area being studied is near the surface of the filament. The technique involved in mounting and sectioning the yarn and the application of this method to other synthetic fibers are discussed.

24. Preparation of Human Cardiac Muscle for Electron Microscope. W. E. ADOLPH, *Department of Investigative Medicine, Birmingham General Hospital, Van Nuys, California* AND R. F. BAKER, *School of Medicine, University of Southern California, Los Angeles, California.*—As a necessary preliminary to a program of pathological research with the electron microscope a study has been made of various fixation techniques on human tissues. Fixatives compared were osmic tetroxide, phosphotungstic acid, formalin, and Zenkers solution. Tissues prepared for the electron microscope in this laboratory are sectioned with a modification of the ordinary microtome. A critical selection of fixative is necessary because fixation artefacts become increasingly prominent with thin (0.2-micron) sections and high magnifications. Limitations peculiar to the use of pathological human material in a hospital are discussed. Illustrative micrographs of human tissues are shown.

25. Thin Metal Sections for Electron Microscopy and Electron Diffraction. R. D. HEIDENREICH, *Bell Telephone Laboratories, Inc., Murray Hill, New Jersey.*—A technique for the preparation of thin sections of metals and alloys is described which does not mechanically deform or distort metal crystals. This method employs electropolishing conditions with a suitable holder for the specimen disk during thinning. The type of results obtained will be demonstrated with pure aluminum and an aluminum-copper alloy under various conditions of heat treatment. The electron image intensity distribution is determined almost entirely by diffraction and is therefore very sensitive to distortion of the crystals. From results with annealed and cold-worked aluminum, it appears that the thin sections offer a method of investigating dislocations in metals. A detailed analysis of such images has not been carried out as yet and, consequently, the interpretation is at present of a speculative nature.

26. Electron Microscopy of Some Plant Viruses (Invited paper). ROBLEY C. WILLIAMS, *Department of Physics, University of Michigan, Ann Arbor, Michigan.*

27. The Philips Electron Microscope (Invited paper). A. C. VAN DORSTEN,* J. B. LEPOOLE,** AND A. VERHOEFF,* to be read by W. J. OOSTERKAMP.*—The instrument is of the electromagnetic type. The design is based on the electron-optical principles, developed by the second author in the course of his investigations at the Institute for Electron Microscopy of the Institute of Technology at Delft. A description of the ideas underlying the design of the microscope and the way these have been realized in the instrument as it is now being manufactured will be given, illustrated with a number of slides.

* Philips Research Laboratory, Eindhoven, Holland.
** Institute for Electron Microscopy, Delft, Holland.

28. Phase Contrast in Electron Microscope Images. E. G. RAMBERG, *RCA Laboratories, Princeton, New Jersey.*—Image contrast in electron microscope images may arise from absorption, scattering, or phase changes impressed on the illuminating electron wave. The last factor may, in particular, be significant in the observation of very thin specimens with objectives of sufficient effective aperture that only very few electrons fail to contribute to the formation of the image. A theoretical treatment is given of the expected intensity distribution in the image of the edge of uniform films impressing phase delays on an incident parallel beam. The aperture of the ideal objective is assumed to be finite, corresponding to a condition approached with normal objectives and perfect physical limiting apertures smaller than the optimum aperture. With the finite aperture a fringe system appears at the image of the edge even at perfect focus. As the edge is defocused this fringe system gradually passes over into the normal Fresnel pattern. The contrast increases, of course, as the phase delay is increased from 0 to π for both in-focus and out-of-focus images. It is not expected that the intensity distributions calculated show very close correspondence to observed patterns since the theory does not take into account the prismatic action of the film edge.

29. Artifacts in Electron Microscopy. J. J. KELSCH, *Interchemical Corporation, New York, New York.*—Artifacts in electron microscopy are figures appearing in the final image, or in the finished electromicrograph which are not inherent in the specimen under observation. These figures, or false structures, originate as a result of forces acting on the specimen during preparation or while under electron bombardment. The purpose of this paper is to bring to the attention of electron microscopists in general, and the newcomer in particular, the need for a careful study of the artifacts which may appear in almost any field under observation, and which only too often lead to erroneous interpretations. A number of the common artifacts will be discussed and several illustrative slides will be presented.

30. The Illuminating System of the Electron Microscope. JAMES HILLIER AND S. G. ELLIS, *RCA Laboratories, Princeton, New Jersey.*—Using a self-biased electron gun, data has been obtained on the angular aperture of the illumination, the distribution of illumination at the specimen, and the total current reaching the specimen. These results are compared with those obtained with a zero-bias electron gun. For the same intensity the self-biased gun provides an angular aperture of the illumination only one-tenth of that provided by the zero-biased gun. The significance of the results is discussed with particular attention to problems arising in the practical use of the electron microscope.

31. Auxiliary Supporting Nets for Fragile Electron Microscope Specimens. MARY S. JAFFE, *Lamp Department, General Electric Company, Cleveland, Ohio.*—Very fragile specimen films, and also coarse particles on normal films, tend to move under the electron beam, due to rupturing of the film. This can be avoided by providing additional support for the specimen with a fine resin net which lies on the customary 200-mesh metal support. The resin net is made by condensing water vapor on a wet film of Formvar or other resin while it is draining on a glass slide. The nets can be strengthened by coating with evaporated metals or silica. They can be used as test specimens for objective pole-piece compensation, and also as filters on which to catch smokes, dusts, or centrifuged suspensions.

32. On the Adjustment and Manipulation of the Electron Microscope (Invited paper). JAMES HILLIER, *RCA Laboratories, Princeton, New Jersey.*—A number of points with regard to the adjustment and manipulation of an electron microscope will be discussed. These will include problems of alignment, instrument cleanliness, extraneous magnetic fields, objective lens astigmatism, vibration and specimen stability, etc. Critical tests will be described in most cases.

33. Diffraction Microscopy. D. GABOR, *British Thomson-Houston Co., Research Laboratories, Rugby, Warwickshire, England,* presented by F. W. CUCKOW, *Royal Cancer Hospital, London.*—Diffraction microscopy is a new way of attack on the problem of improved resolving power, which appears insoluble by the conventional means of electron microscopy. The new method is a two-step process of image formation. In the first step a new type of diffraction diagram is taken, with electrons, using divergent coherent illumination of the object. Coherence is assured if the source is a small aperture, or the image of a small aperture, with a nominal or Gaussian diameter smaller than the resolution limit. The physical diameter can be thousands of times larger, as spherical aberration and other defects of the electron lenses used in the condenser system do not affect the coherence. The diffraction diagram thus obtained has little or no likeness to the original, but the likeness is restored by the second step, in which the diffraction photograph is illuminated by a light beam, which is an optical limitation of the original electron beam, scaled up in the ratio of light to electron wave-length. The principle has been successfully tested in optical experiments, in which light waves were used both for taking the diffraction diagram and for the reconstruction. Calculations show that a resolving power of 1A ought to be attainable without excessive difficulties.

34. An Experimental 400-kv Electron Microscope. A. C. VAN DORSTEN,* J. B. LEPOOLE,** AND W. J. OOSTERKAMP.*—The desirability of realizing a 400-kv electron microscope resulted from the experience, that the penetration and resolving power of the Delft 150-kv microscope was not always sufficient for thick specimens of several μ thickness, e.g., relatively large biologic objects as yeast cells or microtome coupe's. The apparatus which has been designed along the same lines as the Delft microscope comprises an electron gun with three stages of acceleration; the high voltage supply is obtained from a cascade generator. It is shown that at these high voltages sufficient contrast can be retained, even for thin specimens. An additional advantage is a reduced energy absorption in the specimen.

By the use of a primary and secondary stabilizer the tension is kept adequately constant to obtain good resolution. In order to get sufficient depth of field to cover the whole thickness of the specimen the condenser beam should have a very small aperture. Special devices were necessary to limit the amount of x-rays emitted. The instrument has been built in the Philips Research Laboratory and is put at the disposal of the Institute for Electron microscopy at Delft for special investigations, requiring high penetrating power.

* Philips Research Laboratory, Eindhoven, Holland.
** Institute for Electron Microscopy, Delft, Holland.

35. A Study of the Simultaneous Electron and Molecular Bombardment of Electron Microscope Specimens. JAMES HILLIER, *RCA Laboratories, Princeton, New Jersey.*—Specimens in the electron microscope were bombarded simultaneously by electrons and various gases and vapors at pressures of the order of 10^{-2} mm Hg. Magnesium oxide smoke, collodion, and bacteria were used for test specimens. Air, helium, hydrogen, acetylene, benzene, and water were used for the molecular bombardment. Numerous interactions were observed. These involved a change in the rate of contamination, a removal of previously deposited contamination and an etching of the specimens. In no case was a deposit observed. The increased reactivity of some of the gases is attributed in some cases to simple heating of the specimen and in others to an activation of the specimen by the electron bombardment.

36. Further Researches on the Electron Microanalyzer. S. G. ELLIS, *RCA Laboratories, Princeton, New Jersey.*—The present form of the microanalyzer is briefly described. Attention is then given to the factors which limit the performance of the instrument. Results are presented which show that an element, to be detected, must constitute more than 10 percent (approx.) by weight of the region illuminated by the probe. Contamination presents the chief limit at present to the use of very small probes.

37. Observations of Carbon Crystal Structure. J. D. BOADWAY, *Shawinigan Chemicals Limited, Shawinigan Falls, Quebec.*—Crystallite structure in carbon is shown in both light and dark field electron micrographs. The advantage of the electron microscope in crystalline study is that systems with a double distribution of crystallite sizes can be studied.

38. The Growth of Colloidal Crystals. JOHN H. L. WATSON, *The Edsel B. Ford Institute for Medical Research, Henry Ford Hospital, Detroit, Michigan.*—Colloidal crystals of tungstic oxide, iron oxide, and vanadium pentoxide, grown in solution are used as subjects for these experiments.

The crystal morphology and its changes with such factors as washing, concentration, and time are investigated. Micrographs are reproduced to illustrate the observations, and quantitative results are given. The major emphasis is laid on tungstic oxide investigations. In it the growth of the particles is traced from its beginning, through a pre-crystal stage until well formed crystals of almost constant shape and size are detected. A change of shape as well as size is demonstrated with respect to both time and the number of washings. The thickness of the "somatoids" is measurable and information may be gained concerning the "Schiller layer" properties of this material. The kinetics of the growth are considered and theories concerning it are supported by particle size data and bombardment experiments. Micrographs of iron oxide particles are produced to show their change in appearance with solution concentration. The appearance of vanadium pentoxide is described as it ages and both negative and positive "tactoid" forms are shown. Similarities between its growth and that of viri are discussed.

39. An Electron Microscope Technique for the Study of Polymeric Molecules. WILBUR KAYE, *Tennessee Eastman Corporation, Kingsport, Tennessee.*—A technique is presented for the reproducible preparation of polymer molecules for study with the electron microscope. The method differs from existing shadow casting techniques in the arrangement of mounting layers, in the use of aluminum-beryllium alloys for the abstrate, and a hydrophilic stripping layer. Several micrographs of different types of polymers are discussed.

40. The Effect of Shadowing, by Metallic Evaporation, upon Determination of Particle Size. H. KAHLER AND B. J. LLOYD, JR., *National Cancer Institute, Bethesda, Maryland.*—The precision attainable in the measurement of small particle dimensions after metallic shadowing is a neglected phase of investigation. For a satisfactory study of this subject the material selected was the common strain of tobacco mosaic virus. This material is known from x-ray, ultracentrifuge diffusion, and viscosity data, as well as electron microscopic investigations, to have a diameter of 15 mμ. A survey of the literature would lead one to expect that heavy coats of metal would increase the apparent diameter of the particle and that as the coating became thinner the apparent diameter would extrapolate to the true diameter. This expectation has been found to be true only to within a rather large range of variation. A detailed study was made of the manner in which the metal accumulates on the particles, as well as the growth of the background granularity and its effect on apparent size of particle. It is shown that the limits of the cast shadow depend upon the distribution of metal upon the particle. From this data the most reliable technique for estimation of particle size is presented.

41. Particle Size Correlation with X-Ray Methods. K. L. YUDOWITCH, *Department of Physics, University of Missouri, Columbia, Missouri.*—A new x-ray technique has been developed which offers a means for correlation of electron microscope particle size studies through a large range of sizes. Such an alternative method of measurement offers a means of clarifying ambiguities arising in the interpretation of electron micrographs. The usual methods of small angle x-ray scattering and x-ray line broadening become increasingly inaccurate as the particle size is increased beyond a hundred angstroms. Probably the largest portion of the useful range for electron microscopy still lies above a hundred angstroms. A technique employing very long wave-length x-rays permits ready measurement on particles up to a micron in diameter. An additional means of particle size determination by the location of certain intensity maxima is described. Examples are shown of measurements on samples of colloidal gold of several sizes.

Supplementary Paper

Electron Microscope Studies on the Structure of Larger Animal Viruses. PIERRE LEPINE, *Viruses Division, Pasteur Institute, Paris, France.*

Author Index to Volume 19

References with (L) are to Letters to the Editor.

Akeley, Edward S. (see Feuer, Paula)—39

Alexander, Leroy. Geometrical factors affecting the contours of x-ray spectrometer maxima. I. Factors causing asymmetry—1068

——, **Harold P. Klug, and Elizabeth Kummer.** Statistical factors affecting the intensity of x-rays diffracted by crystalline powders—742

Anderson, R. B. and P. H. Emmett. Measurement of carbon black particles by the electron microscope and low temperature nitrogen adsorption isotherms—367

Anderson, Robert A. (see Gilbarg, David)—127

Asp, E. T. (see Decker, B. F.)—388

Auld, Mary Jane. Temperature gradients for convection in well models—218(L)

Avery, W. H. and J. R. Morrison. Errata: Infra-red spectra of hydrocarbons. II. Analysis of octane mixtures by the use of infra-red spectra obtained at low temperatures —472

Axilrod, B. M. and J. J. Lamb. Tensile properties of rolled silver chloride—213

Badger, Richard M. (see Doyle, George J.)—373

Barker, C. B. (see Riblet, H. J.)—63

Barss, W. M. (see Yearian, H. J.)—700

Barton, H. M. (see Dunaway, R. E.)—799 (L)

Beams, J. W. (see Lapsley, A. C.)—111 (L)

Beck, F. J. and J. M. Kelly. Magnetization in perpendicularly superposed direct and alternating fields—551

Beck, Paul A. Effect of recrystallized grain size on grain growth—507 (L)

Belevitch, Vitold. Transmission losses in $2n$-terminal networks—636

Benedikt, E. T. On the flow of a perfect fluid between two plates from a circular inlet channel—1094 (L)

Birchenall, C. Ernest and Robert F. Mehl. Self-diffusion in iron—217 (L)

Birkhoff, Garrett, Duncan P. MacDougall, Emerson M. Pugh, and Sir Geoffrey Taylor. Explosives with lined cavities—563

Birnbaum, M. (see dePackh, D. C.)—795 (L)

Blackburn, Wayne E. Temperature coefficient of electrical resistivity for crystalline selenium containing various percentages of bromine—51

Bleakney, Walker (see Stoner, Richard G.)—670, 1129

Bond, W. L. Alignment chart giving the polarization correction of equi-inclination Weissenberg photographic intensities—82

—— Simple procedure for the making of alignment charts —83

Bouwkamp, C. J. and N. G. de Bruijn. Errata: The electrostatic field of a point charge inside a cylinder, in connection with wave-guide theory—105

Bridgman, P. W. Large plastic flow and the collapse of hollow cylinders—302

Brillouin, L. Wave guides for slow waves—1023

Brooks, Hamilton (see Epstein, Benjamin)—544

Brown, George W. (see Goldberg, Edwin A.)—339

Buerger, M. J. Book review—112, 218

Campbell, William L. (see Dunn, Cecil G.)—605

Cassen, B. and J. Stanton. Decay of shock waves—803

Christ, C. L. Erratum: Remarks on some recently developed devices for summing Fourier series for crystal structure analysis—225

Chu, L. J. Physical limitations of omnidirectional antennas —1163

Clark, C. L., R. A. Peck, Jr., and W. F. Hollander. Homing pigeon in electromagnetic fields—1183 (L)

Coffin, L. F., Jr. (see MacGregor, C. W.)—291

Cooley, J. P. (see Wantuch, E.)—1092 (L)

Copeland, L. E. Thermodynamics of a strained elastomer. II. Compressibility—445

—— **and M. Mooney.** Thermodynamics of a strained elastomer. III. The thermal coefficient of modulus and the statistical theory of elasticity—450

Cross, W. G. (see Deacon, Beatrice M.)—704

Crouch, G. E., Jr. (see Surber, W. H., Jr.)—1130

Crout, Prescott D. An extension of LaGrange's equations to electromagnetic field problems—1007

Cullen, A. B., Jr. and J. H. Greig. Resonant cavity linear accelerator—47

Cunningham, W. J. Simple relations for calculating certain transient responses—251

Davidson, W. L. and I. G. Geib. Effects of pile bombardment on uncured elastomers—427

Davis, Leverett, Jr. Remarks on: "The physical basis of bird navigation"307 (L)

Deacon, Beatrice M., S. G. Ellis, W. G. Cross, and R. S. Sennett. Some observations on the Formvar replica method, with a note on glass surfaces—704

de Bruijn, N. G. (see Bouwkamp, C. J.)—105

Decker, B. F., E. T. Asp, and D. Harker. Preferred orientation determination using a Geiger counter x-ray diffraction goniometer—388

dePackh, D. C. and M. Birnbaum. Prebunching: a method controlling synchrotron radial oscillation amplitudes—795 (L)

de Quevedo, José L. García and William V. Smith. Frequency stabilization of microwave oscillators by spectrum lines. II—831

Doyle, George J. and Richard M. Badger. Visco-elastic behavior of a highly plasticized nitrocellulose in compression under constant load—373

Dunaway, R. E. and H. M. Barton. Notes on electron diffraction with the universal electron microscope—799 (L)

Dunn, Cecil G., William L. Campbell, Harvey Fram, and Ardelia Hutchins. Biological and photo-chemical effects of high energy, electrostatically produced Roentgen rays and cathode rays—605

Elenbaas, W. The dissipation of heat by free convection from vertical and horizontal cylinders—1148
Ellis, S. G. (see Deacon, Beatrice M.)—704
Elmore, W. C. Transient response of damped linear networks with particular regard to wideband amplifiers—55
Emmett, P. H. (see Anderson, R. B.)—367
Epstein, Benjamin. Statistical aspects of fracture problems—140
—— **and Hamilton Brooks.** Theory of extreme values and its implications in the study of the dielectric strength of paper capacitors—544

Fairbanks, A. F. (see McCormick, W. W.)—221
Farrant, J. L. and A. J. Hodge. Interferometric method for the calibration of electron microscope magnification—840
Feuer, Paula and Edward S. Akeley. Scattering of electromagnetic radiation by a thin circular ring in a circular wave guide—39
Fisher, J. C. (see MacGregor, C. W.)—291
——, **J. H. Hollomon, and D. Turnbull.** Nucleation—775
Fisher, John C. The fracture of liquids—1062
Fowler, Franklin H., Jr. Statistical aspects of fracture problems—1092 (L)
Fram, Harvey (see Dunn, Cecil G.)—605
Frissel, H. F. (see Kammer, E. W.)—265
Fuchs. Henry O. Gyrograms—796 (L)
Fullam, Ernest F. and Robert H. Savage. Carbon film formation and commutator brush-wear as revealed by the electron microscope—654

Gardner, C. S., H. F. Ludloff, and F. Reiche. Drag of an airfoil in accelerated, supersonic flight—1179 (L)
Gardner, Irvine C. Range-finder testing laboratory—721
—— Testing of range finders—729
Gehman, S. D. Creep, recovery, and permanent set for GR-S and Hevea—456
Geib, I. G. (see Davidson, W. L.)—427
Geisler, A. H., J. K. Hill, and J. B. Newkirk. Divergent beam x-ray photography with standard diffraction equipment—1041
Gemant, Andrew. Measurement by radioactive tracers of diffusion in liquids—1160
Germer, L. H. (see Lander, J. J.)—910
Geschwind, S. (see Townes, C. H.)—795 (L)
Geyer, Charles J., Jr., C. H. Reichardt, and George Halsey. Theory of commercial yarn testing—464
Gibbs, Norman E. (see Pike, Eugene W.)—106
Gilbarg, David and Robert A. Anderson. Influence of atmosphere pressure on the phenomena accompanying the entry of spheres into water—127
Glasser, Otto J. and John D. Kraus. Measured impedances of helical beam antennas—193
Goldberg, Edwin A. and George W. Brown. Electronic simultaneous equation solver—339
Gordon, W. E. (see Straiton, A. W.)—524
Greig, J. H. (see Cullen, A. B., Jr.)—47
—— (see Wantuch, E.)—1092 (L)
Grimminger, G. Probability that a meteorite will hit or penetrate a body situated in the vicinity of the earth—947
Gross, B. On creep and relaxation. II—257
Gunn, Ross. Electric field intensity inside of natural clouds—481

Hahn, W. C. (see Lawton, Elliott J.)—642
Hall, C. E. Dark-field electron microscopy. I. Studies of crystalline substances in dark-field—198
—— Dark-field electron microscopy—271
Hallen, Erik. Properties of a long antenna—1140
Halsey, George (see Geyer, Charles J., Jr.)—464
Hamm, F. A. and Earl Van Norman. Transformations in organic pigments—1097
Hanley, T. E. Spectral emissivity and electron emission constants of thoria cathodes—583
Hansen, W. W. and R. F. Post. On the measurement of cavity impedance—1059
Harker, D. (see Decker, B. F.)—388
Harris, Louis, David Jeffries, and Benjamin M. Siegel. Electron microscope study of gold smoke deposits—791
—— **and Benjamin M. Siegel.** Method for the evaporation of alloys—739
Henry, Hugh F. Velocity of the anode spark in copper sulfate solutions under application of impulsive potential—988
Hermans, P. H. and A. Weidinger. Quantitative x-ray investigations on the crystallinity of cellulose fibers. A background analysis—491
Hershberger, W. D. Minimum detectable absorption in microwave spectroscopy and an analysis of the Stark modulation method—411
Hicks, Bruce L., Donald J. Montgomery, and Robert H. Wasserman. Erratum: On the one-dimensional theory of steady compressible fluid flow in ducts with friction and heat addition—523
Hill, Edward L. Book review—114
Hill, J. K. (see Geisler, A. H.)—1041
Hillier, James. On the investigation of specimen contamination in the electron microscope—226
—- (see Ramberg, E. G.)—678
Hodge, A. J. (see Farrant, J. L.)—840
Hok, Gunnar. Response of linear resonant systems to excitation of a frequency varying linearly with time—242; erratum—623
Hollander, W. F. (see Clarke, C. L.)—1183 (L)
Hollenberg, A. V., N. Kroll, and S. Millman. Rising sun magnetrons with large numbers of cavities—624
Hollomon, J. H. (see Fisher, J. C.)—775
Holm, Ragnar. Calculation of the temperature development in a contact heated in the contact surface, and application to the problem of the temperature rise in a sliding contact—361
Horton, C. W. (see Watson, R. B.)—661, 836
Hutchins, Ardelia (see Dunn, Cecil G.)—605

Iberall, Arthur S. The effective "gamma" for isentropic expansions of real gases—997

Jaffee, Robert I. Magnetic properties of ordered nickel-manganese alloys—867
Jeffries, David (see Harris, Louis)—791
Jelatis, J. G. Measurements of dielectric constant and dipole moment of gases by the beat-frequency method—419
Jen, C. K. Method for measuring the complex dielectric constant of gases at microwave frequencies by using a resonant cavity—649

Kammer, E. W., T. E. Pardue, and H. F. Frissel. Determination of the elastic constants for beta-quartz—265
Kê, T'ing-Sui. Viscous slip along grain boundaries and diffusion of zinc in alpha-brass—285
Kelly, J. M. (see Beck, F. J.)—551
Kelso, J. M. Note on the phase difference between two waves reflected from the ionosphere—590 (L)
Keogh, C. T. and A. H. Weber. Electron diffraction study of particle size in thin Bi films deposited by evaporation in vacuum—1077
King, Ronold (see Papas, C. H.)—808
Kirkwood, J. G. and R. J. Seeger. Surface waves from an underwater explosion—346
Klug, Harold P. (see Alexander, Leroy)—742
Klute, C. H. Some remarks concerning a proposed method for testing the brittleness of elastomers—1093 (L)
Koehler, J. S. Electronic differential analyzer—148
Kofoid, M. J. Observations on arc discharges at low pressures—399
Kraus, John D. (see Glasser, Otto J.)—193
—— **and J. Claude Williamson.** Characteristics of helical antennas radiating in the axial mode—87
Kroll, N. (see Hollenberg, A. V.)—624
Kroll, Norman M. and Willis E. Lamb, Jr. Resonant modes of the rising sun and other unstrapped magnetron anode blocks—166
Kuczynski, G. C. New method of measuring diffusion coefficient in solids with radioactive tracers—308 (L)
—— **and J. T. Norton.** Young's modulus and strain coefficient of resistivity of some bismuth rich alloys—683
Kummer, Elizabeth (see Alexander, Leroy)—742
Kunkel, Wulf B. Magnitude and character of errors produced by shape factors in Stokes' law estimates of particle radius—1056
—— Growth of charged particles in clouds—1053

LaGrone, A. H. (see Straiton, A. W.)—524
Lamb, J. J. (see Axilrod, B. M.)—213
Lamb, Willis E., Jr. (see Kroll, Norman M.)—166
Lander, J. J. Use of an electron diffraction camera as an ultraoscilloscope and suggested application to contact erosion—1128
—— **and L. H. Germer.** Bridge erosion of electrical contacts. Part I—910
Lapsley, A. C., L. B. Snoddy, and J. W. Beams. Use of a cavity oscillator for a Kerr electro-optical light shutter —111 (L)
Lawton, Elliott J. Choice of operating mode for standing wave type linear accelerators for electrons—534
—— **and W. C. Hahn.** Experimental results on standing wave type linear accelerators for electrons—642
Ling, Chih-Bing. On the stresses in a plate containing two circular holes—77
—— Stresses in a plate containing an overlapped circular hole—405
Loeb, Leonard B. Recent developments in analysis of the mechanisms of positive and negative coronas in air—882
—— **and Robert A. Wijsman.** Theortical criterion for streamer advance in an electrical field—797 (L)
Ludloff, H. F. (see Gardner, C. S.)—1179 (L)
Lutton, E. S. (see Stewart, C. B.)—507 (L)
Lyons, W. James and Irven B. Prettyman. Method for the absolute measurement of dynamic properties of linear structures at sonic frequencies—473

MacDougall, Duncan P. (see Birkhoff, Garrett)—563
MacGregor, C. W., L. F. Coffin, Jr., and J. C. Fisher. Plastic flow of thick-walled tubes with large strains—291
Mack, Charles. Plastic flow, creep, and stress relaxation. Part IV. Anomalous flow as an order-disorder transition —1082
Madansky, L. (see McCormick, W. W.)—221
Mahla, E. M. and N. A. Nielson. Oxide replica technique for the electron microscope examination of stainless steel and high nickel alloys—378
Manning, Laurence A. Theory of the radio detection of meteors—689
Mark, Herman (see Singer, Seymour J.)—97
Marton, L. Electron optical "Schlieren" effect—687 (L)
—— Electron optical observation of magnetic fields—863 (L)
Mason, W. P. and H. J. McSkimin. Energy losses of sound waves in metals due to scattering and diffusion—940
May, Albert and Jean C. Woodhull. Drag coefficients of steel spheres entering water vertically—1109
McCormick, W. W., L. Madansky, and A. F. Fairbanks. Microflash unit for ballistic photography—221
McKinney, C. M. (see Watson, R. B.)—871
McSkimin, H. J. (see Mason, W. P.)—940
Mehl, Robert F. (see Birchenall, C. Ernest)—217 (L)
Middleton, David. Spurious signals caused by noise in triggered circuits—817
Millman, S. (see Hollenberg, A. V.)—624
—— **and A. T. Nordsieck.** Rising sun magnetron—156
Minorsky, N. Self-excited mechanical oscillations—332
Minter, Clarke C. Note on the anomalous physical properties of processed atmospheric nitrogen—217 (L)
Mirabelli, Eugene. Book review—113
Monk, G. W. Apparatus for weighing in vacuum—485
Montgomery, Donald J. (see Hicks, Bruce L.)—523
Mooney, M. Thermodynamics of a strained elastomer. I. General analysis—434
—— (see Copeland, L. E.)—450
Morgan, Karl Z. Shipping of radio-isotopes—593
Morrison, J. R. (see Avery, W. H.)—472
Morrison, Philip. Physics in 1947—311
Moses, H. E. Head-on collision of a shock wave and a rarefaction wave in one dimension—383

Mueller, Robert Emmett. Analogy between isopachic stress lines and equipotential lines—590 (L)
Munk, Max M. and Robert C. Prim. On the canonical form of the equations of steady motion of a perfect gas—957

Newkirk, J. B. (see Geisler, A. H.)—1041
Nielson, N. A. (see Mahla, E. M.)—378
Nolle, A. W. Methods for measuring dynamic mechanical properties of rubber-like materials—753
Nordsieck, A. T. (see Millman, S.)—156
Norton, J. T. (see Kuczynski, G. C.)—683
Norton, John T. A technique for quantitative determination of texture of sheet metals—1176

Okress, E. C. Erratum: A magnetron resonator system—338
Oliner, A. A. Remarks on slow waves in cylindrical guides—109 (L)
Oosterkamp, W. J. Calculation of the temperature development in a contact heated in the contact surface, and application to the problem of the temperature in a sliding contact—1180 (L)

Pachner, Jaroslav. Theory of the positive column in an annular discharge tube—1072
Papas, C. H. and Ronold King. Surface currents on a conducting sphere excited by a dipole—808
Papet, Robert M. Remarks on "The efficiency of thermoelectric generators"—1180 (L)
Papp, G. and K. Sasvári. The application of electron multiplier tubes in the measurement of x-ray beam intensities and in the determination of crystal structure—1182 (L)
Pardue, T. E. (see Kammer, E. W.)—265
Peck, R. A., Jr. (see Clarke, C. L.)—1183 (L)
Pekeris, C. L. Effect of ground constants on the characteristic values of the normal modes in non-standard propagation of microwaves—102
Penner, S. S. Mass emissivity of powder gases in solid fuel rockets—278
—— Effect of radiation on the rate of burning of solid fuel rocket propellants—392
—— Qualitative experimental verification of the change of burning rate of rocket powders with radiation path length—511
Pierce, J. R. Possible fluctuations in electron streams due to ions—231
Piispanen, Väinö. Theory of formation of metal chips—876
Pike, Eugene W. and Norman E. Gibbs. Study on anaeroid capsules—106
Pipes, Louis A. Analysis of retarded control systems—617
Plesset, Milton S. and Philip A. Shaffer, Jr. Cavity drag in two and three dimensions—934
Post, R. F. (see Hansen, W. W.)—1059
Powell, R. W. Bidwell's intercept relation and the thermal conductivity of liquid metals—995
Prager, W. Theory of plastic flow *versus* theory of plastic deformation—540
Prettyman, Irven B. (see Lyons, W. James)—473
Prim, Robert C. (see Munk, Max M.)—957
Pugh, Emerson M. (see Birkhoff, Garrett)—563

Ramberg, E. C. and J. Hillier. Chromatic aberration and resolving power in electron microscopy—678
Reichardt, C. H. (see Geyer, Charles J., Jr.)—464
Reiche, F. (see Gardner, C. S.)—1179 (L)
Reissner, E. Book review—114
Riblet, H. J. and C. B. Barker. General divergence formula—63
Rinehart, R. F. Solution of the problem of rapid scanning for radar antennae—860
Robertson, W. D. and H. H. Uhlig. Observation of corrosion cracking without stress—864 (L)
Robinson, Lawrence Baylor. Application of the Laplace transform in the solution of linear integral equations—237
Rohrbaugh, J. H. (see Wantuch, E.)—1092 (L)
Rojansky, V. Gyrograms for simple harmonic systems subjected to external forces—297
Roth, W. Scattering of ultrasonic radiation in polycrystalline metals—901
Rothstein, Jerome. On the possibility of Hg type arcs with hot refractory cathodes—1181 (L)

Sasaki, Nobuji. An ion microscope with a transverse magnetic field—1050
Sasvári, K. (see Papp, G.)—1182 (L)
Savage, Robert H. Graphite lubrication—1
—— (see Fullam, Ernest F.)—654
Schelkunoff, S. A. Book review—115
Seeger, R. J. (see Kirkwood, J. G.)—346
Seitz. Frederick. The contribution of modern physics to metallurgy—973
Sennett, R. S. (see Deacon, Beatrice M.)—704
Shaffer, Philip A., Jr. (see Plesset, Milton S.)—934
Shankland, Robert S. Book review—800
Sheppard, C. W. Theory of the study of transfers within a multi-compartment system using isotopic tracers—70
Shmoys, J. Note on reflection from dielectric structures in wave guide—797 (L)
—— (see Wantuch, E.)—1092 (L)
Sidhu, S. S. Transmission of monoenergetic slow neutrons through solid solutions and mechanical mixtures of TiC and WC—639
Siegel, Benjamin M. (see Harris, Louis)—739, 791
Singer, Seymour J. and Herman Mark. On the structure of cellulose acetate molecules in acetone solution—97
Skellett, A. M. Palletron, a new electron resonator and its proposed application to the generation of potentials in the million-volt range—187
Slepian, Joseph. Physical basis of bird navigation—306 (L)
Smith, P. D. P. Conical dipole of wide angle—11
Smith, William V. (see De Quevedo, José L. García)—831
Snoddy, L. B. (see Lapsley, A. C.)—111 (L)
Spedding, F. H. Book review—115
Stanton, J. (see Cassen, B.)—803
Stevenson, A. F. Theory of slots in rectangular wave guides—24

Stewart, C. B. and E. S. Lutton. Convenient methods for obtaining d/n values from x-ray diffraction patterns—507 (L)
Stoffregen, W. Ionosphere reflections recorded mechanically by means of a repetition frequency converter—487
Stoner, Richard G. and Walker Bleakney. Attenuation of spherical shock waves in air—670; erratum—1129
Straiton, A. W., W. E. Gordon, and A. H. LaGrone. Method of determining the angle of arrival—524
Surber, W. H., Jr. Universal curves for dielectric-filled wave guides and microwave dielectric measurement methods for liquids—514
—— **and G. E. Crouch, Jr.** Dielectric measurement methods for solids at microwave frequencies—1130

Tai, C. T. On the theory of biconical antennas—1155
Taylor, Sir Geoffrey (see Birkhoff, Garrett)—563
Thomas, D. E. Measurement of stress by means of x-rays—190
Townes, C. H. and S. Geschwind. Limiting sensitivity of a microwave spestrometer—795 (L)
Trillat, Jean-Jacques. Electronic radiography and microradiography—844
Trump, J. G. and R. J. Van de Graaff. Irradiation of biological materials by high energy Roentgen rays and cathode rays—599
Turnbull, D. (see Fisher, J. C.)—775

Uhlig, H. H. (see Robertson, W. D.)—864 (L)

Vand, V. Temperature-controlled Frevel focusing x-ray powder camera—852
Van de Graaff, R. J. (see Trump, J. G.)—599
van der Ziel, A. On the mixing properties of non-linear condensers—999
Van Norman, Earl (see Hamm, F. A.)—1097
Varian, Russell H. Remarks on: "A preliminary study of a physical basis of bird navigation"—306 (L)
Victoreen, John A. Absorption of incident quanta by atoms as defined by the mass photoelectric absorption coefficient and the mass scattering coefficient—855
Vonnegut, Bernard. Production of ice crystals by the adiabatic expansion of gas—959 (L)

Wagner, Carl. Heat transfer from a rotating disk to ambient air—837
Walsh, T. J. Book review—113
Wannier, Gregory H. An observation on heat sources placed at random on a surface—1020
Wantuch, E., J. H. Rohrbaugh, J. P. Cooley, J. H. Greig, and J. Shmoys. Transmission properties of materials in the millimeter wave region—1092 (L)
Wasserman, Robert H. (see Hicks, Bruce L.)—523
Watson, John H. L. Specimen contamination in electron microscopes—110 (L)
—— Pseudostructures in electron microscope specimens—713
Watson, R. B. and C. W. Horton. Radiation patterns of dielectric rods—experiment and theory—661; on the calculation of radiation patterns of dielectric rods—836
—— **and C. M. McKinney.** Gains and effective areas of horn antennas—871
Weber, A. H. (see Keogh, C. T.)—1077
Weidinger, A. (see Hermans, P. H.)—491
Weinbaum, Sidney. Alloying of metal powders by diffusion—897
Wijsman, Robert A. (see Loeb, Leonard B.)—797 (L)
Williamson, J. Claude (see Kraus, John D.)—87
Wood, John K. Analytical discussion of the construction of pole figures—784
Woodhull, Jean C. (see May, Albert)—1109
Worrell, Francis T. Twinning in tetragonal alloys of copper and manganese—929; erratum—1154

Yearian, H. J. and W. M. Barss. Aids to analysis of patterns obtained in the diffraction of electrons by gases—700
Yuan, L. C. Homing and navigational courses of automatic target-seeking devices—1122

Subject Index to Volume 19

References with (L) are to Letters to the Editor.

Absorption of incident quanta by atoms as defined by the mass photoelectric absorption coefficient and the mass scattering coefficient, John A. Victoreen—855

Accelerator, Resonant cavity linear accelerator, A. B. Cullen, Jr. and J. H. Greig—47

Accelerators for electrons, standing wave type linear, Choice of operating mode for, Elliott J. Lawton—534

Accelerators, Experimental results on standing wave type linear accelerators for electrons, Elliott J. Lawton and W. C. Hahn—642

Aids to analysis of patterns obtained in the diffraction of electrons by gases, H. J. Yearian and W. M. Barss—700

Airfoil, Drag of an, in accelerated, supersonic flight, C. S. Gardner, H. F. Ludloff, and F. Reiche—1179 (L)

Alignment chart giving the polarization correction of equi-inclination Weissenberg photographic intensities, W. L. Bond—82

Alignment charts, Simple procedure for the making of, W. L. Bond—83

Alloying of metal powders by diffusion, Sidney Weinbaum —897

Alloys, Method for the evaporation of, Louis Harris and Benjamin M. Siegel—739

Alloys, tetragonal, of copper and manganese, Twinning in, Francis T. Worrell—929; erratum—1154

Alpha-brass, Viscous slip along grain boundaries and diffusion of zinc in, T'ing-Sui Kê—285

Amplifiers, wideband, Transient response of damped linear networks with particular regard to, W. C. Elmore—55

Anaeroid capsules, Study on, Eugene W. Pike and Norman E. Gibbs—106

Analogy between isopachic stress lines and equipotential lines, Robert Emmett Mueller—590 (L)

Analysis of retarded control systems, Louis A. Pipes—617

Analytical discussion of the construction of pole figures, John K. Wood—784

Analyzer, Electronic differential, J. S. Koehler—148

Angle of arrival, Method of determining, A. W. Straiton, W. E. Gordon, and A. H. LaGrone—524

Annular discharge tube, Theory of the positive column in, Jaroslav Pachner—1072

Anode spark, Velocity of the, in copper sulfate solutions under application of impulsive potential, Hugh F. Henry—988

Anomalous physical properties of processed atmospheric nitrogen, Clarke C. Minter—217 (L)

Antenna, long, Properties of a, Erik Hallen—1140

Antennas, biconical, Theory of, C. T. Tai—1155

Antennas, helical beam, Measured impedances of, Otto J. Glasser and John D. Kraus—193

Antennas, horn, Gains and effective areas of, R. B. Watson and C. M. McKinney—871

Antennas, omnidirectional, Physical limitations of, L. J. Chu—1163

Apparatus for weighing in vacuum, G. W. Monk—485

Application of electron multiplier tubes in the measurement of x-ray beam intensities and in the determination of crystal structure, G. Papp and K. Sasvári—1182 (L)

Application of the Laplace transform in the solution of linear integral equations, Lawrence Baylor Robinson —237

Arc discharges at low pressures, Observations on, M. J. Kofoid—399

Arcs, Possibility of Hg type arcs with hot refractory cathodes, Jerome Rothstein—1181 (L)

Atmosphere pressure, Influence of, on the phenomena accompanying the entry of spheres into water, David Gilbarg and Robert A. Anderson—127

Atoms, Absorption of incident quanta by atoms as defined by the mass photoelectric absorption coefficient and the mass scattering coefficient, John A. Victoreen—855

Attenuation of spherical shock waves in air, Richard G. Stoner and Walker Bleakney—670; erratum—1129

Ballistic photography, Microflash unit for, W. W. McCormick, L. Madansky, and A. F. Fairbanks—221

Beat-frequency method, Measurements of dielectric constant and dipole moment of gases by the, J. G. Jelatis —419

Beta-quartz, Determination of the elastic constants for, E. W. Kammer, T. E. Pardue, and H. F. Frissel—265

Bidwell's intercept relation and the thermal conductivity of liquid metals, R. W. Powell—995

Biological materials, Irradiation of, by high energy Roentgen rays and cathode rays, J. G. Trump and R. J. Van de Graaff—599

Biological and photo-chemical effects of high energy, electrostatically produced Roentgen rays and cathode rays, Cecil G. Dunn, William L. Campbell, Harvey Fram, and Ardelia Hutchins—605

Bird navigation, Physical basis of, Joseph Slepian—306 (L)

Bird navigation, Remarks on "The physical basis of," Leverett Davis, Jr.—307 (L)

Bird navigation, Remarks on "A preliminary study of a physical basis of," Russell H. Varian—306 (L)

Bismuth, Young's modulus and strain coefficient of resistivity of some bismuth rich alloys, G. C. Kuczynski and J. T. Norton—683

Bridge erosion of electrical contacts, Part I, J. J. Lander L. H. Germer—910

Brittleness of elastomers, Some remarks concerning a proposed method for testing the, C. H. Klute—1093 (L)

Bromine, Temperature coefficient of electrical resistivity for crystalline selenium containing various percentages of, Wayne E. Blackburn—51

Calculation of radiation patterns of dielectric rods, R. B. Watson and C. W. Horton—836

Calculation of the temperature development in a contact heated in the contact surface, and application to the

problem of the temperature rise in a sliding contact, Ragnar Holm—361; W. J. Oosterkamp—1180 (L)
Camera, electron diffraction, Use of, as an ultraoscilloscope and suggested application to contact erosion, J. J. Lander—1128
Camera, Temperature-controlled Frevel focusing x-ray powder camera, V. Vand—852
Canonical form of the equations of steady motion of a perfect gas, Max M. Munk and Robert C. Prim—957
Carbon black particles, Measurement of, by the electron microscope and low temperature nitrogen adsorption isotherms, R. B. Anderson and P. H. Emmett—367
Carbon film formation and commutator brush-wear as revealed by the electron microscope, Ernest F. Fullam and Robert H. Savage—654
Cathode rays, Biological and photo-chemical effects of high energy, electrostatically produced Roentgen rays and, Cecil G. Dunn, William L. Campbell, Harvey Fram, and Ardelia Hutchins—605
Cathode rays, Irradiation of biological materials by high energy Roentgen rays and, J. G. Trump and R. J. Van de Graaff—599
Cavities, lined, Explosives with, Garrett Birkhoff, Duncan P. MacDougall, Emerson M. Pugh, and Sir Geoffrey Taylor—563
Cavity drag in two and three dimensions, Milton S. Plesset and Philip A. Shaffer, Jr.—934
Cavity impedance, Measurement of, W. W. Hansen and R. F. Post—1059
Cavity, Method for measuring the complex dielectric constant of gases at microwave frequencies by using a resonant cavity, C. K. Jen—649
Cavity oscillator, Use of a, for a Kerr electro-optical light shutter, A. C. Lapsley, L. B. Snoddy, and J. W. Beams —111 (L)
Cellulose acetate molecules, Structure of, in acetone solution, Seymour J. Singer and Herman Mark—97
Cellulose fibers, crystallinity of, Quantitative x-ray investigations on. A background analysis, P. H. Hermans and A. Weidinger—491
Characteristics of helical antennas radiating in the axial mode, John D. Kraus and J. Claude Williamson—87
Choice of operating mode for standing wave type linear accelerators for electrons, Elliott J. Lawton—534
Chromatic aberration and resolving power in electron microscopy, E. G. Ramberg and J. Hillier—678
Circuits, triggered, Spurious signals caused by noise in, David Middleton—817
Clouds, Growth of charged particles in, Wulf Kunkel—1053
Clouds, natural, Electric field intensity inside of, Ross Gunn—481
Commutator brush-wear, Carbon film formation and, as revealed by the electron microscope, Ernest F. Fullam and Robert H. Savage—654
Condensers, non-linear, Mixing properties of, A. van der Ziel—999
Conical dipole of wide angle, P. D. P. Smith—11
Contact, sliding, Calculation of the temperature development in a contact heated in the contact surface, and application to the problem of the temperature rise in a, Ragnar Holm—361; W. J. Oosterkamp—1180 (L)
Contact surface, Calculation of the temperature development in a contact heated in the, and application to the problem of the temperature in a sliding contact, Ragnar Holm—361; W. J. Oosterkamp—1180 (L)
Contacts, electrical, Bridge erosion of, Part I, J. J. Lander and L. H. Germer—910
Contamination, Investigation of specimen contamination in the electron microscope, James Hillier—226
Contamination, Specimen, in electron microscopes, John H. L. Watson—110 (L)
Contribution of modern physics to metallurgy, Frederick Seitz—973
Control systems, retarded, Analysis of, Louis A. Pipes—617
Convection in well models, Temperature gradients for, Mary Jane Auld—218 (L)
Convenient methods for obtaining d/n values from x-ray diffraction patterns, C. B. Stewart and E. S. Lutton—507 (L)
Copper sulfate solutions, Velocity of the anode spark in, under application of impulsive potential, Hugh F. Henry—988
Copper, Twinning in tetragonal alloys of copper and manganese, Francis T. Worrell—929; erratum—1154
Coronas, Recent developments in analysis of the mechanisms of positive and negative coronas in air, Leonard B. Loeb—882
Corrosion cracking without stress, Observation of, W. D. Robertson and H. H. Uhlig—864 (L)
Creep, Plastic flow, creep, and stress relaxation. Part IV. Anomalous flow as an order-disorder transition, Charles Mack—1082
Creep, recovery, and permanent set for GR-S and Hevea, S. D. Gehman—456
Creep and relaxation. II. B. Gross—257
Crystal structure analysis, Remarks on some recently developed devices for summing Fourier series for, C. L. Christ—225 (erratum)
Crystal structure, Application of electron multiplier tubes in the measurement of x-ray beam intensities and in the determination of, G. Papp and K. Sasvári—1182 (L)
Crystalline powders, Statistical factors affecting the intensity of x-rays diffracted by, Leroy Alexander, Harold P. Klug, and Elizabeth Kummer—742
Crystalline substances, Studies of, in dark-field. Dark-field electron microscopy. I, C. E. Hall—198
Cylinders, Large plastic flow and the collapse of hollow cylinders, P. W. Bridgman—302

Dark-field electron microscopy, C. E. Hall—198, 271
Decay of shock waves, B. Cassen and J. Stanton—803
Determination of the elastic constants for beta-quartz, E. W. Kammer, T. E. Pardue, and H. F. Frissel—265
Dielectric measurement methods for solids at microwave frequencies, W. H. Surber, Jr. and G. E. Crouch, Jr.—1130
Dielectric rods, Calculation of radiation patterns of, R. B. Watson and C. W. Horton—836

Dielectric rods, Radiation patterns of—experiment and theory, R. B. Watson and C. W. Horton—661
Diffusion coefficient, New method of measuring, in solids with radioactive tracers, G. C. Kuczynski—308 (L)
Dipole, Conical, of wide angle, P. D. P. Smith—11
Dipole, Surface currents on a conducting sphere excited by a, C. H. Papas and Ronold King—808
Disk, Heat transfer from a rotating disk to ambient air, Carl Wagner—837
Dissipation of heat by free convection from vertical and horizontal cylinders, W. Elenbaas—1148
Divergent beam x-ray photography with standard diffraction equipment, A. H. Geisler, J. K. Hill, and J. B. Newkirk—1041
Drag of an airfoil in accelerated, supersonic flight, C. S. Gardner, H. F. Ludloff, and F. Reiche—1179 (L)
Drag coefficients of steel spheres entering water vertically, Albert May and Jean C. Woodhull—1109

Effect of ground constants on the characteristic values of the normal modes in non-standard propagation of microwaves, C. L. Pekeris—102
Effect of radiation on the rate of burning of solid fuel rocket propellants, S. S. Penner—392
Effect of recrystallized grain size on grain growth, Paul A. Beck—507 (L)
Effective "gamma" for isentropic expansions of real gases, Arthur S. Iberall—997
Effects of pile bombardment on uncured elastomers, W. L. Davidson and I. G. Geib—427
Elastic constants, Determination of, for beta-quartz, E. W. Kammer, T. E. Pardue, and H. F. Frissel—265
Elastomer, strained, Thermodynamics of. I. General analysis, M. Mooney—434; II. Compressibility, L. E. Copeland—445; III. The thermal coefficient of modulus and the statistical theory of elasticity, L. E. Copeland and M. Mooney—450
Elastomers, brittleness of, Some remarks concerning a proposed method for testing, C. H. Klute—1093 (L)
Elastomers, uncured, Effects of pile bombardment on, W. L. Davidson and I. G. Geib—427
Electric field intensity inside of natural clouds, Ross Gunn—481
Electromagnetic field problems, Extension of LaGrange's equations to, Prescott D. Crout—1007
Electromagnetic radiation, Scattering of, by a thin circular ring in a circular wave guide, Paula Feuer and Edward S. Akeley—39
Electron diffraction camera, Use of, as an ultraoscilloscope and suggested application to contact erosion, J. J. Lander—1128
Electron diffraction, Notes on, with the universal electron microscope, R. E. Dunaway and H. M. Barton—799 (L)
Electron diffraction study of particle size in thin Bi films deposited by evaporation in vacuum, C. T. Keogh and A. H. Weber—1077
Electron microscope, Carbon film formation and commutator brush-wear as revealed by the, Ernest F. Fullam and Robert H. Savage—654
Electron microscope examination of stainless steel and high nickel alloys, Oxide replica technique for, E. M. Mahla and N. A. Nielson—378
Electron microscope, Investigation of specimen contamination in the, James Hillier—226
Electron microscope magnification, Interferometric method for the calibration of, J. L. Farrant and A. J. Hodge—840
Electron microscope, Measurement of carbon black particles by the, and low temperature nitrogen adsorption isotherms, R. B. Anderson and P. H. Emmett—367
Electron Microscope Society of America, Proceedings of—118; E. F. Burton Memorial Meeting—1186
Electron microscope specimens, Pseudostructures in, John H. L. Watson—713
Electron microscope study of gold smoke deposits, Louis Harris, David Jeffries, and Benjamin M. Siegel—791
Electron microscope, universal, Notes on electron diffraction with the, R. E. Dunaway and H. M. Barton—799 (L)
Electron microscopes, Specimen contamination in, John H. L. Watson—110 (L)
Electron microscopy, Chromatic aberration and resolving power in, E. G. Ramberg and J. Hillier—678
Electron microscopy, Dark-field, C. E. Hall—198, 271
Electron multiplier tubes, Application of, in the measurement of x-ray beam intensities and in the determination of crystal structure, G. Papp and K. Sasvári—1182 (L)
Electron optical observation of magnetic fields, L. Marton—863 (L)
Electron optical "Schlieren" effect, L. Marton—687 (L)
Electron streams due to ions, Possible fluctuations in, J. R. Pierce—231
Electronic differential analyzer, J. S. Koehler—148
Electronic radiography and microradiography, Jean-Jacques Trillat—844
Electronic simultaneous equation solver, Edwin A. Goldberg and George W. Brown—339
Electrons, Aids to analysis of patterns obtained in the diffraction of electrons by gases, H. J. Yearian and W. M. Barss—700
Electrons, Choice of operating mode for standing wave type linear accelerators for, Elliott J. Lawton—534
Electrons, Experimental results on standing wave type linear accelerators for, Elliott J. Lawton and W. C. Hahn—642
Electrostatic field of a point charge inside a cylinder, in connection with wave-guide theory, C. J. Bouwkamp and N. G. de Bruijn—105 (errata)
Energy losses of sound waves in metals due to scattering and diffusion, W. P. Mason and H. J. McSkimin—940
Equation solver, Electronic simultaneous, Edwin A. Goldberg and George W. Brown—339
Erosion, Bridge, of electrical contacts, Part I, J. J. Lander and L. H. Germer—910
Evaporation of alloys, Method for the, Louis Harris and Benjamin M. Siegel—739
Experimental results on standing wave type linear accelerators for electrons, Elliott J. Lawton and W. C. Hahn—642

Explosives with lined cavities, Garrett Birkhoff, Duncan P. MacDougall, Emerson M. Pugh, and Sir Geoffrey Taylor—563
Extension of LaGrange's equations to electromagnetic field problems, Prescott D. Crout—1007
Extreme values, Theory of, and its implications in the study of the dielectric strength of paper capacitors, Benjamin Epstein and Hamilton Brooks—544

Flow of a perfect fluid between two plates from a circular inlet channel, E. T. Benedikt—1094 (L)
Formvar replica method, Some observations on, with a note on glass surfaces, Beatrice M. Deacon, S. G. Ellis, W. G. Cross, and R. S. Sennett—704
Fracture of liquids—John C. Fisher—1062
Fracture problems, Statistical aspects of, Benjamin Epstein —140; Franklin H. Fowler, Jr.—1092 (L)
Frequency stabilization of microwave oscillators by spectrum lines. II. Jose L. Garcia de Quevedo and William V. Smith—831
Frevel focusing x-ray powder camera, Temperature-controlled, V. Vand—852

Gains and effective areas of horn antennas, R. B. Watson and C. M. McKinney—871
Gas, adiabatic expansion of, Production of ice crystals by, Bernard Vonnegut—959 (L)
Gas, perfect, Canonical form of the equations of steady motion of a, Max M. Munk and Robert C. Prim—957
Gases, Measurements of dielectric constant and dipole moment of gases by the beat-frequency method, J. G. Jelatis—419
Gases, Method for measuring the complex dielectric constant of gases at microwave frequencies by using a resonant cavity, C. K. Jen—649
Gases, real, Effective "gamma" for isentropic expansions of, Arthur S. Iberall—997
Geiger counter x-ray diffraction goniometer, Preferred orientation determination using a, B. F. Decker, E. T. Asp, and D. Harker—388
General divergence formula, H. J. Riblet and C. B. Barker —63
Generators, thermoelectric, Efficiency of, Robert M. Papet —1180 (L)
Geometrical factors affecting the contours of x-ray spectrometer maxima. I. Factors causing asymmetry, Leroy Alexander—1068
Gold smoke deposits, Electron microscope study of, Louis Harris, David Jeffries, and Benjamin M. Siegel—791
Grain growth, Effect of recrystallized grain size on, Paul A. Beck—507 (L)
Graphite lubrication, Robert H. Savage—1
Growth of charged particles in clouds, Wulf Kunkel—1053
GR-S and Hevea, Creep, recovery, and permanent set for, S. D. Gehman—456
Gyrograms, Henry O. Fuchs—796 (L)
Gyrograms for simple harmonic systems subjected to external forces, V. Rojansky—297

Harmonic systems, Gyrograms for simple harmonic systems subjected to external forces, V. Rojansky—297
Head-on collision of a shock wave and a rarefaction wave in one dimension, H. E. Moses—383
Heat, Dissipation of, by free convection from vertical and horizontal cylinders, W. Elenbaas—1148
Heat sources, Observation on, placed at random on a surface, Gregory H. Wannier—1020
Heat transfer from a rotating disk to ambient air, Carl Wagner—837
Helical antennas, Characteristics of, radiating in the axial mode, John D. Kraus and J. Claude Williamson—87
Hevea, Creep, recovery, and permanent set for GR-S and, S. D. Gehman—456
Homing and navigational courses of automatic target-seeking devices, L. C. Yuan—1122
Homing pigeon in electromagnetic fields, C. L. Clark, R. A. Peck, Jr., and W. F. Hollander—1183 (L)
Hydrocarbons, Infra-red spectra of. II. Analysis of octane mixtures by the use of infra-red spectra obtained at low temperatures, W. H. Avery and J. R. Morrison—472 (errata)

Ice crystals, Production of, by the adiabatic expansion of gas, Bernard Vonnegut—959 (L)
Influence of atmosphere pressure on the phenomena accompanying the entry of spheres into water, David Gilbarg and Robert A. Anderson—127
Infra-red spectra of hydrocarbons. II. Analysis of octane mixtures by the use of infra-red spectra obtained at low temperatures, W. H. Avery and J. R. Morrison—472 (errata)
Interferometric method for the calibration of electron microscope magnification, J. L. Farrant and A. J. Hodge —840
Investigation of specimen contamination in the electron microscope, James Hillier—226
Ion microscope with a transverse magnetic field, Nobuji Sasaki—1050
Ionosphere, Note on the phase difference between two waves reflected from the, J. M. Kelso—590 (L)
Ionosphere reflections record 1 mechanically by means of a repetition frequency converter, W. Stoffregen—487
Ions, Possible fluctuations in electron streams due to, J. R. Pierce—231
Iron, Self-diffusion in, C. Ernest Birchenall and Robert F. Mehl—217 (L)
Irradiation of biological materials by high energy Roentgen rays and cathode rays, J. G. Trump and R. J. Van de Graaff—599
Isotopes, Shipping of radio-isotopes, Karl Z. Morgan—593
Isotopic tracers, Theory of the study of transfers within a multi-compartment system using isotopic tracers, C. W. Sheppard—70

Kerr electro-optical light shutter, Use of a cavity oscillator for, A. C. Lapsley, L. B. Snoddy, and J. W. Beams— 111 (L)

LaGrange's equations, Extension of, to electromagnetic field problems, Prescott D. Crout—1007
Laplace transform, Application of, in the solution of linear integral equations, Lawrence Baylor Robinson—237
Large plastic flow and the collapse of hollow cylinders, P. W. Bridgman—302
Limiting sensitivity of a microwave spectrometer, C. H. Townes and S. Geschwind—795 (L)
Linear integral equations, Application of the Laplace transform in the solution of, Lawrence Baylor Robinson—237
Linear networks, damped, Transient response of, with particular regard to wideband amplifiers, W. C. Elmore—55
Linear resonant systems, Response of, to excitation of a frequency varying linearly with time, Gunnar Hok—242; erratum—623
Linear structures at sonic frequencies, Method for the absolute measurement of dynamic properties of, W. James Lyons and Irven B. Prettyman—473
Liquids, Fracture of, John C. Fisher—1066
Liquids, Measurement by radioactive tracers of diffusion in, Andrew Gemant—1160
Liquids, Universal curves for dielectric-filled wave guides and microwave dielectric measurement methods for, W. H. Surber, Jr.—514
Lubrication, Graphite, Robert H. Savage—1

Magnetic fields, Electron optical observation of, L. Marton —863 (L)
Magnetic properties of ordered nickel-manganese alloys, Robert I. Jaffee—867
Magnetization in perpendicularly superposed direct and alternating fields, F. J. Beck and J. M. Kelly—551
Magnetron anode blocks, Resonant modes of the rising sun and other unstrapped magnetron anode blocks, Norman M. Kroll and Willis E. Lamb, Jr.—166
Magnetron resonator system, E. C. Okress—338 (erratum)
Magnetron, Rising sun, S. Millman and A. T. Nordsieck —156
Magnetrons, Rising sun, with large numbers of cavities, A. V. Hollenberg, N. Kroll, and S. Millman—624
Magnitude and character of errors produced by shape factors in Stokes' law estimates of particle radius, Wulf B. Kunkel—1056
Manganese, Magnetic properties of ordered nickel-manganese alloys, Robert I. Jaffee—867
Manganese, Twinning in tetragonal alloys of copper and manganese, Francis T. Worrell—929; erratum—1154
Mass emissivity of powder gases in solid fuel rockets, S. S. Penner—278
Measured impedances of helical beam antennas, Otto J. Glasser and John D. Kraus—193
Measurement of carbon black particles by the electron microscope and low temperature nitrogen adsorption isotherms, R. B. Anderson and P. H. Emmett—367
Measurement of cavity impedance, W. W. Hansen and R. F. Post—1059
Measurement by radioactive tracers of diffusion in liquids, Andrew Gemant—1160
Measurement of stress by means of x-rays, D. E. Thomas —190
Measurements of dielectric constant and dipole moment of gases by the beat-frequency method, J. G. Jelatis—419
Metal chips, Theory of formation of, Väinö Piispanen—876
Metal powders, Alloying of, by diffusion, Sidney Weinbaum—897
Metallurgy, Contribution of modern physics to, Frederick Seitz—973
Metals, Energy losses of sound waves in metals due to scattering and diffusion, W. P. Mason and H. J. McSkimin—940
Metals, liquid, Bidwell's intercept relation and the thermal conductivity of, R. W. Powell—995
Metals, polycrystalline, Scattering of ultrasonic radiation in, W. Roth—901
Metals, sheet, Technique for quantitative determination of texture of, John T. Norton—1176
Meteorite, Probability that a meteorite will hit or penetrate a body situated in the vicinity of the earth, G. Grimminger—947
Meteors, Theory of the radio detection of, Laurence A. Manning—689
Method for the absolute measurement of dynamic properties of linear structures at sonic frequencies, W. James Lyons and Irven B. Prettyman—473
Method of determining the angle of arrival, A. W. Straiton, W. E. Gordon, and A. H. LaGrone—524
Method for the evaporation of alloys, Louis Harris and Benjamin M. Siegel—739
Method for measuring the complex dielectric constant of gases at microwave frequencies by using a resonant cavity, C. K. Jen—649
Methods for measuring dynamic mechanical properties of rubber-like materials, A. W. Nolle—753
Microflash unit for ballistic photography, W. W. McCormick, L. Madansky, and A. F. Fairbanks—221
Microradiography, Electronic radiography and, Jean-Jacques Trillat—844
Microscope, Ion, with a transverse magnetic field, Nobuji Sasaki—1050
Microwave oscillators, Frequency stabilization of, by spectrum lines. II. Jose L. Garcia de Quevedo and William V. Smith—831
Microwave spectrometer, Limiting sensitivity of a, C. H. Townes and S. Geschwind—795 (L)
Microwave spectroscopy, Minimum detectable absorption in, and an analysis of the Stark modulation method, W. D. Hershberger—411
Microwaves, non-standard propagation of, Effect of ground constants on the characteristic values of the normal modes in, C. L. Pekeris—102
Minimum detectable absorption in microwave spectroscopy and an analysis of the Stark modulation method, W. D. Hershberger—411
Mixing properties of non-linear condensers, A. van der Ziel—999

Networks, Transmission losses in $2n$-terminal networks, Vitold Belevitch—636

Neutrons, Transmission of monoenergetic slow neutrons through solid solutions and mechanical mixtures of TiC and WC, S. S. Sidhu—639
New method of measuring diffusion coefficient in solids with radioactive tracers, G. C. Kuczynski—308 (L)
Nickel-manganese alloys, ordered, Magnetic properties of, Robert I. Jaffee—867
Nitrocellulose, Visco-elastic behavior of a highly plasticized nitrocellulose in compression under constant load, George J. Doyle and Richard M. Badger—373
Nitrogen, processed atmospheric, Anomalous physical properties of, Clarke C. Minter—217 (L)
Note on the phase difference between two waves reflected from the ionosphere, J. M. Kelso—590 (L)
Note on reflection from dielectric structures in wave guide, J. Shmoys—797 (L)
Notes on electron diffraction with the universal electron microscope, R. E. Dunaway and H. M. Barton—799 (L)
Nucleation, J. C. Fisher, J. H. Hollomon, and D. Turnbull —775

Observation of corrosion cracking without stress, W. D. Robertson and H. H. Uhlig—864 (L)
Observation on heat sources placed at random on a surface, Gregory H. Wannier—1020
Observations on arc discharges at low pressures, M. J. Kofoid—399
Observations on the Formvar replica method, with a note on glass surfaces, Beatrice M. Deacon, S. G. Ellis, W. G. Cross, and R. S. Sennett—704
One-dimensional theory of steady compressible fluid flow in ducts with friction and heat addition, Bruce L. Hicks, Donald J. Montgomery, and Robert H. Wasserman—523 (erratum)
Oscillations, Self-excited mechanical, N. Minorsky—332
Oxide replica technique for the electron microscope examination of stainless steel and high nickel alloys, E. M. Mahla and N. A. Nielson—378

Palletron, a new electron resonator and its proposed application to the generation of potentials in the million-volt range, A. M. Skellett—187
Paper capacitors, Theory of extreme values and its implications in the study of the dielectric strength of, Benjamin Epstein and Hamilton Brooks—544
Particle radius, Magnitude and character of errors produced by shape factors in Stokes' law estimates of, Wulf B. Kunkel—1056
Particle size in thin Bi films deposited by evaporation in vacuum, Electron diffraction study of, C. T. Keogh and A. H. Weber—1077
Photography, x-ray, Divergent beam, with standard diffraction equipment, A. H. Geisler, J. K. Hill, and J. B. Newkirk—1041
Physical basis of bird navigation, Joseph Slepian—306 (L)
Physical limitations of omnidirectional antennas—L. J. Chu—1163
Physics, modern, Contribution of, to metallurgy, Frederick Seitz—973
Physics in 1947, Philip Morrison—311
Pigeon, Homing, in electromagnetic fields, C. L. Clark, R. A. Peck, Jr., and W. F. Hollander—1183 (L)
Pigments, organic, Transformations in, F. A. Hamm and Earl Van Norman—1097
Pile bombardment, Effects of, on uncured elastomers, W. L. Davidson and I. G. Geib—427
Plastic deformation, theory of, Theory of plastic flow *versus*, W. Prager—540
Plastic flow, creep, and stress relaxation. Part IV. Anomalous flow as an order-disorder transition, Charles Mack —1082
Plastic flow, Large, and the collapse of hollow cylinders, P. W. Bridgman—302
Plastic flow, Theory of, *versus* theory of plastic deformation, W. Prager—540
Plastic flow of thick-walled tubes with large strains, C. W. MacGregor, L. F. Coffin, Jr. and J. C. Fisher—291
Plate containing an overlapped circular hole, Stresses in a, Chih-Bing Ling—405
Pole figures, Analytical discussion of the construction of, John K. Wood—784
Possibility of Hg type arcs with hot refractory cathodes, Jerome Rothstein—1181 (L)
Possible fluctuations in electron streams due to ions, J. R. Pierce—231
Powder gases, Mass emissivity of, in solid fuel rockets, S. S. Penner—278
Prebunching: a method controlling synchrotron radial oscillation amplitudes, D. C. dePackh and M. Birnbaum —795 (L)
Preferred orientation determination using a Geiger counter x-ray diffraction goniometer, B. F. Decker, E. T. Asp, and D. Harker—388
Probability that a meteorite will hit or penetrate a body situated in the vicinity of the earth, G. Grimminger—947
Proceedings of the Electron Microscope Society of America —118, 1186
Production of ice crystals by the adiabatic expansion of gas, Bernard Vonnegut—959 (L)
Properties of a long antenna, Erik Hallen—1140
Pseudostructures in electron microscope specimens, John H. L. Watson—713

Qualitative experimental verification of the change of burning rate of rocket powders with radiation path length, S. S. Penner—511
Quanta, Absorption of incident quanta by atoms as defined by the mass photoelectric absorption coefficient and the mass scattering coefficient, John A. Victoreen—855
Quantitative determination of texture of sheet metals. A technique for, John T. Norton—1176
Quantitative x-ray investigations on the crystallinity of cellulose fibers. A background analysis, P. H. Hermans and A. Weidinger—491

Radar antennae, Solution of the problem of rapid scanning for, R. F. Rinehart—860
Radiation patterns of dielectric rods, R. B. Watson and C. W. Horton—661, 836

Radiation, ultrasonic, Scattering of, in polycrystalline metals, W. Roth—901
Radio detection of meteors, Theory of, Laurence A. Manning—689
Radioactive tracers, New method of measuring diffusion coefficient in solids with, G. C. Kuczynski—308 (L)
Radiography, Electronic, and microradiography, Jean-Jacques Trillat—844
Range-finder testing laboratory, Irvine C. Gardner—721, 729
Recent developments in analysis of the mechanisms of positive and negative coronas in air, Leonard B. Loeb —882
Relaxation, Creep and, II, B. Gross—257
Remarks on "The efficiency of thermoelectric generators," Robert M. Papet—1180 (L)
Remarks on "The physical basis of bird navigation," Leverett Davis, Jr.—307 (L)
Remarks on "A preliminary study of a physical basis of bird navigation," Russell H. Varian—306 (L)
Remarks concerning a proposed method for testing the brittleness of elastomers, C. H. Klute—1093 (L)
Remarks on some recently developed devices for summing Fourier series for crystal structure analysis, C. L. Christ —225 (erratum)
Resonant cavity linear accelerator, A. B. Cullen, Jr. and J. H. Greig—47
Resonant modes of the rising sun and other unstrapped magnetron anode blocks, Norman M. Kroll and Willis E. Lamb, Jr.—166
Resonator, Palletron, a new electron resonator and its proposed application to the generation of potentials in the million-volt range, A. M. Skellett—187
Response of linear resonant systems to excitation of a frequency varying linearly with time, Gunnar Hok—242; erratum—623
Rising sun magnetron, S. Millman and A. T. Nordsieck— 156
Rising sun magnetrons with large numbers of cavities, A. V. Hollenberg, N. Kroll, and S. Millman—624
Rising sun and other unstrapped magnetron anode blocks, Resonant modes of the, Norman M. Kroll and Willis E. Lamb, Jr.—166
Rocket powders, Qualitative experimental verification of the change of burning rate of rocket powders with radiation path length, S. S. Penner—511
Rocket propellants, solid fuel, Effect of radiation on the rate of burning of, S. S. Penner—392
Rockets, Mass emissivity of powder gases in solid fuel rockets, S. S. Penner—278
Roentgen rays, Biological and photo-chemical effects of high energy, electrostatically produced Roentgen rays and cathode rays, Cecil G. Dunn, William L. Campbell, Harvey Fram, and Ardelia Hutchins—605
Roentgen rays and cathode rays, high energy, Irradiation of biological materials by, J. G. Trump and R. J. Van de Graaff—599
Rubber-like materials, Method for measuring dynamic mechanical properties of, A. W. Nolle—753
Scanning, rapid, for radar antennae, Solution of the problem of, R. F. Rinehart—860
Scattering of electromagnetic radiation by a thin circular ring in a circular wave guide, Paula Feuer and Edward S. Akeley—39
Scattering of ultrasonic radiation in polycrystalline metals, W. Roth—901
"Schlieren" effect, Electron optical, L. Marton—687 (L)
Selenium, crystalline, Temperature coefficient of electrical resistivity for, containing various percentages of bromine, Wayne E. Blackburn—51
Self-diffusion in iron, C. Ernest Birchenall and Robert F. Mehl—217 (L)
Self-excited mechanical oscillations, N. Minorsky—332
Shipping of radio-isotopes, Karl Z. Morgan—593
Shock wave, Head-on collision of a, and a rarefaction wave in one dimension, H. E. Moses—383
Shock waves, Decay of, B. Cassen and J. Stanton—803
Shock waves, spherical, in air, Attenuation of, Richard G. Stoner and Walker Bleakney—670; erratum—1129
Silver chloride, rolled, Tensile properties of, B. M. Axilrod and J. J. Lamb—213
Simple procedure for the making of alignment charts, W. L. Bond—83
Simple relations for calculating certain transient responses, W. J. Cunningham—251
Slots, Theory of, in rectangular wave guides, A. F. Stevenson—24
Slow waves in cylindrical guides, A. A. Oliner—109 (L)
Solution of the problem of rapid scanning for radar antennae, R. F. Rinehart—860
Sound waves in metals, Energy losses of, due to scattering and diffusion, W. P. Mason and H. J. McSkimin—940
Specimen contamination in electron microscopes, John H. L. Watson—110 (L)
Spectral emissivity and electron emission constants of thoria cathodes, T. E. Hanley—583
Spectrum lines, Frequency stabilization of microwave oscillators by. II. Jose L. Garcia de Quevedo and William V. Smith—831
Spheres, Influence of atmosphere pressure on the phenomena accompanying the entry of spheres into water, David Gilbarg and Robert A. Anderson—127
Spheres, steel, entering water vertically, Drag coefficients of, Albert May and Jean C. Woodhull—1109
Spurious signals caused by noise in triggered circuits, David Middleton—817
Stark modulation method, Minimum detectable absorption in microwave spectroscopy and an analysis of the, W. D. Hershberger—411
Statistical aspects of fracture problems, Benjamin Epstein —140; Franklin H. Fowler, Jr.—1092 (L)
Statistical factors affecting the intensity of x-rays diffracted by crystalline powders, Leroy Alexander, Harold P. Klug, and Elizabeth Kummer—742
Stress, Measurement of, by means of x-rays, D. E. Thomas —190
Stress relaxation, Plastic flow, creep, and. Part IV. Anomalous flow as an order-disorder transition, Charles Mack —1082

Stresses in a plate containing an overlapped circular hole, Chih-Bing Ling—405
Stresses in a plate containing two circular holes, Chih-Bing Ling—77
Structure of cellulose acetate molecules in acetone solution, Seymour J. Singer and Herman Mark—97
Study on anaeroid capsules, Eugene W. Pike and Norman E. Gibbs—106
Surface currents on a conducting sphere excited by a dipole, C. H. Papas and Ronold King—808
Surface waves from an underwater explosion, J. G. Kirkwood and R. J. Seeger—346
Synchrotron, Prebunching: a method controlling synchrotron radial oscillation amplitudes, D. C. dePackh and M. Birnbaum—795 (L)

Target-seeking devices, automatic, Homing and navigational courses of, L. C. Yuan—1122
Technique for quantitative determination of texture of sheet metals, John T. Norton—1176
Temperature coefficient of electrical resistivity for crystalline selenium containing various percentages of bromine, Wayne E. Blackburn—51
Temperature-controlled Frevel focusing x-ray powder camera, V. Vand—852
Temperature development, Calculation of the, in a contact heated in the contact surface, and application to the problem of the temperature rise in a sliding contact, Ragnar Holm—361; W. J. Oosterkamp—1180 (L)
Temperature gradients for convection in well models, Mary Jane Auld—218 (L)
Tensile properties of rolled silver chloride, B. M. Axilrod and J. J. Lamb—213
Testing of range finders, Irvine C. Gardner—729
Theoretical criterion for streamer advance in an electrical field, Leonard B. Loeb and Robert A. Wijsman—797 (L)
Theory of biconical antennas, C. T. Tai—1155
Theory of commercial yarn testing, Charles J. Geyer, Jr., C. H. Reichardt, and George Halsey—464
Theory of extreme values and its implications in the study of the dielectric strength of paper capacitors, Benjamin Epstein and Hamilton Brooks—544
Theory of formation of metal chips, Väinö Piispanen—876
Theory of plastic flow *versus* theory of plastic deformation, W. Prager—540
Theory of the positive column in an annular discharge tube, Jaroslav Pachner—1072
Theory of the radio detection of meteors, Laurence A. Manning—689
Theory of slots in rectangular wave guides, A. F. Stevenson—24
Theory of the study of transfers within a multi-compartment system using isotopic tracers, C. W. Sheppard—70
Thermal conductivity of liquid metals, Bidwell's intercept relation and the, R. W. Powell—995
Thermodynamics of a strained elastomer. I. General analysis, M. Mooney—434; II. Compressibility, L. E. Copeland—445; III. The thermal coefficient of modulus and the statistical theory of elasticity, L. E. Copeland and M. Mooney—450
Thoria cathodes, Spectral emissivity and electron emission constants of, T. E. Hanley—583
Transformations in organic pigments, F. A. Hamm and Earl Van Norman—1097
Transient response of damped linear networks with particular regard to wideband amplifiers, W. C. Elmore—55
Transmission losses in 2*n*-terminal networks, Vitold Belevitch—636
Transmission of monoenergetic slow neutrons through solid solutions and mechanical mixtures of TiC and WC, S. S. Sidhu—639
Transmission properties of materials in the millimeter wave region, E. Wantuch, J. H. Rohrbaugh, J. P. Cooley, J. H. Greig, and J. Shmoys—1092 (L)
Tubes, thick-walled, Plastic flow of, with large strains, C. W. MacGregor, L. F. Coffin, Jr., and J. C. Fisher—291
Twinning in tetragonal alloys of copper and manganese, Francis T. Worrell—929; erratum—1154

Ultraoscilloscope, Use of an electron diffraction camera as an ultraoscilloscope and suggested application to contact erosion, J. J Lander—1128
Underwater explosion, Surface waves from an, J. G. Kirkwood and R. J. Seeger—346
Universal curves for dielectric-filled wave guides and microwave dielectric measurement methods for liquids, W. H. Surber, Jr.—514
Use of a cavity oscillator for a Kerr electro-optical light shutter, A. C. Lapsley, L. B. Snoddy, and J. W. Beams—111 (L)
Use of an electron diffraction camera as an ultraoscilloscope and suggested application to contact erosion, J. J. Lander—1128

Vacuum, Apparatus for weighing in, G. W. Monk—485
Velocity of the anode spark in copper sulfate solutions under application of impulsive potential, Hugh F. Henry—988
Visco-elastic behavior of a highly plasticized nitrocellulose in compression under constant load, George J. Doyle and Richard M. Badger—373
Viscous slip along grain boundaries and diffusion of zinc in alpha-brass, T'ing-Sui Kê—285

Wave guide, circular, Scattering of electromagnetic radiation by a thin circular ring in a, Paula Feuer and Edward S. Akeley—39
Wave guide, Note on reflection from dielectric structures in, J. Shmoys—797 (L)
Wave-guide theory, in connection with, Electrostatic field of a point charge inside a cylinder, C. J. Bouwkamp and N. G. de Bruijn—105 (errata)
Wave guides for slow waves, L. Brillouin—1023
Wave guides, Theory of slots in rectangular wave guides, A. F. Stevenson—24
Wave guides, Universal curves for dielectric-filled wave guides and microwave dielectric measurement methods for liquids, W. H. Surber, Jr.—514
Waves, shock, Decay of, B. Cassen and J. Stanton—803

Weissenberg photographic intensities, Alignment chart giving the polarization correction of equi-inclination Weissenberg photographic intensities, W. L. Bond—82

X-ray beam intensities, Application of electron multiplier tubes in the measurement of, and in the determination of crystal structure, G. Papp and K. Sasvári—1182 (L)

X-ray diffraction goniometer, Preferred orientation determination using a Geiger counter x-ray diffraction goniometer, B. F. Decker, E. T. Asp, and D. Harker—388

X-ray diffraction patterns, Convenient methods for obtaining d/n values from, C. B. Stewart and E. S. Lutton—507 (L)

X-ray investigations, Quantitative, on the crystallinity of cellulose fibers. A background analysis, P. H. Hermans and A. Weidinger—491

X-ray photography, Divergent beam, with standard diffraction equipment, A. H. Geisler, J. K. Hill, and J. B. Newkirk—1041

X-ray powder camera, Temperature-controlled Frevel focusing, V. Vand—852

X-ray spectrometer maxima, Geometrical factors affecting the contours of. I. Factors causing asymmetry, Leroy Alexander—1068

X-rays diffracted by crystalline powders, Statistical factors affecting the intensity of, Leroy Alexander, Harold P. Klug, and Elizabeth Kummer—742

X-rays, Measurement of stress by means of, D. E. Thomas —190

Yarn testing, commercial, Theory of, Charles J. Geyer, Jr., C. H. Reichardt, and George Halsey—464

Young's modulus and strain coefficient of resistivity of some bismuth rich alloys, G. C. Kuczynski and J. T. Norton —683

Zinc, Viscous slip along grain boundaries and diffusion of, in alpha-brass, T'ing-Sui Kê—285

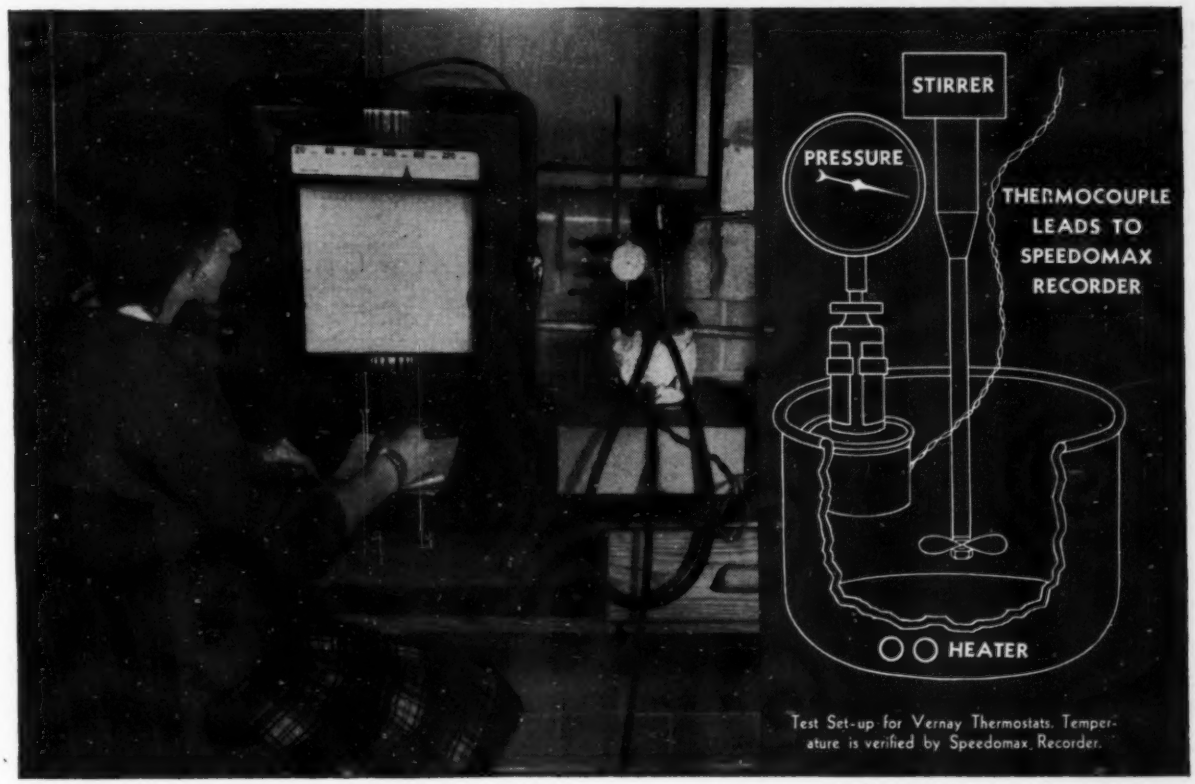

Test Set-up for Vernay Thermostats. Temperature is verified by Speedomax Recorder.

Counting Millivolts To Protect People

This young woman is helping to safeguard the comfort and safety of air travellers. She is testing the thermostats which will operate certain aircraft engine oil temperature control valves which must maintain very close oil temperature control from take-off to landing in tropic or arctic atmospheric conditions.

To check and record the operating temperatures of thermostats in this responsible service, Vernay Laboratories employ the Speedomax Recorder shown above. It comes as near as possible to removing the "human equation," for it never forgets to standardize itself, and it makes no mistakes in writing down what it finds. Furthermore, it is fast—it handles its twin jobs of measuring and recording in less time than the user would need for measuring only, if he were using a manually-operated potentiometer of comparable sensitivity.

If you're recording voltages and want to save time, trouble or money, there's a Speedomax or Micromax Recorder to fit your needs. Write to Leeds & Northrup Co., 4978 Stenton Ave., Philadelphia 44, Pennsylvania.

MEASURING INSTRUMENTS · TELEMETERS · AUTOMATIC CONTROLS · HEAT-TREATING FURNACES

LEEDS & NORTHRUP CO.

Jrl. Ad N-33A-420(1)

Wherever you Employ Magnets, Check with us on the Advantages of using

ARNOLD

PERMANENT MAGNETS

As electrical constituents go, permanent magnets are relatively new. They made tremendous advances within the past decade, especially in the communications and aviation industries, and in the general fields of instruments, controls, meters and mechanical holding devices.

Many of these uses were problems that just couldn't be solved until permanent magnet materials were developed to do the job—a work of pioneering to which Arnold contributed a heavy share. Many other applications were those where permanent magnets supplanted older materials because of their inherent ability to save weight, size and production time, as well as greatly improve the performance of the equipment.

To these advantages, Arnold Permanent Magnets add another very important value—standards of quality and uniformity that are unmatched within the industry. Arnold Products are 100% quality-controlled at every step of manufacture. What's more, they're available in all Alnico grades and other types of magnetic materials, in cast or sintered forms, and in any shape, size or degree of finish you need. ● Let's get our engineers together on *your* magnet applications or problems.

THE ARNOLD ENGINEERING CO.

Subsidiary of

ALLEGHENY LUDLUM STEEL CORPORATION

147 East Ontario Street, Chicago 11, Illinois

Specialists and Leaders in the Design, Engineering and Manufacture of PERMANENT MAGNETS

W&D 1296

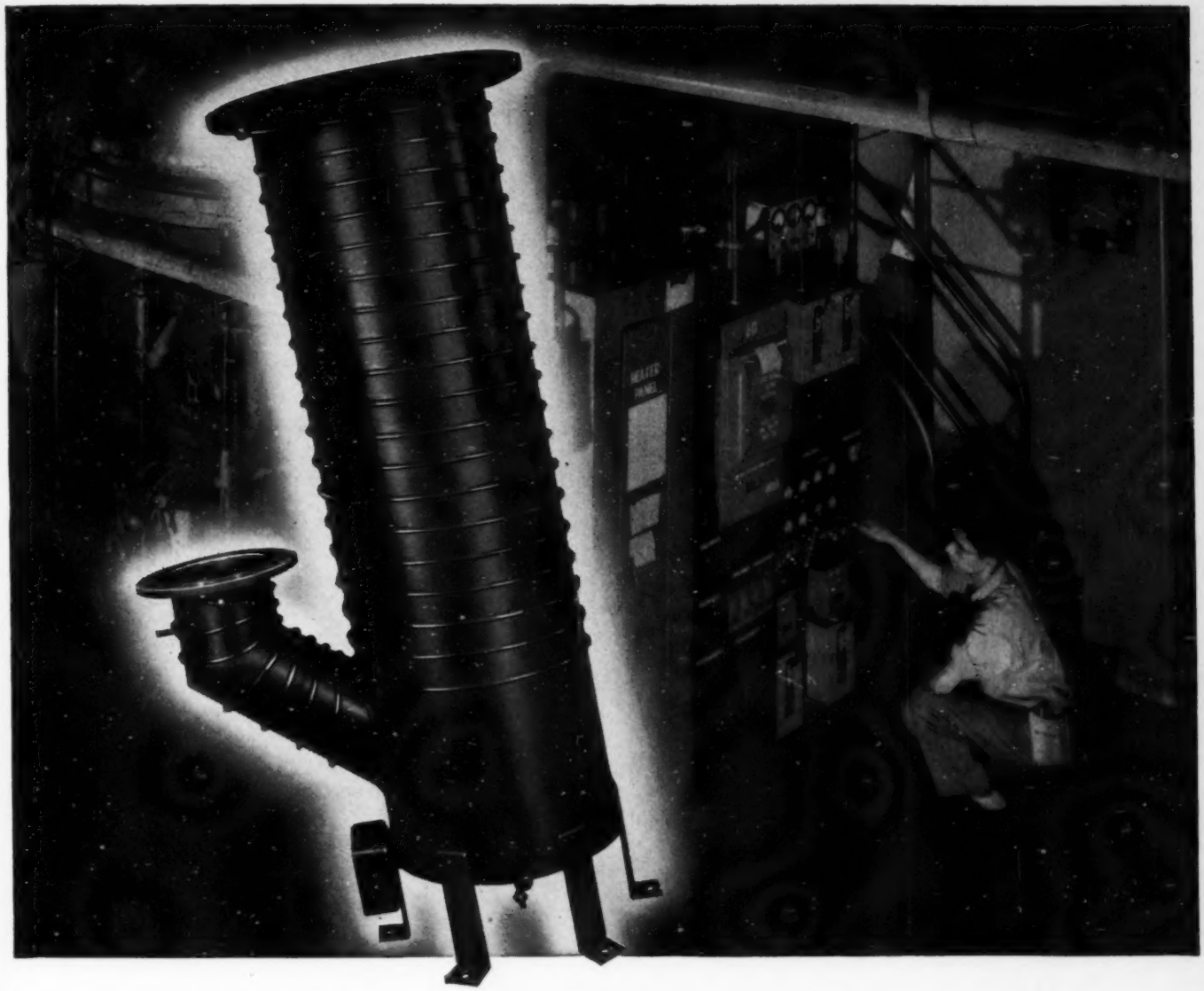

BIG CAPACITY PUMPS **FOR VACUUM**

OF ONE-BILLIONTH OF AN ATMOSPHERE

AMERICAN production is discovering startling ways to use high vacuum. Commercial applications in the broad fields of electronics, metallurgy, physical chemistry and nuclear physics are demanding large capacity pumps and components for fast, large-scale production.

To provide the necessary equipment, DPI's engineering department has developed a wide variety of diffusion pumps of rugged, all-metal construction capable of pumping many thousands of cubic feet per minute without sacrificing low ultimate vacuum achieved by the finest laboratory apparatus. This line of large-capacity, high-vacuum equipment and the technical knowledge acquired by DPI research men and engineers are available to industries interested in the possibilities of high-vacuum processing—or in improving present high-vacuum installations. Write:

DPi
HIGH VACUUM RESEARCH AND ENGINEERING

Vacuum Equipment Division

DISTILLATION PRODUCTS, INC.

769 RIDGE ROAD WEST • ROCHESTER 13, N. Y.

DP I

570 Lexington Ave.
New York 22, N. Y.

135 So. La Salle St.
Chicago 3, Illinois

Manufacturers of Molecular Stills and High-Vacuum Equipment; Distillers of Oil-Soluble Vitamins and other Concentrates for Science and Industry

PRINCIPLES OF MECHANICS. *New second edition*

By JOHN L. SYNGE, Carnegie Institute of Technology and B. A. GRIFFITH, University of Toronto. *In press.*

A revision of a well-known text for intermediate course in mathematics, physics, antl engineering mechanics departments. Changes throughout clarify the material, and a number of sections dealing with units and dimensions have been added. An outstanding feature of the revision is the account of the motion of a charged particle in an electromagnetic field.

RADIO FUNDAMENTALS

By ARTHUR L. ALBERT, Oregon State College. 590 *pages.* $4.50

A simply written, up-to-date text presenting recent developments in radio, including broadcast and point-to-point services. Major topics covered include acoustics, radio circuits, transmission lines and cables, vacuum tubes, rectifiers, amplifiers, oscillators, amplitude and frequency modulation and detection, radio transmitters and receivers and antennas.

VACUUM TUBE AMPLIFIERS

Volume 18 in the Massachusetts Institute of Technology Radiation Laboratory Series. OSRD–NDRC

Edited by GEORGE E. VALLEY, JR. and HENRY WALLMAN, Massachusetts Institute of Technology. 743 *pages.* $10.00

This book seeks to analyze completely, to give design principles of, and to describe the special constructional techniques pertaining to many important types of amplifiers. The amplifiers selected for treatment are, in general, characterized either by very high gain, by large bandwidth, by great dynamic range, or by precise response. Following a theoretical introduction, video amplifiers, wide-band high-frequency bandpass amplifiers, low-frequency bandpass amplifiers, and direct-coupled amplifiers are discussed. Noise in amplifiers is treated rigorously, and the practical design of minimal noise amplifiers described.

WAVEFORMS

Volume 19 in the Massachusetts Institute of Technology Radiation Laboratory Series. OSRD–NDRC

Edited by BRITTON CHANCE, University of Pennsylvania, VERNON HUGHES, Columbia University, EDWARD MACNICHOL, University of Pennsylvania, DAVID SAYRE, Alabama Polytechnic Institute, and FREDERICK C. WILLIAMS, Manchester University. *Approximately* 750 *pages.* $10.00. *In press.*

This volume describes the generation and use of precisely controlled voltages and currents having various time dependence and duration. Introductory chapters present new methods of wave shaping by linear circuit elements and negative feedback amplifiers. The properties of vacuum tubes as non-linear circuit elements and their applications to waveform manipulations are presented in detail.

Send for copies on approval

McGRAW-HILL BOOK COMPANY, INC.

330 WEST 42ND STREET, NEW YORK 18, N. Y.

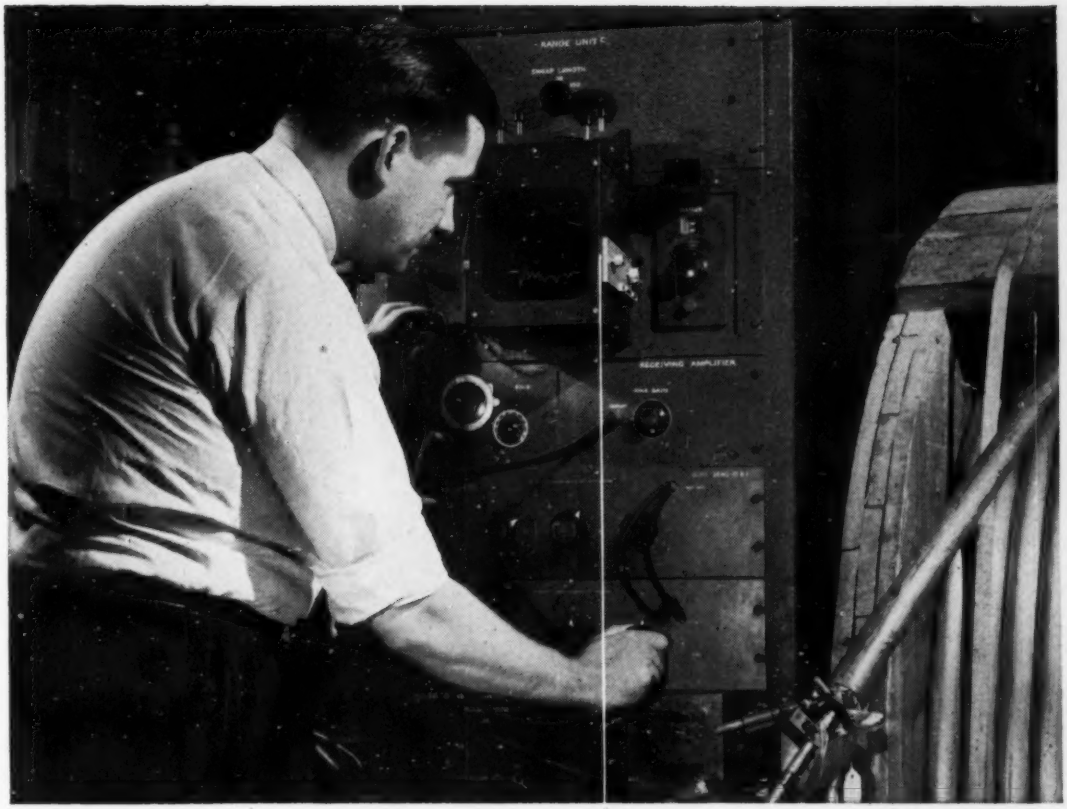

He asks an echo

Radar sends out pulses of electric waves which, reflected from a target, return to reveal the target's location.

Likewise, the apparatus pictured above sends electric waves over a coaxial telephone cable. Minute irregularities reflect the waves back to their origin; the echo makes a trace on an oscilloscope screen and so tells where to look for the trouble.

Telephone messages need smooth "highways" over which to travel across country: circuits able to transmit every talking frequency, without distortion. Television needs even smoother highways and at many more frequencies. So Bell Laboratories devised this method of spot-testing the cable over the entire frequency band needed for telephone or television. It is so delicate that any possible interference with transmission is detected at once. Its use makes sure that every inch of highway is clear.

This is another important example of how Bell Telephone Laboratories constantly develop finer communications for the nation.

BELL TELEPHONE LABORATORIES

Exploring and inventing, devising and perfecting for continued improvements and economies in telephone service

An Unusual Line of

IMPULSE REGISTERS

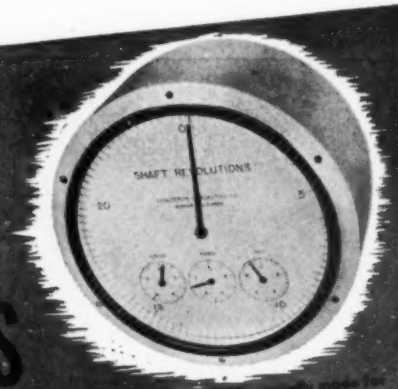

PRECISION Standard, specially made for the United States Navy [illegible] used for precision propulsion measurements. Has 6-inch dial, and indicates up to 100 impulses per second.

FLUSH MOUNTED Type with single hole mounting and plastic case. Widely used for panel mounting.

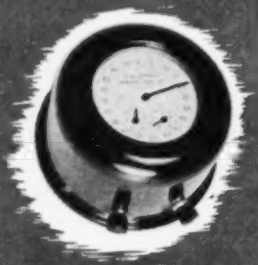

TYPE 401-A with fully enclosed plastic desk case and non-removable-top binding posts. See the complete specifications opposite. →

FLUSH MOUNTED Type with four auxiliary dials making possible direct readings to 999,999 impulses. Similar in construction to regular Flush Mounting.

In addition to the Cyclotron Specialties Registers illustrated, other types include higher speeds, electrical reset, add and subtract type and higher totalization. Inquiries for these special types will receive prompt attention.

Cyclotron Specialties Impulse Registers were originally designed to meet the exacting requirements of radio-activity research workers. Their outstanding performance has attained for them acceptance in nearly every scientific field and today, many special types are in use by scientific workers throughout the world.

Cyclotron Specialties Registers are unique in their ability to operate at exceptionally high speeds with complete accuracy and without adjustment or maintenance. They are unexcelled for high speed impulse recording and mechanical operations requiring counting in precise quantities.

SPECIFICATIONS of Cyclotron Specialties Impulse Register No. 401-A

Accurately Registers Up to 60 *Impulses Per Second*

Main, easily-read sweep dial reads 0 to 100 directly

Sweep dial plus auxiliaries read 0 to 9,999 impulses without extra equipment

4000 ohm D. C. resistance

Operates on as low as 100 milliwatt

Small, compact, light weight

Durable, rugged construction to withstand unavoidable accidents

Dimensions: 3" x 4" Weight: 2 lbs.

Immediate Delivery of all Types in Reasonable Quantities

Cyclotron Specialties Company

MORAGA 3, CALIFORNIA

STATHAM

ACCELEROMETERS

MODEL C

Illustration Actual Size

Increased production to meet the popular demand for Statham Model C accelerometers has resulted in a substantial price reduction. Unchanged is the craftsmanship which is the identifying mark of Statham instruments.

Combining excellent frequency response with small size, ruggedness, and simplicity of operation, the Model C type is extremely versatile, both in its application (which carries no license limitation) and in the auxiliary equipment which may be used with it.

This precision instrument is but 3/4 in. high, 1 13/16 in. long, and 1 1/2 in. wide. It weighs approximately 2 oz. The Model C type is supplied either with solder terminals as illustrated, or with a 2 foot length of 4-conductor cable and connector.

A new catalog sheet, Bulletin No. 401A, listing ranges, resistances, natural frequencies, and outputs for Model C accelerometers is available upon request.

Statham Laboratories manufactures a variety of Accelerometers, Dynamometers, Load Cells, and Pressure Transmitters. Request our catalog together with Instrument Notes, our house organ.

STATHAM LABORATORIES SCIENTIFIC INSTRUMENTS

9328 SANTA MONICA BOULEVARD • BEVERLY HILLS, CALIFORNIA

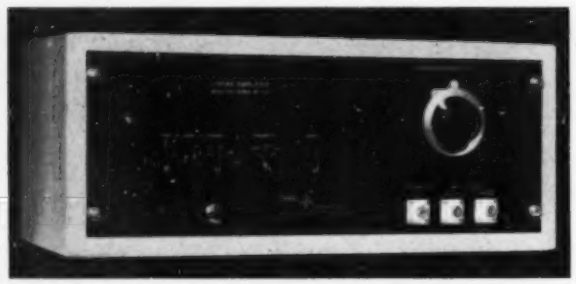

MODEL 204-C

featuring independent selection of input time constants and rise times.

SPECIFICATIONS:

PULSE RESPONSE: By means of selector switches on the front panel the input time constant can be varied from 0.16 μs to 16 μs in seven steps, and the rise time can be varied from 0.2 μs to 2 μs in five steps.

AMPLIFICATION: The voltage amplification varies between 1600 X and 9000 X depending upon the choice of input time constant and rise time. Control of gain is effected by an attenuator having 6 db steps in the range from 0 to 30 db.

GAIN STABILITY: By virtue of the inverse feedback employed, a high order of gain stability is achieved. Variations in line voltage between 105 and 125 volts cause negligible gain change.

INPUT VOLTAGE: Model 204 operates on pulses of either positive or negative polarity . . . minimum usable input signal varies from about 200 microvolts to 1 millivolt depending on bandwidth.

AMPLIFIER OUTPUTS: Two provided: Low level output gives a maximum signal of about 5 volts, high level output maximum signal of about 100 volts.

NOISE: Maximum noise output, including A-C hum, less than 1 volt at maximum gain for all rise times.

DISCRIMINATOR: A pulse amplitude discriminator operates from the high level output of the amplifier . . . pulses above predetermined level cause the discriminator to give out a 10 volt pulse of 0.4 microsecond duration . . . discrimination level is determined by a dial calibrated for output pulses from 0 to 100 volts.

ACCESSORIES AVAILABLE

The Model 205 Linear Pre-amplifier is used with the Model 204 for nuclear measurements where an ionization chamber is employed. This compact unit, connected to main amplifier by 8 foot flexible cable, enables experimenter to eliminate excessive input capacitance by placing first few stages of amplfier close to counting tube or ionization chamber. The Model 205 is exceptionally compact and features a gain of about 20 and a 0.2 microsecond rise time. In other applications where added gain is not required, use of the Model 206 pre-amplifier is recommended. The Model 206 acts as an impedance transformer having a gain of slightly less than unity.

Plate and heater voltages for either model pre-amplifier are available from a power connector at the rear of the Model 204.

Linear Amplifiers

Available now in two versatile models

MODEL 204-B

The characteristics of this model are similar to those of the 204-C with the following exceptions.

PULSE RESPONSE: By means of a selector switch on the front panel any one of three bandwidths may be selected, providing rise and decay times as follows:

Rise Time	*Decay Time*
5.0μs.	25
0.8μs.	4.0
0.2μs.	0.4

In case a longer decay time is required an additional capacitor may be easily switched into the input coupling circuit, as may be required in certain experiments employing ionization chambers.

AMPLIFICATION: The maximum voltage amplification for each rise time is approximately:

Rise Time	*Amplification*
5.0 μs.	15,000
0.8 μs.	10,000
0.2 μs.	3,500

Gain control is effected by two attenuators. The coarse gain control permits attentuation in 6 db steps from 0 to 30 db. Between these positions the fine gain control provides continuously variable attenuation between 0 and 6 db.

IMPORTANT USES IN NUCLEAR RESEARCH

These Linear Amplifiers have been designed specifically for use in nuclear research where the small pulses from an ionization chamber, proportional counter, electron multiplier or other such transducer must be amplified to a level sufficient for observation on an oscilloscope or for counting with a scaler.

The amplifier consists of two sections of three tubes each. Within each section degenerative feedback is employed to effect gain stabilization and to improve the linearity of pulse response.

PRICES

Model 204-B Linear Amplifier	**$395.00**
Model 204-C Linear Amplifier	**395.00**
Model 205 Linear Pre-amplifier including 8 foot power and signal cables	**100.00**
Model 206 Pre-amplifier including 8 foot power and signal cables	**50.00**

ATOMIC *Instrument Company*

158 CHARLES STREET, BOSTON 14, MASSACHUSETTS

ACCURACY • RELIABILITY • CONVENIENCE • EASY SERVICING

The New
FULLY AUTOMATIC
Berkeley **DECIMAL SCALER**

MODEL 2000

Now in Production

The new fully automatic Berkeley Decimal Scaler, Model 2000, is a development based on extensive field research by the Berkeley staff in cooperation with nuclear scientists and laboratory technicians. The Model 2000 is the result of our effort to design and produce an outstanding instrument meeting the exacting requirements of the modern laboratory.

Fully automatic. The operator sets the scaler for a predetermined number of counts. The instrument stops automatically when this number is reached, registering the total count directly in numerical form (decimal presentation—no interpolation required). Elapsed time is recorded by the built-in time clock. (Optional accessory available for counting over pre-determined time intervals.)

Designed for continuous, accurate operation. Uses components of highest quality; conservative rating of all parts. Scale of 1000 to improve statistical accuracy at high counting rates. High voltage supply exceptionally well regulated over wide input range.

Convenient and flexible in use. All controls and connectors on front panel. Light and compact, easy to handle. Built-in pre-amplifier for Geiger Muller work. Pre-amplifier accessory available for proportional counting.

Easy servicing. New plug-in unit construction permits rapid testing and servicing. Three interchangeable decimal counting units make up the scale of 1000. Input and output amplifiers, high voltage power supply and voltage regulator also housed in conveniently removable plug-in units.

The new Model 2000 assures more productive work in your laboratory. For complete specifications and details, let us send you Bulletin No. BDS-203.

Berkeley Scientific Company

SIXTH AND NEVIN AVENUE • RICHMOND, CALIF.

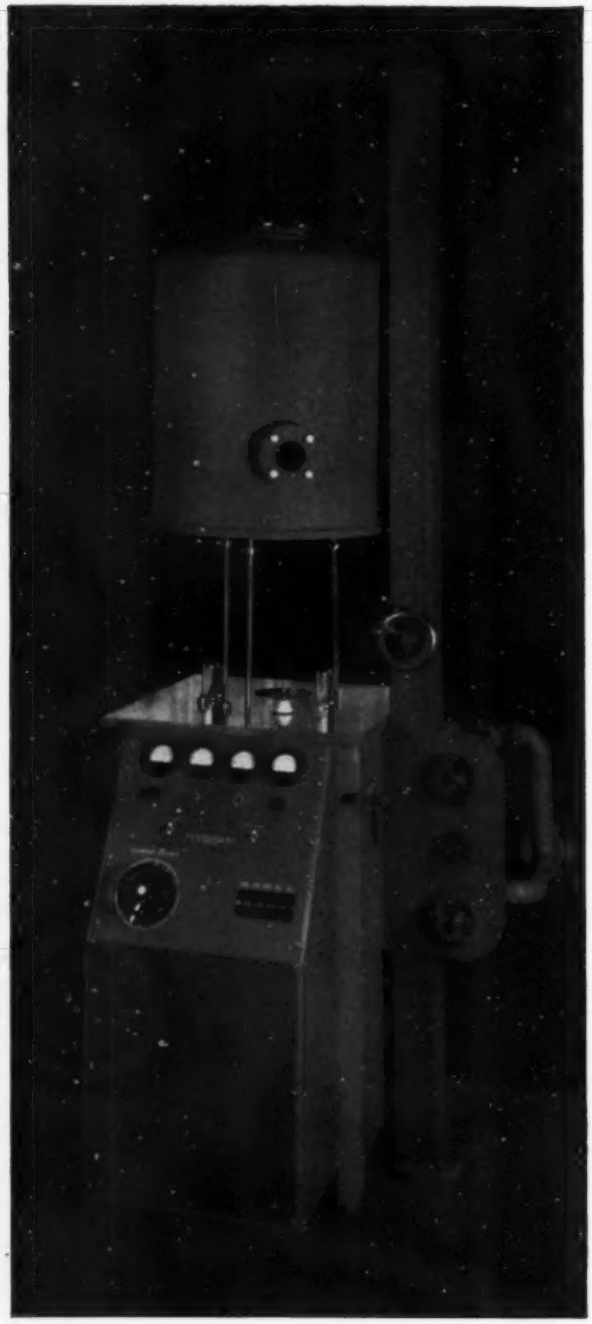

Type 3102

EVAPORATOR

A new high vacuum coating unit for optical work or other applications requiring low-pressure bell jar equipment.

This unit has high pumping capacity and a quick-acting high vacuum valve for rapid cycles. It is designed for use with bell jars up to 24" inside diameter. Complete facilities for coating, including filament power and high voltage clean-up, are provided.

The design of the Type 3102 Evaporator is the result of our experience in building coating equipment and in operating in the coating field since 1940. For full particulars, write VACUUM ENGINEERING DIVISION, National Research Corporation, Cambridge 42, Massachusetts.

We supply a complete line of diffusion pumps, vacuum gauges, valves, seals, coating equipment, dehydration equipment and special high vacuum apparatus.

HIGH VACUUM FOR INDUSTRY

NATIONAL RESEARCH CORPORATION

Vacuum ENGINEERING DIVISION

The NEW *and* IMPROVED

RADIATION SURVEY METER

This newest version of the "Cutie Pie" ionization chamber SU-1A Portable Radiation Survey Meter possesses many improved features. For example, its large three inch meter, calibrated directly in milliroentgens per hour, permits faster more accurate readings to be made. Three scale ranges of 25, 250 and 2500 milliroentgens per hour permit precise readings to be made from well below tolerance dosage rate to values far above those normally encountered in most radioactivity laboratories. Batteries need be renewed only after 800 hours of operation. A moveable circular shield permits differentiation between beta and gamma radiation. The convenient pistol grip handle and light weight of only five pounds permit a high degree of portability and ease of carrying. The SU-1A Radiation Survey Meter is suitable for monitoring not only radioisotopes but also for X-rays of energies as low as 50 kilovolts. Write for complete specifications.
PRICE ..... $275.00 F.O.B. Boston

Tracerlab

Commercial Radioactivity Center

instruments • radiochemicals • isotope processing • geiger tubes • industrial applications • health physics • research

TRACERLAB INC., 55 OLIVER STREET, BOSTON 10, MASS.

PROUDLY PRESENTS

MODEL 616A UHF SIGNAL GENERATOR

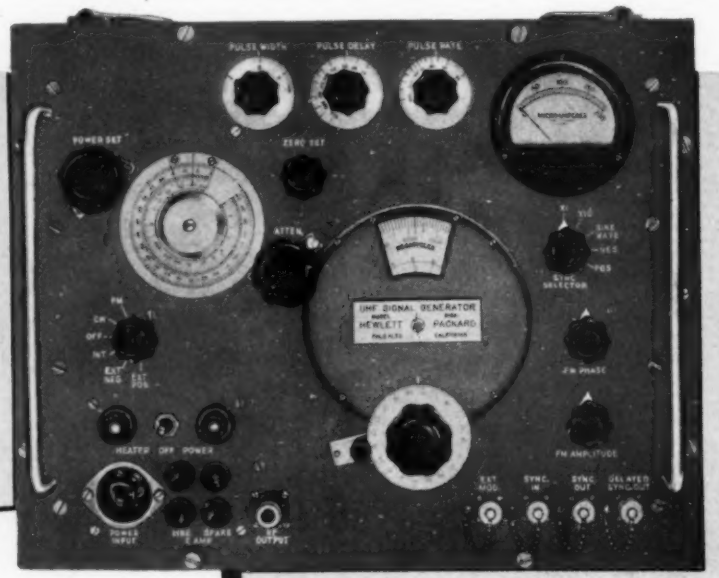

NOW! for the first time

Fast, direct readings 1800 to 4000 mc

Here for the first time is an uhf signal generator that combines direct reading scales, simplified controls, and c-w, pulsed, or a limited f-m output with a wide frequency range and a rugged, compact design.

Direct Reading, Direct Control

Carrier frequency in mc may be directly *set* and *read* on the large central frequency dial. R-f output from the reflex klystron oscillator is also *directly set* and *directly read*, in microvolts or db, on the simplified output dial. No calibration charts or interpolations are necessary. And because the unique coupling device causes oscillator repeller voltage to automatically track frequency changes, no voltage adjustments are necessary during operation. Even the bolometer circuit is automatically compensated for temperature changes.

C-W, F-M, or Pulsed Output

R-f output ranging from 0.1 volt to 0.1 microvolt is available. Output may be continuous or pulsed, or frequency modulated at power supply frequency. Maximum deviation is approximately ±5 megacycles. Pulse modulation may be supplied from an external source or provided internally. Pulse rate is variable between 40 and 4000 cps, and pulse width ranges from 1 to 10 microseconds. Internal pulsing may be accurately synchronized with either positive or negative external pulses, or external sine waves. R-f pulse may be delayed 3 to 300 microseconds with respect to the external synchronizing pulse. Output trigger pulses are also available. They may be simultaneous with the r-f pulse or in advance of the r-f pulse from 3 to 300 microseconds.

Wide Range, Great Stability

A twist-of-the-wrist precision tunes the *-hp-* Model 616A to any frequency between 1800 and 4000 mc. Accuracy of calibration is within ±1% and stability is of the order of 0.005% per degree centigrade in ambient temperature. Line voltage changes of ±10% cause frequency changes of less than 0.02%.

Wide Applicability

The *-hp-* Model 616A UHF Generator is ideal wherever precision ultra-high frequencies are needed for measuring purposes. Some of its many uses include determining of receiver sensitivity, signal-noise or standing-wave ratios, conversion gain, alignment, antenna or transmission line characteristics.

HEWLETT-PACKARD CO.
1380J Page Mill Road, Palo Alto, Calif.
Export Agents: FRAZAR AND HANSEN
301 Clay St., San Francisco 11, Calif., U. S. A.

hp laboratory instruments
FOR SPEED AND ACCURACY

L A N E - W E L L S P R E S E N T S

PEN-RECORDING RAMAN EQUIPMENT

with Photographic Features

Pen-Recording Intensity vs. Raman frequency photo-electrically.

Photographic Spectra immediately available, short exposures.

Write for bulletin on Industrial Raman Spectroscopy and this new equipment

LANE-WELLS COMPANY

INSTRUMENT DIVISION

717 NORTH LAKE AVENUE

PASADENA 6, CALIFORNIA

An

X-ray Diffraction Development

..... as IMPORTANT as it is NEW!

To meet the increasingly varied demands imposed upon present-day diffraction equipment, Philips has introduced at the Philadelphia National Metals Congress a new X-ray Diffraction instrument. This new apparatus will not only enlarge the sphere of applications but also the speed of analysis. It will fulfill many industrial needs for research and control techniques not possible with standard diffraction equipment—and further, it will simplify operation.

Outstanding in design and performance, this new Philips achievement represents a major advance, with exclusive features unique in the field of X-ray Diffraction. It will be applicable to both old and new apparatus.

The applications of this new instrument embrace the fields of Metallurgy, Petroleum Refining, Corrosion Study, Paint, Varnish and Protective Coating Manufacture, Organic Chemicals, Minerals and Geologicals, Inorganic Chemicals, Refractories and Ceramics, Food Processing, Biologicals and Pharmaceutical Synthesis.

Write for the new 24-page illustrated booklet describing Philips Diffraction equipment and related products. See them in operation at the National Metals Congress.

• Inquiries are invited regarding the fall and spring sessions of the Philips Diffraction School to be held in New York City. The school offers an opportunity for becoming conversant with the principles and modern techniques of operating spectrometric and diffraction and fluorescence analysis apparatus.

NORTH AMERICAN PHILIPS COMPANY, INC. Norelco

ELECTRONIC PRODUCTS

NORTH AMERICAN PHILIPS COMPANY, INC.

RESEARCH and CONTROL INSTRUMENTS DIVISION ★ DEPT. XI-12, 750 S. FULTON AVENUE, MT. VERNON, N. Y.

IN CANADA: Philips Industries Ltd., 1203 Philips Square, Montreal ★ EXPORT REPRESENTATIVE: Philips Export Corporation, 750 South Fulton Avenue, Mt. Vernon, N. Y.

*Van de Graaff** TWO-MILLION-VOLT
POSITIVE ION ACCELERATOR
TYPE A—MODEL H

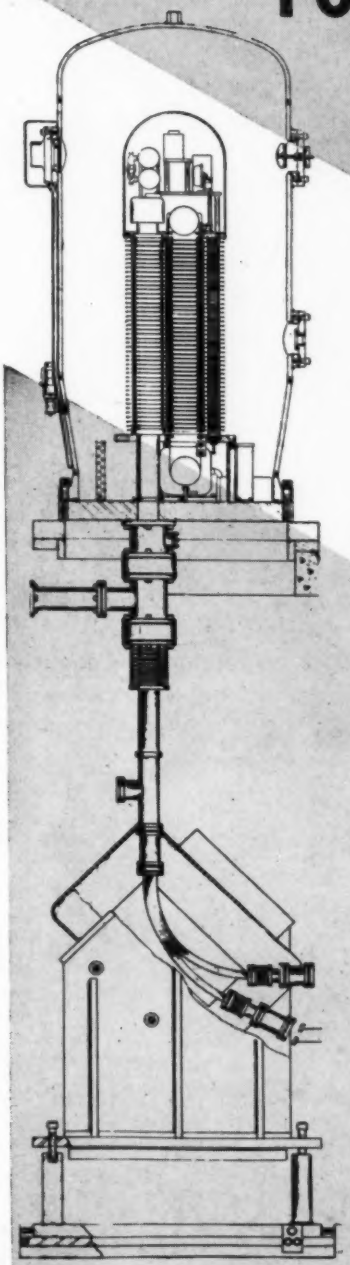

- Sharpness of the ion beam, with low radiation background, characterizes the output of this apparatus.
- Desirable flexibility of operation is provided by external adjustments of the ion source and generator controls.
- Beam analysis to separate Mass-1 and Mass-2 particles is accomplished with a highly stable magnet.
- Voltage stabilization is obtained by the feed-back of data from the Mass-2 portal to corona electrodes discharging to the generator terminal.

*Trade mark

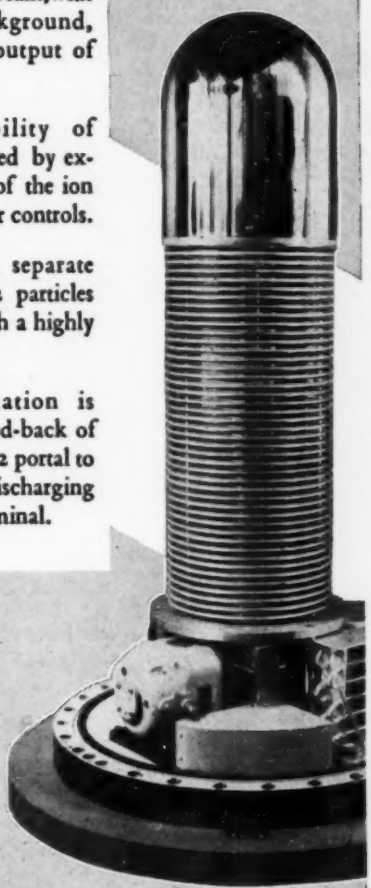

Your inquiries will receive prompt attention. Other electrostatic accelerators can be quoted to meet special requirements of voltage range and beam intensity.

The complete unit weighing approximately 5 tons is shown for a typical installation. The positive ion source is inside the generator terminal. The accelerator tube extends through the base flange to the high-speed pumping system and analyzing magnet which is complete with battery supply and charger. The voltage stabilizer also operates from the remote-control panel.

HIGH VOLTAGE ENGINEERING CORPORATION

7 UNIVERSITY ROAD CAMBRIDGE 38, MASSACHUSETTS

CONTINUOUS STRIP GAUGING AT MILE-A-MINUTE SPEEDS

The heart of this continuous strip gauge is the Machlett AEG-50 X-ray tube.

● In growing use by some of the leading rolling mills, this accurate, dependable, non-contact, time saving gauge is made possible by an X-ray tube of special design.

This tube, developed by Machlett Laboratories, employs a beryllium window in place of the conventional X-ray port and provides a new source of high intensity soft X-radiation which is readily absorbed by thin sheet. The degree of absorption varies with the thickness of the sheet. Through the use of a fluorescent screen and photocell combination and suitable dial calibration, the degree of absorption, i.e., thickness, can be accurately indicated and checked against predetermined tolerances. Continuous and uninterrupted gauging is possible. The necessity for stopping the mill for spot checking is eliminated. Uniformity through the entire strip can be maintained by use of roll compensating devices to provide for fully-automatic control of strip thickness.

The gauge may be embodied in new equipment or installed on existing equipment. The tube is shockproof and rayproof and may be positioned at the most convenient gauging location.

Write us for further information on how this new tube can save you time and money in your application.

MACHLETT

XRAY TUBES SINCE 1897

TODAY THEIR LARGEST MAKER

MACHLETT LABORATORIES, INC.

Springdale, Connecticut

S·S·White MOLDED RESISTORS

INSURE ACCURACY AND RELIABILITY IN *Hipot* INSULATION TESTERS

The "All-Weather" Resistors

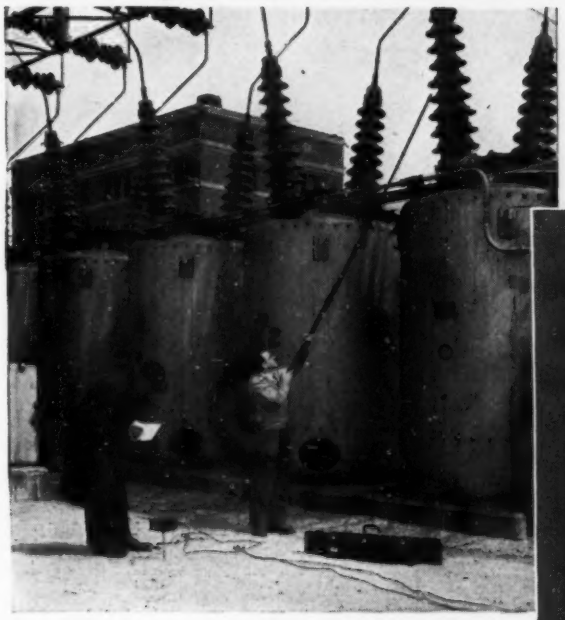

Illustration, courtesy of Canadian Line Materials, Ltd. Toronto, Canada

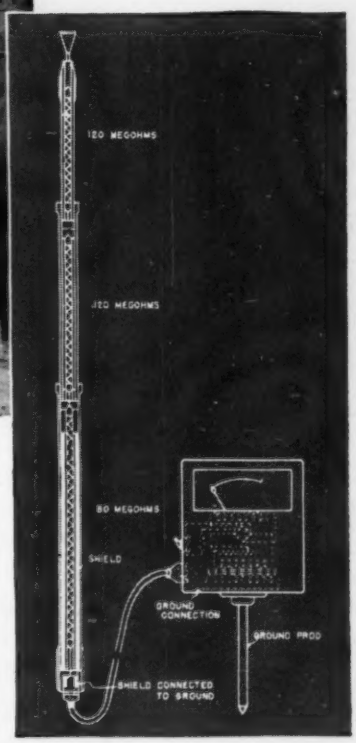

(Above) Schematic wiring diagram of the "Hipot" test stick. Each telescoping stick section contains a number of S.S.White Resistors hooked up in series. This permits the resistances to be varied from 72 to 372 megohms.

THE "Hipot" Test Stick is used to test Bushings and Insulators on high voltage transmission lines from 11 to 230 KV. It consists of telescoping bakelite stick sections each containing a series of S.S.White Resistors to step the voltages down to minute values for measurement.

The manufacturer, Canadian Line Materials, Ltd., Toronto, Canada says—"We have always found S.S.White Resistors of highest quality. They have characteristics which insure consistently accurate and dependable readings on the indicating instruments."

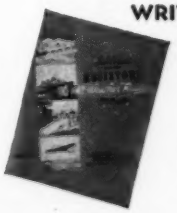

WRITE FOR BULLETIN 4505

It gives essential data about S.S.White Resistors, including construction, characteristics, dimensions, etc. Copy on request.

S.S.WHITE INDUSTRIAL DIVISION

THE S. S. WHITE DENTAL MFG. CO. DEPT. F, 10 EAST 40th ST., NEW YORK 16, N. Y.

FLEXIBLE SHAFTS • FLEXIBLE SHAFT TOOLS • AIRCRAFT ACCESSORIES
SMALL CUTTING AND GRINDING TOOLS • SPECIAL FORMULA RUBBERS
MOLDED RESISTORS • PLASTIC SPECIALTIES • CONTRACT PLASTICS MOLDING

One of America's AAAA Industrial Enterprises

SUPER SLEUTH

THE CONSOLIDATED LEAK DETECTOR MODEL 24-101A

TRACKING DOWN minute leaks, rapidly and accurately, is the everyday function of a Consolidated Leak Detector. With this sensitive detection instrument, leaks as small as 10^{-9} cc per second can be accurately located in a matter of seconds.

Helium gas, used as the testing agent, is both nondestructive and noncontaminating, easily obtainable, and inexpensive to use. Through the DIATRON,* a miniature version of the analyzer tube found in the world-famous Consolidated Mass Spectrometers, minute quantities of helium molecules are quickly separated from the atmosphere, giving instantaneous response both on a visual meter and an audio alarm.

Whether your leak problem is in checking vacuum or pressure laboratory equipment, in maintaining pressure-tight systems in petroleum and chemical processing, in assembly-line inspection of refrigeration units, in checking vacuum tubes, in testing high-vacuum equipment in large-scale plant operations, or in the location of leaks in municipal gas-filled cables and pipe lines buried underground, the Consolidated Leak Detector may well be the ideal solution.

For further information write for Bulletin CEC-1801-X3.

*Trademark

CONSOLIDATED ENGINEERING CORPORATION
Analytical Instruments for Science & Industry
620 N. LAKE AVE., PASADENA 4, CALIFORNIA

MIRACLES DO HAPPEN!

WITH

KINNEY

HIGH VACUUM PUMPS

Kinney High Vacuum Pumps are performing modern-day miracles in industrial production. Already they have greatly improved countless products and have made possible many spectacular new developments. Further miracles continue to unfold almost daily. Kinney Pumps are playing a vital part in producing pharmaceuticals, dehydrating foods, coating lenses, sintering metals, exhausting lamps and tubes, and performing many other low pressure operations. The high pumping speed, long life, and dependability of Kinney High Vacuum Pumps have indeed put vacuum processing on a full production basis. Investigate the new possibilities—and increased profits, too—in low pressure processing with Kinney High Vacuum Pumps.

Write for Bulletin V-45

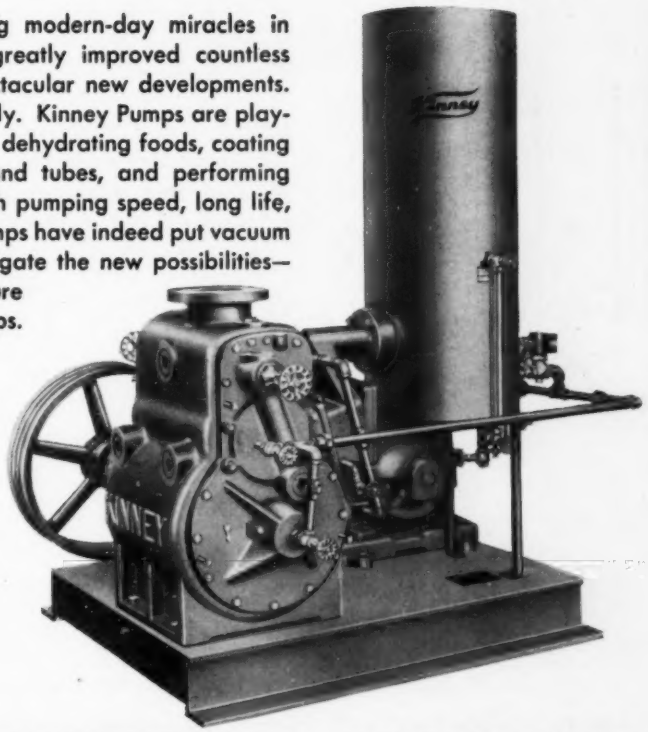

KINNEY SINGLE STAGE PUMP. 8 sizes with displacements from 13 to 702 cu.ft. per min. for low absolute pressures to 10 microns or better. Also Compound Pumps in 2 sizes (15 and 46 cu.ft. per min. displacements) for low absolute pressures to and below 0.5 micron.

KINNEY MANUFACTURING COMPANY

3556 WASHINGTON ST., BOSTON 30, MASS.

NEW YORK • CHICAGO • PHILADELPHIA • LOS ANGELES • SAN FRANCISCO

Foreign Representatives

GENERAL ENGINEERING CO. (RADCLIFFE), LTD., Station Works, Bury Road, Radcliffe, Lancashire, England
HORROCKS, ROXBURGH PTY., LTD., Melbourne, C.I. Australia
W. S. THOMAS & TAYLOR PTY., LTD., Johannesburg, Union of South Africa
NOVELECTRIC, LTD., Zurich, Switzerland

WE ALSO MANUFACTURE LIQUID PUMPS, EJECTORS AND BITUMINOUS DISTRIBUTORS

DUBROVIN VACUUM GAUGE

• UNIQUE MAGNIFIED SCALE • SIMPLE TO USE • DIRECT READING • ECONOMICAL

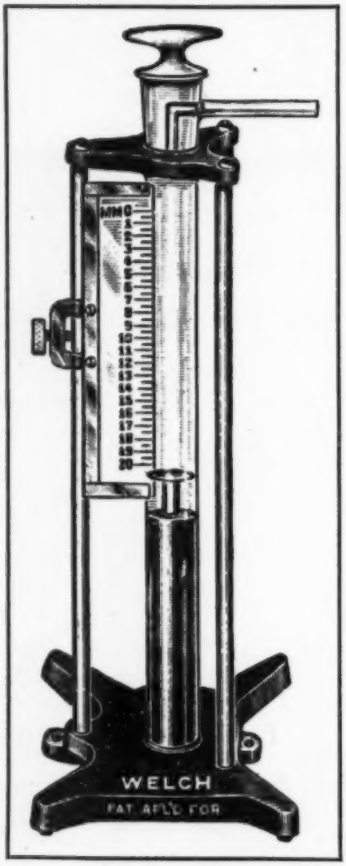

No. 1451C

Instantly responsive to pressure variations

This Gauge is principally a straight glass tube mounted on a metal base. The lower half of the tube is filled with mercury, in which is immersed an indicating float. As the air is evacuated through the outlet provided in the upper part of the glass tube, the indicator shows pressure variations directly on the scale.

Absolute direct reading and instantly responsive to pressure variations. This gauge is superior to the U type manometer because of the magnification of the scale. One type is offered with a 6 to 1 magnification and another with a 9 to 1 magnification. This means that if you are attempting to measure the vacuum indicated by 1 mm. of difference in level on the ordinary closed U type manometer, this new gauge will point out a difference 6 mm. long (or 9 mm. long). Type A is 40 cm. high and Type B is 57 cm. high.

1451C. DUBROVIN GAUGE TYPE A
table model, 20 mm. range, 6 to 1 scale, without mercury. **Each, $40.00**

1451G. DUBROVIN GAUGE TYPE A
wall model, 20 mm. range, 6 to 1 scale, without mercury. **Each, $40.00**

1451E. DUBROVIN GAUGE TYPE B
table model, 20 mm. range, 9 to 1 scale, without mercury. **Each, $48.00**

1451J. DUBROVIN GAUGE TYPE B
wall model, 20 mm. range, 9 to 1 scale, without mercury. **Each, $48.00**

Available in PYREX glass at the same prices.

W. M. WELCH SCIENTIFIC COMPANY

Established 1880

1515 SEDGWICK STREET, DEPT. C-I CHICAGO 10, ILLINOIS, U.S.A.

Manufacturers of Scientific Instruments and Laboratory Apparatus

3 ways photography shows composition of materials

1 Spectrography . . . To record composition quantitatively and qualitatively, Kodak offers 108 specialized materials. For general spectrographic use, however, Kodak recommends two emulsions: *Kodak Spectrum Analysis No. 1 Plates and Films* for high contrast, low background density, and low granularity; and for a more uniform contrast-wavelength relation, *Kodak Spectrum Analysis No. 2 Plates and Films.*

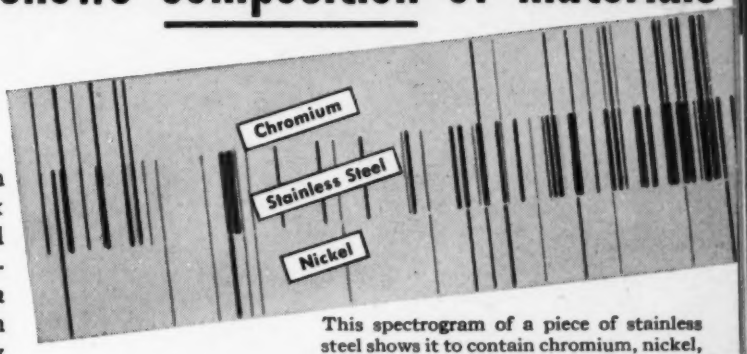

This spectrogram of a piece of stainless steel shows it to contain chromium, nickel, and iron, but none of the other alloying elements commonly found in commercial stainless steel.

2 X-ray diffraction . . . To record crystalline composition, stresses, and thermal history by x-ray diffraction, the fastest film to use is *Kodak Industrial X-ray Film, Type K.* When smooth microdensitometer traces rather than highest film speed are required, use fine-grain *Kodak Industrial X-ray Film, Type A.*

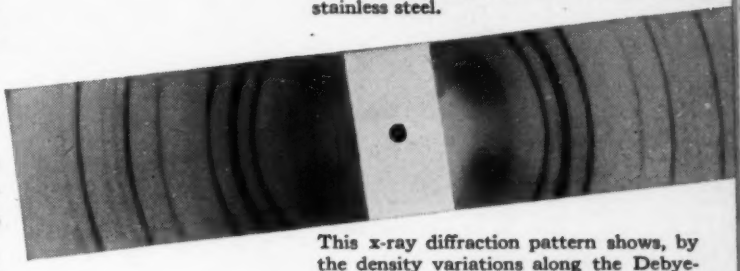

This x-ray diffraction pattern shows, by the density variations along the Debye-Scherrer rings, notably by the patchy center, that the stainless steel used above is not isotropic in its properties.

3 Electron diffraction . . . To record the nature and composition of thin films, layers, surface reaction products of materials by electron diffraction, Kodak offers the following products: *Kodak Medium Lantern Slide Plates,* and *Kodak Contrast Lantern Slide Plates,* and for the most critical work, *Kodak Spectroscopic Plates, Type 548-0.* Users also report that many highly informative electron diffraction patterns have been recorded on *Kodak Verichrome Film.*

This electron diffraction study (below) of the surface of the same stainless steel shows the presence of a thin layer, formed when the steel was treated with concentrated nitric acid for greater resistance to corrosion.

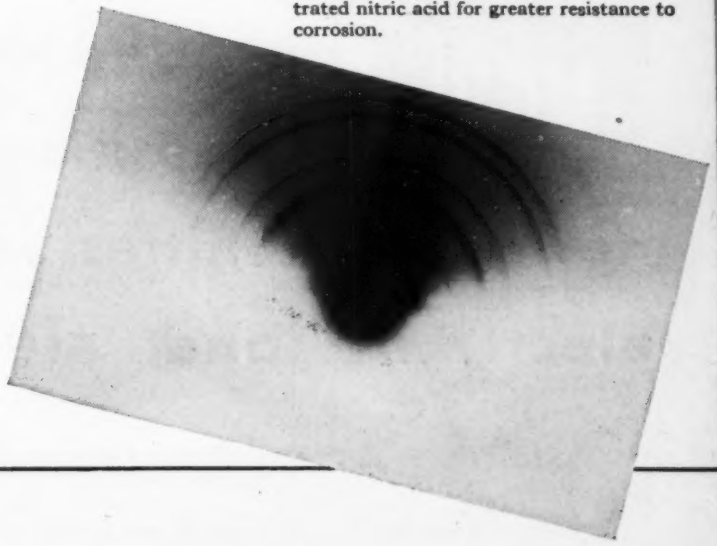

FUNCTIONAL PHOTOGRAPHY

. . . is advancing scientific technics

Kodak will send you free: a copy of the booklet "Materials for Spectrum Analysis" and a chart that tabulates Kodak films for x-ray diffraction. Your specific questions on Kodak Lantern Slide Plates for electron diffraction, and on other products mentioned above, will gladly be answered by correspondence.

Eastman Kodak Company, Rochester 4, N. Y.

"Kodak" is a trade-mark

Kodak

This NEW IRC type B

NOW an ADVANCED insulated fixed composition resistor that offers new opportunities to radio, television, electronic and electrical engineers.

At desks and drawing boards across the country resistor requirements are being reviewed in the light of this *advanced* resistor. Quiet huddles in engineering departments and research labs are rapidly disclosing present performance standards for fixed composition resistors to be obsolete.

The new IRC Type BT resistor *meets* JAN-R-11 specs. At ⅓, ½, 1 and 2 watts, the *new* IRC Type BT is an *advanced* resistor in every respect.

You may specify this *advanced* IRC resistor immediately. It is in production now, with hundreds of thousands coming off production lines daily.

BT *means* **B***etter* **T***echnically* **BTS** *means* **B***eats* **T***oughest* **S***pecs* **BTR** *me*

pe BT resistor will change your standards of performance for fixed composition resistors

Get the full performance facts on this ADVANCED resistor

Standards for resistor performance set by this *new* IRC Type BT are so advanced, you need complete information to fully evaluate its significance. Test result charts will show you how this *advanced* resistor easily performs the rigorous requirements of television. Performance curves prove its excellence in every characteristic . . . particularly in high ambient temperatures.

Technical Data Bulletin B-1 gives the full story. We shall be glad to rush it to your desk or drawing board . . . or to have our representative review your requirements in the light of this *advanced* resistor. Use the handy coupon below.

IRC MEETS JAN-R-11

IRC

power resistors • precisions • insulated composition resistors • low wattage wire wounds • rheostats • controls • voltmeter multipliers • voltage dividers • HF and high voltage resistors.

INTERNATIONAL RESISTANCE CO., 401 N. Broad Street, Philadelphia 8, Pa.
IN CANADA: *International Resistance Co., LTD., Toronto, Licensee*

International Resistance Co.
401 N. Broad St., Phila. 8, Pa.

I want to know more about IRC's *advanced* BT Resistor:

☐ Send me Technical Data Bulletin B-1.
☐ Have your representative call—no obligation.

Name .....
Title .....
Company .....
Address .....
.....

R me tter Test Results **BT** *means* **B***etter* **T***elevision*

EVAPORATED metal films CORPORATION OF ITHACA

FIRST-SURFACE MIRRORS

1—Are all *optical image-formers* alike?
No! There are lenses and there are *mirrors*

2—Are all *mirrors* alike?
No!! There are silver-on-glass mirrors and there are *first-surface* mirrors.

3—Are all *first-surface* mirrors alike?
No!!! There are ordinary first-surface mirrors and

there are { CHROLUMINUM / DUOLUX / RHODIUM } mirrors

made by **EVAPORATED** at Ithaca

Write for descriptive folder

EVAPORATED METAL
FILMS CORPORATION
ITHACA, NEW YORK

Theory and Practice of HEAT ENGINES

By VIRGIL M. FAIRES

Designed primarily for students, taking a terminal course in heat power, this new text also provides an excellent preliminary course in theoretical thermodynamics. Containing much descriptive matter traditional with heat engines courses, it also represents an independent appraisal of the appropriate theoretical developments. *Published October* 26th, 1948. $5.00.

The Engineering Metals and Their Alloys

By CARL A. SAMANS

This text explains the basic theories of pure metals and alloys, and emphasizes particularly their many engineering applications. The book also contains a clear description of nearly all the processes in the molding of metals, stating or indicating the answers to all the questions student engineers might ask. *To be published in the winter.* $7.50 (probable)

Theory of Modern Steel Structures, Vol. II

Revised Edition

By L. E. GRINTER

In the new edition of this text, which is completely reorganized and rewritten, every effort has been made to simplify, clarify and make easier the study of statically indeterminate structures. All the material is presented consistently in such a way as to be of equal value to civil engineers, architects, and aeronautical structural engineers. *To be published in January.* $5.50 (probable)

THE MACMILLAN COMPANY
60 Fifth Avenue New York 11

announcing

A Completely New SCALING TYPE Geiger Müller Laboratory Set Incorporating EVERY modern up to the minute innovation.

Featuring . . .

HERMETICALLY SEALED COMPONENTS

for long life.

MODEL LS100 (Scale of 100) PRICE $385.
MODEL LS1000 (Scale of 1000) PRICE $425.

•

Regulated High Voltage Supply . . . Zero Reset Type Impulse Register Oscilloscope and Timer Connections and dozens of other features.

•

DIRECT READING DECIMAL DECADE SYSTEM . . . Scale of **100** or Scale of **1000** . . . Incorporating the famous positive, reliable, foolproof, Higinbotham scaling circuit.

INDICATES TOTAL COUNT UP TO 999,999 or 9,999,999 BEFORE RECYCLING . . . Direct reading of total count without multiplication, addition or mathematics of any kind.

STYLED TO OCCUPY MINIMUM SPACE ON THE LABORATORY TABLE . . . ONLY 11" wide 9" high . . . 18" deep.

SEND FOR DESCRIPTIVE BULLETIN NO. 485

GEIGER MÜLLER INTEGRATING RATE METER ATTACHMENT

An accessory for use with scaling sets
A complete Self-Contained Unit . . Direct Reading

Four Full Scale Ranges of 5, 50, 500, and 5000 Pulses Per Second.

Built-In Loudspeaker For Aural Monitoring of Operation.

Provision For 5 M. A. Pen Recorder.

MODEL SA4—(complete with tubes) PRICE $240.

A modern fully equipped plant of 15,000 square feet devoted to the manufacture of Geiger Müller apparatus.

El-Tronics INC.

Manufacturers of Geiger Müller counter apparatus for nearly 14 years.

2647-67 N. HOWARD STREET, PHILADELPHIA 33, PA.

NUCLEAR PARTICLES FOR RESEARCH

Highly compressed mixtures of radium: beryllium or polonium: beryllium for use as a source of fast neutrons. Put up in standard monel alloy metal capsule, or magnetic metal if desired. Ratio of active material to beryllium as required. Standard ratio 1:10 by weight.

Sources of gamma, alpha, and beta particles also available.

For prices and further details write to:

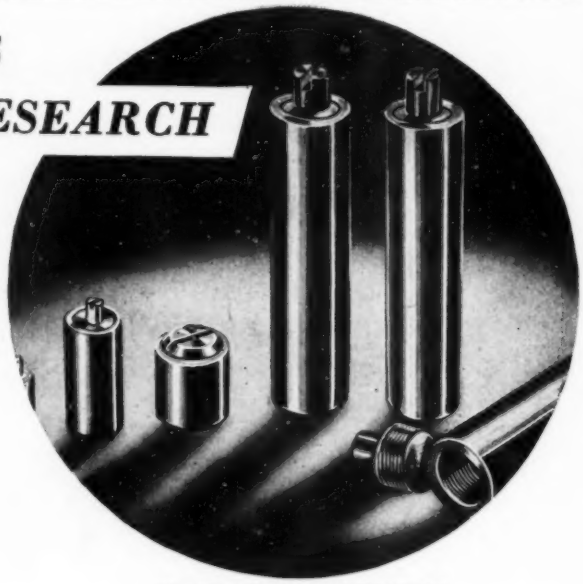

NEUTRON SOURCES

ELDORADO RADIUM

ELDORADO MINING & REFINING (1944) LIMITED

P.O. BOX 379 - OTTAWA, CANADA

. . . Today's schools . . . . .

must train for TOMORROW—a challenge intensified by the accelerating pace of scientific and engineering advance.

Specially designed to meet the needs of modern education, is the NEW

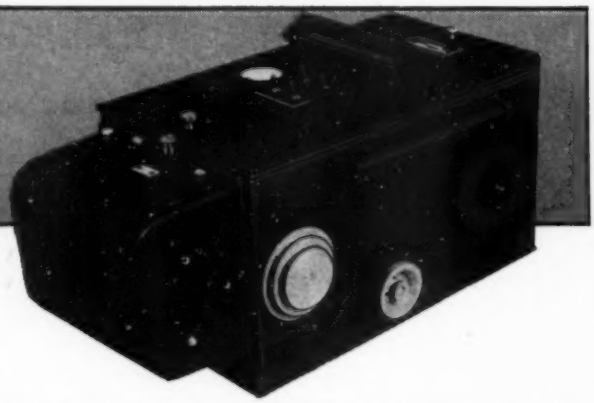

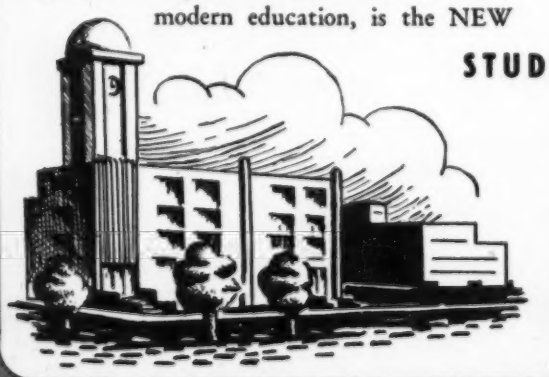

STUDENT'S OSCILLOGRAPH—TYPE S-14

An Essential part of the modern college laboratory

- Accuracy, for the critical researcher
- Simplicity, for the undergraduate student
- 6 to 12 channels, precision components

WRITE FOR TECHNICAL BULLETIN SP-183E

Hathaway INSTRUMENT COMPANY
1315 SO. CLARKSON STREET • DENVER 10, COLORADO

CREEP TEST INSTRUMENTS • TELESCOPES • TOOLMAKER MICROSCOPES • COMPARATORS • OPTICAL INSTRUMENTS • SPECTROMETERS **Gaertner** REFRACTOMETERS • MICROMETER SLIDES • INTERFEROMETERS • SPECTROPHOTOMETERS • LABORATORY SUPPORTS CATHETOMETERS • CHRONOGRAPHS • OPTICAL BENCHES • SPHEROMETERS • SPECTROSCOPES • DIVIDING MACHINES PHOTOELASTICITY POLARISCOPES • MICROSCOPES • SPECTROGRAPHS • POLARIMETERS • MONOCHROMATORS

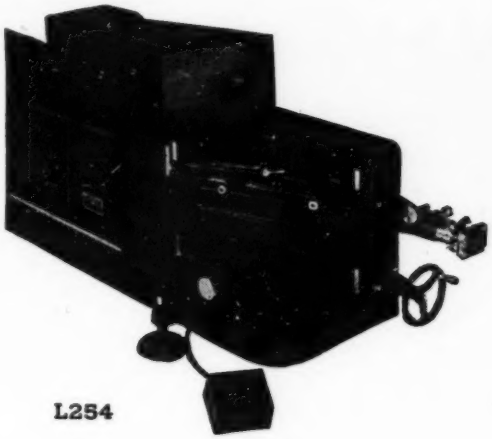

L254

LARGE TWO LENS

QUARTZ SPECTROGRAPH

meets the most exacting requirements

GOOD DEFINITION—NO STRAY LIGHT

EXQUISITE RESOLUTION

1850 TO 12,000 ANGSTROMS

Request New Bulletin 151-74

THE GAERTNER SCIENTIFIC CORPORATION
1212 WRIGHTWOOD AVE. • CHICAGO 14 • U.S.A.

INSTRUMENTS YOU CAN *AFFORD* TO USE

. . . on everyday jobs!

INEXPENSIVE

ACCURATE

RUGGED

EASILY REPAIRED

WRITE FOR BULLETINS
on any desired electrical measuring instrument type.

Hundreds of production testing jobs, field investigations and laboratory tests require dependable instruments that don't have to be kept under lock and key because of their extreme delicacy and high cost. Shallcross answers this need with many types of

BRIDGES • RESISTANCE STANDARDS
DECADE BOXES • DECADE POTENTIOMETERS
HIGH-VOLTAGE TEST EQUIPMENT, etc.

These instruments are accurate up to the point of the most exacting research in pure physics. They are rugged, easy to operate, moderate in price. In case of misuse, they can quickly be repaired by any reasonably competent individual without returning them to the factory.

SHALLCROSS MFG. CO., DEPT. P-128, Collingdale, Pa.

SHALLCROSS

ENGINEERS
DESIGNERS
MANUFACTURERS

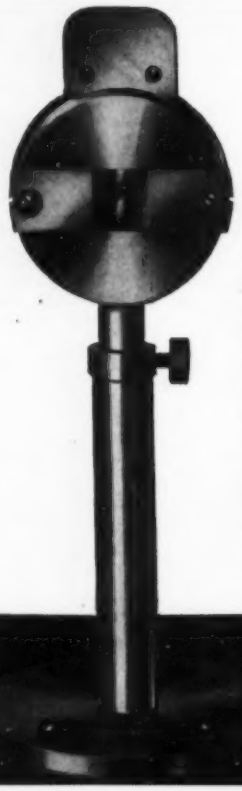

EPLAB

Thermopiles

For many years the thermopile has been the accepted instrument for measuring Radiant Heat from Radiant Heaters at the American Gas Association Testing Laboratory in Cleveland, Ohio. Since 1930, when Vandaveer first described his work in this field,* an Eppley thermopile has been used for this purpose in hundreds of tests and the results have been consistent and accurate to within 1 per cent.

This is but one of many applications in the field of radiant energy measurements for which Eppley Thermopiles are ideally suited. They may be obtained with windows of different materials, and various types of black are available for receiver coatings.

All Eppley Thermopiles are supplied with a certificate of calibration, this calibration being made against a Standard Lamp from the National Bureau of Standards.

If you have a problem involving the measurement of radiant energy we invite you to write us, describing your problem in as much detail as possible. We will be glad to make recommendations and there will be no obligation.

*Vandaveer, Industrial & Engineering Chemistry, Vol. 22, page 596, June 1930.

BULLETIN No. 3 ON REQUEST

THE EPPLEY LABORATORY, INC.

SCIENTIFIC INSTRUMENTS

NEWPORT, RHODE ISLAND, U. S. A.

Again Represented in U. S. A.

P. J. KIPP & ZONEN of Delft, Holland

FORTUNATELY for science, the factory of this renowned concern was undamaged by war. P. J. Kipp & Zonen continues to build precision galvanometers, microphotometers, thermopiles, spectrometers, monochromators, and other highly specialized scientific instruments and apparatus.

We are now the exclusive representatives for Kipp & Zonen in the United States and in the U. S. possessions. Accordingly we invite your inquiries for their apparatus and are prepared to quote prices and delivery.

JAMES G. BIDDLE CO.

ELECTRICAL & SCIENTIFIC INSTRUMENTS

1316 ARCH STREET • PHILADELPHIA 7, PENNA.

Sole Agents in U.S.A. for P. J. Kipp & Zonen

HARMONIC ANALYSIS

Each Fourier coefficient of a curve plotted on rectangular coordinates can be found in less than five minutes using Harmonic Analysis Grids.

A Harmonic Analysis Grid is a transparent plastic template which is used as an overlay chart to locate certain ordinates on the curve such that the sum of these ordinates is equal to the Fourier coefficient corresponding to the template used.

Harmonic Analysis Grids yield results which compare very favorably with the accuracy obtained using other commercial analysers; in fact, the results are more accurate than the curve can be plotted unless extreme care is taken.

The prices of the girds are, including mailing costs:

Harmonic Analysis Grids, set of six templates, mean-value and 1st to 5th harmonics $11.00

Harmonic Analysis Grids, set of eleven templates, mean-value and 1st to 10th harmonics $19.00

Orders will be sent postage prepaid, payment due when billed. Satisfaction guaranteed; order may be canceled provided the Harmonic Analysis Grids are returned within thirty days of their receipt.

Gary Collins Company, P.O. Box 264, Cambridge 39, Mass.

WAR SURPLUS BARGAINS

8 POWER ELBOW TELESCOPE

Gov't Cost $200.00! Our Price $17.50. Big 2" diameter objective. All lenses Achromatic. Amici prism erects the image. 4 built-in filters—clear, amber, neutral and red. Slightly used condition but all guaranteed for perfect working order. Weight 5 lbs. Can be carried but a trifle bulky. Excellent for finder on Astronomical Telescope.
Stock #943-C.....$17.50 Postpaid

POLARIZING OPTICAL RING SIGHT (Unmounted) Used in gun sights—especially for shotguns. As you look through, you see a series of rings that you superimpose on your target. No front sight required. Increases degree of accuracy.
Stock #2067-C.....$4.00 Postpaid.

SLIDE PROJECTOR SETS—Consist of all unmounted lenses you need to make the following size projectors:
Stock #4038-C—2¼" X 2¼".....**$3.35 Postpaid**
Stock #4039-C—2¼" X 3¼".....**$3.35 Postpaid**
Stock #4029-C—35 mm.....**$2.85 Postpaid**

Government's 7 X 50 Binoculars

You Assemble them! Complete Optics! Complete Metal Parts! Save More Than ½ Regular Cost! METAL PARTS—All Metal Parts—completely finished—for assembly of 7 X 50 Binoculars. No machining required. Bodies factory hinged and covered. Sturdy Binocular Carrying Case optional with each set of Metal Parts.
Stock #842-C.....$39.40 Postpaid, plus $4.80 for Case—Total **$44.20**

OPTICS—All Lenses and Prisms for assembling 7 X 50 Binoculars. Excellent condition—perfect or near-perfect—new low reflection coating.
Stock #5102-C.....$25.00 Postpaid

(These are standard American-made parts . . . not Japanese, French or German) Include 20% Federal Excise Tax if you buy both Optics and Metal Parts.
Other items of interest: 6 X 30 Gov't Binoculars, Drift Meters, Gun Sights.

MOUNTED ANASTIGMAT LENSES—Used for Projectors, Enlargers, Copying Cameras. Complete with Shutter and Diaphragm. Value about $20. An excellent buy. WE WILL INCLUDE FREE ILLUSTRATED BOOKLET on HOW TO MAKE YOUR OWN ENLARGER.
Stock #8004-C—Speed of f/7.7, focal length approx. 127 mms. Suitable for pictures, negatives, positives up to 3½" X 4½".....**$7.50 Postpaid**
Stock #8006-C—Speed of f/7.7, focal length approx. 100 mms. Suitable for pictures, etc. up to 2¼" X 3¼".....**$8.50 Postpaid**

We have literally millions of war surplus lenses and prisms for sale at bargain prices. Write for Catalog "C" Sent Free!

Order by Stock No. *Satisfaction Guaranteed*

EDMUND SALVAGE CO. P. O. AUDUBON, NEW JERSEY

ACCELEROMETER TRANSDUCERS

Unique linear Acceleration Transducers . . . Measure the acceleration of launching and additional thrust and the deacceleration of aerodynamic drag. These instruments provide large electrical potentiometer-type outputs proportional to acceleration Magnetically damped with ranges from ±5 G's to ±100 G's. The type 2414 provides expansion of potentiometer output for special ranges. Standard resistance for these instruments is 5,000 ohms.

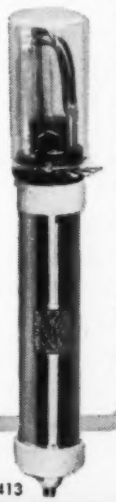

Type 2413

Write for complete information

GM Giannini & CO INC

REACTION POWER PLANTS • AUTOMATIC FLIGHT EQUIPMENT
785 WEST COLORADO STREET • PASADENA 1, CALIFORNIA

BETA HIGH VOLTAGE POWER SUPPLIES

PROBLEM: A physicist doing research work on jet propulsion fuels required a *stable, adjustable, low-ripple* power supply for a photo multiplier tube.

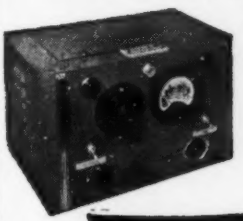

BETA *Built it!*

MAJOR SPECIFICATIONS

Input: 115 volts, 50/60 cycles; 50 volt-amperes

Output: 0–2 KV, negative grounded. More than 2 ma available at 2 KV. Short circuit current limited to 10 ma.

Ripple: Less than ½%.

Size: 14" x 10" x 10".

Power Supplies up to 200,000 volts DC, regulated or unregulated, built to specifications. Compactness, low cost and rapid delivery featured.

Submit your high voltage power supply requirements to us for a prompt bid on price and delivery.

Other BETA products include:

KILOVOLTMETERS: Up to 50 KV at 50,000 ohms per volt. 20 μa drain.

PORTABLE POWER SUPPLIES: Adjustable from 0 to 30 KV DC. Regulated and unregulated units available.

ELECTRONIC MICROAMMETERS: 0.01 μa full-scale to 100 μa full-scale in 5 decade ranges. Cannot be damaged by overload.

ELECTRONIC RHEOSTATS: Resistance continuously variable from above 100,000 megohms to below 100,000 ohms. Good for voltages up to 15 KV.

SEND FOR DESCRIPTIVE LITERATURE

Sales Engineers throughout the country are at your service to discuss our products more thoroughly with you.

BETA ELECTRONICS CO.
1762 Third Ave., New York 29, N. Y.

LABORATORY PANELS AND SWITCHBOARDS

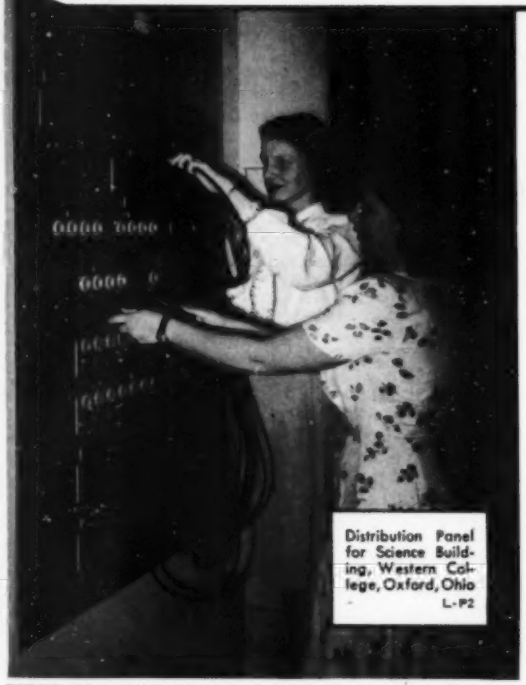

Distribution Panel for Science Building, Western College, Oxford, Ohio L-P2

For over twenty years, The Standard Electric Time Company has specialized in designing and building laboratory equipment. Throughout the nation, in every conceivable kind of college or industrial laboratory, Standard distribution panels, control panels, table and wall units and other associated equipment, are daily proving themselves.

Standard maintains a competent staff of laboratory engineers whose wide experience enables them to be of vital assistance to the architects and engineers who do the planning as well as the instructors who use the equipment. The greatest asset of this staff is its ability to specify complete experimental electrical services efficiently, yet economically.

If you are planning new laboratories, or intend to improve present ones, we shall be happy to work with you without any obligation. Booklet 142 gives more information about this equipment, and will be furnished you on request. Why not write for it today?

THE Standard Electric Time Co.
SPRINGFIELD 2 STANDARD MASSACHUSETTS

Announcing a new book...

COLLEGE PHYSICS

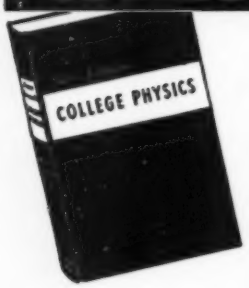

by
Francis Weston Sears
Professor of Physics
Massachusetts Institute of Technology
Mark W. Zemansky
Associate Professor of Physics
College of The City of New York

Teachers of college physics who have regretted that they were unable to adopt the three-volume series of Sears' PRINCIPLES OF PHYSICS because of its use of calculus will welcome this adaptation and revision by Professor Zemansky.

Those parts of the original text that were treated with the aid of calculus have been either removed or rewritten. COLLEGE PHYSICS consists exclusively of material suitable for first-year college students whose mathematical preparation goes no further than the elements of trigonometry. The number of topics has been reduced so that a complete course in general physics may be covered in one year.

Part 1 (one semester)
Mechanics, Heat and Sound
June 1947 $3.50

Part 2 (one semester)
Electricity, Magnetism and Optics
January 1948 $3.50

Complete (two semesters)
January 1948 $6.00

ADDISON-WESLEY PRESS INC.
KENDALL SQUARE BUILDING CAMBRIDGE 42, MASS.

PHYSICISTS FOR RESEARCH

Theoretical and experimental physicists interested in research are invited to investigate the variety of attractive employment opportunities in our research laboratories. Immediate vacancies require men from recent graduates without experience to Ph. D.s with extensive research experience. A few of the variety of problems involve atomic energy, solid state physics, electrostatic and electro-optical properties of materials, and engineering physics. Responsibility, salary, and advancement commensurate with capabilities. All inquiries acknowledged promptly and treated confidentially. Please address replies directly to

Battelle Memorial Institute
505 King Avenue
Columbus 1, Ohio

VYCOR BRAND LABORATORY WARE

...FOR HIGH TEMPERATURE SERVICE

VYCOR brand glass provides exceptional chemical stability. Its low thermal expansion gives it great resistance to heat shock. Available in beakers, crucibles, dishes, flasks and other shapes at leading laboratory supply dealers everywhere.

VYCOR

CORNING GLASS WORKS
CORNING, NEW YORK

PHYSICISTS

During the coming year the Armour Research Foundation is planning to expand considerably its research activities in the following fields: nuclear physics, electricity and magnetism, acoustics and vibrations, optics, spectroscopy, and high-pressure phenomena. Unusual opportunities are available for fundamental and applied research and for professional advancement. The Foundation will welcome applications from persons with several years of research and/or administrative experience.

Write:

Chairman, Physics Research
Armour Research Foundation
35 West 33rd Street
Chicago 16, Illinois

ELECTRONIC LINE VOLTAGE SENTRY

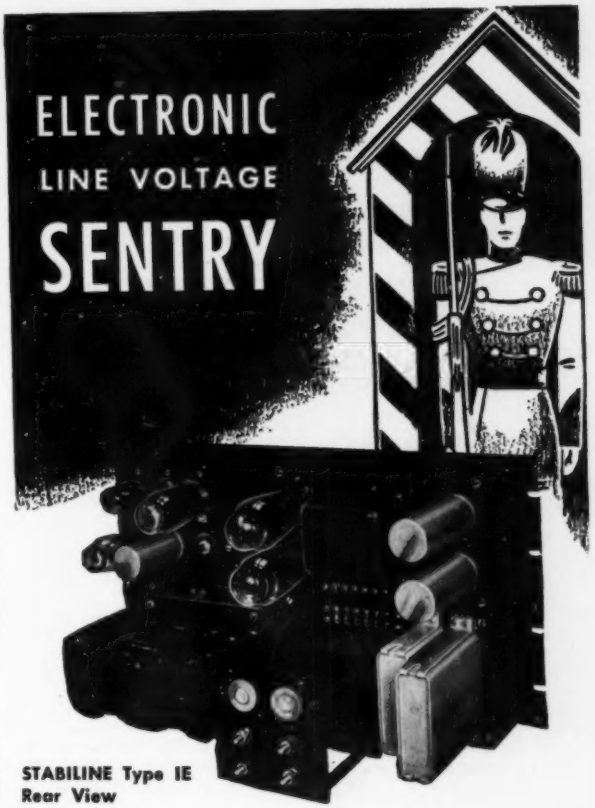

STABILINE Type IE
Rear View

The Superior Electric STABILINE Automatic Voltage Regulator acts as a sentry—always "on duty" to maintain a constant voltage to electrical apparatus. Type IE, an *all-electronic* regulator, acts instantaneously to keep delivered voltage to within ±0.1 volts of the preset value, regardless of line variations. STABILINE Type IE will hold the output to within ±0.15 volts for any load current change or load power factor change from lagging .5 to leading .9. Waveform distortion never exceeds 3 percent — a negligible error not recognized in instrument readings.

Bulletin 547 gives you information on this and other Superior Electric voltage control equipment. Write for your copy today.

1112 Meadow Street, Bristol, Connecticut

THE SUPERIOR ELECTRIC CO.
BRISTOL, CONNECTICUT

POWERSTAT VARIABLE TRANSFORMERS • VOLTBOX A-C POWER SUPPLY • STABILINE VOLTAGE REGULATORS

PLUMMER AND KERSHAW

Understanding
YOUR NEEDS
In Precision Optics
IS OUR JOB

At Plummer and Kershaw we say that the production of fine optics is an attitude of mind—that the correct approach to our work is of utmost importance. To do the best work for you we follow a well defined production system—

FIRST . . . At the outset, we thoroughly study each job to determine the *best* method of work.

SECOND . . . Our highly skilled workers carefully perform each production step assuring a precise finished product.

Whether your needs require the manufacture of complete optical instruments to specifications, the designing of optical systems using glass, crystal or other transmission media, or the production of one or many lenses, we believe you will find our attitude toward your work of distinct advantage to you.

Your inquiry will receive prompt attention.

PLUMMER AND KERSHAW

PRECISION OPTICS
2761 Frankford Ave., Phila. 34, Pa.

PROJECT ENGINEERS

Real opportunities exist for Graduate Engineers with design and development experience in any of the following: Airplane Stability and control, Servomechanisms, radar, microwave techniques, microwave antenna design, communications equipment, electron optics, pulse transformers, fractional h.p. motors.

SEND COMPLETE RESUME TO EMPLOYMENT OFFICE.

SPERRY
GYROSCOPE CO.,
DIVISION OF THE SPERRY CORP.
GREAT NECK, LONG ISLAND

POSITIONS OPEN

Position available on University of California research project for research metallurgist and research physicist. Excellent opportunity for fundamental research in mechanical metallurgy. Ph.D. preferred. Reply Engineering Projects Office, 206 California Hall, University of California, Berkeley 4, California.

Research Engineer: With degree in Mechanical Engineering or Physics and five to ten years experience in research or development work. For applied research on the flow of water, steam and air; metals under simulated service conditions; heat transfer; experimental stress analysis; all as applied to steam boilers and related equipment. Unusual opportunity for men in new research and development laboratory. The Babcock and Wilcox Co., Research and Development Department, Alliance, Ohio.

WANTED: Graduate engineer to head Quality Control Department for large Company making small precision instruments. Ability to deal with and analyze statistics required. Engineering and manufacturing experience necessary. Visiting branch plants in U. S. A. and abroad would be part of duties. Write Box 1248, 57 East 55 Street, New York 22, New York.

Physicist with genuine interest in fundamental, original research in the fields of gas dynamics, thermodynamics, statistical mechanics and/or related fields; advanced degrees preferred; excellent working conditions, salary commensurate to qualifications, good opportunities for advancement and for the establishment of a personal scientific reputation. Write Cornell Aeronautical Laboratory, Employment Office, Buffalo 21, New York.

IN SOLID-STATE RESEARCH AT RCA LABORATORIES
Opening for experimental physicist with originality and thorough fundamental training in solid-state physics, to do research on semi-conductor devices for applications in the radio and electronics field. This position offers an excellent opportunity in a well-equipped laboratory located at Princeton, New Jersey, free from production and factory problems, in a university community with many research and cultural advantages. Write to Personnel Supervisor, RCA Laboratories, Radio Corporation of America, Princeton, N. J.

Laboratory and Research Instruments
ENGINEERED FOR ENGINEERS

OSCILLOSYNCHROSCOPE
Model OL-15B

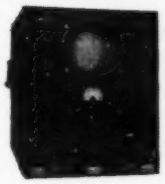

Provides a variety of time bases, triggers, phasing and delay circuits, and extended-range amplifiers in combination with all standard oscilloscope functions.

THESE FEATURES ARE IMPORTANT TO YOU

Extended-range amplifiers: vertical, flat within 3 db 5 cycles to 6 megacycles; horizontal, flat within 1 db 5 cycles to 1 megacycle ● High sensitivity: vertical, 0.05 RMS volts per inch; horizontal 0.1 RMS volts per inch ● Single-sweep-triggered time base permits observation of transients or irregularly recurring phenomena ● Variable delay circuit usable with external or internal trigger or separate from 'scope ● Sawtooth sweep range covers 5 cycles to 500 kilocycles per second ● 4,000-volt acceleration gives superior intensity and definition.

For complete data request Bulletin PO-812

SWEEP CALIBRATOR Model GL-22

This versatile source of timing markers provides these requisites for accurate time and frequency measurements with an oscilloscope:

Positive and negative markers at 0.1, 0.5, 1.0, 10, and 100 microseconds ● Marker amplitude variable to 50 volts ● Gate having variable width and amplitude for blanking or timing ● Trigger generator with positive and negative outputs.

Further details given in Bulletin PC-812

STANDING WAVE RATIO METER & HIGH GAIN AUDIO AMPLIFIER

Model TAA-16

Standing wave voltage ratios are read directly on the panel meter of this sensitive, accurate measuring instrument. ● Frequency range 500 to 5,000 cycles per second ● Two input channels with separate gain control for each ● "Wide-band" sensitivity 15 microvolts full scale ● "Selective" sensitivity 10 microvolts full scale ● Bolometer crystal switch adjusts input circuit to signal source.

Write for Bulletin PA-812 containing full details of this useful instrument.

BROWNING
LABORATORIES, INC
WINCHESTER, MASS
ENGINEERED FOR ENGINEERS

Silicone News
DC

More Power Per Pound†

Call it plain laziness or call it "divine discontent", some potent force has driven us to seek more concentrated motive power ever since man started to move on wheels. But each increase in horsepower per pound has increased operating temperatures and created a need for more heat resistant materials. Dow Corning Silicones help to supply

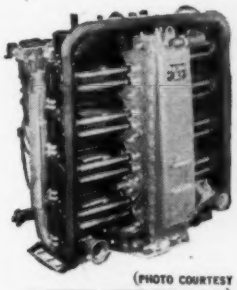

(PHOTO COURTESY CONTINENTAL MOTORS CORPORATION)

Horsepower per pound in Continental's new line of air-cooled gasoline engines is increased as much as 100% in engines below 250 hp . . . more than 300% (down from 2400 to 777 lbs.) in the horizontally opposed 8 cylinder 250 hp engine shown above. In this type of engine, Silastic gaskets are essential parts of the standard push-rod and tube assembly.*

that need in such major developments as the new air-cooled gasoline engine by Continental Motors Corporation of Detroit.

Among the many problems solved by Continental engineers in designing this compact power plant, was the leakage of oil around the push-rod tube assembly. Hot oil and operating temperatures up to 500° F. severely limited the life of conventional gasketing materials. Continental engineers, however, knew about Silastic, the rubber-like Silicone by Dow Corning, and they asked for samples and technical assistance.

Silastic solved this problem because it is more heat-stable and more resistant to hot oils and to permanent deformation at temperatures above 200° F. than any other resilient material. Use of engines in sub-zero weather is not restricted by these gaskets of Silastic 161 because they are serviceable from −90° to 500° F. For more information about Silastic, ask for data sheet No. F-5R.

†See Silicone News, Dec. 1947, for story on 50% reduction in size and weight of electric motors made possible by Dow Corning Silicone Insulation.

*TRADE MARK REGISTERED U. S. PAT. OFF.

DOW CORNING CORPORATION
MIDLAND, MICHIGAN

Atlanta • Chicago • Cleveland
Dallas • Los Angeles
New York
In Canada: Fiberglas Canada, Ltd., Toronto
In England: Albright and Wilson, Ltd., London

Dow Corning
FIRST IN SILICONES

INDEX TO ADVERTISERS

Name	Page
ADDISON-WESLEY PRESS, INC.	xxx
ARNOLD ENGINEERING COMPANY — Alnico Permanent Magnets.	ii
ATOMIC INSTRUMENT COMPANY — Quality Instrumentation for Nuclear Research; Scalers; Linear Amplifiers; Radio Activity Demonstrators; Regulated High-Voltage Supplies; Oscilloscopes; Pulse Generators; Counting Rate Meters; Radiation Meters; and Special Electronic Equipment.	viii
BELL TELEPHONE LABORATORIES	v
BERKELEY SCIENTIFIC COMPANY	ix
BETA ELECTRONICS COMPANY	xxix
JAMES G. BIDDLE COMPANY — "Jagabi" Rheostats; "Pointolite" Lamps; Electrical Testing and Speed-Measuring Instruments; Vibrating-Reed Tachometers and Frequency Meters.	xxviii
BROWNING LABORATORIES, INC.	xxxiii
CENTRAL SCIENTIFIC COMPANY — Manufacturers of Cenco Physical Apparatus and Instruments to meet all requirements of University, College, and High School Physics Laboratories. Specializing in high vacuum pumps and development of instruments and apparatus for various sciences.	Cover 4
GARY L. COLLINS COMPANY	xxviii
CONSOLIDATED ENGINEERING CORPORATION	xviii
CORNING GLASS WORKS — Manufacturers of Pyrex brand Laboratory Glassware including Fritted Ware and Vycor brand Laboratory Ware.	xxxi
CYCLOTRON SPECIALTIES COMPANY — Manufacturers of Scientific, Industrial and Medical Electronic Specialties and Cyclotron components including Geiger-Müller Counter Sets, Geiger Tubes, High Speed Electro-Mechanical Impulse Registers and Ion Gauges.	vi
DISTILLATION PRODUCTS, INC. — Glass fractionating vacuum diffusion pumps, glass-metal diffusion pumps, a complete line of all metal vacuum pumps including the horizontal and vertical fractionating type, booster pumps, low-vapor pressure pump fluids, vacuum greases, Pirani gauges, Ionization gauges and tubes, complete vacuum coating apparatus, molecular distillation units, and other aids to high vacuum technology.	iii
DOW CORNING CORPORATION	xxxiii
EASTMAN KODAK COMPANY — Purified Organic Chemicals for research purposes; Plates for Photography, Photomicrography, Spectroscopy, Photometry, Astronomy; Wratten Light Filters; Cameras and Films.	xxi
EDMUND SALVAGE COMPANY — Retailers of seconds and surpluses in Lenses, Prisms and miscellaneous items . . . currently specializing in the disposal of war surplus optics.	xxix
ELDORADO MINING & REFINING LTD.	xxvi
EL-TRONICS INC.	xxv
THE EPPLEY LABORATORY, INC. — Standards of e.m.f. (standard cells). Precision electrical instruments; potentiometers, bridges, temperature bridges, volt boxes. Thermopiles and pyrheliometers.	xxviii
EVAPORATED METAL FILMS CORPORATION — First surface and semi-transparent mirrors by high vacuum deposition.	xxiv
THE GAERTNER SCIENTIFIC CORP. — Spectroscopes, Spectrometers, Spectrographs, Spectrophotometers, Heliostats, Measuring Microscopes, Comparators, Cathetometers, Reading Telescopes, Interferometers, Chronographs, Dividing Machines, etc.	xxvii
GENERAL RADIO COMPANY — Manufacturers of electronic measuring instruments; vacuum-tube voltmeters, amplifiers and oscillators; wave analyzers, noise meters and analyzers, stroboscopes; laboratory standards of capacitance, inductance and frequency; impedance bridges, decade resistors and condensers, air condensers and variable inductors; rheostats, Variacs, transformers; other laboratory accessories.	Cover 3
G. M. GIANNINI & CO., INC.	xxix
HATHAWAY INSTRUMENT COMPANY	xxvi
HEWLETT-PACKARD COMPANY — Resistance-Tuned Audio Oscillators; Audio Signal Generators; Harmonic Analyzers, Square Wave Generator; Vacuum Tube Voltmeter; Frequency Standards; Frequency Meters; Automatic Welding Machine Controls.	xii
HIGH VOLTAGE ENGINEERING CORPORATION	xv
INTERNATIONAL RESISTANCE COMPANY	xxii, xxiii
KINNEY MANUFACTURING COMPANY	xix
LANE-WELLS COMPANY	xiii
LEEDS & NORTHRUP COMPANY — Manufacturers of Galvanometers, Resistors, Bridges, Condensers, Inductances, Potentiometers, Testing Sets; Temperature Measuring, Recording, and Controlling Apparatus; Instruments for Measuring and Controlling Conductivity of Electrolytes and Hydrogen Ion Concentrations.	i
MACHLETT LABORATORIES INCORPORATED — X-ray tubes for medical, industrial and scientific uses; high voltage rectifying valves for x-ray apparatus; special electronic tubes.	xvi
THE MACMILLAN COMPANY	xxiv
McGRAW-HILL BOOK COMPANY, INC.	iv
NATIONAL RESEARCH CORPORATION — Specialists in industrial applications of high vacuum in the fields of physics and chemistry; research, design, consulting; low reflection glass surfaces, freeze drying, vacuum distillation, vacuum metallurgy and special products manufactured or processed under low pressure.	x
NORTH AMERICAN PHILIPS COMPANY, INC. — Manufacturers of Searchray (X-Ray) Apparatus; X-Ray Diffraction Apparatus; Electronic Measuring Instruments; Direct Reading Frequency Meters; High Frequency Heating Equipment; Tungsten and Molybdenum in powder, rod, wire and sheet form; Fine Wire; Diamond Dies.	xiv
PLUMMER AND KERSHAW	xxxii
SHALLCROSS MFG. COMPANY — Taylor High Voltage Resistors, Kilovoltmeters, Megohm Decade Resistance Boxes, Bridges, Resistance Standards, Test Sets, Attenuators, and other laboratory apparatus. Solid Silver contact rotary selector switches, Super Akraohm, non-reactive wirewound resistors. Special apparatus built to specifications.	xxvii
THE STANDARD ELECTRIC TIME COMPANY	xxx
STATHAM LABORATORIES	vii
THE SUPERIOR ELECTRIC COMPANY — Manufacturers of POWERSTAT variable voltage transformers; SECO Automatic Voltage Regulators; VOLTBOX a-c power supplies; SECO d-c power supplies, and other electrical equipment.	xxxi
TRACERLAB, INC.	xi
W. M. WELCH SCIENTIFIC COMPANY — Manufacturers of high-vacuum pumps, both mechanical and diffusion; vacuum gauges; electrical measuring instruments; physics equipment; and other items for the physical and chemical laboratories.	xx
THE S. S. WHITE DENTAL MFG. CO. — *Industrial Division*—Flexible Shafts for rotary power transmission and remote control—Molded Resistors—Contract plastics molding—Special rubbers.	xvii

The EASIEST Way To Measure

INDUCTANCE • RESISTANCE • CAPACITANCE

● Completely self-contained, portable and always set up for immediate use, this impedance bridge is indispensable in any laboratory where electrical equipment is used. No hastily putting together a circuit, finding an oscillator, detector and power supply . . . they are all here permanently assembled in an accurate instrument . . . always ready for use at any time.

Over the major portion of its ranges this bridge is accurate for the majority of routine measurements in any laboratory. Its ranges are:

INDUCTANCE: 1 microhenry to 100 henrys
RESISTANCE: 1 milliohm to 1 megohm
CAPACITANCE: 1 micromicrofarad to 100 microfarads
STORAGE FACTOR (X/R): 0.02 to 1000
DISSIPATION FACTOR (R/X): 0.002 to 1

Included in the walnut cabinet are built-in standards, batteries, a 1000-cycle tone source for a-c measurements, a zero-center d-c galvanometer null detector and terminals for a headset for 1,000-cycle detection. Terminals are provided for an external generator for measurements from a few cycles to 10 k.c. Direct-reading dials add greatly to the ease and rapidity with which measurements can be made.

TYPE 650-A IMPEDANCE BRIDGE . . . $240

WRITE FOR COMPLETE INFORMATION

GENERAL RADIO COMPANY

Cambridge 39, Massachusetts

90 West St., New York 6 — 920 S. Michigan Ave., Chicago 5 — 950 N. Highland Ave., Los Angeles 38

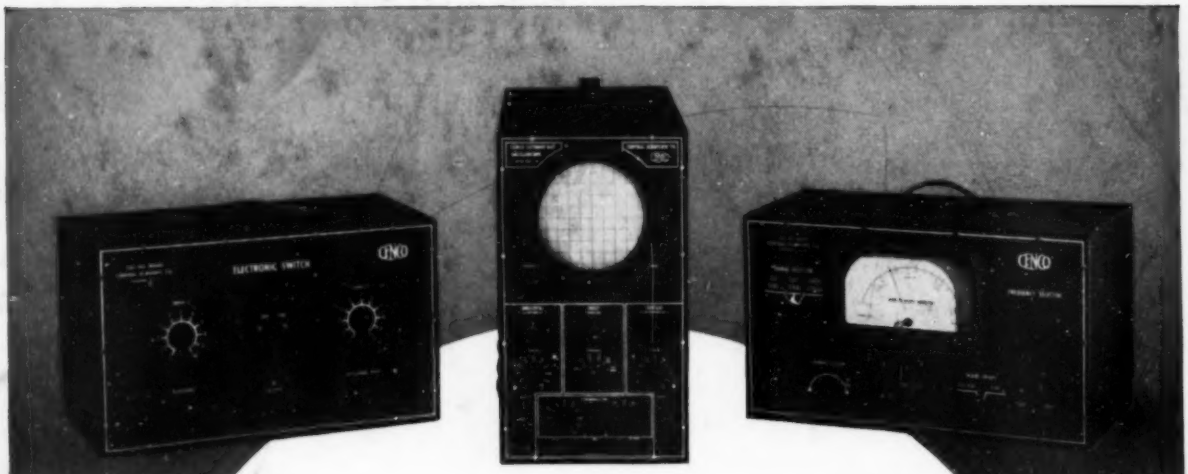

The CENCO SINE WAVE AND SQUARE WAVE GENERATOR will produce both sine waves and square waves in the frequency range from 20–20,000 cps. This range is obtained in three steps selected by means of a range switch on the front panel of the instrument. The three ranges are from 20–200 cps., 200–2000 cps. and 2000–20,000 cps. The oscillator is calibrated with an accuracy of ± 3% of the setting, or 3 cps.

The CENCO ELECTRONIC SWITCH permits the simultaneous observation of two or more separate signals on the screen of a cathode ray oscilloscope. A single Electronic Switch will allow two signals to be observed, while if two Electronic Switches are connected in cascade, three signals may be observed with but one oscilloscope. The Electronic Switch may be used to observe the input signal to an amplifier and the output signal from the same amplifier simultaneously on the same oscilloscope. Thus, wave form, amplitude and phase distortion of the amplifier may be quickly examined. The effects of added components to circuits, differentiation and integration of a square wave, and many other phenomena may be seen.

No. 80592 Cenco Sine Wave and Square Wave Audio Oscillator..Each $100.00
No. 80600 Electronic Switch Each $85.00
No. 71552 Cenco Cathode Ray Oscilloscope, 5 inch screen .....Each $135.00

Write for literature

CENTRAL SCIENTIFIC COMPANY

Scientific (CENCO) Apparatus

1700 IRVING PARK ROAD CHICAGO 13

NEW YORK BOSTON SAN FRANCISCO NEWARK LOS ANGELES TORONTO MONTREAL

LANCASTER PRESS, INC., LANCASTER, PA.